Universidad Autónoma de Madrid
Facultad de Ciencias
Departamento de Biología Molecular

STUDY OF THE IMPACT OF REDUCED SOX4 EXPRESSION LEVELS IN HOMEOSTASIS, CANCER AND AGEING

DOCTORAL THESIS

MIGUEL FORONDA ÁLVARO
Madrid, 2014

Universidad Autónoma de Madrid
Facultad de Ciencias
Departamento de Biología Molecular

STUDY OF THE IMPACT OF REDUCED SOX4 EXPRESSION LEVELS IN HOMEOSTASIS, CANCER AND AGEING

Miguel Foronda Álvaro
BSc, Biochemistry

The entirety of the work presented in this Thesis has been carried out at the Telomeres and Telomerase Group in the Spanish National Cancer Research Centre (CNIO, Madrid), under the direction and supervision of Dr. Maria Antonia Blasco Marhuenda

Madrid, 2014

Dr. Maria Antonia Blasco Marhuenda, Scientific Director of the Spanish National Cancer Research Centre (CNIO) and Head of the Telomeres and Telomerase group (CNIO)

CERTIFIES:

That the Doctoral Thesis entitled "**STUDY OF THE IMPACT OF REDUCED SOX4 EXPRESSION LEVELS IN HOMEOSTASIS, CANCER AND AGEING**" developed by **Mr. Miguel Foronda Álvaro, BSc, MSc** meets all the requirements to obtain the degree of **Doctor of Philosophy (PhD) in Molecular Biology** that will, with the aforementioned objective, be defended at the Universidad Autónoma de Madrid. This Thesis has been carried out under my direction and I authorize it to be presented to the Thesis Tribunal accordingly.

I hereby issue this certification in Madrid on February, the 20th 2014.

Maria A. Blasco, PhD
PhD Thesis Director.

Maria A. Blasco
Director
Telomeres and Telomerase Group Head
Molecular Oncology Program

Spanish national Cancer Research Centre (CNIO)
C/Melchor Fernández Almagro, 3
E-28029, Madrid (Spain)
Phone: 0034-91 732 80 00

A mis padres y a mi hermano.

A Lucía, mi maga.

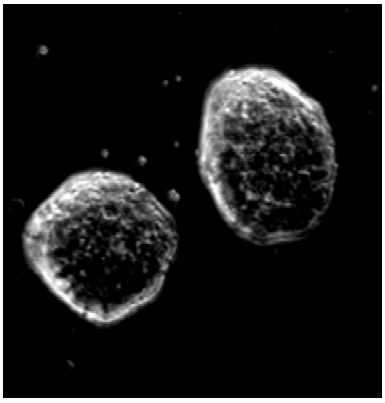

Acknowledgements

"(…) Morelli había pensado una lista de acknowledgments que nunca llegó a incorporar a su obra publicada. Dejó varios nombres: Jelly Roll Morton, Robert Musil, Dasetz Teitaro Suzuki, Raymond Roussel, Kurt Schwitters, Vieira da Silva, Akutagawa, Anton Webern, Greta Garbo, José Lezama Lima, Buñuel, Louis Armstrong, Borges, Michaux, Dino Buzzati, Max Ernst, Pevsner, Gilgamesh (?), Garcilaso, Arcimboldo, René Clair, Piero di Cosimo, Wallace Stevens, Izak Dinesen. Los nombres de Rimbaud, Picasso, Chaplin, Alban Berg y otros habían sido tachados con un trazo muy fino, como si fueran demasiado obvios para citarlos. Pero todos debían serlo al fin y al cabo, porque Morelli no se decidió a incluir la lista en ninguno de los volúmenes (…)".

Julio Cortázar. Rayuela, Cap. 60

La escritura de esta Tesis representa para mí el final de una etapa que he vivido muy intensamente, tanto a nivel personal como profesional. A todos vosotros que me habéis inspirado, apoyado, comprendido, soportado, disfrutado, y, en definitiva, me habéis hecho crecer GRACIAS.

Maria, muchas gracias por acogerme en tu grupo (*and giving me shelter!*). Gracias por confiar en mí, por arriesgar conmigo, por tener en cuenta mis opiniones e intuiciones, por guiarme cuando éstas no eran acertadas y por emocionarte conmigo cuando lo fueron. Trabajar en tu equipo ha sido enormemente enriquecedor.

Gracias a todos los miembros del grupo de **Telómeros y Telomerasa** en el CNIO, presentes y pasados, por hacer de esta aventura una experiencia fantástica. **Susa Alcamí**, *you are my idol, you don't fear problems but they rather fear* you! **Paula**, voy a echar de menos las risas y los consejos; *keep the lab in shape while I'm out!* **Nani**, gracias por tener siempre en la recámara una conversación divertida. **Águeda**, **Elisa**, **Isabel,** gracias por compartir vuestra experiencia conmigo! **Juanma**, **Aksi**, **Miguel Ángel** *on your hands is the future of the lab; make a good place of it!* **Marinela**, no te olvides nunca del *Método 2 (*aunque sea para unas risas*)*. **Christian,** *thanks for sharing with me fun, stress, runs, laughs and GSEAs (YEAH!).* **Smarty**, *yours is attitude (and thanks for sweetening my PhD experience!).* **Maria G**, *rock it wherever you go!* Te dejo en herencia el cuaderno de paridas, *keep it updated* ;) **Nora**, sirenita! A ver quién me toca de compi en natación ahora, que ahí también te echaré de menos. **Merche** echaré mucho de menos tu visión sevillana de la realidad, ha sido genial trabajar contigo. **Ianire**, compi de fatigas y de cuadrilla! Reprográmate y vente con nosotros a Edimburgo, que ya te estoy echando de menos, *caracoles!* **Iole**, *so brief and yet so cool! Good luck*, y *fuggire* a tope cuando la situación lo pida! **Judit**, buena suerte con todo, hazte una científica de provecho (no me dejes en mal lugar, jeje). **Rosa**, Rose, Rosita! Para ti me faltan palabras, pero ante todo: gracias por hacerte cargo de las fieras! Sin ti no sólo mi tesis sino todo el labo sería un completo desastre. Gracias también a **Esther**, que tiene la paciencia de una hermana; tenerte echando un ojo a los animalillos hace la vida mucho más sencilla. **Ale**, *we miss your know-how and your endless curiosity. See you in the heart of the Kingdom*! **Fabian**, *holaqué! Our lab lost part of its enthusiasm and self when you left, thanks for your positivity and friendly attitude.* **Bruno**, *the time we coincided in the lab seemed so brief! It was great to work with you, but even greater to share so many good moments out of the cage*. **Ralphie**, *albondiguilla! Since you left I'm getting fat and slow, my only hope is that cheese and chocolate are spoiling you as well! Thanks for sharing the Söla experience with us.* **Ben**, *my other favourite businessman, keep a place for me wherever you are when you become rich and famous! Thanks for the good times, and keep your enthusiasm and smart-thinking, the world needs brains like yours.* **Gina**, *bella!* Gracias por cambiar mi rumbo para mejor con un sólo e-mail (pobre *Kaji-san*!). Ha sido genial intercambiar libros y abrazos. Trabajar sin ti cerca va a ser horrible, por muy bueno que sea todo lo demás.

I want also to thank our neighbours from the **Tumour Suppression group***, with whom we share much more than just lab space and reagents. Thanks* ***Manolo*** *for your advice and attention. Thanks to* **Han**, **Tim, Cian**, **Lluc**, **Noelia** y **Raquel** *for your sense of humour and freshness*. Gracias a **Antonio** y **Dani** por ser tan auténticos. **Sandrina**, *I liked a lot your calm ways and I really admire your hard-working and efficiency.* **Luis***, I miss your acid, British sense of humour. I wish I had a tenth of your vocabulary and writing elegance.* Gracias a **Ade** por aportar siempre su contrapunto con una sonrisa de oreja a oreja. Gracias a **Manuel Collado** por compartir los secretos de la Eterna Juventud y de la Literatura. Sigamos en contacto siempre! **Pablo**, my *Rayuela soul-mate!* Ha sido genial tenerte cerca, gracias por aportar tu inteligencia y tu candor (y tus películas!). **Kathi**, *come back to the lab!! We need your spontaneity and deep mind.* **Elena**, qué guay que Manchester sea feo, así podéis venir siempre a visitarnos, que queda cerquita! **Daniela**, *knowing you has been a fantastic experience. You'll succeed in everything you attempt to; I only wish I ever get to have a quarter of your common sense, your intelligence, your persistence and your empathy.*

luck, bella! Gracias a **Susana Llanos**, porque es simplemente genial trabajar cerca de ti, gracias por tu *positive-thinking!* **Panto**, *guapa*! Gracias por cuidarme como una madre (pero en jovencita) y por darme tanto cariño; guárdame alguno de tus abrazos para cuando venga de visita (y luego, a nadar!). **Meri Abad**, mi rubia favorita!! Qué fuerte estar escribiendo *ésto* aquí y ahora. Gracias por dar ese toque de alegría a todo lo que miras. No te olvides de nosotros ahora que YA eres una gran estrella. Orgullo máximo por haber compartido contigo pasillo, dudas, opiniones, manifestaciones, y sobre todo sobre todo, amistad. GRACIAS!

Quiero agradecer también a todos los amigos que compartieron mis inicios en la investigación en el **CNIC**. Gracias **Miguel Ángel** por acogerme, gracias a **Raffaele** por tu profundidad y tu amistad, has sido un gran profe y a **Ana Cerezo** (eres mi científica modelo!). Gracias a **Rubén** y **Vane** por compartir conmigo tantos buenos momentos, ser amigo vuestro me hace sentir privilegiado, y también a **Íñigo, Laura** y **Salomón**, qué pena no haber llegado una "F" antes al labo!. *Thanks* **Jacky** *for sharing that much with me, even years after we met there!* Gracias también a **Olivia, Marta, Pilar, Dácil, Teijo, Aga, Ángela, Inma, Tere, Sara, Susana**, **Olga**, **Maria Casanova**, **Ara** y **Enara** no tengo más que buenas palabras para agradeceros el tiempo que pasé con vosotros.

Un apartado especial merece el **Running Team del CNIO**, empezamos siendo cuatro gatos y terminamos siendo casi seis, y hemos salido tanto si hacía buen tiempo como si hacía MEJOR. Os debo mucho más que mis piernas de atleta, y aunque hayamos coincidido tan tarde (o a mí se me ha hecho muy breve) os habéis convertido en una parte muy importante de mi ser. **Oli**, eres el *mechero* alemán mejor fabricado del mundo y mi héroe del *running*! **Lola**, quisiera tener tu energía y tu capacidad de *multi-tasking* y *multi-tascas*! **Nuria**, para mí eres el descubrimiento del año, cuánta alegría traes de casa! **Jacinto**, eres único e inimitable! **Juan Guinea**, oooolé! **Narciso**, qué genial coincidir contigo en alguna carrerilla! **Silvia**, eres de las mejores adquisiciones del grupo, te lo digo. **Laura**, gracias por vigilar las pertenencias y por las cañitas de después. Gracias **Enara**, el núcleo duro del grupo; tú y **Ara** sois mis viejas glorias preferidas, espero coincidir con vosotras en todos los próximos Centros de Excelencia que tengamos de *target*! Súper-**Juanma**, de verdad no te conozco de toda la vida? A todos, UN MILLÓN DE GRACIAS por compartir momentos tan buenos conmigo, por ser mi gasolina del día; donde vaya, corra con quien corra, siempre os llevaré grabados en la memoria y seréis mi motivación para seguir.

I would also like to thank all the people I have met at the **CNIO** *and made out of this time something even more special, if possible. Thanks to* **Isabel Morgado** (hermana! ahora los domingos tendremos que llorar juntos por skype), **Metehan, Laura** (-Paula!)**, Direna, Andrés J. López, Eva Pérez, Jarek, Paloma Olave, Patri Nieto, Ciara Ambroggio, Sarah Francoz, Carmen Lechuga, David Santamaría, Yolanda Ripoll, Susana Velasco, Emma** (qué crack!!) y la gente de cafetería, **Celeste** y la gente de **Mantenimiento y Seguridad**, **Nabil**, *all the CNIO Core Units, especially* **Histopathology** (sin vosotras todo habría sido imposible), **Transgenic Mice**, **Genomics** (**Guada, Orlando**, GRACIAS de nuevo), **Bioinformatics** (**Osvaldo**, gracias por tu paciencia en los cursos! **Gonzalo**, GRACIAS por tu profesionalidad y rapidez! **David Pisano**, es siempre un placer hablar contigo!), **Confocal** (**Diego, Manu, Ximo**, sois unos genios, es genial hacer microscopía con vosotros!), *and* **Flow Cytometry** (**Lola, Ultan, Miguel Ángel, Elena**, hacer citometría ha valido la pena aunque sólo sea para coincidir con vosotros!). *To all of you, BIG THANKS, you know you deserve a special place in this thesis.*

Quiero también agradecer a todos mis profesores de la **Universidad Autónoma de Madrid, la UAM,** por darme una sólida formación y por imbuirme la pasión por la Biología. Quería hacer una mención a **Elena Escudero**, **Elena Bogónez**, **Mauricio García-Mateu** y con especial cariño a **Jose M. (Pepe) Cuezva**, que guió mis primeros pasos en su laboratorio en el CX. GRACIAS por ilusionarme.

*Also, big special thanks to Drs***. Andrew Ramsay, Elías Campo** and **Carlos López-Otín**. *It has been a big pleasure to have the opportunity to work with you, and I have deeply enjoyed doing science with you. THANK YOU.*

Gracias mis amigos, a quienes siempre veo mucho menos de lo que quisiera pero que hacen que la distancia y el tiempo sean insignificantes porque a su lado, todo parece pequeño. Gracias a **Pilar**, uno de mis principales apoyos (*como su propio nombre indica*) y a **Alfons**, ya sabéis todo lo que os quiero; ser amigo vuestro es uno de los raros privilegios de la vida, gracias por ser exactamente como sois. Gracias a **Alejo** y **Jimi Race**, por subir el nivel intelectual de todo lo que hemos compartido, gracias también a **Jaime de Juan, Lara Durán-Trio, Cris Gutierrecina, David Lara, Piñero-Carlos, Dani Mateos, Edu Pis, Irene Guijarro, David Ruano, Marta Moris, Alex Macías, Elisa Lucas, Bea Rodríguez, Inés Soro, Jara Moreno, Jesús Curt, Ana del Río, Alba Maiques** y todos los demás; algunos de mis mejores recuerdos son del tiempo que he pasado con gente tan genial como vosotros! Gracias a **Diegocepe**, mi alma gemela, y también a **Emilio**, **Raqui** y **Fernan** por haber compartido conmigo momentos inolvidables. Gracias a **Bea** y **Maldo** y a todos los **amigos de la sierra**, por crecer conmigo y ser tan diferentes a todo. Gracias a todos mis **amigos de Wushu**, **Rafa, Blanca, Alberto, Marcos, Vane, Óscar, Adri, Ana, Javi, Chema, Almu, Marta, Diego, Irene, Alex** y todos los demás, mis frikis preferidos con quienes comparto obsesión y locura por las artes marciales chinas.

Si tuviera que agradecer a **toda mi familia**, me llevaría todo un tomo como éste que tengo ahora entre las manos, y no sólo porque sois muchos sino porque os debo todo; gracias por estar, siempre. Pero quiero hacer mención a mis raíces, a mis abuelitos **Dolores** y **Lorenzo, Angelita** y **Pedro**. De vosotros me quedo con algo de la entereza, la inteligencia, la persistencia y el amor que siempre habéis irradiado, la memoria puede a veces diluirse en brumas pero a vosotros os llevo indelebles en el corazón. **Ali**, contigo me sentiría a gusto hasta sentado en un cardo. Gracias por saber sintonizar siempre con mis ondas y **David**, siempre has sido un ejemplo a seguir en todo para mí, gracias por ser mis hermanos mayors y enseñarme tanto. **Víctor**, mi hermano preferido, aunque eres el peque, aprendo de ti todos los días. Gracias por ser un diamante en bruto y darme tanto cariño. **Papá**, muchas gracias por enseñarme a vivir con la intensidad con la que siempre has hecho todo y por enseñarme a mantener siempre *los ojos bien abiertos*. **Mamá**, mamita, gracias por cuidar de mí y por estar siempre, en los momentos buenos y en los malos; gracias por la educación y los valores que me habéis dado, gracias por enseñarme a morder la vida y por ser tan alegres y tan cariñosos. Los achuchones que reparto por el labo os los deben a vosotros.

Gracias a **Julio Cortázar**, quien hace 50 años nos dejó una reliquia que es *Rayuela* y hace 30 nos dejó, sin más; las citas incluídas en cada capítulo pertenecen a ésta novela, y su vigencia queda plasmada en su perfecto acoplamiento con cualquier aspecto de la realidad.

Lucecita, todo lo que pueda decirte se queda pequeño. Eres una inteligencia cegadora, un pozo de sabiduría; gracias por ser tan perfeccionista (tan perfecta) y tan exigente, gracias por todo el cariño que guardas para mí y por hacer que la realidad se pliegue a nuestro gusto, por buscar tesoros conmigo, por mantener vivos todos mis sueños.

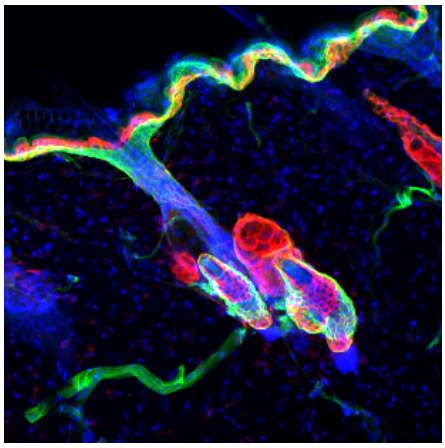

Resumen

"(…)
—Usted escribe, supongo.
—No —dijo Oliveira—. Qué voy a escribir, para eso hay que tener alguna certidumbre de haber vivido.
—La existencia precede a la esencia —dijo Morelli sonriendo. (…)"

Julio Cortázar. Rayuela, Cap 154

Sox4 es un factor de transcripción perteneciente a la clase SoxC (que engloba a Sox4, Sox11 y Sox12), dentro de la superfamilia de proteínas relacionadas con Sry con dominios tipo HMG.

La expresión de Sox4 es máxima durante el desarrollo embrionario en la cresta neural y el mesénquima, donde regula la diferenciación y desarrollo de precursores neuronales y mesenquimales. Así mismo, también se ha detectado expresión de Sox4 en otros tejidos como timo, bazo, páncreas y folículos pilosos.

Durante la embriogénesis, Sox4 está implicado en un vasto panel de procesos que incluyen maduración de linfocitos B y T, modulación de la diferenciación mieloide, desarrollo de islotes pancreáticos y osteoblastos, y adecuada formación del canal auriculoventricular. Ratones deficientes en la expresión de Sox4 presentan letalidad embrionaria debido a profundas malformaciones cardíacas, que cursan con defectos en hematopoyesis y en la formación de islotes pancreáticos.

En adultos la expresión de Sox4 se restringe a unos pocos tejidos como la médula ósea, sistema reproductivo femenino, criptas intestinales, islotes pancreáticos y folículos pilosos activados. Dichas constricciones son sugestivas de una fuerte regulación que asegure una adecuada homeostasis tisular; de hecho, la desregulación de la expresión de Sox4 en adultos se encuentra asociada a transformación celular.

Sox4 puede actuar como un potente oncogén que promueve la supervivencia de células transformadas y favorece el crecimiento independiente de anclaje a substrato. La expresión elevada de Sox4 está estrechamente asociada a leukemogenesis, inhibición de la apoptosis y aumento de la viabilidad celular. Además, el aumento de la expresión de Sox4 se asocia frecuentemente a la adquisición de un fenotipo invasivo dado a que es capaz de promover el programa transcripcional asociado a la EMT, y por lo tanto a menudo se asocial a la colonización metastática de tejidos distantes.

Para estudiar Sox4 en adultos, hemos generado ratones con niveles reducidos de Sox4 en todo el organismo. Dichos ratones muestran un panel de enfermedades asociadas al envejecimiento y resistencia frente al cáncer espontáneo, indicando un papel para Sox4 en el mantenimiento de la homeostasis tisular y en tumorogénesis. Para estudiar en detalle el papel de Sox4 en células madre adultas, hemos delecionado Sox4 de forma condicional en epitelio estratificado (ratones *Sox4*^{cKO}). Estos ratones muestran mayor quiescencia en las células madre de la piel junto a una mayor acumulación de daño en el DNA y resistencia a carcinogénesis química. Dichos fenotipos correlacionan con una regulación negativa de genes implicados en ciclo celular, reparación de daño en el DNA y diferenciación de células madre de la piel. Estos resultados resaltan la importancia de Sox4 en la homeostasis tisular adulta y cáncer.

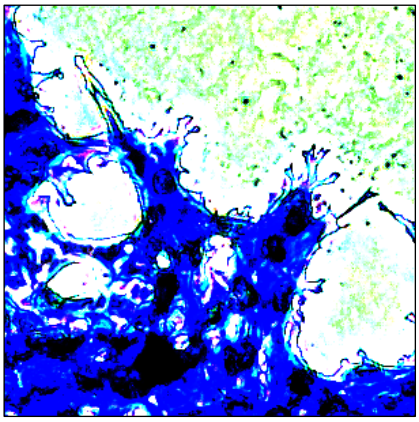

Abstract

“Morelliana.
Si el volumen o el tono de la obra pueden llevar a creer que el autor intentó una suma, apresurarse a señalarle que está ante la tentativa contraria, la de una resta implacable.”

Julio Cortázar. Rayuela, Cap. 137

Sox4 belongs to the SoxC class of transcription factors (encompassing Sox4, Sox11 and Sox12) within the *Sry*-related HMG box-containing superfamily of proteins.

Sox4 expression peaks during embryonic development in neural crest and mesenchyme, where it regulates the differentiation and survival of mesenchymal and neural progenitors. Sox4 expression has also been found in thymus, spleen, developing pancreas and hair follicles. During embryogenesis, *Sox4* has been implicated in a plethora of processes including the maturation of B and T lymphocytes, the modulation of myeloid differentiation, pancreatic islet development, osteoblast development and proper cardiac cushion formation. $Sox4^{-/-}$ mice display embryonic lethality at E14.5, mainly due to profound cardiac malformations, concomitant with defective haematopoiesis and pancreatic islet formation defects.

In adults, the *Sox4* is restricted to few tissues such as haematopoietic compartment, female reproductive system, intestinal crypts, pancreatic islets and activated hair follicles. These constrictions suggest a tight regulation to ensure proper tissue homeostasis; indeed, deregulated Sox4 expression is frequently associated to malignant cellular transformation.

Sox4 can act as a potent oncogene that promotes the survival of transformed cells and favours anchorage-independent cell growth and motility. High expression of Sox4 is associated with leukemogenesis, inhibition of apoptosis and increased cell viability. Moreover, increased Sox4 expression is often linked to the acquisition of an invasive phenotype by promoting the initiation of the EMT transcriptional program, and therefore is often associated to metastatic colonization of distant tissues.

To study the role of *Sox4* in the adult organism, we first generated mice with reduced whole-body *Sox4* expression. These mice display a plethora of age-related degenerative disorders and reduced spontaneous cancer incidence, indicating a role for this protein in maintaining adult tissue homeostasis and in tumour growth. To specifically address a role for Sox4 in adult stem cells, we conditionally deleted *Sox4* ($Sox4^{cKO}$) in stratified epithelia. $Sox4^{cKO}$ mice show increased skin stem cell quiescence and DNA damage accumulation, accompanied by resistance to chemical carcinogenesis. These phenotypes correlate with downregulation of cell cycle, DNA repair and skin stem cell differentiation genes. Altogether, our findings highlight the importance of *Sox4* in adult tissue homeostasis and cancer.

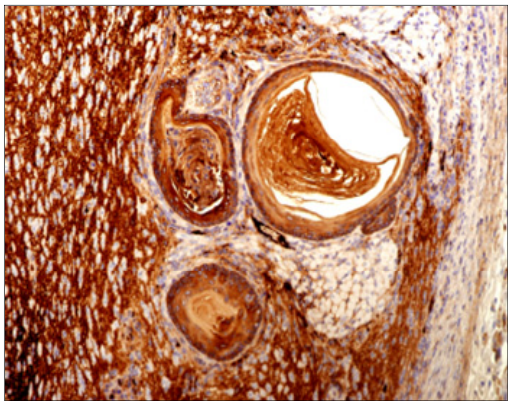

Index

Andábamos sin buscarnos pero sabiendo que andábamos para encontrarnos.

Julio Cortázar. Rayuela, Cap 1

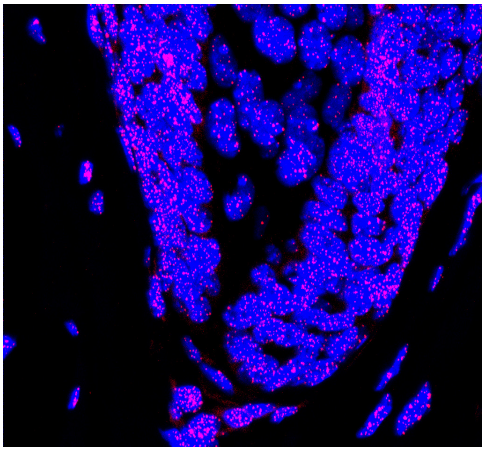

Abbreviations

"(…) No aprendás datos idiotas", le aconsejaba. "Por qué te vas a poner anteojos si no los necesitas. (…)"

Julio Cortázar. Rayuela, Cap. 4

γH2AX	Phosphorylated Histone 2 variant A.X
2i	Two inhibitors, MEK and GSK-3beta inhibitors
ACC	Adenoid cystic carcinoma
AdCre	Adenoviral particles expressing Cre recombinase
a.u.f.	Arbitrary units of fluorescence
Bg	Hair bulge
BM	Basement Membrane
BMD	Bone mineral density
CIS	Common integration site
CK6	Cytokeratin6
DAPI	4',6-Diamidino-2-phenylindole dihydrochloride
DEG	Differentially-expressed genes
DEXA	Dual-energy X-ray absorptiometry
DDR	DNA damage response
DMBA	7,12-Dimethylbenzanthracene
DMEM	Dulbecco's Modified Eagle's Medium
DMSO	Dimethyl sulfoxide
DNA	Deoxyrribonucleic acid
DP	Dermal papilla
dpc	Days post-coitum
DSB	Double-strand DNA break
EB	Embryoid bodies
EDTA	Ethylenediaminetetraacetic acid
EMT	Epithelial to mesenchymal transition
EtOH	Ethanol
ES	Enrichment score
FBS	Foetal bovine serum
FDR	False discovery rate
GFP	Green fluorescent protein
GSEA	Gene set enrichment analysis
HCC	Hepatocellular carcinoma
HSCs	Haematopoietic stem cells

HET	Heterozygous
HFSC	Hair follicle stem cell
HMG	High mobility group
HT-QFISH	High-throughput quantitative fluorescence in-situ hybridization
iPS	Induced pluripotent stem
IRES	Internal ribosome entry site
IFE	Interfollicular epidermis
JZ	Junctional zone
K5	Keratin5 promoter
KI	Knock-In
KO, cKO	Knock-Out, conditional Knock-Out
KSR	Knockout serum replacement
LIF	Leukemia-inhibiting factor
MEF	Mouse embryo fibroblast
MET	Mesenchymal to epithelial transition
mES	Mouse embryonic stem
min	minute(s)
miRNA,miR	micro-RNA
PBS	Phosphate buffer saline
PCR	Polymerase chain reaction
qPCR	Quantitative-Real Time PCR
PNA	Peptide nucleic acid
PFA	Paraformaldehyde
PTH	Parathyroid hormone
RA	Retinoic acid
RIS	Retroviral integration site
ROI	Region of interest
RS	Replicative stress
RT	Room temperature
sec	second(s)
siRNA	small-interference RNA
shRNA	short-hairpin RNA
SG	Sebaceous gland

SDS-PAGE	Sodium dodecyl sulfate-polyacrylamide gel electrophoresis
ssDNA	single-stranded DNA
Sry	Sex-determining region of the Y chromosome
Sox	Sry-related, HMG box-containing protein
T2D	Type 2 diabetes
Terc	Telomerase RNA component
TERT	Telomere end repeat retrotranscriptase
Tg	Transgenic
TPA	12-O-Tetradecanoylphorbol-13-acetate
TRF1	Telomere end repeat binding factor 1
UTR	Untranslated region
UV	Ultra-Violet light
WT	wild type
XEN	Extraembryonic endoderm

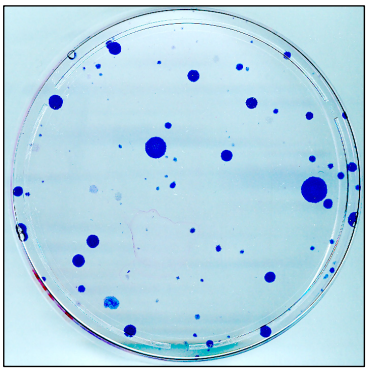

Introduction

"(…) La razón sólo nos sirve para disecar la realidad en calma, o analizar sus futuras tormentas, nunca para resolver una crisis instantánea.(…)".

Julio Cortázar. Rayuela, Cap 28

I. DEVELOPMENT, CANCER AND AGEING

Mammalian embryonic development comprises a plethora of tightly regulated biological processes (spatiotemporal control of specific gene regulation, cell signalling, cell migration and growth, tissue patterning and modulation of metabolism among others) that govern the differentiation of the embryonic stem cells into all the cellular lineages that form the adult organism while maintaining a population of undifferentiated cells that ensure proper input to all cellular lineages (Tam and Loebel 2007; Smith, 2001). Likewise, adult organs and tissues are maintained through a delicate balance of proliferation, differentiation and self-renewal of their tissue-type adult stem cells in order to keep a constant replacement of the damaged cells originated upon injury or during normal tissue homeostasis (Wagers and Weissman, 2004; Blanpain and Simons, 2013). Any perturbation in the aforementioned control of such regulatory mechanisms can cause aberrant loss or gain of cellular fitness. On one hand, accumulation of cellular damage is thought to be the widest accepted cause of ageing (Lopez-Otin et al, 2013); on the other hand, aberrant proliferative potential or increased survival advantage are some of the commonest hallmarks of cancer (Hanahan and Weinberg, 2011).

II. THE MAMMALIAN SKIN AS A MODEL FOR STEM CELL FUNCTION

The skin is the largest of the mammalian organs and its main function consists on covering the entire body surface in order to provide protection from external aggressions (either from biological or from physical sources, such as infections or ionizing radiations, respectively) and to confer a barrier against water loss and thereby prevent dehydration. It also provides an additional layer of functionality with its multiple specialised appendages, such as touch pads for sensing, sweat glands for thermoregulation and excretion, feathers and hairs for thermal isolation and defensive keratinized structures (Fuchs, 2007). The skin structure meets the functional requirements of such a specialised organ, and its repertoire of specialised cell populations and their dynamics in mammals have been broadly studied; this knowledge provides a great tool in cell biology for addressing embryonic and adult stem cell function during development, ageing, regeneration and cancer (Arwert et al., 2012; Blanpain and Fuchs, 2009).

II.1. The structure of the mammalian skin

In mammals, the skin is composed of the dermis and the epidermis. The dermis is a supportive connective tissue which contains fibroblasts and a dense scaffold composed of collagen, elastin and glucosaminoglycans, that is placed on top of a subcutaneous fat pad covering the muscular layer. The epidermis is the external layer, and is attached to the dermis through the basement membrane (BM). The epidermis comprises several layers of differentiating keratinocytes, remaining the less differentiated ones directly attached to the BM (Watt and Huck, 2013). The increased differentiation towards the surface is accompanied by programmed cell death (apoptosis), cornification (accumulation of intermediate filaments, especially keratins, in the cytosol), stratification and sequential expression of differentiation markers (cytokeratin 14 in the basal layer, cytokeratin 10 in the suprabasal or spinous layer, involucrin and filaggrin in the granular layer and loricrin in the cornified layer) (Fuchs, 1994).

Being the most exposed part of the skin, the epidermis is subjected to constant mechanical tension and other types of physicochemical aggressions. In order to prevent the tearing of the skin with such stresses, the epidermal keratinocytes are subjected to constant replacement. The source of this replacement is the basal layer of the epidermis, which proliferates constantly in order to provide with fresh cells the upper epidermal layers, while the cornified, dead cells are constantly desquamated and shed from the skin surface. Similarly, most other epidermal structures are constantly renewed through recurring bouts of proliferation, differentiation and degeneration that take place during the hair cycle, and which depends on the timely activation of the so-called hair follicle stem cells (HFSCs), which provide with their input to all the skin cellular lineages (Alonso and Fuchs, 2006; Fuchs, 2007).

II.2. The hair follicle and the hair cycle

The outermost part of the mammalian epidermis is composed of a multi-layered epithelium known as the Interfollicular Epidermis (IFE) and its adjunct structures: hair follicles (HFs), sebaceous glands (SGs) and sweat glands (SwGs). In mice, the sweat

glands are restricted to hairless regions, such as the paws; therefore, the epidermal stem cell potential is usually assessed in terms of input to the IFE, the HF and the SG. Terminally-differentiated cells from these compartments are constantly lost and thus it has been long known that all the epidermal lineages are maintained by the HFSCs, capable of self-renewal and terminal differentiation (Blanpain and Fuchs, 2006).

Every hair is destroyed and regenerated several times during an organism lifespan, initially in a synchronic manner that gradually becomes less frequent and less coordinated among different parts of the body with ageing. The hair cycle in mice has been deeply characterised, mostly because of its structural resemblance with that of human hair cycle and because it provides an unvaluable tool for modelling adult stem cell function. In fact, each hair follicle is considered to be a mini organ, composed of specialised structures containing differentiated cells and a variety of multipotent stem cells (the HFSCs) that can partially (or totally, under certain circumstances such as wound repair) regenerate the whole hair structure (Blanpain and Fuchs, 2009).

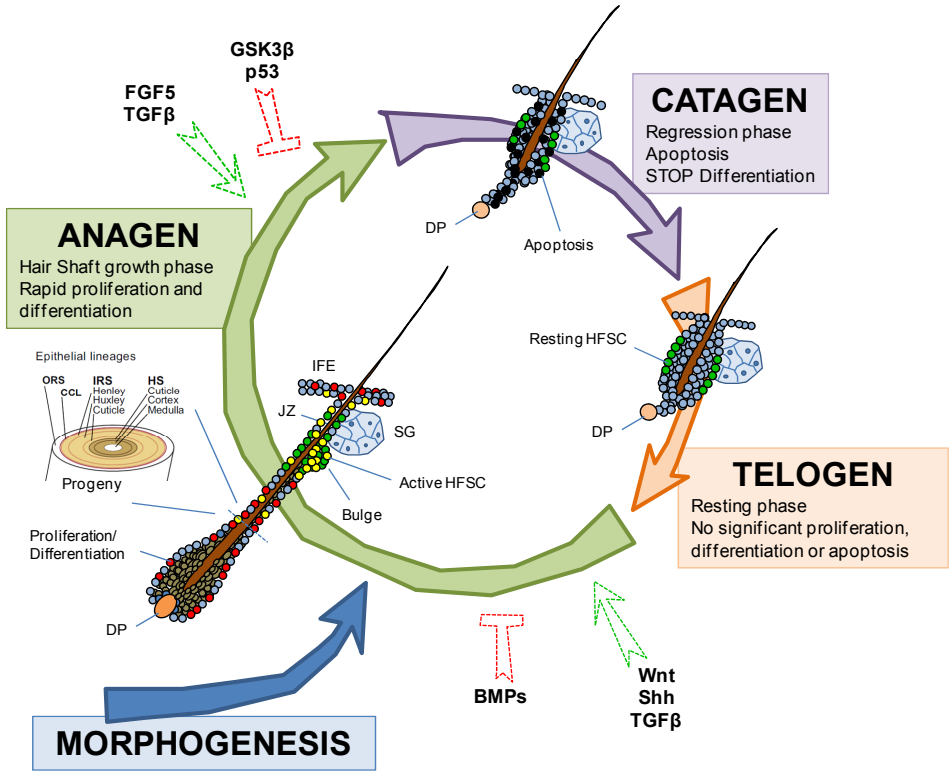

Figure 1. The Hair cycle. Adapted from Alonso and Fuchs, 2006.

The hair cycle is composed of three alternating states, namely the resting phase or telogen (from the Greek *telos:* end, completion, perfection), proliferative phase or anagen (from the Greek *ana*: up, upward, anew) and the destructive phase or catagen (from the Greek *kata*: downward, regression) (Figure 1). After each cycle, the old hair is lost and a new complete fur coat is generated from the hair follicle stem cells (HFSCs) (Alonso and Fuchs, 2006). Every cycle happens in waves that start at the snout and progresses along the mouse back towards the tail, and each of the stages of the hair cycle have been meticulously studied and can therefore be identified through detailed inmunohistochemistry (Muller-Rover et al., 2001). The alternation between these states is orchestrated by the dermal papilla, which provides the appropriate signals required for HFSC activation mainly through the TGFβ, Shh and Wnt/β-catenin pathways (Oshimori and Fuchs 2012; Kobielak et al., 2007; Watt et al. 2008). In mammals, HFSCs reside mainly at the Junctional Zone and Hair bulge regions (Figure 1). The molecular signature of resting and activated HFSC has been extensively studied by transcriptional profiling, showing that while dormant HFSCs are enriched in factors that promote quiescence and/or self-renewal including *Lhx2, Lgr5, Lgr6, Lrig1* and CD34 among others (Braun et al., 2003; Jaks et al., 2008; Jensen et al., 2009; Jensen et al., 2010; Nowak et al., 2008; Rhee et al., 2006; Snippert et al., 2010; Tumbar et al., 2004), activation of HFSC occurs stepwise with increased expression of genes involved in cell cycle progression, extracellular matrix/adhesion and transcription (Greco et al., 2009). Among them, *Sox4* (*Sry*-related High Mobility Group (HMG) box-containing transcription factor 4) has been found upregulated upon hair regeneration cues (Greco et al., 2009; Kobielak et al., 2007; Lien et al., 2014; Lowry et al., 2005).

III. THE HIGH-MOBILITY GROUP SUPERFAMILY

The *Sox4* gene belongs to the *SoxC* class within the Sox family of transcription factors. All Sox proteins share a High-mobility-group (HMG), a functional domain also found in other members of the HMG domain superfamily. To get a better insight into the major roles of Sox4 it becomes indispensable to have first an overview to the history of its discovery, its family diversification and finally a brief description of its functional domain organization. We finally brief the main functions assigned to Sox4 in development and cancer.

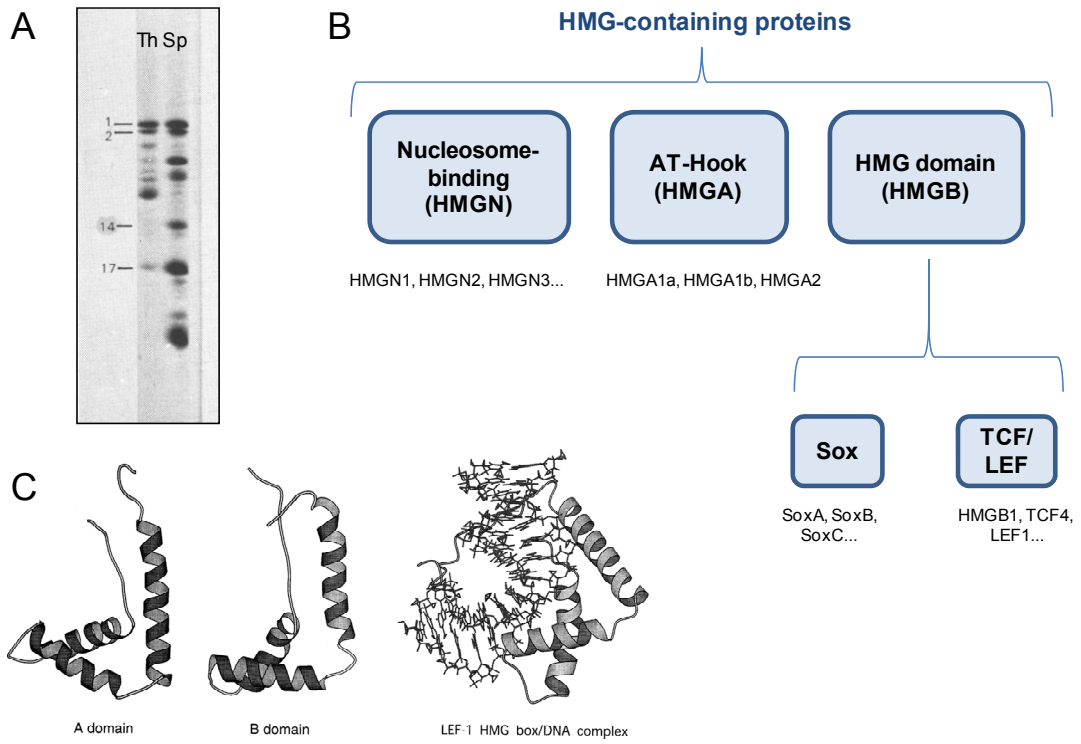

Figure 2. The HMG domain superfamily

(A) Polyacrilamide gel elctrophoresis showing HMG proteins isolated from mouse thymus (Th) or spleen (Sp). Adapted from Rabbani, 1978.
(B) Diversity of HMG-containing proteins.
(C) Schematic representation of two HMG-box domains from LEF-1, either alone or in complex with a DNA molecule.
Source: Biochemical Society Transactions.

III.1. The discovery of the High-mobility-group (HMG) domain proteins

In the early 1970's the search for non-histone DNA-bound proteins led to the discovery of an intriguing group of proteins which clustered together when analysed by SDS-PAGE according to their mobility in acrylamide gels (Goodwin et al., 1973). This group of proteins belonged to three unrelated families of DNA-bound proteins: the nucleosome-binding family (also known as HMG-14/17), the AT-hook family (or HMG-Y) and the HMG domain family (or HMG-1/2). Proteins containing an HMG domain (also known as HMG-box) comprise the T-cell factor (TCF)/lymphoid enhancer binding factor (LEF) family and the Sox family (Figure 2). HMG-box proteins have acquired certain sequence specificity in the binding to DNA that the rest of HMG-containing proteins lack. Moreover, and in contrast to other HMG domain members, HMG-box factors are expressed at very low levels in a limited subset of cell types, suggesting a tight regulation and functional diversification (Harley and Lefebvre, 2009).

Class	Members	Expression	Function
SoxA	Sry	Male germ cells	Male sex determination
SoxB1	Sox1	Neural Progenitor Cells (NPCs)	NPC specification and maintenance
	Sox2	Ectoderm, endoderm and mesoderm derivatives	Embryonic/adult stem cell specification and maintenance
	Sox3	Spermatogonia, NPCs	Spermatogonia differentiation, NPC specification and maintenance
SoxB2	Sox14	Neural tube, limbic ectodermal ridge	Neuronal differentiation, limb development
	Sox21	NPCs	Neuronal differentiation
SoxC	Sox4	NPCs, mesenchymal stem cells, haematopoietic system, pancreas, kidney, heart, uterus, skin...	B/T cell specification, regulation of survival/apoptosis, cardiac development, osteoblast/myeloid/β-cell differentiation
	Sox11	NPCs, heart, pancreas, haematopoietic system,	lymphoid differentiation, cardiac development, osteoblast differentiation, neurogenesis
	Sox12	Cardiac progenitors, NPCs, mesenchymal progenitors	Cardiac development, neural development
SoxD	Sox5	NPCs, bone	Neurogenesis, skeletogenesis
	Sox6	Mesoderm	Cardiac development, skeletogenesis, erythropoiesis
	Sox13	T lymphocytes	Lymphoid differentiation
SoxE	Sox8	Muscle satellite cells	Inhibition of myogenesis
	Sox9	Hair follicle stem cells, NPCs, distal tip cells (lung), pancreatic progenitors, liver duct cells, intestinal progenitors, mammary stem cells	Stem cell specification and maintenance
	Sox10	NPCs, melanocyte	Stem cell maintenance, melanocytic lineage determination
SoxF	Sox7	Cardiac progenitors, haemogenic endothelium, HSCs	Cardiogenesis, erythropoiesis
	Sox17	Extraembryonic endoderm (XEN), haematopoiteic stem cells	XEN gene expression regulation, fetal HSC maintenance
	Sox18	Cardiac progenitors, haemogenic endothelium, hair follicles	Cardiogenesis, angiogenesis, hair follicle development
SoxG	Sox15	ES cells, satellite cells	No obvious phenotype from LOF
SoxH	Sox30	Unknown	NA

Table 1. Sox family members. Adapted from Lefebvre et al 2007, and Sarkar et al 2013

III.2. The Sox family portrait

In the early 90's the search for an elusive male-determining differentiation factor finished when Dr. A. H. Sinclair and colleagues discovered *Sry* (acronym for Sex-

determining region of the Y chromosome), the founding member of the *Sox* family (Sinclair et al., 1990). After the discovery of *Sry*, an intense research activity focused on finding proteins with high degree of identity with this factor, and this lead to the identification of several *Sry*-related genes with important functions in sex determination, development and adult/embryonic stem cell function (Lefebvre et al., 2007; Sarkar and Hochedlinger, 2013). For classification purposes, only genes sharing at least 50% homology with the HMG domain from Sry were included in the Sox family.

In mammals there are twenty Sox factors classified into nine groups (SoxA, SoxB1, SoxB2, SoxC, SoxD, SoxE, SoxF, SoxG and SoxH; see Table 1), according to their protein sequence homology (Harley and Lefebvre, 2009). Each of them regulates diverse aspects related to adult stem cell function and cell fate decissions, nuclear reprogramming to induced pluripotency (generation of iPS cells), cell specification, differentiation and numerous crucial steps of embryonic development (Sarkar and Hochedlinger, 2013). Members from the same group share a high degree of identity along its whole aminoacidic sequence, whereas members from different groups share up to 50% homology in the HMG box domain, by definition, and none in the rest of the protein sequence (Bowles et al., 2000).

III.3. The structure of Sox proteins

All Sox factors share a HMG box, and most of them display several other domains which confer them additional properties such as oligomerization, subcellular localization, transactivation or sequence specificity modulation.

The HMG-box domain features three L-shaped α-helices that allow the HMG-box bind and bend the minor groove of the DNA; this sharp curvature induces a local shift in the chromatin conformation, thereby enabling the assembly of transcriptional activator complexes and subsequent transactivation of gene expression (Figure 2). Besides its role in transactivation (including DNA recognition, and bending), the HMG-box fulfils other basic functions required for the proper functioning of Sox proteins, including nuclear translocation and protein-protein interaction (Lefebvre et al., 2007). DNA motif recognition specificity was studied by in vitro DNA site selection assays, which unveiled a preference for the hexameric sequence 5'-WWCAAW-3' (where W stands for either A or T). In the case of Sox4, its crystal structure has been recently solved in complex with DNA, and this revealed slight structural differences with other Sox members, such as Sox2 or Sox17

(Jauch et al., 2012). In particular, Sox4 can accommodate a primary AACAAG and a secondary AATTGTT motif. Despite these sequence preferences, the HMG-box of Sox proteins displays a very low affinity and a variable sequence specificity, as seen for example in the degree of variability with respect to the consensus sequence that Sox4 shows in some of its bound enhancer sequences, such as the ones belonging to *Tubb3* (TATTGTC, CATTGTG), *CD2* (AACAATA) or *Tead2* (CTTTGTC, CTTTGTT) genes. Therefore, given the low specificity in target recognition and the widespread distribution of consensus sequences along the genome, it remains challenging in general to identify HMG-box recognised sequences and makes it impossible to predict Sox-target sequences based solely on the presence of matching motifs, in contrast to most of the rest of mammalian transcription factors (Lefebvre et al., 2007; Vervoort et al., 2013b).

In the case of Sox4, its protein structure also features a transactivation domain (TAD) whose main function is to activate Sox4 transcriptional activity functions through yet unknown mechanisms. The TAD domain is adjacent to a destruction domain (DD) necessary for regulating the protein stability and proteasomal-dependent degradation, a glicine-rich region (GRR) required for the regulation of Sox4-mediated apoptosis, a serine-rich region with not very well characterised functions (SRR) (Figure 3) (Vervoort et al., 2013b).

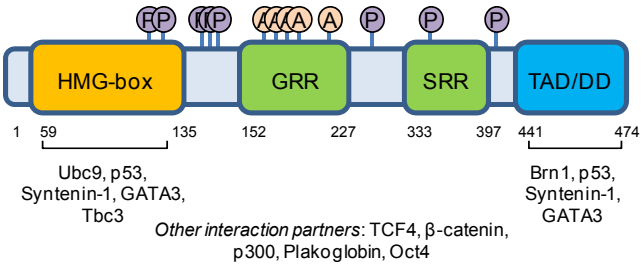

Figure 3. Functional domain organization, interacting proteins and post-translational modifications of Sox4. P, phosphorylation; A, acetylation; GRR, Glicine-rich; SRR, Serine-rich; TADD/DD, transactivation domain/degradation domain; numbers stand for aminoacid position. Adapted from Vervorrt et al, 2013.

IV. SOX4 IN EMBRYONIC DEVELOPMENT

Sox4 belongs to the SoxC class of transcription factors, encompassing Sox4, Sox11 and Sox12 (Harley and Lefebvre, 2010). As mentioned above, Sox4 specificity in

target recognition largely depends on cellular and molecular contexts when binding to different target promoters and enhancers (Jauch et al., 2012). *Sox4* is expressed mainly during embryonic development in neural crest and mesenchyme, and displays a high degree of overlapping in most tissues with its cousin members Sox11 and Sox12 (Dy et al., 2008). *Sox4* mRNA has also been detected in the developing pancreas, thymus, spleen and hair follicles (Dy et al., 2008; Hoser et al., 2008; Lioubinski et al., 2003). Most of the functions of Sox4 have been ascertained from the study of mouse models with deficient expression of either Sox4 alone or in combination with other SoxC class members. *Sox4*-null mice die at midgestation (E14.5) due to profound cardiac malformations, unveiling a role for Sox4 in cardiac outflow formation (Paul et al., 2013; Schilham et al., 1996). Other functions attributed to Sox4 are the regulation of survival and proliferation of neural and mesenchymal progenitors, where its expression peaks in coordination with Sox11 and Sox12 to ensure the survival and proliferation of neural progenitor cells (NPCs) (Bhattaram et al., 2010). Of note, part of the late embryonic lethality seen in $Sox4^{-/-}$ mice is at least partially due to the strong overlap among all SoxC class members, a fact that is evident upon simultaneous knock-out of both Sox4, Sox11 and Sox12, which results in accelerated embryonic lethality (E8) than with either of the single knock-out mice (Bhattaram et al., 2010). Sox4 also intervenes in pancreas development, as $Sox4^{-/-}$ mice display reduced pancreatic islet formation capacities, resulting in impaired insulin secretion and glucose tolerance (Wilson et al., 2005). Moreover, $Sox4^{+/-}$ mice show diminished bone formation and osteoblast developmental defects, an effect related to parathyroid hormone signalling defects observed in osteoblasts (Nissen-Meyer et al., 2007). B and T cell maturation defects have been observed in haematopoietic progenitors obtained from $Sox4^{-/-}$ embryos and Sox4 is induced during TGFβ-mediated differentiation of Th2 lymphocytes (Kuwahara et al., 2012; Laurenti et al., 2013; Schilham et al., 1997; Schilham et al., 1996). Moreover, Sox4 is involved in the regulation of myeloid differentiation, a feature often involved in the onset of myeloid leukemia (see below), by regulating IL5-triggered myelopoiesis, (Aue et al., 2011; Geijsen et al., 2001; Sandoval et al., 2012).

In adults, *Sox4* expression is found in a limited set of tissues such as female reproductive system, hematopoietic system, pancreatic islets, intestinal crypts and activated Hair Follicle Stem Cells (HFSCs) (Deneault et al., 2009; Hunt and Clarke, 1999; Lien et al., 2014; Schilham et al., 1997; Van der Flier et al., 2007; Wilson et al., 2005). These constrictions in expression of *Sox4* by adult cells suggest a tight regulation required to maintain an adequate tissue homeostasis. Indeed, aberrant *Sox4* expression in adult tissues has been linked to cancer onset and progression in mice and humans (Jafarnejad

et al., 2013a; Vervoort et al., 2013b). Some of the most relevant cellular functions of Sox4 have been unveiled by studying its involvement in cancer onset and progression, therefore they will be discussed in closer detail in the next section.

V. ROLES OF SOX4 IN CANCER ONSET AND PROGRESSION

It is widely accepted that given I) their prominent roles in regulating crucial cell-fate decisions along embryonic development and II) the tight spatiotemporal regulation of Sox protein expression levels, uncontrolled expression of these factors during the adulthood leads to loss of cell identity and cancer in general terms. Sox4 is no exception in this regard. There are however few cases in which Sox4 has been reported as a potential tumour suppressor, due to its positive correlation with induction of apoptosis immediately upon Sox4 overexpression; nevertheless, it is not completely clear whether these are in fact autonomous mechanisms triggered by the cell upon oncogenic traits in order to prevent transformation as it is the case of the oncogene c-Myc (Jafarnejad et al., 2013a; Vervoort et al., 2013b). The case of melanoma, in which Sox4 seems to behave specifically as a tumour suppressor, will be discussed in detail (see below).

V.1. Sox4 in blood malignancies

The first proof that *Sox4* could act as an oncogene *in vivo* was the finding of the *Sox4* locus as one of the most common integration sites in genome-wide tagging protocols based on retroviral-mediated activation of proto-oncogenes. In two inbred mouse models bearing random retroviral insertion-mediated gene activation that led to myeloid or B-/T-cell leukemia (BHX-2 mice and AKXD mice, respectively), a high-throughput screening based on inverse PCR sequencing revealed retroviral integration sites (RISs) relevant for cancer and unknown thus far. From a group of B-cell lymphomas from the AKXD strain, a panel of RISs was isolated; interestingly, the authors of the study also found these RIS in myeloid leukaemia samples obtained from the BHX-2 strain. Being these RISs found repeatedly enriched in tumours of different origin vs. normal tissue, they were referred to as CISs, common integration sites; these CIS therefore tagged new genes potentially involved in cancer (Suzuki et al., 2002) (Figure 4). Sox4 was

one of the factors whose promoter was most frequently targeted, and in subsequent studies reproducing retroviral tagging experiments with replication-incompetent, LT-expressing retroviruses, this finding was validated in a number of independent studies (Du et al., 2005; Li et al., 2007; Shin et al., 2004), indicating that Sox4 behaves as an oncogene in haematological tumours such as myeloid leukemia and lymphocytic leukemia.

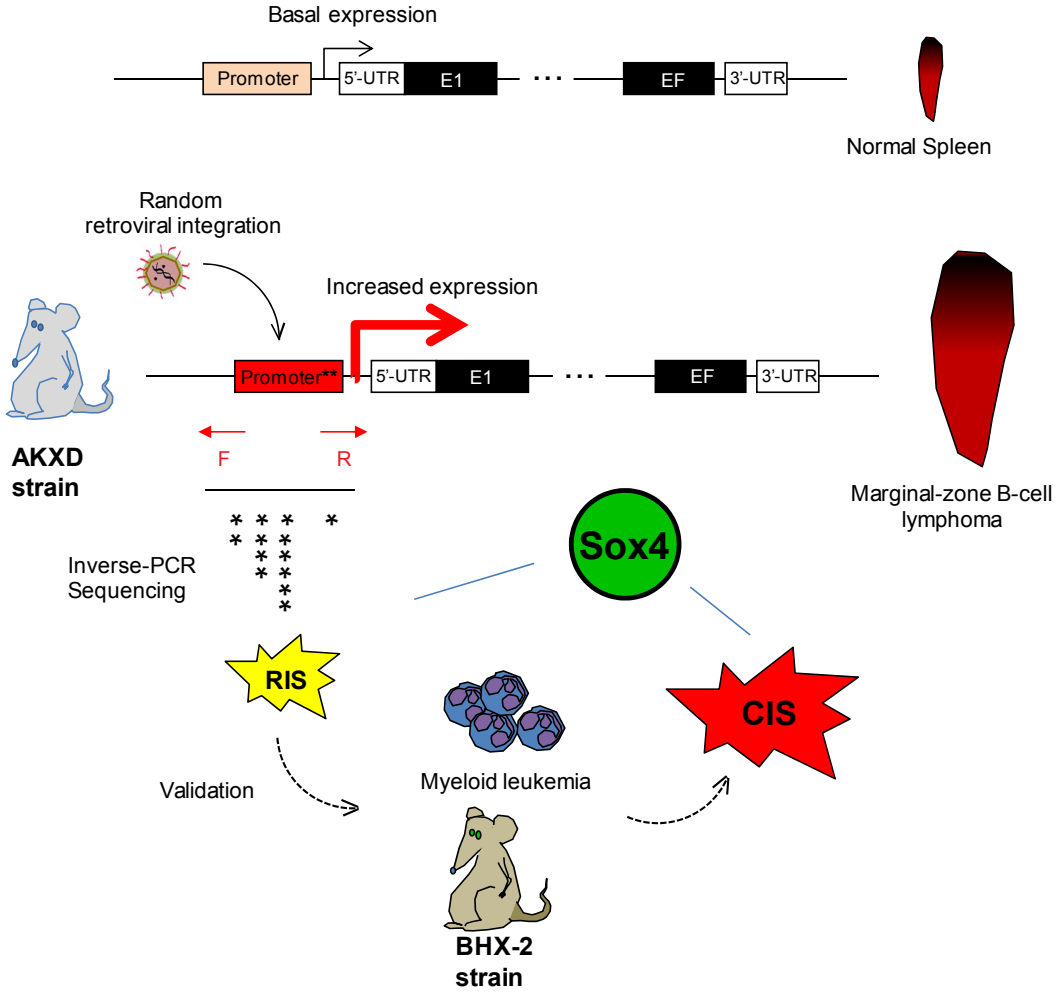

Figure 4. Strategy for High-throughput retroviral tagging and discovery of Sox4 as an oncogene in leukemia

Random integration of retroviruses induces stochastic activation of genes. B-cell tumours are screened for retroviral integration sites (RISs) which are validated in myeloid tumours to unveil common integration sites (CISs).Asterisks denote point mutations induced by retroviral random integration. Source: Suzuki, 2002.

Sox4 in myeloid leukemia: a block in myeloid differentiation

Expression of *Sox4* is a requisite for normal haematopoiesis during embryonic development, but its aberrant expression leads to cellular transformation in the hematopoietic compartment. Indeed, forced expression of Sox4 in bone marrow explants is sufficient to induce malignization, either alone or in cooperation with a variety of pro-oncogenic cues such as proviral insertion of *Evi1* (Boyd et al., 2006), loss of *Cdkn2b* (Bies et al., 2010), upregulation of *CREB* (Sandoval et al., 2012), deregulation of *Mef2C* (Du et al., 2005), *PU.1* haploinsufficiency (Aue et al., 2011), *PML-RARα* translocations (Omidvar et al., 2013), oncogenic *C/EBPβ* mutations (Zhang et al., 2013).

Of note, many of such conditions are incapable of inducing myeloid leukemogenesis per se, in contrast to Sox4; however they notably accelerate the tumourigenesis onset and progression when combined with Sox4 overexpression. The mechanisms whereby Sox4 exerts such a central role in initiating and promoting leukemogenesis range from increased cell survival and proliferation, transcriptional repression of PU.1, increased self-renewal and potentiation of CREB-mediated transcription; all these facts result in a block in myeloid cell differentiation, thus coalescing around the major cause for myeloid leukemogenesis (Figure 5) (Vervoort et al., 2013b). In addition, the intriguing incidence of Sox4 overexpression in myeloid leukaemia patients bearing common chromosomal translocations such as AML1-ETO suggests a selective pressure to activate Sox4, most likely through epigenetic mechanisms, in support of a role for Sox4 as an oncogene that can potentiate the effect of pre-existing genetic lesions and act synergistically with them to drive the disease (Kvinlaug et al., 2011; Vervoort et al., 2013b).

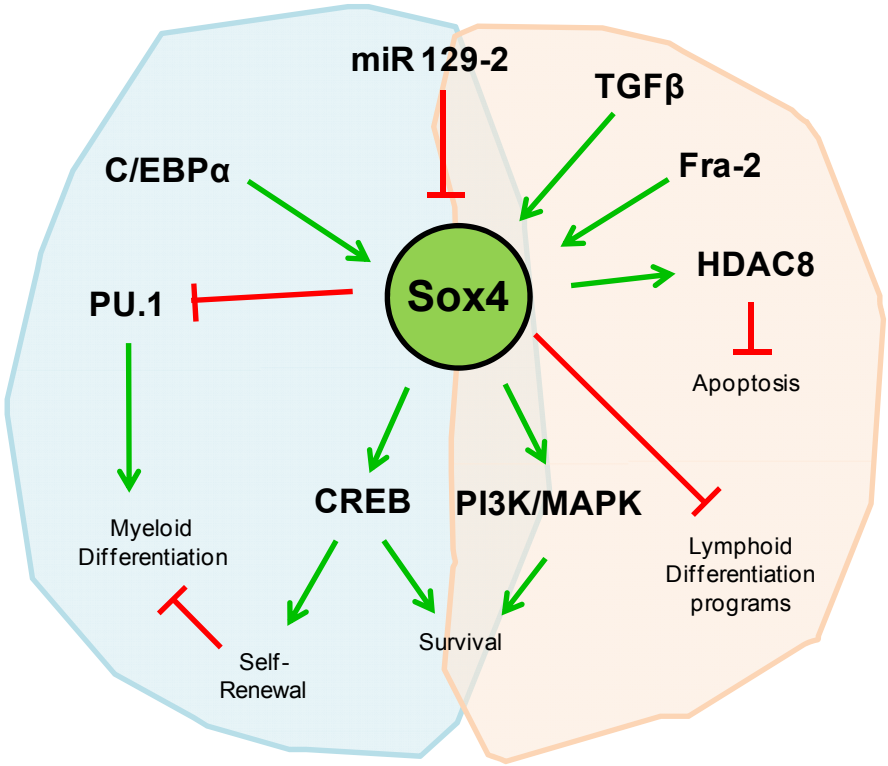

Figure 5. Schematic diagram summarizing the proposed mechanisms for Sox4-mediated oncogenesis in blood malignancies.

Highlighted in blue are the mechanisms linked to myeloid leukemia and in red, mechanisms in lymphoid leukemia.

Sox4 in lymphocytic leukemia: pro-survival & anti-apoptotic

As above-mentioned, and in an analogous manner to myeloid leukemia, Sox4 is required for normal B-/T-cell development during embryogenesis. A prominent role for Sox4 has also been documented in blood malignancies other than myeloid leukemia. Among them, Sox4 has been shown to act as a critical activator of the PI3K/MAPK-dependent signalling to promote survival of tumour cells, and Fra2-mediated expression of HDAC8 (which prevents apoptosis and increases cancer cell proliferation), thereby promoting T-/B-acute lymphocytic leukemia (Higuchi et al., 2013; Ramezani-Rad et al., 2013). The study of the Role of Sox4 during lymphomagenesis has revealed important hints into the molecular pathways that regulate Sox4 expression, such as TGFβ pathway and its regulation through micro-RNAs (miRNAs) (Wong et al., 2013; Zhao et al., 2011) (Figure 5).

V.2. Sox4 in solid malignancies

In parallel to the compelling evidence of the prominent role that Sox4 exerts in blood malignancies, there has been an intense research activity gathered around the study of a possible function for this protein in solid tumourigenesis. Since the discovery that expression of *Sox4* is sufficient to drive tumorigenesis, *Sox4* overexpression has been found in virtually all major cancer types including lung cancer, bladder cancer, prostate cancer, hepatocellular carcinoma (HCC), glioblastoma, endometrial cancer and adenoid cystic carcinoma (ACC). Mirroring the number of molecular phenotypes arising from Sox4 overexpression in leukemia, there has been a number of findings associated to Sox4 upregulation in solid tumours as well (Table 2). Notably, there is a high dependence on tumour and cell-type specific contexts in the nature of such outcomes, which range from regulation of cell survival to activation of specific genes involved in cellular transformation (Jafarnejad et al., 2013a; Vervoort et al., 2013b).

Sox4 regulates cell cycle and apoptosis

Recapitulating the role of Sox4 in neural and mesenchymal progenitors during normal embryonic development and in acute-lymphoblastic leukemia, increased expression of Sox4 in prostate cancer and adenoid cystic carcinoma correlates with enhanced apoptosis resistance and greater cell survival, features that are reversed in ex-vivo cell cultures treated with siRNA targeting Sox4, thus reinforcing the hypothesis that such mechanisms are intrinsically linked to Sox4 expression (Frierson et al., 2002; Liu et al, 2006; Pramoonjago et al., 2006; Veervort et al., 2013b). Indeed, Sox4 expression positively correlates with tumour grade in prostate carcinoma. In addition, forced expression of Sox4 in non-transformed cell lines *ex-vivo* is sufficient to confer colony-forming abilities and support anchorage-independent growth in soft agar *in vitro*, indicating that Sox4 behaves as a potent oncogene also in solid tumours. The suggested mechanisms governing Sox4-mediated inhibition of apoptosis and enhanced survival include the control of cell cycle and proapoptotic regulators such as BCL10, PUMA, CSF1 or CCNB1 as ascertained from microarray-based gene profiling of tumour cells depleted of Sox4 by siRNA (Frierson et al., 2002; Liu et al., 2006; Pramoonjago et al., 2006). Moreover, Sox4 has been shown to inversely correlate with p16, a main hub in cell cycle regulation and a molecular marker of ageing; in healthy lungs Sox4 decreases and p16 increases with ageing, and in small cell lung carcinoma, wherein Sox4 becomes

reactivated to overcome cell cycle breaks (such as p16) and promotes a transcriptional program that boosts tumorigenesis (Castillo et al., 2012).

The interaction among Sox4, p53 and DDR

An interesting observation in some of these studies was the marked upregulation of p53 protein, by means of western-blotting, when Sox4 was targeted with siRNA. Such p53 accumulation was likely due to protein stability rather than transcriptional induction upon Sox4 interference, given the lack of evidence for significant *p53* mRNA upregulation in any of the microarrays included in these studies (Liu et al., 2006; Pramoonjago et al., 2006). Some studies focused thereafter in the putative interaction between Sox4 and p53, leading to an intense debate with paradoxical observations that still remain to be studied in depth and put into appropriate context to provide meaningful insights into Sox4 function in this regard. In particular, several reports postulated an interaction of Sox4 with the DNA damage response (DDR) pathway to modulate p53 levels. There is a substantial upregulation of Sox4 in HCT116 cells after treatment with DNA damage-inducing agents such as doxorubicin, UV irradiation or ionizing radiation (IR) but not with other cellular stressors such as hypoxia, heat shock or H_2O_2 treatment. Interestingly, this was shown to be a p53 independent but ATM/ATR-dependent phenomenon (Pan et al., 2009). Sox4 interacts with p53 whereby it prevents Mdm2-mediated ubiquitination of p53 and its subsequent proteasomal degradation, resulting in increased p53 protein stability. However, in this context and in stark contrast with previous results, Sox4 downregulation resulted in a reduced stability of p53 protein, paradoxically pointing to a putative role for Sox4 as a tumour suppressor (Pan et al., 2009). A negative correlation between tumour prognosis and Sox4 expression (and thus in support of a tumour-suppressive effect of Sox4) was found in subsequent studies in a limited subset of human tumours including bladder cancer, HCC, gall bladder carcinoma and melanoma (Vervoort et al., 2013b). Nonetheless, the only type of tumour showing robust association of Sox4 with tumour-suppressive functions along subsequent studies is melanoma (see below).

An interesting observation is the fact that Sox4 confers resistance to DNA damage in medulloblastoma cell lines, thus alleviating the burden of the DDR upon irradiation. In this setting, Sox4 knock-down (KD) or inhibition through expression of SPARC (a bona-fide endogenous peptide inhibitor of Sox4) renders cancer cells susceptible to IR. Even the mere reduction of Sox4 levels is sufficient to induce a mild DDR, as means of γH2AX accumulation (a marker for DNA lesions such as double-strand breaks or replication-associated ssDNA) (Jackson and Bartek, 2009), and when challenged with sub-lethal IR

apoptotic rates were increased up to six fold. Importantly, these results were reproducible *in vivo* with transplanted tumours (Chetty et al., 2012). Overall, these studies suggest an intimate link of Sox4 with the DDR and p53-dependent apoptotic response in tumours, therefore open new therapeutic windows for certain tumours that could suffer from endogenous replication stress alleviated by Sox4, a feature that could be counterbalanced by means of Sox4 inhibition or downregulation to render cancer cells more susceptible to current treatments such as IR.

Type of tumour	Sox4 status and role
Splenic marginal zone lymphoma	Common retroviral integration site (increased expression), positive correlation with disease progression
Myeloid leukemia	Upregulated in myeloid leukemia, prevents myeloid differentiation, association with disease progression, associated to AML1-ETO translocation
Hpatocellular carcinoma	Overexpressed, good correlation with metastasis
Medulloblastoma	Increased expression compared to normal cerebellum, alleviation of DNA damage response and associated to radiation-resistance
Prostate cancer	Increased expression compared to healthy tissue, associated with aggressiveness, EMT and metastasis
Lung cancer	Gene amplification, prevents p16 activation upon oncogenic cues
Colorectal cancer	Increased expression, associated to metastatic potential
Adenoid cystic carcinoma	Increased expression relaqtive to normal tissue, prevents apoptosis and increases cellular viability
Bladder Cancer	Increased expression and gene amplification
Glioblastoma multiforme	Elevated expression compared to normal brain, favours cancer stem cell phenotype
Gallbladder carcinoma	Elevated in primary tumours, reduced expression in advanced forms of the disease
Gastric cancer	Elevated expression relative to normal tissue
Breast cancer	Elevated in comparison to normal tissue, good correlation with tumour grade, promotes metastasis and EMT phenotype
Pancreatic cancer	Upregulated when compared to normal tissue
Pheochromocytoma	Upregulated when compared to normal tissue

Table 2. Status and role of Sox4 in different tissues. Adapted from Vervoort, 2013

Sox4 and metastasis: the control of EMT

So far, it can be ascertained that Sox4 constitutes a key oncogenic event in the vast majority of tumours, that occurs in the initial stages of tumorigenesis. Nonetheless, a number of reports have demonstrated a prominent role for Sox4 also in regulating late cellular transformation steps. In particular, Sox4 expression levels strongly correlate with disease progression, metastasis and probability of relapse. In the breast cancer line MCF-7, high Sox4 expression was associated to cancer stem cell-like properties in tridimensional collagen scaffolds concomitant with downregulation of epithelial markers such as ECDH, upregulation of cancer stem cell markers such as OCT4 and SOX2, and

higher tumorogeneicity in xenotransplants (Chen et al., 2012). Interestingly, independent studies demonstrated that higher Sox4 expression correlated with the triple-negative breast cancer subtype in humans ($ER^-/PR^-/HER2^-$, associated with more aggressive and difficult to treat forms of breast cancer). In this study, ectopic Sox4 expression in the immortalized cell line MCF-10A was sufficient to induce a mesenchymal phenotype with increased migratory/invasive abilities. Sox4 itself is induced by TGFβ and required for the initiation of the EMT/metastatic programs (Vervoort et al., 2013a), and, in xenografts, Sox4 cooperates with oncogenic Ras mutations to promote tumorigenesis *in vivo* (Zhang et al., 2012). The induction of Sox4 by TGFβ is crucial for the induction of Ezh2 and subsequential epigenetic reprogramming of cancer cells to acquire a phenotype tailored for distant tissue colonization (Tiwari et al., 2013). The relevance of Sox4 in metastasis is evident in studies showing how breast cancer cell lines selected for their metastatic capacities in vivo display a selective pressure for losing endogenous miRNAs that regulate Sox4 expression among other targets (Tavazoie et al., 2008).

The case of melanoma

As aforementioned, the only human type of tumour displaying Sox4 downregulation concomitant with disease progression is melanoma. This is the only setting in which in most cases Sox4 seems to behave as a tumour suppressor rather than as an oncogene (Jafarnejad et al., 2013a; Vervoort et al., 2013b). Tumour microarray analysis in various types of human melanocytic lesions shows that Sox4 is significantly reduced in advanced lesions when compared to primary melanoma or dysplastic nevi. Multivariate Cox analysis in human samples reveals controversial results, pointing out that Sox4 is an independent prognostic marker of disease progression (Jafarnejad et al., 2010), either alone or in combination with a set of markers relevant for melanoma progression (Li et al., 2011) though sometimes despite finding similar trends, no significance was obtained for this marker alone (Zhang and Li, 2012); in human melanoma cell lines Sox4 plays a pivotal role in binding and inducing Dicer, thereby promoting a shift in the set of miRNAs expressed in dysplastic nevi vs invasive melanoma that controls cell proliferation and invasion (Jafarnejad et al., 2013b) or either inhibiting NF-κB subunit p50 transcription through yet unknown mechanisms (Jafarnejad et al., 2010). Despite the mounting results showing correlation of Sox4 downregulation with melanoma progression, there is still a hot debate in this regard and no consensus on the prognostic significance of Sox4 as a biomarker in melanoma, given the lack of meaningful

insights into the molecular mechanism and consistency among studies (Jafarnejad et al., 2013a).

Altogether, the extensive research gathered around Sox proteins, and in particular the interest focused in Sox4, underlines the importance of these proteins in controlling numerous aspects of stem cell biology during important processes often associated to human disease. However, there is still a notable lack of appropriate research models that allow the complete understanding of the molecular properties of this intriguing factor *in vivo* and therefore facilitate the development and testing of new treatments useful to confront and new ideas to comprehend these age-associated pathologies.

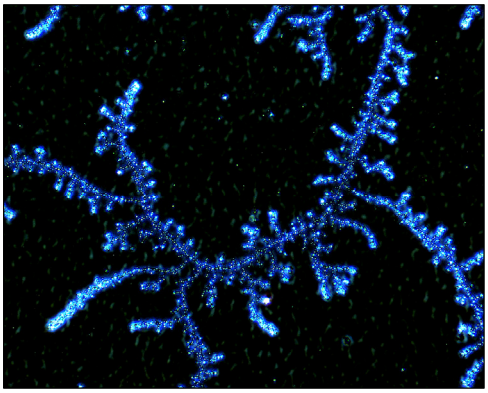

Objetivos

"(…) El hombre es el animal que pregunta. El día en que verdaderamente sepamos preguntar, habrá diálogo. Por ahora las preguntas nos alejan vertiginosamente de las respuestas.(…)"

Julio Cortázar. Rayuela, Cap 147

El objetivo general de la presente Tesis Doctoral fue la generación de nuevas herramientas que permitieran el estudio *in vivo* de las funciones del factor de transcripción Sox4 en células madre y tejidos adultos. Los objetivos específicos fueron los siguientes:

1. Generar un modelo de ratón con un alelo insertado en el locus genómico de Sox4 (ratones *Sox4*$^{lox/lox}$), cuya secuencia está flanqueada por sitios LoxP que permiten su escisión *in vivo*, para estudiar las células que expresan Sox4 y poder estudiar el efecto de la ausencia de expresión en dichas células.

2. Determinar el impacto de la expresión reducida de Sox4 durante los procesos de adquisición de pluripotencia y durante la diferenciación de células madre.

3. Estudiar la importancia de la expresión reducida de Sox4 en la homeostasis global y durante el envejecimiento.

4. Comprobar la contribución específica de Sox4 a la arquitectura de la piel y a su mantenimiento en ratones con deleción condicional de Sox4 en piel.

5. Caracterizar los efectos de la eliminación de Sox4 durante la regeneración del pelo y el cierre de heridas.

6. Descubrir los cambios en los perfiles transcripcionales de la piel durante la regeneración del pelo en ausencia de Sox4.

7. Estudiar la dependencia de Sox4 en la transformación de keratinocitos mediante tratamiento con carcinógenos.

Objectives

"(…)
—Contáselo con todos los detalles —dijo Oliveira.
—Oh, una idea general es bastante —dijo Gregorovius.
—No hay ideas generales —dijo Oliveira..(…)"

Julio Cortázar. Rayuela, Cap 15

The main goal of the present PhD thesis was to generate new tools to *in vivo* study the major functions of the Sox4 transcription factor in stem cells and adult tissues. In that context, we aimed to address the following specific objectives:

1. To generate a reporter and excisable Sox4 KI mouse model for studying and tracking *Sox4*-expressing cells *in vivo* (*Sox4*$^{lox/lox}$ mice)

2. To determine the impact of Sox4 downregulation in acquisition of pluripotency and stem cell differentiation.

3. To study the importance of Sox4 downregulation in global homeostasis and ageing.

4. To address the specific contribution of Sox4 to skin architecture and maintenance when conditionally deleted in skin

5. To characterize the effects of Sox4 abrogation during hair regeneration and wound healing in *Sox4*^{cKO} mice

6. To unveil the changes in the transcriptional profile of skin undergoing hair regeneration in the absence of Sox4.

7. To understand whether Sox4 is required for cellular transformation during chemically-induced skin carcinogenesis.

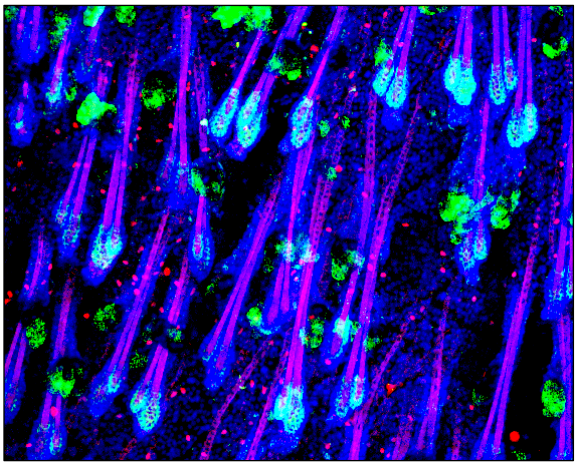

Experimental Procedures

"(...) La rayuela se juega con una piedrita que hay que empujar con la punta del zapato. Ingredientes: una acera, una piedrita, un zapato, y un bello dibujo con tiza, preferentemente de colores. En lo alto está el Cielo, abajo está la Tierra, es muy difícil llegar con la piedrita al Cielo, casi siempre se calcula mal y la piedra sale del dibujo. Poco a poco, sin embargo, se va adquiriendo la habilidad necesaria para salvar las diferentes casillas (rayuela caracol, rayuela rectangular, rayuela de fantasía, poco usada) y un día se aprende a salir de la Tierra y remontar la piedrita hasta el Cielo, hasta entrar en el Cielo, (...), lo malo es que justamente a esa altura, cuando casi nadie ha aprendido a remontar la piedrita hasta el Cielo, se acaba de golpe la infancia y se cae en las novelas, en la angustia al divino cohete, en la especulación de otro Cielo al que también hay que aprender a llegar. (...)"

Julio Cortázar. Rayuela, Cap. 36

I. ANIMAL EXPERIMENTATION

In order to generate the *Sox4*$^{+/KI}$ mice, recombinant ES cells from a 129Sv background were injected into C57BL6 and the chimeras obtained were back-crossed with C57BL6 for a total of four generations and thereafter inter-crossed to expand the colony; therefore, all the mice used in this study were of mixed background C57BL6/129Sv (75%:25%).

All animals were maintained at the Spanish National Cancer Research Centre (CNIO) under specific pathogen-free conditions, in agreement with the recommendations of the Federation of European Laboratory Animal Science Association (FELASA). Mice were fed a standard chow diet (Harland Tekland 2018, 18% of fat-based calorie content) and observed on a weekly basis by trained personnel. All the treatment protocols were evaluated and approved by the Ethical Committee of the Carlos III Health Institute, and the animals were supervised on a weekly basis by trained personnel. All the mice presenting any sign of morbidity (http://dels.nas.edu/global/ilar/Guide) were sacrificed in agreement with the guidelines for Humane End Point for Animals Used in Biomedical Research.

I.1 Generation of a Sox4 Knock-In (*Sox4*^{KI}) mouse model

The targeting construct and the mice carrying the *Sox4*^{KI} allele were generated by genOway (France; see Figure 6A for additional information) by means of standard procedures. In brief, the *Sox4* locus was cloned from mouse ES genomic DNA encompassing the only *Sox4* exon together with the 5'-UTR and 3'-UTRs and surrounding genomic regions. This allowed the generation of the homologous arms of the targeting construct and the targeting cassette containing the endogenous *Sox4* unique exon sequence fused to an IRES-GFP-Luciferase cassette; a neomycin selection region flanked by FRT sites (specifically recognized by the *Flpe* recombinase) was also included for positive selection of recombinant ES cells, and the *Sox4*-IRES-GFP-NEO^{FRT} construct was flanked by *LoxP* sites (specific for *Cre* recombinase), allowing the excision of the whole cassette in a controlled time and tissue-specific manner to be performed.

Mice bearing the NEO^{FRT} sequence (*Sox4*$^{+/loxFRT}$ mice) were viable and fertile, and thus we proceeded further with the crosses with *Flpe*-expressing mice in order to

eliminate the neomycin cassette; we inter-crossed *Sox4*$^{+/lox}$, once the NEO^{FRT} region was deleted, in order to generate homozygous *Sox4*$^{lox/lox}$ mice.

I.2 Genotyping strategy of Sox4 alleles by PCR

30-50ng of total DNA were isolated from mouse tissues following standard procedures were subjected to PCR reaction using Platinum Taq (*Invitrogen* Cat. 10966) by following the manufacturer's instructions (1.5mM $MgCl_2$, 0.2mM/dNTP, 0.5µM/primer, 0.05U Platinum Taq/reaction, 1µl DMSO and milliQ distilled water to reach a final volume of 20 µl per reaction). The PCR program was as follows: 1min 94ºC + 35x(30sec 94ºC + 30sec 60ºC + 3min 72ºC) + 7min 72ºC + keep at 8ºC. The genotyping PCR primers used were (See Figure 6B):

Cre F: TTAATCCATATTGGCAGAACGAAAACG
Cre R: CAGGCTAAGTGCCTTCTCTACA
Genot-*Sox4* F1: CCAGCATCTCTAACCTGGTCTTC
Genot-*Sox4* F2: TTGGAGCACGGAAAGACGAT
Genot-*Sox4* R: CAGGCCAGCTCTATGCACTTT
Genot-*Neo* F: CACTTGTGTAGCGCCAAGTGC

I.3 Body Imaging with DEXA

Lean mass, fat content and bone mineral density were analyzed by Dual-Energy X-Ray Absorptiometry (DEXA) by using a Lunar PIXImus Densitometer (GE Medical Systems) on anesthetized mice with 2% isofluorane. Acquisition time was 5 min. Bone mineral density was calculated from a manually-restricted Region of Interest (ROI) including the whole left femur of the studied animals.

I.4 Plucking and wound healing in mouse skin

For hair plucking protocol, mice were anesthetized in 2.5% Isofluorane / 1% Oxygen (kept during the whole procedure with gas masks adapted for mice) and were intraperitoneally administered Buprex solution as analgesic. 1cm^2 of dorsal hair was then removed by manual plucking with tweezers and tape-stripping until only dorsal skin and no hair was visible in the plucked area. Hair regeneration was assessed by taking pictures from a fixed distance and hair-depleted regions were scored as a percentage of the initial plucked area with the help of ImageJ software.

For wound healing assays, mice were anesthetized as above; 4-6cm^2 of dorsal hair was removed with depilatory cream (Veet) and rinsed with distilled water. 24h later parallel-double wounds were performed under anaesthesia conditions in the upper region of the dorsal skin of the mice with 4mm biopsy punch device. Subsequent wounds were performed following a head-to-tail progression along the back skin of the mice every 3 days and pictures were taken every second day and wound size assessed with a calliper.

I.5 DMBA/TPA-mediated skin carcinogenesis

For skin carcinogenesis assays 12-week-old mice (6-10 mice per genotype) were hair clipped and a single dose (100µl) of a 100nM DMBA solution in acetone was administered topically in the lower part of the back skin in order to promote cancer-initiating mutations. Thereafter, animals were treated every 3 days with 12µg TPA dissolved in 200µl acetone in order to induce a proliferative state in the skin that favours expansion of cells bearing oncogenic mutations. Mice were clipped once weekly right before TPA administration, and tumour burden was evaluated on a weekly basis, recording number and size of lesions (papilloma) as well as appearance of other skin conditions, such as melanocytic growths. Mice were sacrificed whenever signs of morbidity (caquexy, presence of tumours >15mm, etc) were detected and samples collected for assessment by an anatomic-pathologist.

I.6 Histology and IHC. Antibodies

Mice were culled and tissues were collected and fixed immediately in 10% Formalin in PBS during 16h and embed into paraffin blocks. 5µm sections were mounted in poly-L-Lysine glass slides, deparaffinised and rehydrated. After that, either we performed Haematoxylin-Eosin staining or antigen retrieval in 10mM citrate buffer cooked under high pressure for 2min. Spurious peroxidise activity was removed by H_2O_2 and methanol treatment. After blocking, primary antibodies were incubated 16h at 4ºC, washed, further incubated with biotin-conjugated secondary antibodies and processed for standard indirect immune peroxidase detection (Vector Laboratories) using DAB as substrate (Dako). Finally, slides were slightly counter-stained with Haematoxylin-Eosin and analysed by light microscopy. For confocal microscopy, Alexa-fluor conjugated antibodies (Molecular Probes, Invitrogen) were used at 1:500 dilution, washed, counterstained with DAPI and mounted in Vectashield or ProLong Gold antifading reagents. Confocal microscopy acquisition and settings were as described for QFISH (see below).

Antibodies used and dilutions were as follows: mouse monoclonal anti-GFP (Roche, 1:500), rabbit polyclonal anti-CK14 (Covance, 1:1000), rabbit polyclonal anti-CK10 (Covance, 1:300), rabbit polyclonal anti-Loricrin (Covance, 1:500), rabbit polyclonal anti-p53 (CM5 Novocastra, 1:200), mouse monoclonal anti-Ki67 (Master Diagnostica, 1:200), mouse monoclonal anti-Histone 3 phospho-Ser10 (Millipore, 1:200), mouse monoclonal anti-Histone 2 phospho-Ser139 (γH2AX, Millipore, 1:100), mouse monoclonal anti-p63 (Neo Markers, 1:100), rabbit polyclonal anti-TRF1 (homemade, 1:50) (Munoz et al., 2009).

II. CELL CULTURE

Unless otherwise specifically indicated, cells were cultured in DMEM (*Dulbecco's Modified Eagle's Medium,* Gibco) supplemented with 10% FBS (*Foetal Bovine Serum*, Sigma) and 1% antibiotic/antimycotic (Gibco). Culture plates were held in appropriate incubators at 37ºC, 16% O_2 and 5% CO_2.

II.1 Extraction and culture of MEFs and preparation of feeders

Pregnant female mice were euthanized in a CO_2 chamber 13.5dpc, and uterus was removed and kept on 1% Antibiotic/Antimycotic in PBS pre-warmed at 37ºC. Inside a tissue culture hood, each embryo was isolated and the extraembryonic layers were removed with a pair of forceps and tweezers. The embryo head was cut below the eye and preserved in an eppendorf tube placed on dry ice for genotyping. The rest of the embryo was transferred to a p35 dish containing 1ml of 2X Trypsin solution in PBS, chopped during 30sec with a razorblade and incubated at 37ºC. After 20min, the suspension containing the chopped embryo was aspirated up and down 15 times through a glass Pasteur pipette and incubated at 37ºC for 20 additional minutes. Then, the cell suspension was diluted in 15ml of 10% complete medium and transferred to a T75 bottle. When confluent, cells were resuspended in 1ml trypsin and split in a 1:3 ratio every 2-3 days. For long-term preservation, $5x10^6$ cells were frozen in 10% DMSO diluted in FBS.

For generating Feeders, MEF were expanded up to passage 4-5 and when at 75-90% confluence, incubated with 10µg/ml MitomycinC for 3h at 37ºC, washed twice in PBS and frozen at $5x10^6$ cells per vial. For co-culture with iPS or keratinocytes, $2,5x10^6$ cells per p100, $4x10^5$ cells per p35 or $1x10^4$ cells per m96 well were seeded at least 2 days in advance in 10% complete medium on top of a porcine gelatine coating (10ml per p100 dish of 1% porcine gelatin in milliQ distilled water were incubated during 10 min at RT, aspirated, air-dried and the Feeders were seeded in complete DMEM medium). Medium was changed as appropriate medium when co-cultured with iPS or keratinocytes.

II.2 Transfection and Viral Transduction

In order to produce retroviral particles containing the vectors encoding the genes of interest for subsequent transduction into mammalian cells, $4x10^6$ 293T packaging cells were seeded for 30 minutes in p100 dishes and transfected with 4µg of ecotropic packaging vector for mouse cells (pCL-Eco) and 4µg of the vector containing the gene of interest, using Fugene6 (Roche). One day after transfecting the 293T cells, the target MEF were seeded at a density of $2x10^5$ cells per p35 dish or $8x10^5$ cells per p100 plates, and fresh complete DMEM medium was added to the 293T cells. The following day, the

supernatant containing the viral particles was collected and replaced with fresh medium; the supernatant was filtered through a 0.45µm mesh and diluted 1/3 with complete medium. After addition of 8µg/ml of Polybrene, 2ml (p35) or 10ml (p100) of supernatant was added to the target MEF. This procedure was repeated every 8 hours for a total of 4 rounds of infection.

II.3 Generation and maintenance of ES and iPS cells

MEF from the desired genotypes were retrovirally-transduced with pMX-Sox2, pMX-Oct3/4 and pMX-Klf4 at a ratio 1:1:1 as described. 24h after the last transduction round, complete medium was replaced by iPS medium (high-glucose DMEM supplemented with 1000U/ml LIF, 1% non-essential aminoacids, 15% KSR, 1% Glutamax and 0.1% β-mercapto-ethanol, Life Technologies) and subsequently fresh iPS medium was added daily. The cultures were kept until colonies became apparent (typically 10-15 days) and then the dishes were either stained for Alkaline Phosphatase to asses reprogramming efficiency or picked for clonal expansion. Picked colonies were trypsinized and plated onto 96 well plates (1 clone per well), and upon establishment of iPS clones they were split every other day in a 1:5 ratio, and fresh KSR medium was added daily. ES were maintained in ES medium (high-glucose DMEM supplemented with 1000U/ml LIF, 1% non-essential aminoacids, 15% dialysed FBS, 1% Glutamax and 0.1% β-mercapto-ethanol, Life Technologies) For gelatine culture we used 2i medium (Complete iPS medium supplemented with 1µM MEK inhibitor and 3µM GSK3β inhibitor, Stemgent). The ES/iPS clones were preserved in a 2X freezing medium (20% DMSO, 40% KSR, 40% ES medium) after trypsinization, neutralization with ES medium and cell counting. Vials were preserved in liquid Nitrogen for long-term storage.

II.4 Teratoma Formation and RA-mediated differentiation of stem cells

For studying general iPS differentiation by teratoma-forming capabilities, $2x10^6$ iPS cells were injected subcutaneously into nude athymic mice (FOXN1 mutant strain). Typically, the tumours started to form around 1 week post-inoculation, and size was

assessed on a weekly basis with a calliper on grafted tumours. When the grafts reached 1.5cm length mice were sacrified and tumours collected for subsequent IHC analysis.

RA treatment was used to assess neuro-ectodermal differentiation. $1x10^5$ cells grown in gelatine and 2i medium were seeded into p35 gelatin-coated dishes. After 24h, 2i medium was switched to ES medium without LIF (Day 0), and the day after (Day 1) medium was changed to RA-containing ES medium (without LIF) at a concentration of $1x10^{-6}$ M. Thereafter, fresh RA medium was added daily and cells collected as indicated for biochemical characterization.

II.5 Extraction and culture of Peripheral Blood Mononuclear Cells (PBMCs)

100µl of peripheral blood was obtained from the submandibular vein of restrained animals onto EDTA-containing tubes. Immediately after collection, the blood was resuspended in 10ml QIAGEN RBC buffer for erythrocyte lysis. After 15 min at 4ºC the cell suspension was vortexed and cells were pelleted at 450xg for 3min in conical polypropylene tubes; then, cells were either frozen in 10% DMSO-containing FBS or plated in 96-well Greiner plates in RPMI medium (RPMI supplemented with 10%FBS, 1% non-essential aminoacids, 1% sodium pyruvate, 1% HEPES, 0.1% β-mercapto-ethanol, 1% antimycotic/antibiotic) for HT-QFISH analysis (see below).

II.6 Extraction, culture and differentiation of Keratinocytes from adult mice

For adult keratinocyte extraction, mice were clipped and then culled by cervical dislocation. After hair-spraying with 70% EtOH, skin was collected and kept in cold-ice PBS containing 1% antimycotic/ antibiotic. In a tissue culture hood, skins were stretched dermal side up in a p150 lid and subdermal adipose tissue was scraped with a scalpel. Once the fat was removed, skins were subjected to 15sec sequential washes in 10% Povidone Iodine in PBS, 70% EtOH and finally PBS with antibiotics, skins were floated dermis side down in p100 dishes containing 10ml of EDTA-free trypsin and kept overnight at 4ºC. The day after, skins were stretched in sterile p100 lids, epidermal side up, and epidermis was scraped and minced with scalpels. After resuspending in EDTA-free trypsin with a 5ml pipet, cell suspension was filtered through a 70µm nylon mesh and neutralized

with 2ml of trypsin neutralizer. After addition of 10 ml of Keratinocyte Medium 02 (CELLnTEC), cells were spun down at 500xg during 8min. Cell pellet was collected by aspirating 2ml from the bottom of the tube and resuspended in 10ml of Keratinocyte Medium 02 for cell counting.

For keratinocyte differentiation, $5x10^3$ keratinocytes were plated in triplicates in 2ml of Keratinocyte Medium 02 onto p35 dishes containing pre-seeded feeder layers and cultured at 37ºC in a 2% oxygen incubator. Fresh medium was added every 3-5 days, and when 10-50 cell colonies were visible, plates were fixed in 4% Formaldehyde for 30min at RT and stained with 1% Rhodamine B or 0.02% Giemsa in PBS during 30min at RT in an orbital shaker. Plates were rinsed with distilled water, dried o/n and colonies were scored on digital images with ImageJ after scanning the plates.

II.7 Ras/E1a-mediated transformation of MEFs

For assaying cell transformation, MEF were infected with a pBabe-*Ras*^{G12V}-IRES-*E1a* construct following the standard retroviral infection protocol. After selection in 2µg/ml puromycin during 48h, cells were split in the presence of 1µg/ml puromycin and when cells reached confluence, $2x10^3$ or $2x10^4$ cells were seeded in p100 dishes and cultured for 10-15 days adding fresh medium once per week. When macroscopically visible colonies appeared (typically after 10-15 days) cells were fixed by adding 2ml of 37% Formaldehyde solution to the dishes containing 10ml of complete DMEM medium, and kept on an orbital shaker for at least 30min at RT. After removing the fixative, colonies were stained with a 0.02% Giemsa solution in PBS for 30 min at RT. The plates were washed in distilled water until the water run clear and dried overnight placed on top of a filter paper. Plates were scanned and colonies quantified with regard to their relative abundance and size distribution on digital images with ImageJ software.

III. IN VITRO ASSAYS AND CELL IMAGING

III.8. Quantitative-Real Time PCR (qPCR) and Primers

Total RNA isolation and DNA digestion was done with RNA later, RNEasy and DNAse I kits (QIAGEN) following manufacturer's instructions. For cDNA synthesis, 0.5ng of total RNA were retro-transcribed with Advanced iScript and assayed using Power SYBR Green PCR Master Mix (Applied Biosystems). GAPDH and Actin were used as references and results were represented as relative to GAPDH levels. qPCR primers are listed below.

Gene	Forward	Reverse
GAPDH	5' GCA CAG TCA AGG CCG AGA AT 3'	5' GCC TTC TCC ATG GTG GTG AA 3'
Actin	5' GGC ACC ACA CCT TCT ACA ATG 3'	5' GTG GTG GTG AAG CTG TAG CC 3'
Sox4	5' GCC TCC ATC TTC GTA CAA CC 3'	5' AGT GAA GCG CGT CTA CCT GT 3'
Sox11	5' ATC AAG CGG CCC ATG AAC 3'	5' TGC CCA GCC TCT TGG AGA T 3'
Sox12	5' GAG CGG AGA AAA ATC ATG GA 3'	5' CGA GGC CGG TAC TTG TAG TC 3'
p16	5' TAC CCC GAT TCA GGT GAT 3'	5' TTG AGC AGA AGA GCT GCT ACG T 3'
p19	5' GCC GAC CGG AAT CCT 3'	5' TTG AGC AGA AGA GCT GCT ACG T 3'
GATA3	5' TAC CAC CTA TCC GCC CTA TG 3'	5' AGG ATG TCC CTG CTC TCC TT 3'
Tcf3	5' GGA GCC GGG GCA ACC AGT G3'	5' CAT CCT GGG GCC TTC TCA CTT C 3'
Tcf4	5' CAC CCG GCC ATC GTC ACA C 3'	5' GCC ACC TGC GCC CGA GAA T 3'
Sox9	5' GAC TCC CCA CAT TCC TCC TC 3'	5' CCC TCT CGC TTC AGA TCA AC 3'
c-Myc	5' AAG CCA CCG CCT ACA TCC TG 3'	5' AAA GCC CCA GCC AAG GTT G 3'
mTERT	5' GGA TTG CCA CTG GCT CCG 3'	5' TGCCTGACCTCCTCTTGTGAC 3'
Nanog	5' CAGGTGTTTGAGGGTAGCTC 3'	5' CGGTTCATCATGGTACAGTC 3'
Oct4	5' TCTTTCCACCAGGCCCCCGGCTC 3'	5' TGCGGGCGGACATGGGGAGATCC 3'
Rex1	5' ACG AGT GGC AGT TTC TTC TTG GGA 3'	5' TAT GAC TCA CTT CCA CGG GGC ACT 3'

III.1 Transcriptional profiling by microarray hybridization

Total RNA was extracted from pluck skin of the indicated genotypes after immediate preservation in RNA later with the QIAGEN RNEasy Mini Kit, following manufacturer's instructions. RNA Integrity Number (RIN) was in the range 7 to 9.8 when

assayed by Lab-chip technology on an Agilent 2100 Bioanalyzer. 100ng of total RNA were labelled with commercial "One-Color Microarray-Based Gene Expression Analysis (Low Input Quick Amp Labeling)" version 6.5 kit by following manufacturer instructions, and purified with silica-based spin columns (BioRad).

For Microarray hybridization, a Mouse Gene Expression 60K (Agilent) was used in a SureHyb hybridization chamber (Agilent) during 17h at 65ºC. The microarrays were scanned in a G2505C DNA microarray scanner (Agilent). Images were analysed by Agilent Feature Extraction Software (ver. 10.7) without background substraction. The resulting TIF images were transformed into low resolution false-colour JPEG images. The raw data files were used to generate .txt files for further quantification and annotation with the FeatureExtraction software. Genes were ranked according to their FDR, P values and fold enrichment, and only those showing a FDR<0.15 were considered Differentially Expressed Genes (DEGs).

III.2 Gene set enrichment analysis

Gene Set Enrichment Analysis was performed using annotations from the KEGG, Reactome and NCI databases, or by testing in-house made gene lists extracted from the TransFac repository or signatures found in published research articles (indicated when appropriate). Genes were ranked using the t statistic. After Kolmorogov-Smirnoff correction for multiple testing, only those pathways bearing a FDR<0.15 were considered significant. The Gene Ontology GO terms (biological proccesses, cellular components and molecular functions), Genecard and Malacard annotations were included and annotated according to published literature. Enrichment plots were also obtained with GSEA, and ranked according to their enrichment score (ES).

III.3 Telomere Quantitative Fluorescence In-Situ Hybridization (QFISH)

In order to perform QFISH in metaphase nuclei of mouse tissues, paraffin-embed organs were processed as described (Methods, section I.6). Then, 5µm sections were attached to Poly-L-Lysine-covered glass slides. After deparaffinization and antigen retrieval, tissues were fixed in 4% Formaldehyde, washed 3x5min in PBS and incubated

in pepsin solution (0.1% Porcine Pepsin (Sigma) containing 0.01M HCl (Merck)) 10min at 37ºC. After another round of washes and fixation as above-mentioned, slides were dehydrated in a 70% - 90% - 100% Ethanol series (5min each). After 30 min of air drying 50µl of Telomere probe mix (10mM TrisCl pH7, 25mM $MgCl_2$, 9mM Citric Acid, 82mM Na_2HPO_4 (adjusted to pH7), 70% Deionised Formamide (Sigma), 0.25% Blocking Reagent (Roche) and 0.5µg/ml Telomeric PNA probe (Panagene)) were added to each slide. After putting a cover slide on top of it, DNA was denatured by heating during 3min at 85ºC, and further incubated for 2h at RT in a wet chamber in the dark. Finally, slides were washed 2x15min in Washing Solution I (10mM TrisCl pH7, 0.1% BSA in 70% Formamide), then 3x5min in Washing Solution II (TBS 0.08% Tween-20) and then incubated with 4µg/ml DAPI (Sigma) and mounted in Vectashield mounting medium (VectorTM). For analysis, confocal image stacks were acquired every 0.5µm for a total of 10µm by using a Leica SP5-MP confocal microscope and maximum projections were generated and analysed using LAS-AF software and TFL-Telo (A kind gift of Peter Landsorp)

III.4 High-Throughput QFISH (HT-QFISH)

PBMCs were obtained as described above. 96-well Greiner plates were pre-coated with 1:10 Poly-L-Lysine in milliQ distilled water for 30min at 37ºC, at a density of $1{,}2x10^5$ cells per well. The cells were incubated during 2h at 37ºC and then fixed 3x5min in 200µl with a multichannel pipette in Methanol:Acetic Acid 3:1. Fixed cells were preserved at -20ºC until use. Then, plates were dehydrated o/n in an air-jacketed 37ºC incubator, then rehydrated 5min in PBS and fixed again in 4%PFA in PBS. After 3x5min PBS washes, the plates were included in a Styrofoam frame floater and digested in Pepsin 15min in a 37ºC water bath. After digestion, samples were fixed and washed as above mentioned. Then, the plates were dehydrated in EtOH (5minx70% EtOH, 5minx90% EtOH and 5minx100% EtOH) and dried for 30min in a 37ºC incubator. After dehydration, 50µl of Cy3-Telomeric probe mix were added to each well and denatured 5min at 85ºC in a hot plate. The Greiner plates were hybridized then for 2h at RT in the dark and washed 2x15min in washing solution I, then 3x5min in washing solution II, then 1x5min in PBS with DAPI and then mounted using Mowiol solution (Calbiochem).

Images were acquired using an automated Opera Confocal High-throughput microscope (PerkinElmer), and analysed with Acapella software to obtain mean telomere

intensity. Briefly, DAPI signal was used to create nuclei masks in which telomeric spots were identified and classified depending on their intensity. 60 images per well were captured from duplicate wells, and at least $5x10^3$ telomeres were analysed per sample. For normalization and transformation of a.u.f. into Kilobases, LY-R and LY-S reference lymphoma cell lines with known telomere length (70.9Kb and 11.2Kb, respectively) were included in each plate.

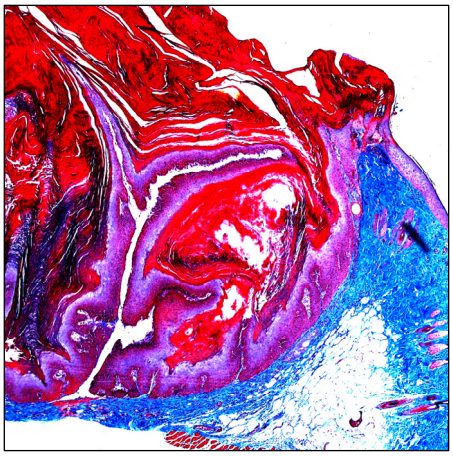

Results

"(…) Pero detrás de toda acción había una protesta, porque todo hacer significaba salir de para llegar a, o mover algo para que estuviera aquí y no allí, o entrar en esa casa en vez de no entrar o entrar en la de al lado, es decir que en todo acto había la admisión de una carencia, de algo no hecho todavía y que era posible hacer, la protesta tácita frente a la continua evidencia de la falta, de la merma, de la parvedad del presente. Creer que la acción podía colmar, o que la suma de las acciones podía realmente equivaler a una vida digna de este nombre, era una ilusión de moralista. (…)"

Julio Cortázar. Rayuela, Cap 3

I. Generation of mice with an excisable Knock-In allele for Sox4

The fact that complete *Sox4* abrogation (*Sox4*$^{-/-}$ mice) results in embryonic lethality (Schilham et al., 1996) has hampered understanding the role of *Sox4* in the adult organism. To circumvent this, we decided to generate a *Sox4* Knock-In (KI) mouse model (*Sox4*$^{lox/lox}$ mice), which would allow us to conditionally delete *Sox4* as well as to *in vivo* track *Sox4*-expressing cells in adult tissues. To do so, we generated a KI construct targeted to the *Sox4* locus including the whole *Sox4* 5'- and 3'-UTR and the full length *Sox4* unique exon adjacent to an Internal Ribosome Entry Site-Green Fluorescent Protein-Luciferase (IRES-GFP-Luc) reporter coding sequence. We flanked the KI allele with LoxP sites in order to allow the excision of the whole cassette with tissue-specific *Cre* recombinase. We included FRT sequences in order to remove the neomycin cassette by crossing the founders with *Flp*-expressing mice. When intact, the KI cassette is regulated by the endogenous *Sox4* promoter and its transcription is expected to give rise to the full-length Sox4 protein simultaneously to a GFP-Luc protein (Figure 6A and B).

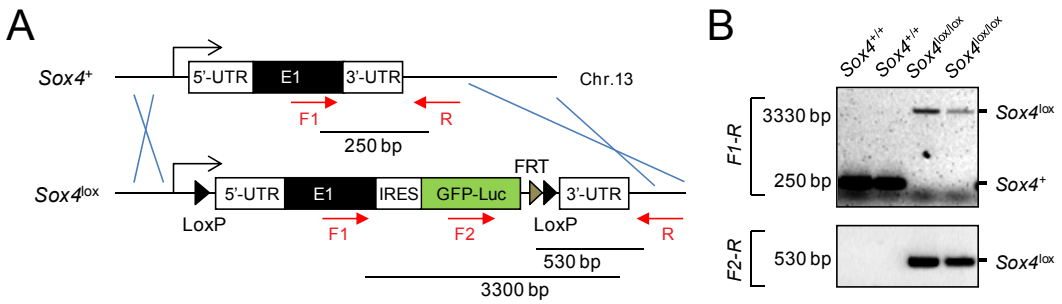

Figure 6. Generation of *Sox4*-IRES-Luc-GFP Knock-In mouse model

(A) Schematic of the different *Sox4* alleles. The Forward-WT (F1), Forward-KI (F2) and Reverse (R) genotyping primers (red arrows) and PCR sizes in base pairs (bp) are depicted. See Supplementary Table 4 for detailed primer sequences.
(B) Genotyping PCR of the different *Sox4* alleles.

II. Sox4 is dispensable for pluripotent cell generation and differentiation

In 2006, Takahashi and Yamanaka demonstrated that it is possible to reprogram the cell's differentiated status to ES-cell like status, giving rise to the so-called induced-Pluripotent Stem cells (iPS cells) by inducing the expression of only four factors, namely Klf4, Oct4, c-Myc and Sox2 a method that soon was proven equally efficient disposing of

c-Myc, allowing the generation of iPS with only three factors (3F) (Marion et al., 2009; Takahashi et al., 2006). Ever since, nuclear reprogramming has become a powerful tool to address the influence of a given condition in the acquisition and maintenance of pluripotency.

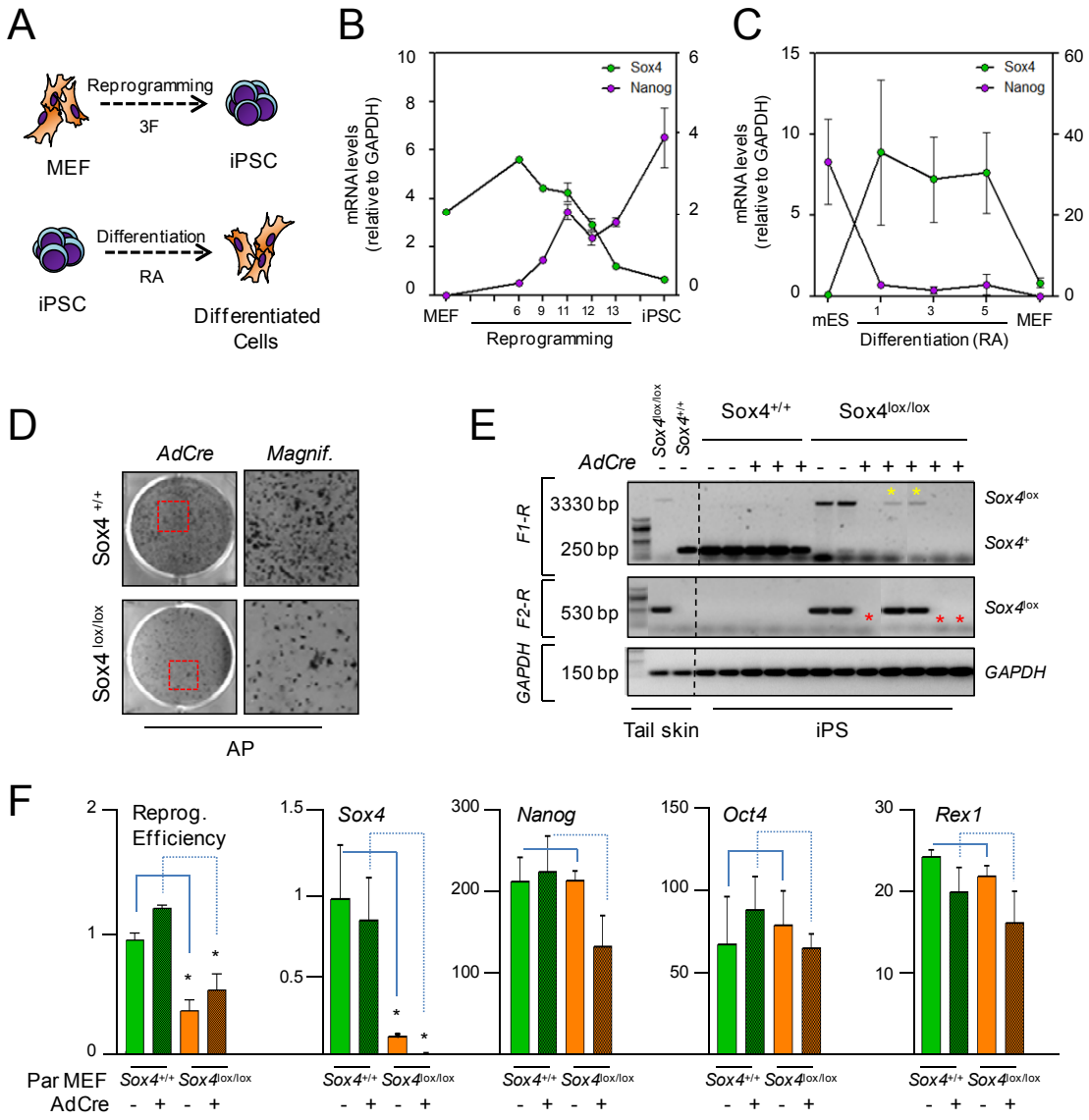

Figure 7. Sox4 is dispensable for the generation of iPS but required for efficient reprogramming

(A) Schematic of reprogramming into iPSC or differentiation of mESC protocols.
(B and C) Dynamics (Days) of Sox4 (green, right Y axis) and Nanog (purple, left Y axis) along reprogramming (left panel) or differentiation (right panel). Data is relative to GAPDHx10^{-3}, n=3 experiments.
(D) Alkaline phosphatase staining of reprogramming plates.
(E) Genotyping PCR to confirm AdCre-mediated excision of Sox4 locus in iPS clones. Yellow asterisks, not excised KI cassette escaper clones; red, excised cassette.
(F) Relative reprogramming efficiency, relative Sox4 mRNA levels and total mRNA expression levels (relative to GAPDHx10^{-3}) of Nanog, Oct4 and Rex1, respectively, in iPSC clones of the indicated genotypes.

Depicted is mean and SEM Only significant P values are shown (two-tailed Student's t test , P<0.01)

Given that most of the principal roles of Sox4 are related to stem cell maintenance and differentiation, we wanted to address a possible role for Sox4 in the biology of pluripotent stem cells. To that end, we performed reprogramming assays in WT MEFs using the Yamanaka cocktail of three factors (3F) and differentiation assays in mESC with retinoic acid (RA; Figure 7A) and measured *Sox4* mRNA. We observed a decrease of *Sox4* expression during reprogramming and a sharp increase during differentiation protocols, as opposed to Nanog (Figure 7B and C), suggesting that Sox4 is induced during the differentiation of mESC and repressed during acquisition of pluripotency. To study the function of Sox4 during reprogramming, we infected *Sox4*$^{lox/lox}$ and *Sox4*$^{+/+}$ MEF with adenoviral vectors expressing Cre recombinase (AdCre) prior to reprogramming. We observed a ≈50% decrease in reprogramming efficiency; however, the iPS clones with proven excised Sox4 cassette expressed largely normal expression levels of pluripotency-associated factors such as Nanog, Oct4 and Rex1(Figure 7D-F). To understand whether these Sox4-deficient iPS clones could have defects during differentiation into specific lineages, we performed teratoma-mediated differentiation by subcutaneous injection into nude athymic mice. We detected slower growth rates in Sox4-depleted iPS undergoing differentiation, without reaching significance (Figure 8A). Nevertheless, we obtained tissues from the three embryonic layers, as assessed by IHC (Figure 8B). These results are indicative that Sox4 is largely dispensable for reprogramming and differentiation.

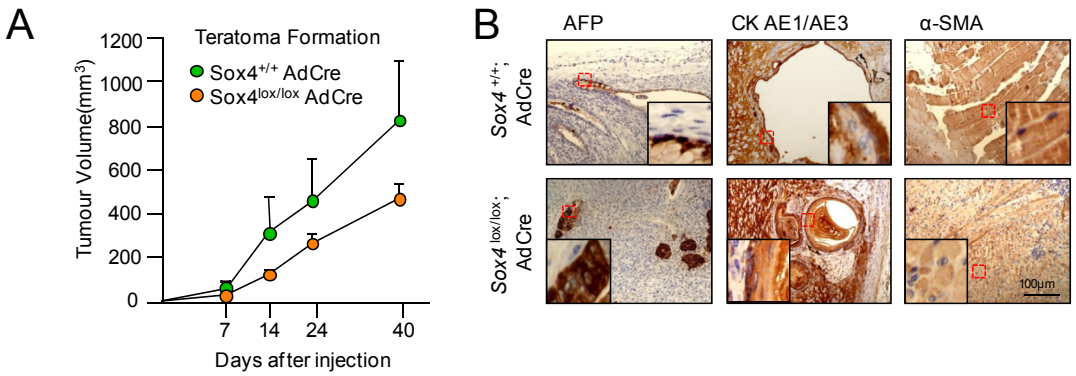

Figure 8. Sox4-deficient iPS are pluripotent

(A) Dynamics of teratoma growth (n=5 clones per genotype).
(B) IHC of the three embryonic layers, obtained from teratomas of the indicated genotypes. AFP, alpha-feto protein (endoderm); CKAE1/AE3, cytokeratins AE1 and AE3 (ectoderm); α-SMA, a-smooth muscle actin (mesoderm). Insets depict magnification.

No significant differences were obtained (Student's t test)

III. *Sox4*$^{lox/lox}$ mice show signs of premature ageing and are cancer-resistant

Sox4$^{lox/lox}$ mice are viable and fertile, but they are born under sub-mendelian ratios (Figure 9A). Moreover, *Sox4*$^{lox/lox}$ mice show a reduced body size and weight compared with their *Sox4*$^{+/+}$ littermates (Figure 9B and C). These differences were increased when mice grew older (Figure 9C). Dual-Energy X-Ray Absorptiometry (DEXA) indicated that reduced weight could be attributed to a decrease in both lean and fat mass (Figure 9D).

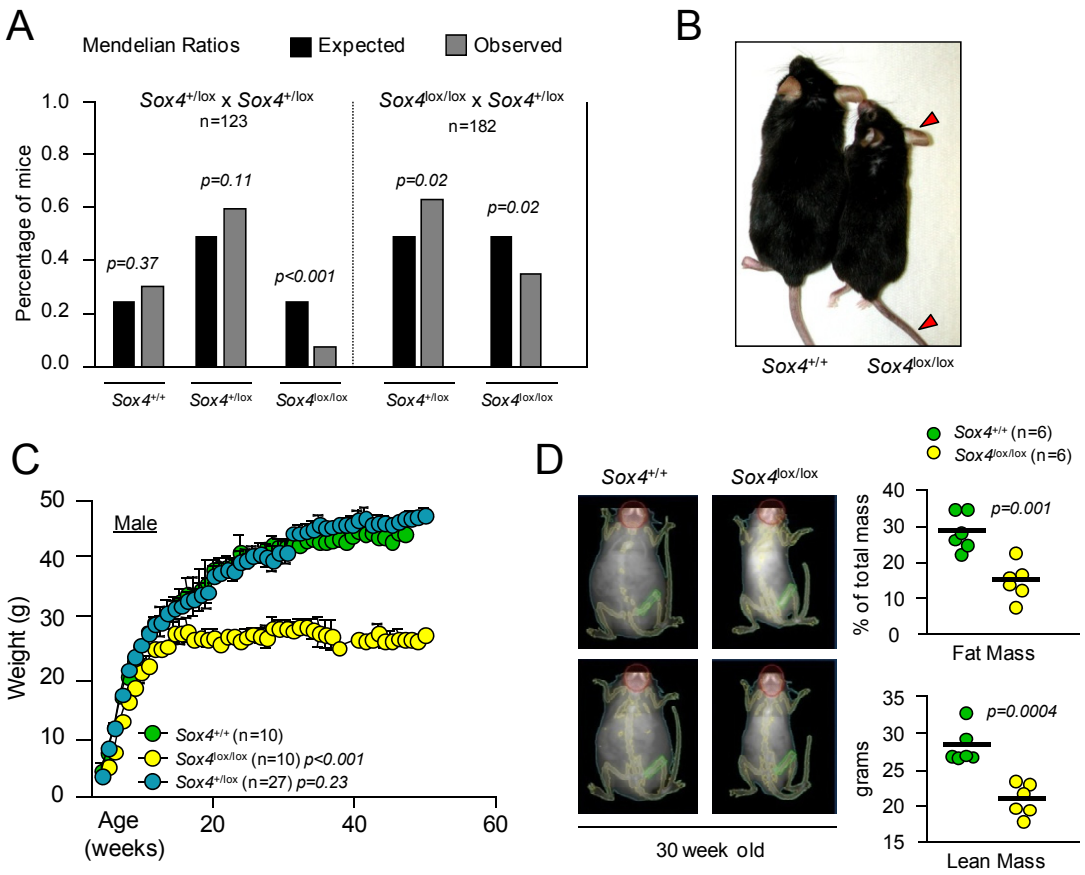

Figure 9. Characterization of *Sox4*-IRES-Luc-GFP Knock-In mouse model

(A) Mendelian ratios, in two different cross settings, of *Sox4*$^{lox/lox}$, *Sox4*$^{+/lox}$ and *Sox4*$^{+/+}$ pups. P values were calculated using Fisher's exact test.
(B) Macroscopic aspect of *Sox4*$^{+/+}$ and *Sox4*$^{lox/lox}$ mice. Genotypes are included. Note the marked size reduction and increased pigmentation in exposed skin (red arrowheads).
(C) Plot of the average weight in grams (g) of a group of male mice of the indicated genotypes.
(D) (Left) DEXA images of adult male *Sox4*$^{+/+}$ and *Sox4*$^{lox/lox}$ mice. (Right) Fat mass (%) and grams of lean mass *Sox4*$^{+/+}$ and *Sox4*$^{lox/lox}$ mice.

In addition, *Sox4*$^{lox/lox}$ mice have a significantly reduced longevity when compared to *Sox4*$^{+/+}$ or *Sox4*$^{+/lox}$ mice (Figure 10A-D). This decreased survival paralleled an early onset of various age-associated pathologies. In particular, *Sox4*$^{lox/lox}$ mice present brittle

bones due to decreased bone mineral density (Figure 10E), and a higher incidence of intestinal failure, chronic hepatic failure, skin hyperpigmentation and dilated cardiomyopathy (Figure 10F and Table3). We also found an increased incidence of congenital diaphragmatic hernia and pyometra (Figure 10F and Table3). Furthermore, the humane end point was significantly anticipated in *Sox4*$^{lox/lox}$ compared to control mice (Figure 10A-D and Table3).

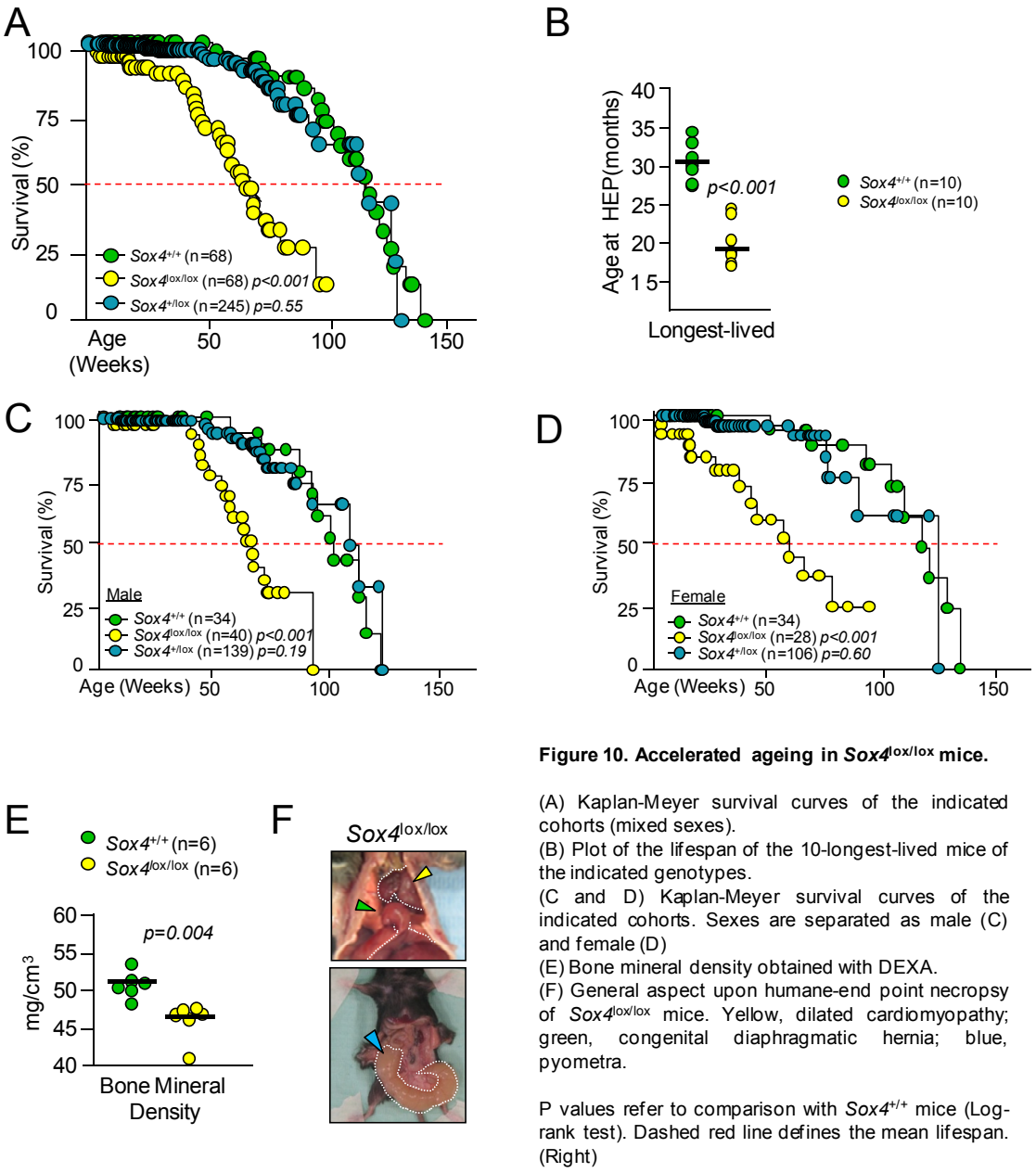

Figure 10. Accelerated ageing in *Sox4*$^{lox/lox}$ mice.

(A) Kaplan-Meyer survival curves of the indicated cohorts (mixed sexes).
(B) Plot of the lifespan of the 10-longest-lived mice of the indicated genotypes.
(C and D) Kaplan-Meyer survival curves of the indicated cohorts. Sexes are separated as male (C) and female (D)
(E) Bone mineral density obtained with DEXA.
(F) General aspect upon humane-end point necropsy of *Sox4*$^{lox/lox}$ mice. Yellow, dilated cardiomyopathy; green, congenital diaphragmatic hernia; blue, pyometra.

P values refer to comparison with *Sox4*$^{+/+}$ mice (Log-rank test). Dashed red line defines the mean lifespan. (Right)

These signs of accelerated ageing and decreased longevity are coincidental with a notable reduction in the mean telomere length of peripheral blood cells, a bona fide indicator of biological aging (Canela et al., 2007; de Jesus and Blasco, 2012; Lopez-Otin et al., 2013; Vera et al., 2012) (Figure 11A). Interestingly, these mice also display

resistance to spontaneous cancer incidence when compared with Sox4$^{+/+}$ mice (Figure 11B).

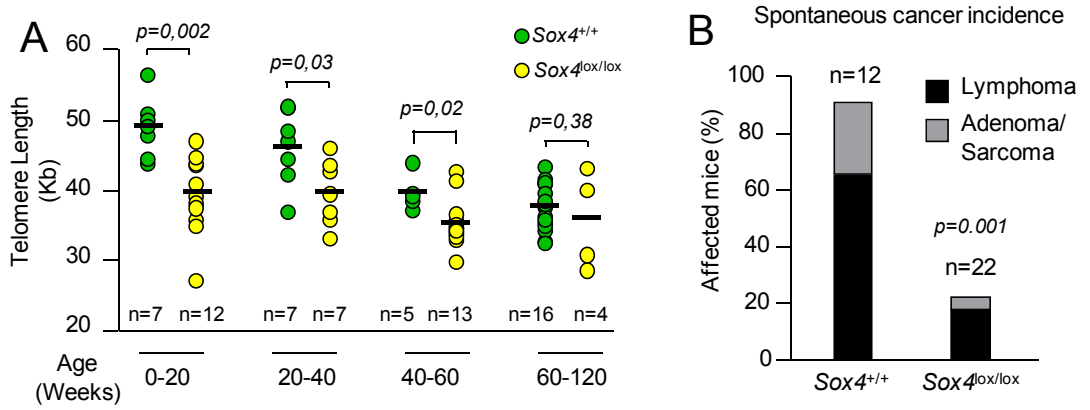

Figure 11. Reduced telomere length and cancer incidence in Sox4 hypomorphic mice

(A) HTQFISH in mice of the indicated age and genotype. Indicated is the number of mice per group of age and genotype. P=Student's t test, n=number of mice per age group and genotype.
(B) Spontaneous cancer incidence in the indicated genotypes, classified according to the type of cancer; bars represent the percentage of affected mice. Fisher's exact test was used for comparison.

Together, these findings indicate that *Sox4*$^{lox/lox}$ mice show signs of premature loss of tissue homeostasis and a subsequent accelerated onset of age-associated pathologies. In addition, *Sox4*$^{lox/lox}$ mice also show a significant cancer resistance.

IV. *Sox4*$^{lox/lox}$ mice are hypomorphic

The above results point out to hypomorphic behaviour of the *Sox4* KI allele. In order to demonstrate this, we performed indirect inmunohistochemistry (IHC) for GFP in tail skin sections given that *Sox4* mRNA has been detected in skin (Dy et al., 2008; Greco et al., 2009; Lowry et al., 2005). We failed to detect any positive GFP signal in any skin region, indicating either very low expression levels of KI cassette or absence of *Sox4* expression in adult mouse skin (Figure 12A). To confirm this, we performed *Sox4* quantitative-Real Time RT-PCR (qPCR) in a panel of tissues from both *Sox4*$^{lox/lox}$ and *Sox4*$^{+/+}$ mice. We found an approximated 10-fold reduction in the *Sox4* mRNA levels in all the analyzed tissues, therefore demonstrating reduced *Sox4* expression in *Sox4*$^{lox/lox}$ mice. Notably, we did not detect a significant deregulation of the other *SoxC* class members (*Sox11* and *Sox12*) in the analyzed tissues (Figure 12B). Altogether, these findings demonstrate that our *Sox4*$^{lox/lox}$ mouse model behaves as a functional hypomorph for

Sox4 mRNA expression levels, and thus constitutes the first viable adult mouse model with whole-body reduced *Sox4* expression.

Parameter	Category	$Sox4^{+/+}$ n=12	$Sox4^{lox/lox}$ n=22	Fisher's exact test
Sex	Male (%)	6 (50.0%)	14 (63.6%)	p=0.34
Age at H. E. P. (Weeks)	Mean (Range)	106.9 (72-139)	53.8 (17-81)	p<0.001
Diaphragmatic hernia	Affected (%)	0 (0%)	16 (72.7%)	p<0.001
Dilated Cardiomyopathy and heart hypertrophy	Affected (%)	1 (8.3%)	8 (36.4%)	p=0.083
Pyometra	Affected (% of Female)	0 (0%)	4 (50.0%)	p=0.03
Intestinal failure (oedema, amiloidosis, hyperthropic caecum, etc)	Affected (%)	1 (8.33%)	7 (31.8%)	p=0.13
Renal failure (chronic glomerulonephritis, amiloidosis, calculus, etc	Affected (%)	4 (33.3%)	5 (22.7%)	p=0.58
Hepatic failure (necrosis, chronic hepatitis, amiloidosis, congestion, steatosis, etc)	Affected (%)	2 (16.7%)	12 (54.5%)	p=0.035
Skin atrophy	Affected (%)	5 (41.7%)	8 (36.4%)	p=0.52
Skin hyperpigmentation	Affected (%)	0 (0%)	5 (22.7%)	p=0.09

Table 3. Main histopathological findings in Sox4 hypomorphic ($Sox4^{lox/lox}$) mice compared to their wild type counterparts ($Sox4^{+/+}$) at humane end point.

V. Generation of a *Sox4* conditional KO mouse model in stratified epithelia

The above results indicate that adult mice with reduced *Sox4* levels show a faster loss of normal tissue homeostasis. As the latter relies on a controlled balance between tissue replenishment and degeneration, we hypothesized that organ failure could be due to defects in the activity of adult stem cells. In order to test this, we abrogated Sox4 in skin as a model for adult stem cell function. *Sox4* is hitherto the only *SoxC* class member whose expression has been detected in developing and adult skin (Dy et al., 2008; Lien et

al., 2014; Lowry et al., 2005). To this end, we crossed *Sox4*$^{lox/lox}$ mice with K5Cre transgenic mice (Ramirez et al., 2004), giving rise to *Sox4*$^{+/+}$; K5Cre$^{Tg/+}$ (*Sox4*^{WT}) and *Sox4*$^{lox/lox}$; K5Cre$^{Tg/+}$ (*Sox4*^{cKO}) mice. As expected, *Sox4*^{cKO} mice lack *Sox4* mRNA expression in tail skin epidermis when compared to *Sox4*^{WT} and show no differences in the expression levels of *Sox11* and *Sox12* (Figure 13A and B).

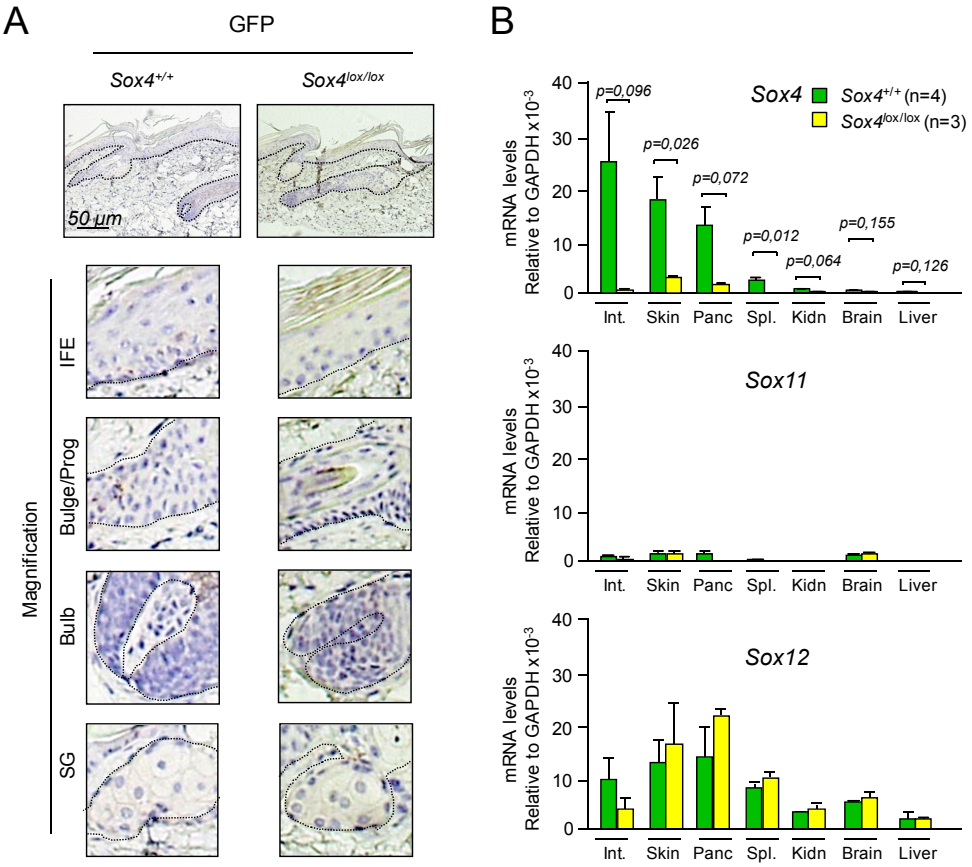

Figure 12. Expression of SoxC factors in Sox4 hypomorphic mice

(A) GFP IHC in tail skin sections from *Sox4*$^{+/+}$ *and Sox4*$^{lox/lox}$ *mice.*
(B) *Sox4, Sox11 and Sox12 qPCR* in the indicated tissues from *Sox4*$^{+/+}$ and *Sox4*$^{lox/lox}$ mice. P values are obtained with Student's t test, n=number of mice per genotype.

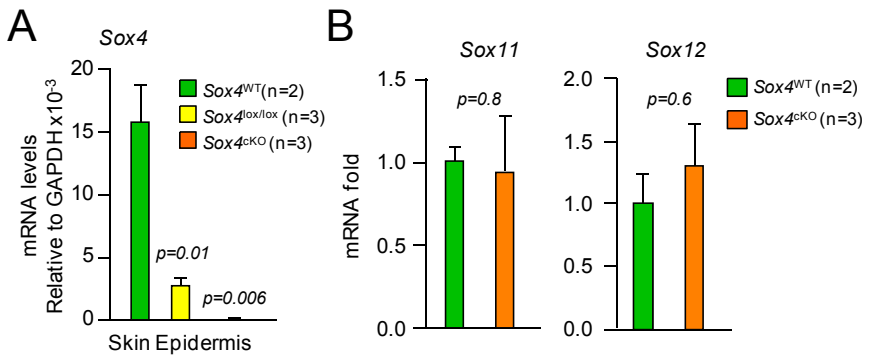

Figure 13. Expression of SoxC factors in Sox4 hypomorphic and *Sox4*^{cKO} mice

(A) *Sox4 qPCR* in the indicated tissues from *Sox4*^{WT}, *Sox4*$^{lox/lox}$ and *Sox4*^{cKO} mice.
(B) *Sox11 and Sox12 qPCR* in the indicated tissues from *Sox4*^{WT} and *Sox4*^{cKO} mice.

Finally, we did not find any significant change in the lifespan of mice with or without the K5Cre transgene (Figure 14), therefore unless specifically mentioned we refer hereafter to *Sox4*$^{+/+}$; K5Cre$^{Tg/+}$ and *Sox4*$^{+/+}$; K5Cre$^{+/+}$ mice collectively as *Sox4*^{WT} mice.

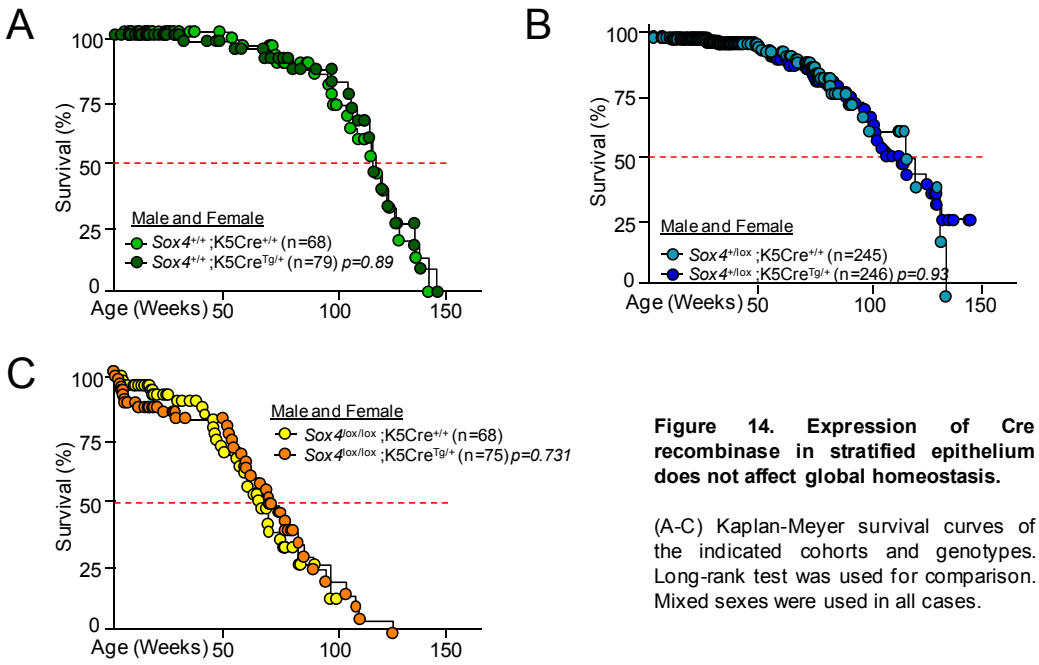

Figure 14. Expression of Cre recombinase in stratified epithelium does not affect global homeostasis.

(A-C) Kaplan-Meyer survival curves of the indicated cohorts and genotypes. Long-rank test was used for comparison. Mixed sexes were used in all cases.

VI. Sox4 is dispensable for normal skin development

In order to assess a role for *Sox4* during skin development, we studied skin differentiation markers in *Sox4*^{cKO} and *Sox4*^{WT} mice. We did not find differences in the assembly or disposition of Cytokeratin 10 (CK10, committed basal keratinocytes), Cytokeratin 14 (CK14, epidermal keratinocytes) or Loricrin (terminally-differentiated, cornified layer of keratinocytes) (Fuchs, 1994) (Figure 15A). In addition, *Sox4*^{cKO} mice displayed a normal hair coat in a gross examination (Figure 15B), indicating that *Sox4* is largely dispensable for normal skin specification and stratification. Being hypomorphic in all other tissues *Sox4*^{cKO} mice also display reduced weight and lifespan, (Figure 15C and Figure 14A-C).

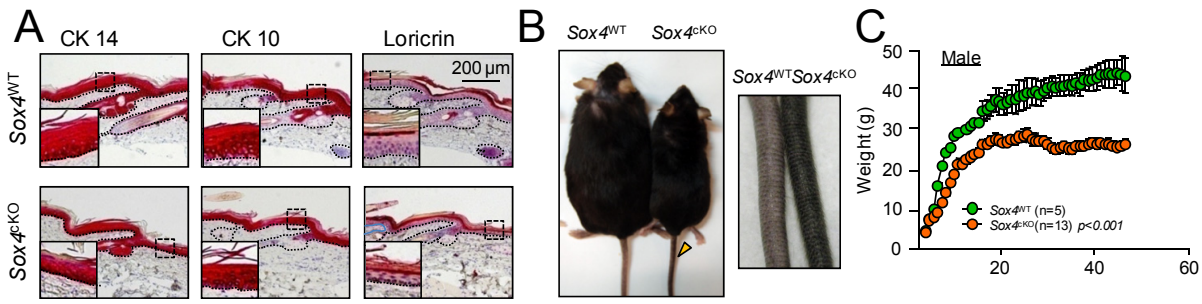

Figure 15. Sox4 is dispensable for skin stratification

(A) IHC of tail skin sections from mice of the indicated genotypes.
(B) General aspect of *Sox4*^{cKO} and *Sox4*^{WT} mice. Orange arrowhead, hyperpigmentation (magnified)
(C) Weight plots of male *Sox4*^{cKO} and *Sox4*^{WT} mice.

VII. Sox4 deficiency results in premature skin ageing

Decreased *Sox4* expression resulted in skin hyperpigmentation and a thinning of the IFE (Figure 15B and Figure 16). These phenotypes are also observed in mice with increased DNA damage in the skin owing to telomere dysfunction (Martinez et al., 2009; Munoz et al., 2005; Tejera et al., 2010).

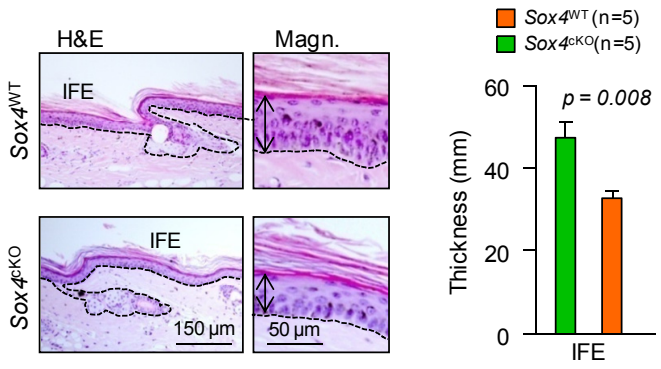

Figure 16. Reduced epidermal thickness in the absence of Sox4

(Left) Haematoxylin and Eosin labeling (H&E) in tail skin section of adult *Sox4*^{WT} and *Sox4*^{cKO} mice. (Right) Quantification of the epidermal thickness shown in left panel. N=number of mice per genotype, p values arise from Student's t test.

We also detected decreased proliferation rates at the IFE and Infundibulum but not at low proliferative compartments such as the bulge (Bg) and the sebaceous glands (SG) (Figure 17). This points out to a possible defect in the response to proliferative stimuli in the absence of *Sox4* in proliferative skin compartments, which in turn may lead to premature skin aging phenotypes.

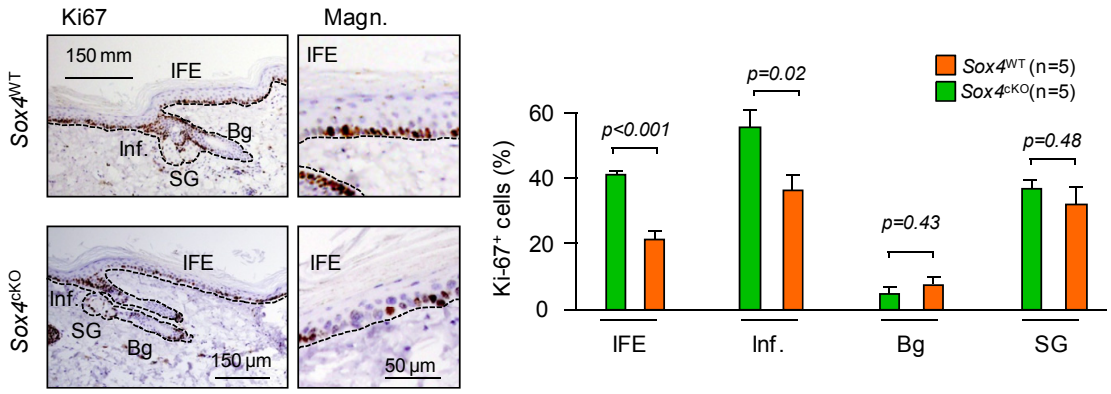

Figure 17. Reduced proliferation in *Sox4*^{cKO} mouse tail skin

Ki67 staining in tail skin sections of mice from the indicated genotypes (left) and quantification of the percentage of proliferative cell per compartment (right). N=number of mice per genotype, Student's t test.

To address whether *Sox4* deletion leads to accelerated skin degeneration, we studied several molecular biomarkers of ageing. First, we performed Quantitative telomere Fluorescent In-Situ Hybridization (QFISH), which allows determination of telomere length at a single cell level (Flores et al., 2008) in tail skin sections from 6-month old mice. We detected a marked decrease in the mean telomere length in the differentiated skin compartments, such as the IFE in *Sox4*^{cKO} mice (Figure 18A and B), indicative of replicative ageing. This was paralleled by significant accumulation of short telomeres and reduced abundance of long telomeres in the IFE (Flores et al., 2008) (Figure 18B). Strikingly, we observed a tendency to accumulate long telomeres in the hair bulge of *Sox4*^{cKO} mice (Figure 18C and D), suggestive of decreased replicative history of *Sox4*-depleted HFSC and possible defects in exiting quiescence (see below).

Dysfunctional or critically short telomeres have been shown to behave as DSBs by inducing a DNA damage response at chromosome ends, forming the so-called Telomere-Induced foci (TIFs) (de Lange, 2009). In order to assess whether the increased abundance of short telomeres could be a source of damage to *Sox4*-depleted IFE keratinocytes, we performed co-staining of γH2AX and Telomere End Repeat binding Factor 1 (TERF1, hereafter referred to as TRF1) to visualize DNA damage at telomeres in tail skin sections. We detected increased amounts of γH2AX in *Sox4*^{cKO} mouse IFE (Figure 19A and B). While we observed a preferential distribution of γH2AX foci in non-telomeric regions in *Sox4*^{WT} keratinocytes, in agreement with normal telomere length, *Sox4*^{cKO} mouse skin showed a shift towards increased presence of γH2AX foci at telomeres or TIFs, thus suggesting increased DNA damage arising from telomeres in the absence of Sox4 (Figure 19C).

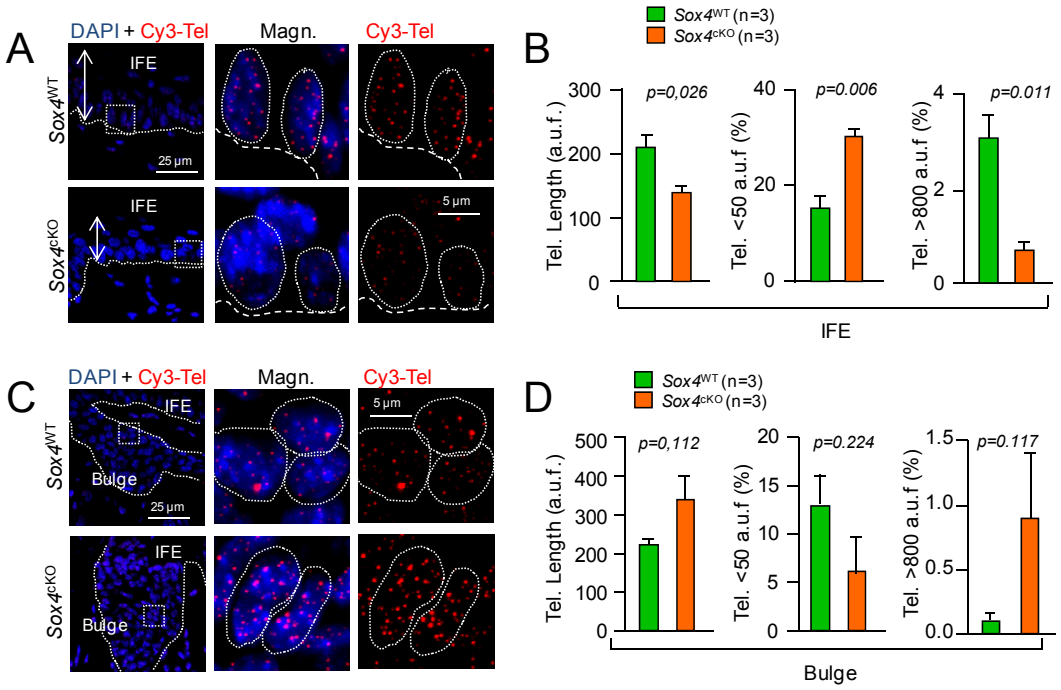

Figure 18. Accumulation of molecular markers of ageing in *Sox4*-depleted mouse skin (I)

(A) QFISH on adult mouse (6 month-old) tail skin IFE. Dermis and Epidermis are indicated, depicted is also magnification (Magn.).
(B) Mean telomere length (left), percentage of short telomeres (middle) and long telomeres (right) at the IFE.
(C) QFISH on adult mouse tail skin (Bulge region).
(D) Mean telomere length (left), percentage of short telomeres (middle) and long telomeres (right) from the bulge region.

N=number of mice per genotype, Student's t test was done for comparison.

Given that skin hyperpigmentation is also linked to DNA-damage-dependent p53 upregulation (Cui et al., 2007), we next determined p53 expression in *Sox4*-depleted skin, which is also a marker of replicative senescence and DNA damage in vivo (Collado et al., 2007). We observed a moderate but significant increase in the amount of p53-positive cells by IHC at the IFE compartment of the skin (Figure 19D). This was paralleled by a significant increase in the age/senescence markers p16 and p19 as detected by qPCR in isolated epidermal sheets of 6 month-old mice (Figure 19E).

Altogether, our results showing shortened telomeres, accumulation of DNA damage, and increase senescence markers as a consequence of *Sox4* deletion confirm a contribution of *Sox4* to skin maintenance and a pro-ageing phenotype in *Sox4*-depleted tissues.

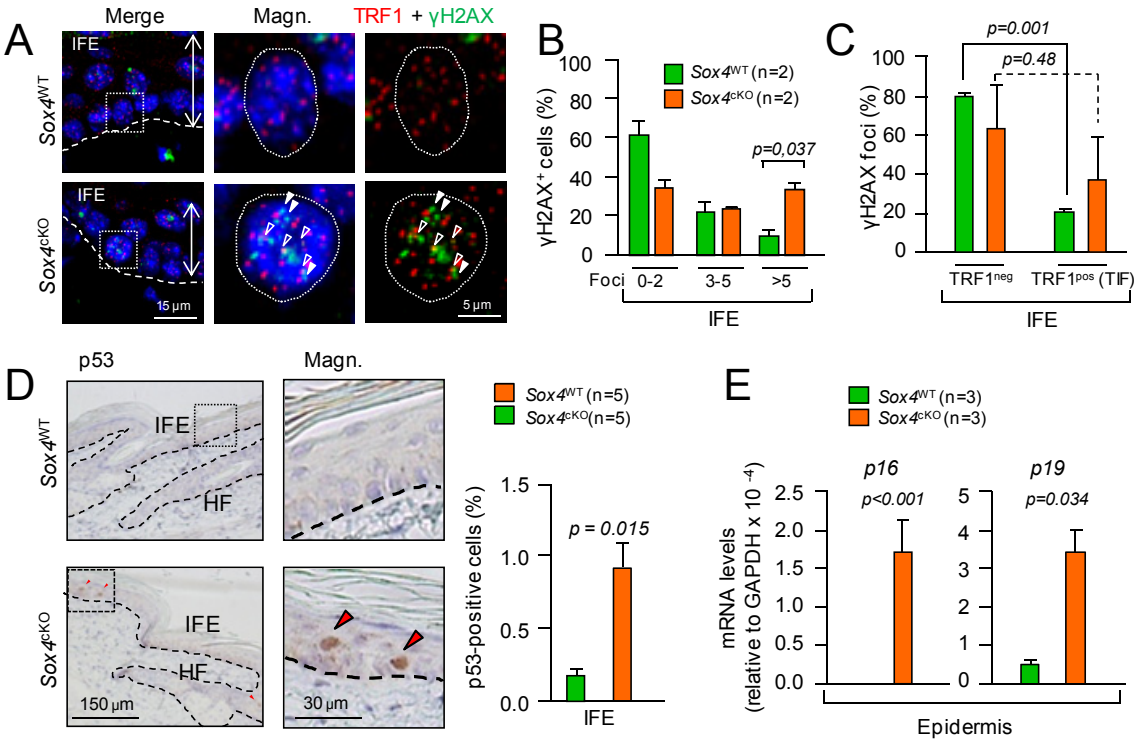

Figure 19. Accumulation of molecular markers of ageing in *Sox4*-depleted mouse skin (II)

(A) TRF1 and γH2AX staining in tail skin IFE from *Sox4*^{WT} and *Sox4*^{cKO} mice. TIFs are indicated with empty arrowheads, non-telomeric γH2AX foci are indicated by white arrowheads.
(B) Proportion of cells with the indicated γH2AX foci at the IFE from mice of the indicated genotypes.
(C) Distribution of H2AX staining between telomeric (TIFs) and non-telomeric foci.
(D) (Left) p53 IHC in 6 month-old mouse tail skin. (Right) p53-positive cells at the IFE (%).
(E) p16 (left) and p19 (right) qPCR analysis of tail skin epidermal extracts from adult *Sox4*^{WT} and *Sox4*^{cKO} mice.

N=number of mice per genotype, Student's t test was done for comparison.

VIII. Sox4 is induced upon plucking and modulates hair regeneration and wound healing

It is possible to force unscheduled entry into the hair cycle by physically removing a portion of the hair coat. Following plucking, resting HFSCs exit quiescence, become activated and proliferate while differentiating into all the hair lineages (Keyes et al., 2013; Muller-Rover et al., 2001) (Figure 20A). To test whether *Sox4* expression is induced during the plucking-induced anagen response, we depilated a group of *Sox4*^{WT} mice and determined mRNA expression levels for several markers of HFSC activity. We found upregulation of *GATA3, Tcf3/4, mTERT*, *Sox9* and *c-Myc* in a step-wise manner, confirming sequential activation of HFSCs after plucking (Greco et al., 2009) (Figure 20B).

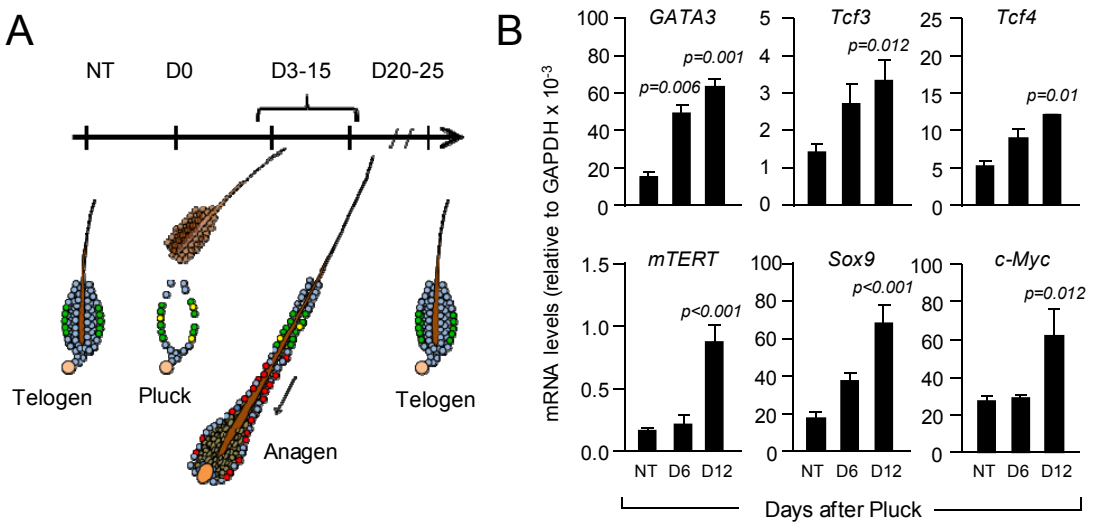

Figure 20. Sox4 is induced in the anagen phase upon plucking response

(A) Schematic of the timing of HFSC activation dynamics upon plucking. Symbols are: green, resting bulge HFSC; blue, differentiated cells; yellow, activated HFSC; and red, hair progeny. The timeline (in Days, D) is indicated on top of the graph.
(B) qPCR analysis of genes relevant for epidermal activation along hair regeneration (mid and late anagen, D6 and D12, respectively). 2-3 mice per condition were analyzed. Student's t test was used for comparison.

Sox4 was similarly induced during hair regeneration (Figure 21A). None of the other *SoxC* class members showed significant changes after plucking, indicating functional specificity of Sox4 in the context of epidermal stem cell activation (Figure 21A). To test whether *Sox4* increased expression was required for hair regeneration we plucked *Sox4*^{WT} and *Sox4*^{cKO} mice. We observed complete fur regeneration in *Sox4*^{WT} mice 12-15 days after plucking, while *Sox4*^{cKO} mice displayed a delayed hair growth although eventually they also resumed full hair coat regeneration (Figure 4D).

Hair regeneration relies on the activity of HFSCs, located in the hair bulge in mice (Fuchs, 2009). Other HFSC populations can also contribute to tissue replenishment in other regions than the hair progeny. Among them, the Junctional Zone (JZ)/Lrig1-positive cells can also contribute to the IFE regeneration (Jensen et al., 2009). To understand whether *Sox4* could be required also for proper IFE regeneration, we performed wound-healing assays. In accordance with delayed hair regeneration, *Sox4*^{cKO} mice also displayed a significant delay in replenishing the epidermis after wounding (Figure 21C), indicating a general delayed response of *Sox4*-deficient skin to proliferative stimuli.

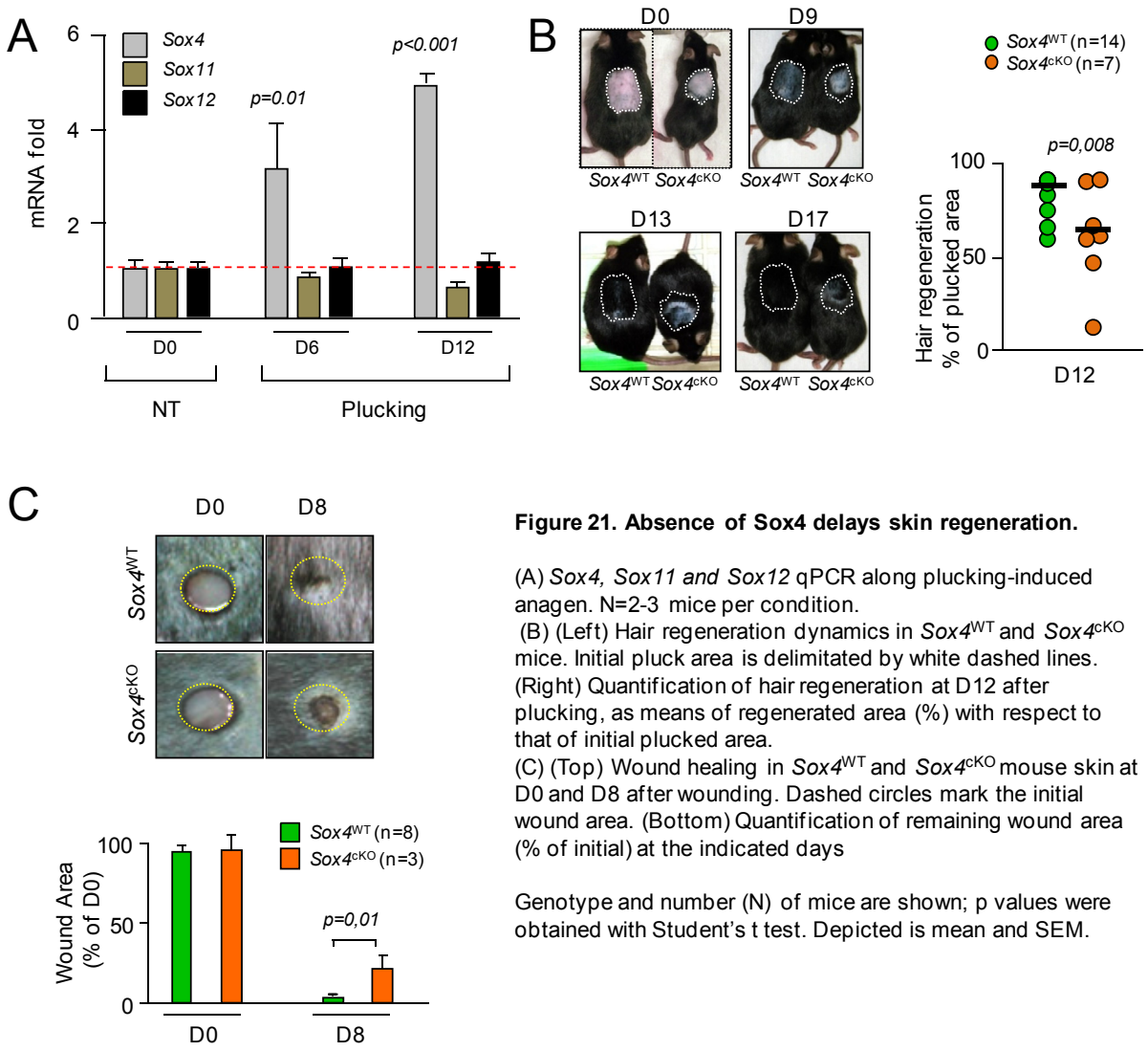

Figure 21. Absence of Sox4 delays skin regeneration.

(A) *Sox4, Sox11 and Sox12* qPCR along plucking-induced anagen. N=2-3 mice per condition.
(B) (Left) Hair regeneration dynamics in *Sox4*^{WT} and *Sox4*^{cKO} mice. Initial pluck area is delimitated by white dashed lines. (Right) Quantification of hair regeneration at D12 after plucking, as means of regenerated area (%) with respect to that of initial plucked area.
(C) (Top) Wound healing in *Sox4*^{WT} and *Sox4*^{cKO} mouse skin at D0 and D8 after wounding. Dashed circles mark the initial wound area. (Bottom) Quantification of remaining wound area (% of initial) at the indicated days

Genotype and number (N) of mice are shown; p values were obtained with Student's t test. Depicted is mean and SEM.

IX. Defective HFSC activation and DNA damage accumulation upon plucking in the absence of Sox4

In order to understand the cause of the delayed hair regeneration and wound-healing in *Sox4*^{cKO} mice, we tested the ability of HFSCs to regenerate the skin after plucking (Keyes et al., 2013; Muller-Rover et al., 2001). To this end, we performed skin histology and IHC analysis 12 days after plucking. We noted a significant reduction in hair follicle length, epidermal thickness and dermis size in *Sox4*^{cKO} compared to *Sox4*^{WT}, indicating reduced hair cycle induction in the absence of Sox4 (Figure 22A and B) (Flores et al., 2005; Keyes et al., 2013; Muller-Rover et al., 2001). Simultaneously, there was an overall decrease in the number of proliferating cells, as evidenced by Ki67 staining, in the differentiating areas of the skin such as the IFE, the hair bulb and the hair progeny

compartments, further supporting limited induction of hair cycling (Figure 22C and D). This was accompanied by an increase in the percentage of γH2AX-positive cells (Figure 22E and F) and p53-positive cells (Figure 22G and H). To confirm that the delayed HFSC activation was a cell-autonomous event, we extracted keratinocytes from adult mice and cultured them in clonogenic conditions. After 2 weeks in culture we observed a significant reduction in the number of big, differentiated colonies in keratinocytes depleted of *Sox4* (Figure 23)

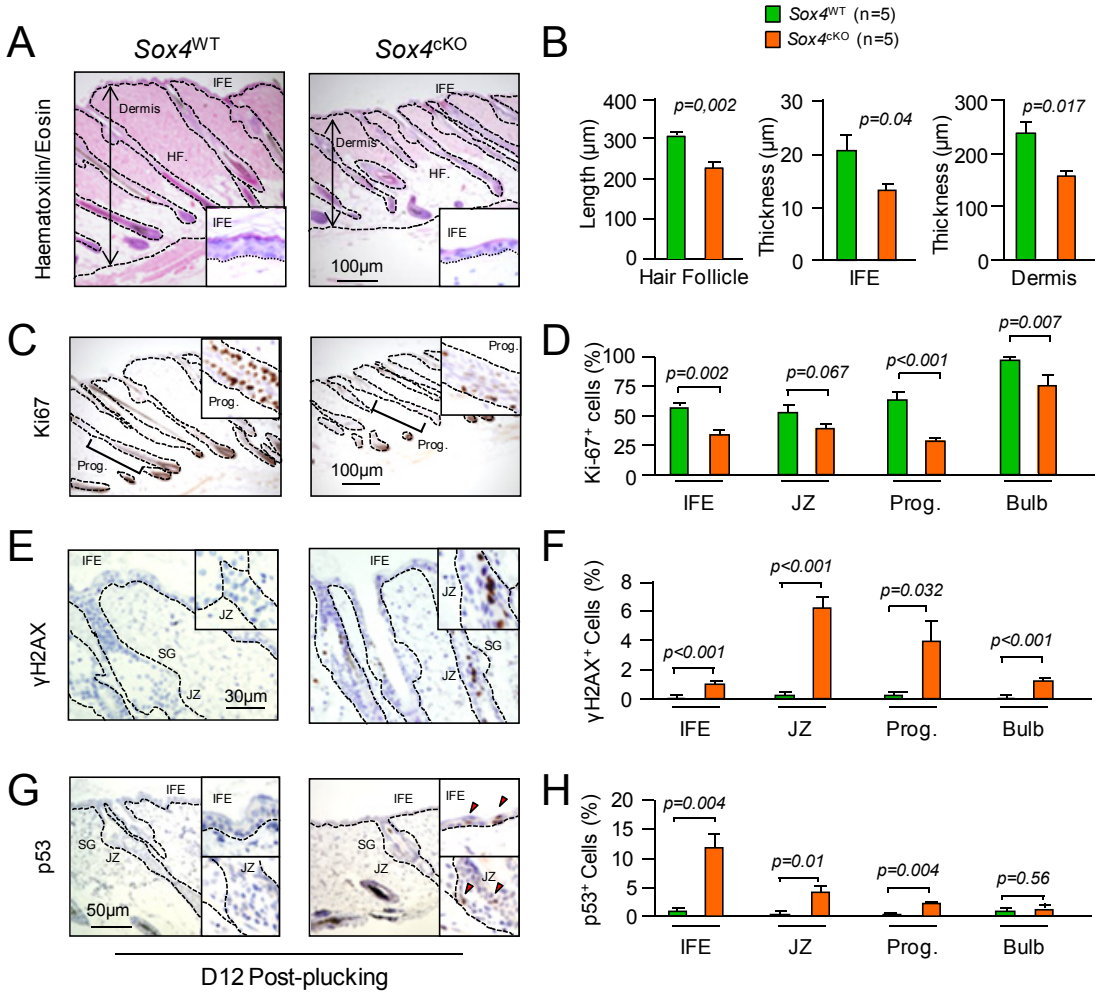

Figure 22. Requirement of *Sox4* for normal HFSC activation during hair regeneration.

(A) H&E staining in *Sox4*^{WT} and *Sox4*^{cKO} mouse back skin sections, at D12 after plucking. Skin regions are delimitated with dashed lines.
(B) Hair follicle length, epidermis thickness and dermal size from the experiment described in A.
(C-H) (Left) Ki67 (C), γH2AX (E) and p53 (G) IHCs on back skin sections from *Sox4*^{WT} and *Sox4*^{cKO} mice, at D12 post-pluck. Insets show magnification. Abbreviations are: Prog, Hair Progeny; IFE, Interfollicular Epidermis; JZ, Junctional Zone; HF, Hair Follicle; Bulb, Hair Bulb. Scale bars are indicated; depicted is a representative picture of 5 mice per genotype. (Right) Ki67 (D), γH2AX (F) and p53 (H) positive cells (% in the indicated compartments) found 12 days after plucking.

Number of mice (n) is 5 mice per genotype unless indicated. Student's t test was used. Depicted is average and SEM. Scale bars are included within graphs.

These results indicate that Sox4 is necessary for the skin response to proliferative stimuli such as hair plucking, suggesting an impaired ability of stem cells to exit quiescence and regenerate the hair (Flores and Blasco, 2009; Flores et al., 2005; Keyes et al., 2013).

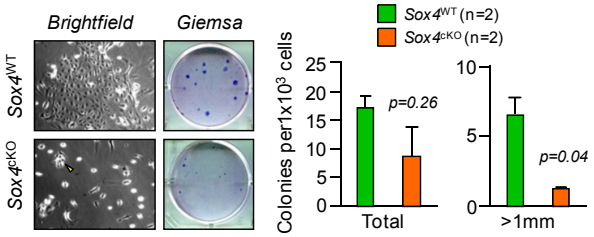

Figure 23. Requirement of *Sox4* for normal HFSC activation during hair regeneration (II).

(Left) Micrographs of differentiating primary keratinocytes under bright field (magnification is 20X) and Giemsa-stained 35mm dishes. Images are representative of 6 plates from 2 mice per genotype (n=2). (Right) Total colonies and colonies >1mm found in differentiating keratinocytes, as described in left panels. Student's t test was used for comparison.

X. Sox4 is required for the coordinated initiation of differentiation and proliferative programs upon HFSC activation

To dissect the molecular pathways underlying the delayed hair regeneration in *Sox4*-deficient skin, we performed microarray-based gene expression profiling in anagen skin 12 days after plucking, when Ki67 peaks (Figure 24A and B). Given that *Sox4* acts as a transcriptional activator (van de Wetering et al., 1993), we first focused in the genes negatively regulated in *Sox4*^{cKO} mice. A stringent (FDR<0.15) analysis revealed 12 differentially expressed genes (DEGs) between *Sox4*^{WT} and *Sox4*^{cKO} mouse skin undergoing hair regeneration (Table 4).

Among them, *Sox4* was the most downregulated gene ($log_2FC=4.87$; ≈30-fold decrease) (Figure 24B and Table 4), thus validating the microarray. The rest of DEGs were involved in nervous system development, heart function, cytoskeleton remodeling and cancer, as determined by GO studies (Table 4). All these processes have been previously linked to *Sox4* (Vervoort et al., 2013) and therefore provide a biologically-relevant quality control.

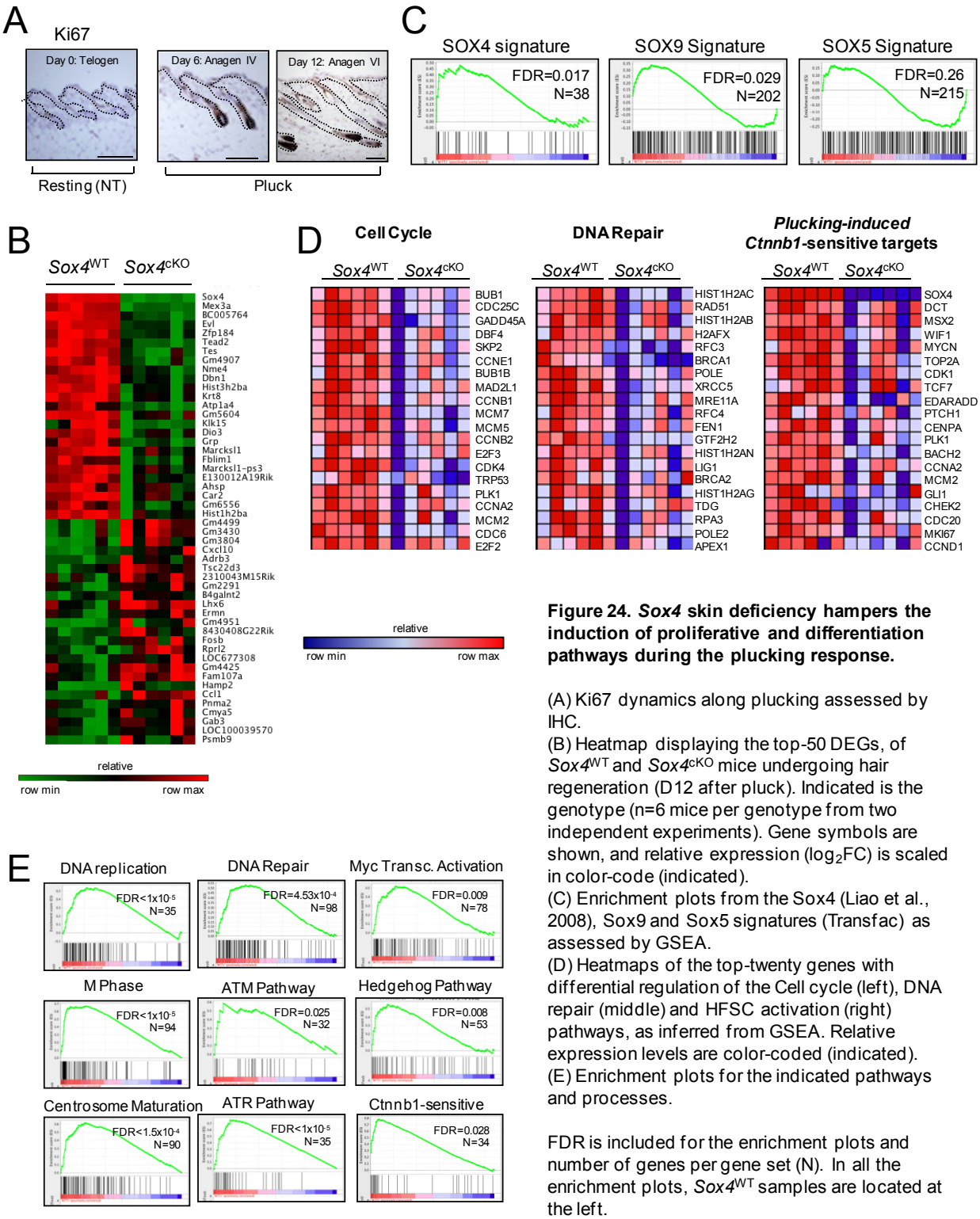

Figure 24. *Sox4* skin deficiency hampers the induction of proliferative and differentiation pathways during the plucking response.

(A) Ki67 dynamics along plucking assessed by IHC.
(B) Heatmap displaying the top-50 DEGs, of *Sox4*^{WT} and *Sox4*^{cKO} mice undergoing hair regeneration (D12 after pluck). Indicated is the genotype (n=6 mice per genotype from two independent experiments). Gene symbols are shown, and relative expression (log_2FC) is scaled in color-code (indicated).
(C) Enrichment plots from the Sox4 (Liao et al., 2008), Sox9 and Sox5 signatures (Transfac) as assessed by GSEA.
(D) Heatmaps of the top-twenty genes with differential regulation of the Cell cycle (left), DNA repair (middle) and HFSC activation (right) pathways, as inferred from GSEA. Relative expression levels are color-coded (indicated).
(E) Enrichment plots for the indicated pathways and processes.

FDR is included for the enrichment plots and number of genes per gene set (N). In all the enrichment plots, *Sox4*^{WT} samples are located at the left.

Symbol	Name	log_2FC	p value	Annotated Diseases	GO ID	Biological/Molecular GO term
Sox4	SRY (Sex Determining Region Y)-Box 4	4,872	9,01E-13	Neuronitis, Splenic marginal zone lymphoma, Adenoid cystic carcinoma, Endometrial adenocarcinoma, Ependymoma, Mantle cell lymphoma, Colorectal cancer, Melanoma, Hepatitis, Breast cancer, Lung cancer, Prostate cancer, Obesity, Myeloma, Hepatocellular carcinoma, Adenocarcinoma, Glioblastoma, Medulloblastoma, Bladder carcinoma	GO:0001841	neural tube formation
					GO:0002328	pro-B cell differentiation
					GO:0003211	cardiac ventricle formation
					GO:0006355	regulation of transcription, DNA-dependent
					GO:0008284	positive regulation of cell proliferation
					GO:0035019	somatic stem cell maintenance
					GO:0090263	canonical Wnt signaling pathway
Mex3a	Mex-3 RNA Binding Family Member A	2,231	2,47E-08	NA	GO:0003723	RNA binding
					GO:0005515	protein binding
					GO:0008270	zinc ion binding
BC005764 (*Prg-2, Lpppr3*)	Plasticity-Related Gene 2 Protein Lipid Phosphate Phosphatase-Related Protein Type	1,923	6,24E-07	Melanoma, Pancreatitis	GO:0003824	catalytic activity
					GO:0005515	protein binding
					GO:0008195	phosphatidate phosphatase activity
Evl	Ena/VASP-Like Protein	1,423	1,07E-05	Splenic abscess, Esophageal varix, Hypersplenism, Portal hypertension, Wiskott-aldrich syndrome, Liver cirrhosis, Hypertension, Esophagitis, Colorectal cancer, Gastric cancer, Endotheliitis, Breast cancer	GO:0007015	actin filament organization
					GO:0007166	cell surface receptor signaling pathway
					GO:0007399	nervous system development
					GO:0007411	axon guidance
					GO:0008154	actin polymerization or depolymerization
Zfp184 (Znf184)	Zinc Finger Protein 184 (Kruppel-Like)	1,261	3,97E-05	Choriocarcinoma, Schizophrenia	GO:0006351	transcription, DNA-dependent
					GO:0006355	regulation of transcription, DNA-dependent
Tead2	TEA Domain Family Member 2	1,017	5,48E-05	Patulous eustachian tube, Alpha-mannosidosis, Plasmodium falciparum malaria, Pharyngitis, Neuronitis	GO:0001570	vasculogenesis
					GO:0001843	neural tube closure
					GO:0003143	embryonic heart tube morphogenesis
					GO:0006355	regulation of transcription, DNA-dependent
					GO:0006367	transcription initiation from RNA polymerase II promoter

Table 4. Annotated ranked list of genes significantly downregulated in *Sox4*^{cKO} vs. *Sox4*^{WT} mice undergoing hair regeneration 12 days after plucking.

Next, we performed Gene Set Enrichment Analysis (GSEA) to gain insights into the biological significance of the DEGs. GSEA revealed significant alteration (FDR<0.05) of 92 signaling pathways (extracted from the KEGG, Reactome and NCI repositories) in *Sox4*^{WT} vs. *Sox4*^{cKO} mice (Table 5). We confirmed a *Sox4* signature in the microarray by analyzing genes identified by Liao and colleagues (Liao et al., 2008) (Figure 24C; FDR=0.017). This group of gene sets showed downregulation in pathways controlling progression throughout cell cycle, epidermal stem cell activation and DNA repair (24 D and E; Table 5). These included critical mitotic regulators such as *CDK4*, *Bub1*, *Ccnb1*; genes of the DNA replication origin assembly, such as *Mcm2, 5 and 7*; and centrosome maturation genes such as *Mad2l1 and Plk1* (Figure 24D and E). We also found downregulation of DNA repair and replicative stress pathways in *Sox4*^{cKO} mice undergoing hair regeneration, in agreement with the observed DNA damage accumulation upon plucking (Figure 24D and E). Interestingly, several of the gene sets significantly downregulated in the absence of *Sox4* have been shown crucial for proper hair follicle cycling and activation/differentiation of HFSCs (Berta et al., 2010; Lien et al., 2014; Nowak et al., 2008; Oro and Higgins, 2003). In particular, we found downregulation in the *Myc* and *Hedgehog* pathways, in support of the previously shown delayed hair follicle activation (Figure 24D and E). We further confirmed a defective HFSC function by testing a home-made list of genes obtained from the *Sox9* signature in the Transfac repository. We observed a significant (FDR=0.029) overlap among genes regulated by *Sox9* and those specifically downregulated in *Sox4*^{cKO} mice undergoing anagen in contrast to *Sox4*^{WT} controls. We used the *Sox5* signature as a negative control, which did not show significant variation in our microarray (Figure 24C). Finally, we compared our microarray data with the plucking-induced, Wnt-upregulated, β-catenin-sensitive gene signature obtained by Lien and colleagues, a bona fide set of genes governing HFSC activation (Lien et al., 2014). Interestingly, we found a significant downregulation (FDR=0.028) of this set of genes in Sox4-depleted HFSC 12 days after plucking, when compared to their WT controls (Figure 24D and E). This overlapping regulation points out to a cooperation of β-catenin and Sox4 in regulating target genes relevant for Wnt-induced HFSC activation and normal hair regeneration.

Altogether, these results demonstrate that absence of *Sox4* in skin results in delayed epidermal stem cell activation and subsequent deficient induction of proliferative and differentiation pathways, concomitant with defects in DNA damage repair and therefore pointing out to Sox4 as a crucial regulator of pathways that master the exit of

epidermal stem cell quiescence. The coalescence of Sox4-mediated transcription with β-catenin targets further confirms the importance of Sox4 in governing the hair regeneration process.

Gene Set Name	# Genes	NES	FDR q-val	Source	Status
DNA REPLICATION	35	23.419.375	< 1E-05	KEGG	DOWN
CELL CYCLE	108	22.575.436	< 1E-05	KEGG	DOWN
CELL CYCLE, MITOTIC	317	2.670.456	< 1E-05	REACTOME	DOWN
M PHASE	94	25.053.108	< 1E-05	REACTOME	DOWN
MITOTIC PROMETAPHASE	90	24.785.168	< 1E-05	REACTOME	DOWN
G2/M CHECKPOINTS	45	24.457.316	< 1E-05	REACTOME	DOWN
ACTIVATION OF THE PRE-REPLICATIVE COMPLEX	29	23.832.464	< 1E-05	REACTOME	DOWN
ACTIVATION OF ATR IN RESPONSE TO REPLICATION STRESS	35	23.366.392	< 1E-05	REACTOME	DOWN
DNA STRAND ELONGATION	29	22.902.646	< 1E-05	REACTOME	DOWN
PLK1 SIGNALING EVENTS	40	25.397.267	< 1E-05	NCI	DOWN
FANCONI ANEMIA PATHWAY	42	2.312.326	< 1E-05	NCI	DOWN
ATR SIGNALING PATHWAY	37	22.004.871	< 1E-05	NCI	DOWN
ELONGATION AND PROCESSING OF CAPPED TRANSCRIPTS	129	21.529.381	6.39E-05	REACTOME	DOWN
E2F MEDIATED REGULATION OF DNA REPLICATION	37	2.168.428	6.74E-05	REACTOME	DOWN
EXTENSION OF TELOMERES	22	21.894.016	7.14E-05	REACTOME	DOWN
E2F TRANSCRIPTIONAL TARGETS AT G1/S	22	21.906.655	7.58E-05	REACTOME	DOWN
FORMATION AND MATURATION OF MRNA TRANSCRIPT	146	21.985.574	8.09E-05	REACTOME	DOWN
LOSS OF PROTEINS REQUIRED FOR INTERPHASE MICROTUBULE ORGANIZA	81	22.046.125	8.67E-05	REACTOME	DOWN
G2/M TRANSITION	97	22.255.423	9.34E-05	REACTOME	DOWN
DOUBLE-STRAND BREAK REPAIR	31	22.309.527	1.01E-04	REACTOME	DOWN
HOMOLOGOUS RECOMBINATION REPAIR OF REPLICATION-INDEPENDENT D	26	22.312.896	1.10E-04	REACTOME	DOWN
LOSS OF NLP FROM MITOTIC CENTROSOMES	81	22.381.098	1.21E-04	REACTOME	DOWN
HOMOLOGOUS RECOMBINATION REPAIR	26	22.718.346	1.35E-04	REACTOME	DOWN
CENTROSOME MATURATION	90	22.736.535	1.52E-04	REACTOME	DOWN
ASSEMBLY OF THE RAD50-MRE11-NBS1 COMPLEX AT DNA DOUBLE-STRANI	16	20.962.038	1.58E-04	REACTOME	DOWN
CELL CYCLE CHECKPOINTS	116	21.012.824	1.65E-04	REACTOME	DOWN
ATM MEDIATED PHOSPHORYLATION OF REPAIR PROTEINS	17	21.284.003	1.72E-04	REACTOME	DOWN
LAGGING STRAND SYNTHESIS	19	21.374.292	1.80E-04	REACTOME	DOWN
ELONGATION OF INTRON-CONTAINING TRANSCRIPTS AND CO-TRANSCRIPTI	129	21.416.466	1.89E-04	REACTOME	DOWN
AURORA B SIGNALING	39	20.790.722	2.09E-04	NCI	DOWN
GAP-FILLING DNA REPAIR SYNTHESIS AND LIGATION IN TC-NER	16	20.626.438	2.23E-04	REACTOME	DOWN
E2F-ENABLED INHIBITION OF PRE-REPLICATION COMPLEX FORMATION	15	20.684.686	2.32E-04	REACTOME	DOWN
MRN COMPLEX RELOCALIZES TO NUCLEAR FOCI	16	20.856.543	2.41E-04	REACTOME	DOWN
ATM MEDIATED RESPONSE TO DNA DOUBLE-STRAND BREAK	17	20.860.016	2.50E-04	REACTOME	DOWN
BARD1 SIGNALING EVENTS	27	20.733.442	3.50E-04	NCI	DOWN
DNA REPLICATION	96	20.064.106	3.89E-04	REACTOME	DOWN
G1/S TRANSITION	109	2.009.477	4.02E-04	REACTOME	DOWN
CYTOSOLIC TRNA AMINOACYLATION	27	20.106.726	4.15E-04	REACTOME	DOWN
METABOLISM OF NON-CODING RNA	17	20.236.602	4.30E-04	REACTOME	DOWN
DNA REPAIR	98	19.992.706	4.53E-04	REACTOME	DOWN
GAP-FILLING DNA REPAIR SYNTHESIS AND LIGATION IN GG-NER	16	19.747.477	6.90E-04	REACTOME	DOWN
HOMOLOGOUS RECOMBINATION	27	20.180.893	0.001285787	KEGG	DOWN
PYRIMIDINE METABOLISM	89	2.018.695	0.001353652	KEGG	DOWN
MISMATCH REPAIR	22	19.752.159	0.001968444	KEGG	DOWN
DNA REPLICATION PRE-INITIATION	75	18.913.058	0.002422943	REACTOME	DOWN
APC/C:CDC20 MEDIATED DEGRADATION OF CYCLIN B	30	18.631.127	0.003491783	REACTOME	DOWN
MITOTIC SPINDLE CHECKPOINT	22	18.565.638	0.003697891	REACTOME	DOWN
FOXM1 TRANSCRIPTION FACTOR NETWORK	39	19.572.923	0.0037972662	NCI	DOWN
APC-CDC20 MEDIATED DEGRADATION OF NEK2A	27	18.275.056	0.004728567	REACTOME	DOWN
CLEAVAGE OF GROWING TRANSCRIPT IN THE TERMINATION REGION	26	18.290.805	0.004823893	REACTOME	DOWN
ABC TRANSPORTERS - GENERAL	41	-20.396.116	0.005750482	KEGG	UP
FORMATION OF THE EARLY ELONGATION COMPLEX	32	1.806.907	0.005861847	REACTOME	DOWN
BASE EXCISION REPAIR	17	18.014.127	0.006018174	REACTOME	DOWN
APC/C-MEDIATED DEGRADATION OF CELL CYCLE PROTEINS	84	17.948.378	0.006361603	REACTOME	DOWN
INHIBITION OF THE PROTEOLYTIC ACTIVITY OF APC/C REQUIRED FOR THE C	21	17.887.087	0.006581755	REACTOME	DOWN
RHOA SIGNALING PATHWAY	43	-20.495.057	0.007478651	NCI	UP

Table 5. Ranked list of gene sets significantly changed in *Sox4*^{cKO} vs. *Sox4*^{WT} mice undergoing hair regeneration 12 days after plucking.

Gene Set Name	# Genes	NES	FDR q-val	Source	Status
HEDGEHOG SIGNALING PATHWAY	53	1.873.602	0.007613374	KEGG	DOWN
BASAL CELL CARCINOMA	55	18.676	0.007957148	KEGG	DOWN
AMINOACYL-TRNA BIOSYNTHESIS	42	1.851.659	0.008033624	KEGG	DOWN
SYSTEMIC LUPUS ERYTHEMATOSUS	87	18.603.351	0.00830677	KEGG	DOWN
GENE EXPRESSION	353	17.621.422	0.008675053	REACTOME	DOWN
VALIDATED TARGETS OF C-MYC TRANSCRIPTIONAL ACTIVATION	78	18.829.532	0.0091759	NCI	DOWN
HEDGEHOG SIGNALING EVENTS MEDIATED BY GLI PROTEINS	47	18.652.664	0.009426778	NCI	DOWN
INACTIVATION OF APC/C VIA DIRECT INHIBITION OF THE APC/C COMPLEX	21	1.746.477	0.010122311	REACTOME	DOWN
BASE EXCISION REPAIR	33	18.169.132	0.010572486	KEGG	DOWN
IL23-MEDIATED SIGNALING EVENTS	37	-19.667.697	0.011410583	NCI	UP
E2F TRANSCRIPTION FACTOR NETWORK	67	18.426.008	0.011725595	NCI	DOWN
GLOBAL GENOMIC NER (GG-NER)	34	1.729.057	0.011841513	REACTOME	DOWN
GLUCOSE METABOLISM	77	-18.421.031	0.014822196	REACTOME	UP
CYTOCHROME P450 - ARRANGED BY SUBSTRATE TYPE	50	-18.640.511	0.017167443	REACTOME	UP
PHASE 1 - FUNCTIONALIZATION OF COMPOUNDS	71	-18.427.429	0.018527746	REACTOME	UP
AURORA A SIGNALING	29	17.860.239	0.019656735	NCI	DOWN
ACTIVATION OF APC/C AND APC/C:CDC20 MEDIATED DEGRADATION OF MIT	77	16.652.274	0.02164067	REACTOME	DOWN
NUCLEOTIDE EXCISION REPAIR	40	1.751.457	0.022095194	KEGG	DOWN
ATM PATHWAY	32	17.544.352	0.024574187	NCI	DOWN
MITOCHONDRIAL TRNA AMINOACYLATION	26	16.489.309	0.024760392	REACTOME	DOWN
HDL-MEDIATED LIPID TRANSPORT	26	-18.641.241	0.025751164	REACTOME	UP
NUCLEOTIDE EXCISION REPAIR	50	16.393.281	0.026672386	REACTOME	DOWN
CONVERSION FROM APC/C:CDC20 TO APC/C:CDH1 IN LATE ANAPHASE	19	16.323.775	0.027763184	REACTOME	DOWN
UREA CYCLE AND METABOLISM OF AMINO GROUPS	27	1.704.583	0.029192088	KEGG	DOWN
COLLAGEN-MEDIATED ACTIVATION CASCADE	16	16.171.777	0.030529834	REACTOME	DOWN
THYROID CANCER	27	17.080.088	0.030887974	KEGG	DOWN
GENERATION OF SECOND MESSENGER MOLECULES	20	15.895.758	0.036932748	REACTOME	DOWN
M/G1 TRANSITION	61	15.907.022	0.037230276	REACTOME	DOWN
APC/C:CDC20 MEDIATED DEGRADATION OF MITOTIC PROTEINS	74	15.929.469	0.037267175	REACTOME	DOWN
FGFR4 LIGAND BINDING AND ACTIVATION	15	-18.798.758	0.039966363	REACTOME	UP
ASSEMBLY OF THE PRE-REPLICATIVE COMPLEX	61	15.754.787	0.040402573	REACTOME	DOWN
METABOLISM OF BILE ACIDS AND BILE SALTS	47	-17.318.394	0.044718016	REACTOME	UP
MELANOGENESIS	100	16.441.392	0.04555292	KEGG	DOWN
P53 SIGNALING PATHWAY	65	16.359.637	0.04618583	KEGG	DOWN
SELENOAMINO ACID METABOLISM	22	16.455.731	0.04809926	KEGG	DOWN
FORMATION OF RNA POL II ELONGATION COMPLEX	43	15.488.114	0.049070586	REACTOME	DOWN

Table 5 (Cont.). Ranked list of gene sets significantly changed in *Sox4*^{cKO} vs. *Sox4*^{WT} mice undergoing hair regeneration 12 days after plucking.

XI. Sox4 deficiency prevents chemically-induced skin carcinogenesis

We have shown that *Sox4* levels correlate with resistance to spontaneous carcinogenesis in hypomorphic *Sox4*$^{lox/lox}$ mice. Moreover, *Sox4*-deficient keratinocytes are resilient to HFSC activation when facing proliferative stimuli, and several of the *Sox4*-regulated genes in our microarray profiling point to severe impairment of cell division capacity of cells. We therefore speculated that *Sox4*-deficient keratinocytes could be resistant to oncogenic signals required for rapid proliferation, thereby preventing expansion of malignant cells during skin carcinogenesis. To test that, we performed a two-step chemically induced carcinogenic protocol. We treated the mice with a single dose of DMBA and administered TPA twice weekly during 15 additional weeks in order to promote expansion of cells bearing oncogenic mutations. We monitored tumor burden once a week during a total of 35 weeks after the first DMBA administration (Figure 25A). We observed

that the onset of papillomas was delayed in *Sox4*^{cKO} mice after DMBA/TPA administration (Figure 25B). Moreover, the average number of tumors per mouse was notably reduced across the duration of experiment (Figure 25B and 26A and B). Of note, most of the papillomas that appeared in *Sox4*^{cKO} mice regressed upon TPA withdrawal, while up to 30% of the tumours formed in *Sox4*^{WT} became independent of TPA administration and progressed (Figure 25B and Figure 26A and B). In addition, *Sox4*-depleted mice did not display any papilloma bigger than 6mm after 30 weeks of treatment, in contrast to more than 80% of *Sox4*^{WT} mice (Figure 26B).

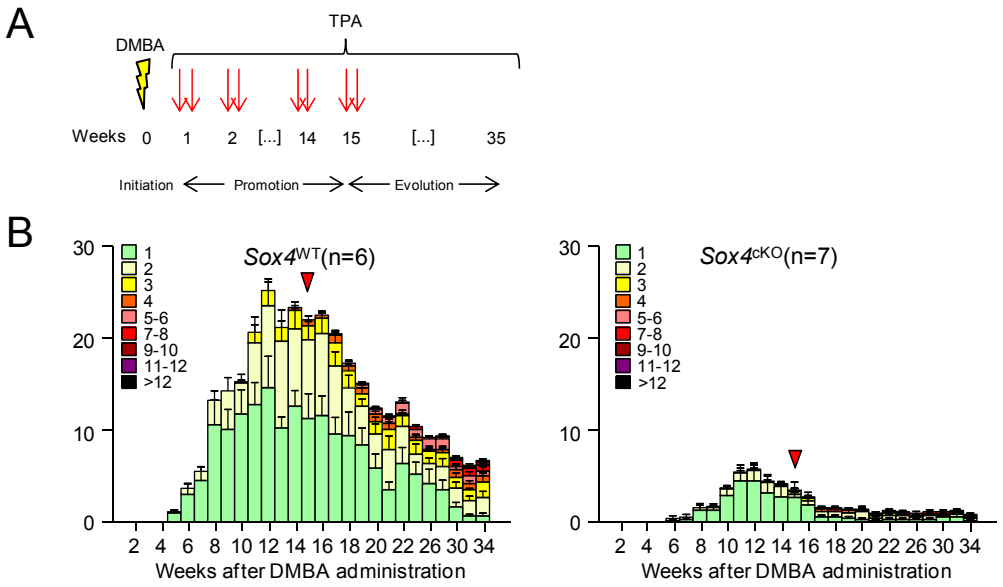

Figure 25. Absence of Sox4 prevents chemically-induced tumorigenesis

(A) Schematic representation of the two-step chemically-induced carcinogenesis protocol. Red arrows denote the twice-weekly administration of TPA during the first 15 weeks of the treatment.
(B) Average number of papillomas, stratified by size (colour-coded), at the indicated weeks after the TPA/DMBA treatment in *Sox4*^{WT} (left) and *Sox4*^{cKO} (right) mice. Red arrowhead marks the end of the TPA treatment.

In order to rule out possible non-cell autonomous effects of *Sox4* in chemically induced skin carcinogenesis, we performed *in vitro* transformation protocols. For that, we assayed *Sox4*$^{lox/lox}$ and *Sox4*$^{+/+}$ Mouse Embryonic Fibroblasts (MEFs) previously transduced with Adeno-Cre viruses to induce recombination of the KI allele (hereafter *Sox4*$^{lox/lox;}$ AdCre and *Sox4*$^{+/+;}$ AdCre MEFs). In order to transform the MEFs, we further transduced them with HRasG12V and E1A oncogenes, and subsequently plated them at a very low density to quantify appearance of transformed foci. *Sox4*$^{lox/lox;}$ AdCre MEFs showed a dramatically reduced foci formation compared to the *Sox4*$^{+/+}$ controls, indicative of reduced transformation ability (Figure 26C). These results indicate that the impairment of tumorigenesis in the absence of Sox4 is cell autonomous.

We also studied carcinogenesis in *Sox4*^{HET} and *Sox4* hypomorphic (*Sox4*$^{lox/lox}$) mice. We observed a good correlation between *Sox4* gene dosage and tumour burden, as assessed by the total number of tumours and the percentage of mice bearing big tumours (Figure 26B). These results point out to *Sox4* as a gene necessary for skin cell transformation and tumorigenesis, in agreement with the fact that *Sox4* is upregulated in many different cancer types.

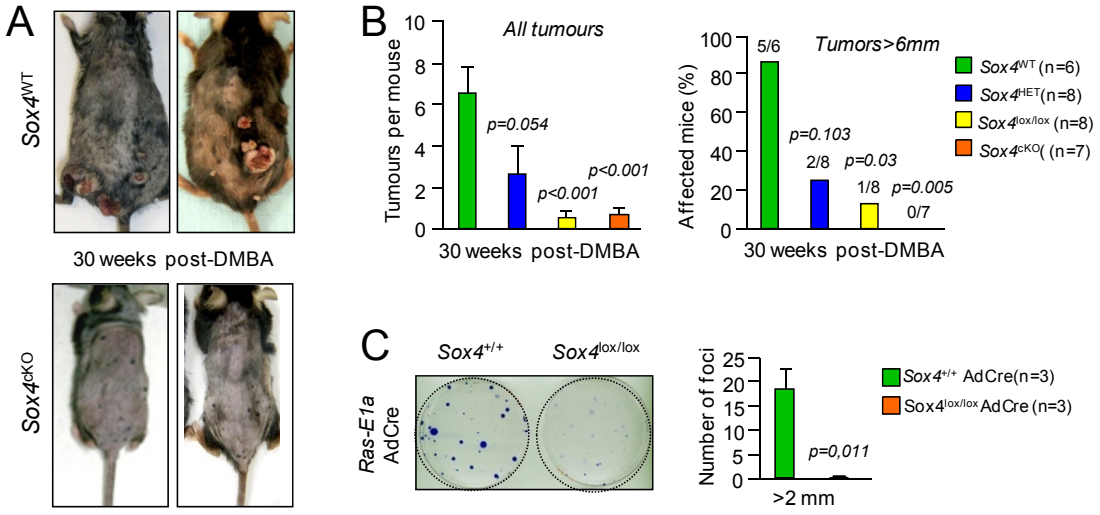

Figure 26. Absence of Sox4 prevents chemically-induced tumorigenesis

(A) Representative pictures of *Sox4*^{WT} (top) and *Sox4*^{cKO} mice (bottom), 30 weeks after the DMBA application.
(B) Average number of tumors (Left; Student's t test, all groups were compared to *Sox4*^{WT}) and percentage of mice bearing tumors >6mm (Left: two-tailed Student's t test; right, Fisher's exact test, compared to *Sox4*^{WT}).
(C) (Left) Colony-forming assay using transformed *Sox4*$^{+/+}$ and *Sox4*$^{lox/lox}$ MEF, previously transduced with AdCre and further transduced with Ras-IRES-E1A. (Right) 100mm dishes seeded with $2x10^3$ cells grown for 2 weeks and stained with Giemsa. (Right) Number of transformed foci >2mm per mouse. Two-tailed Student's t test.

XII. A resistance to TPA-induced proliferation limits the skin tumour burden in the absence of Sox4

Having demonstrated the essential role that *Sox4* plays on keratinocyte transformation, we wanted to understand the mechanism by which this protein could exert its function during carcinogenesis. Given that papilloma burden in *Sox4*^{WT} mice peaks between 6 and 8 weeks after TPA/DMBA administration (Figure 25), we decided to sacrifice a group of animals after 6 weeks of treatment for histological examination of skin. Interestingly, we found a strong reduction in the percentage of proliferating cells, as assessed by Ki67 staining, at the IFE of *Sox4*^{cKO} mice (Figure 27A and B). Accordingly, these mice showed a reduced thickening of this compartment and a reduced hair follicle

length, indicating that *Sox4* is needed for cell expansion upon mitogenic stimulation. We also studied the levels and distribution of phosphorylated Histone-3 (P-H3) by IHC in equivalent regions of benign lesions (collected at 30 weeks of treatment) from *Sox4*^{WT} and *Sox4*^{cKO} mice, as determined from the distribution of the Loricrin and Cytokeratin-6 markers (Figure 27C). We observed a notable reduction in the amount of cells positive for P-H3. In addition, the majority of P-H3-positive cells in *Sox4*^{cKO} mouse skin showed a dotted pattern, indicating that these cells could not progress through the cell cycle beyond G2 (Goto et al., 1999) (Figure 27C). These findings are in line with defective activation and proliferation of HFSCs upon stimulation that we have observed both through IHC and microarray profiling, which include downregulation of many genes required for cell division. All these results provide a molecular proof of tumour suppression mediated by loss of *Sox4* by preventing entry into cell cycle and account for the reduced tumour formation abilities in *Sox4*-reduced contexts.

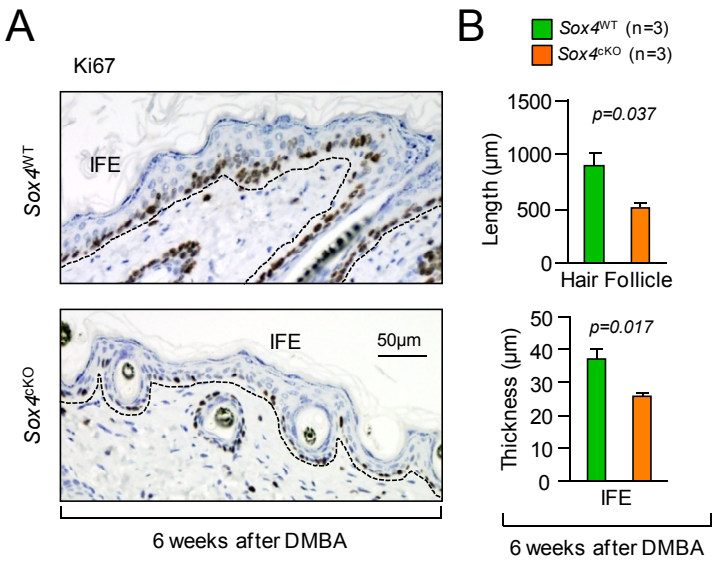

Figure 27. Defective proliferation in Sox4cKO mice upon TPA stimulation and along cellular transformation.

(A) Ki67 IHC in skin from *Sox4*^{WT} and *Sox4*^{cKO} mice, 6 weeks after initiation of DMBA/TPA treatment. Note the reduced Ki67-positive cells in *Sox4*-depleted mice.
(B) IFE thickness and hair follicle length after 6 weeks of TPA treatment.
(C) Loricrin, Cytokeratin 6 (CK6), p53 and phospho-Histone 3 (P-H3) IHC in benign lesions after 30 weeks of TPA treatment, in *Sox4*^{WT} and *Sox4*^{cKO} mice. Insets show magnification; yellow arrowheads, pan-nuclear P-H3-positive cells; red arrowheads, dotted P-H3.

N=number of mice per genotype. Student's t test was used for comparison.

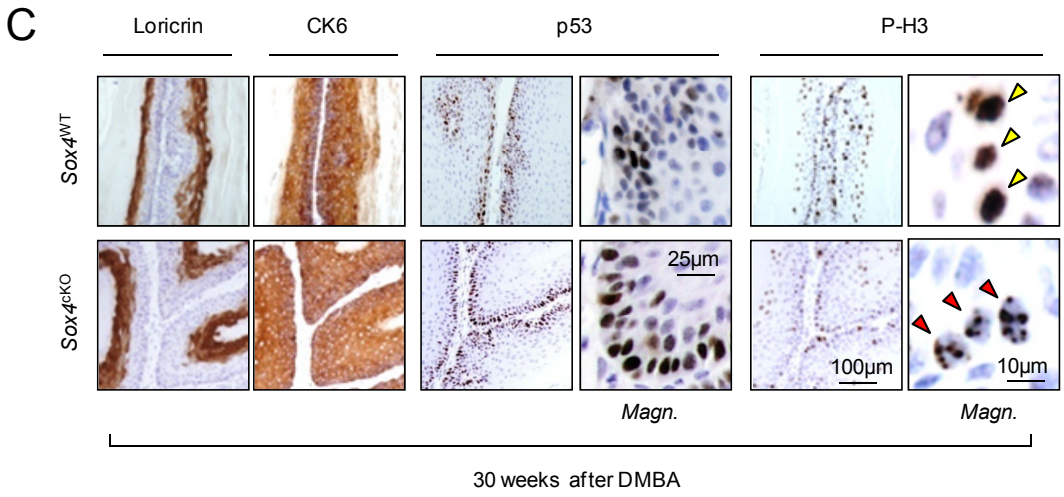

XIII. DMBA/TPA treatment favours melanocytic lesions in the absence of Sox4

Melanoma is the only tumour type in which reduced expression or genomic loss of *Sox4* has been consistently reported in correlation with increased malignancy hitherto (Jafarnejad et al.; Jafarnejad et al.; Zhang and Li, 2012). We have shown that *Sox4*^{cKO} mice have reduced susceptibility to skin tumorigenesis. Nevertheless, we noted that upon TPA/DMBA stimulation a number of melanocytic lesions started to appear in mice from all the studied genotypes. However, both the rate of growth and the number of such lentiginous lesions were notably increased in *Sox4*^{cKO} and Sox4 hypomorphic *Sox4*$^{lox/lox}$ mice. These melanocytic hyperplasias stopped growing after TPA withdrawal, according to the correlation of melanocytic growth with skin stress (Cui et al., 2007). However, in reduced *Sox4* expression contexts (such as in *Sox4*^{cKO}, hypomorphic *Sox4*$^{lox/lox}$ and, though to a lesser extent, in *Sox4*^{HET} mice) these lesions progressed in size and number in good correlation with *Sox4* dosage (Figure 28). Interestingly, we even detected one malignant melanoma with metastasis in the axilar lymph nodes of a *Sox4*^{HET} mouse (Figure 28). This paradoxical result indicates that reduced *Sox4* expression can be causal of melanoma initiation and/or progression, in agreement with the observation that *Sox4* can behave as a tumour suppressor in melanoma despite it prominent role as oncogene in most cellular contexts (Cai et al.; Jafarnejad et al.; Jafarnejad et al.; Zhang and Li, 2012) (Figure 28).

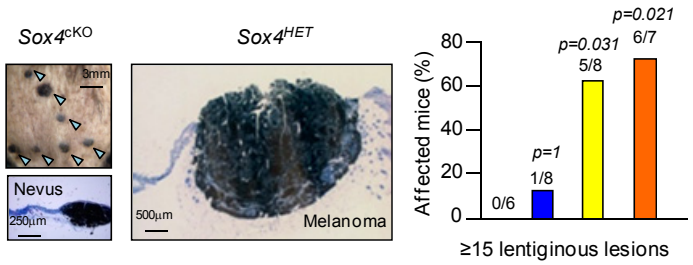

Figure 28. Reduced Sox4 expression levels favour the appearance of melanoma under forced proliferative stimulus.

(Left) Melanocytic lesions in DMBA/TPA-treated *Sox4*^{cKO} mouse skin (blue arrowheads), nevus and melanoma (*Sox4*^{HET}). (Right) proportion of mice bearing >15 melanocytic lesions in mice from the indicated genotypes. Fisher's exact test was used for comparison.

.

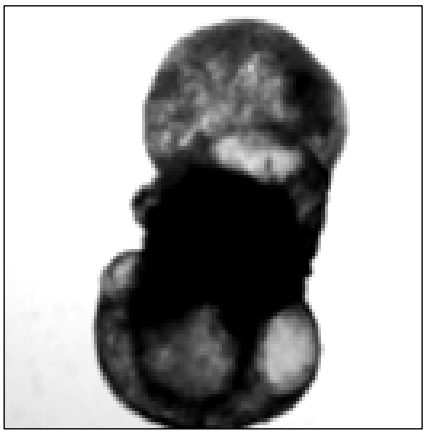

Discussion

"(…) Cuántas veces me pregunto si esto no es más que escritura, en un tiempo en que corremos al engaño entre ecuaciones infalibles y máquinas de conformismos. Pero preguntarse si sabremos encontrar el otro lado de la costumbre o si más vale dejarse llevar por su alegre cibernética, ¿no será otra vez literatura? Rebelión, conformismo, angustia, alimentos terrestres, todas las dicotomías: el Yin y el Yang, la contemplación o la Tatigkeit, avena arrollada o perdices faisandées, Lascaux o Mathieu, qué hamaca de palabras, qué dialéctica de bolsillo con tormentas en piyama y cataclismos de living room. El solo hecho de interrogarse sobre la posible elección vicia y enturbia lo elegible. Que sí, que no, que en ésta está... Parecería que una elección no puede ser dialéctica, que su planteo la empobrece, es decir la falsea, es decir la transforma en otra cosa. Entre el Yin y el Yang, ¿cuántos eones? Del sí al no, ¿cuántos quizá? Todo es escritura, es decir fábula. ¿Pero de qué nos sirve la verdad que tranquiliza al propietario honesto? (…)".

Julio Cortázar. Rayuela, Cap. 1

I. Sox4 is dispensable for mES differentiation and iPS generation

Mammalian embryonic development consists on the generation of specialised tissues composed of a variety of cells that arise from an original multipotent embryonic stem cell (Smith, 2001). Likewise, adult tisular homeostasis is maintained through input coming from the tissue stem cells that fuel with fresh cells those tissues that have lost their integrity during normal tissue homeostasis or wounding (Blanpain and Simons, 2013).

The dogma of the Waddington's deterministic, irreversible epigenetic landscape along differentiation was first challenged when Gurdon demonstrated in the late 1950's that it was indeed possible to revert a cell's fate by means of nuclear transfer when he generated the first cloned organism, obtained from somatic cells (Gurdon et al., 1958). More than 40 years later, Yamanaka and colleagues achieved another milestone in the field of somatic nuclear reprogramming when they demonstrated that it was possible to revert a differentiated cell's status to that of embryonic stem-like by transducing a differentiated cell with a cocktail of just four transcription factors. These induced-pluripotent stem cells (iPS cells) were capable of giving rise to all the cellular lineages in a similar fashion to that of mES cells and therefore overcome the ethical issues that arise from the use of human embryonic stem cells (Takahashi et al., 2007; Takahashi and Yamanaka, 2006).

However in nature, while stem cells specialize and differentiate they also lose part of their potency, and as so in adult organisms the so-called somatic (or adult) stem cells are uni-, bi-, or multi-potent, therefore being capable of giving rise to only few, but not all, cellular lineages, as opposed to embryonic stem cells (Wagers and Weissman, 2004). To prevent stem cell exhaustion, the other main feature of stem cells besides differentiation into specialised tissues through asymmetrical cell division is that they are also capable of self-renew through symmetrical division whereby they generate identical daughter cells that ensure a stable population of stem cells (Sharpless and DePinho, 2007). The decisions that govern the balance between self-renewal and differentiation are tightly controlled through the interaction of extrinsic cues (such as fluctuating environmental stimuli) with intrinsic mediators of the cell behaviour (such as chromatin remodelers and transcription factors) (Simons and Clevers, 2011). Among the above-mentioned intrinsic factors, the family of Sox proteins is known to play major roles in regulating processes associated to cell fate decisions (Lefebvre et al., 2007; Sarkar and Hochedlinger, 2013). Not surprisingly, some of the Sox factors also play crucial roles in the differentiation and

maintenance of somatic stem cells, such as Sox1 or Sox9 in neural and skin stem cells respectively (Nowak et al., 2008; Sarkar and Hochedlinger, 2013), or in the generation of iPS cells, such as Sox2 (Takahashi and Yamanaka, 2006).

In this work we have focused our attention in Sox4, one of the poorest-studied Sox members in the context of adult tissues and embryonic/somatic stem cell biology (Sarkar and Hochedlinger, 2013). For that, we have generated mice bearing an excisable KI cassette that would allow us to track cells expressing Sox4 *in vivo;* the KI cassette was flanked by LoxP sites to functionally address the results of its ablation in adult organisms and stem cells (Figure 6).

First of all, we have observed an upregulation of Sox4 mRNA expression levels in WT mES cells treated with retinoic acid to promote neuroectoderm differentiation inversely paralleled by a progressive reduction along acquisition of pluripotency (Figure 7A-C). These results were exciting, as they suggested that Sox4 could constitute a break during reprogramming. In this regard, promising results arising from high-throughput mRNA sequencing in iPS treated with 2i (*naïve* pluripotent cells) compared to FBS-treated cells (*primed* state) showed upregulation of Sox4 in primed iPS cells, suggesting indeed that this factor could represent an early trigger during the loss of pluripotency (Marks et al., 2012). Taking advantage of our mouse model bearing a KI-excisable cassette at the Sox4 locus, we first tested whether Sox4 could boost reprogramming. We actually observed decreased reprogramming efficiency in the absence of Sox4, but we obtained iPS cells depleted of Sox4 expression that besides displayed normal expression levels of pluripotency factors (Figure 7). Aiming to test whether Sox4 could be relevant during stem cell differentiation instead, we performed teratoma-mediated assays and detected contribution to all embryonic layers, indicating that Sox4 is largely dispensable at least during the first stages of mammalian embryonic development. These results go in line with the observation that Sox4-null embryos can develop until midgestation (E14.5) (Penzo-Mendez, 2010; Schilham et al., 1996), in contrast to Sox2-null embryos, for example, whose development in severely impaired at the two-cell stage (Sarkar and Hochedlinger, 2013). Interestingly, the reduction in reprogramming efficiency and the slightly reduced velocity of teratoma growth are suggestive of imperfect induction of proliferation, required for both reprogramming and differentiation, an effect that we later observed also in adult stem cells from the skin (see below).

II. Sox4 is required for normal adult tissue homeostasis

We next sought to address the role of *Sox4* in the adult organism. We generated a KI cassette targeted to the Sox4 locus in order to achieve expression of a reporter protein driven by the endogenous Sox4 promoter. This would allow us to *in vivo* track cells expressing Sox4, by means of direct GFP or Luciferase detection. Unfortunately, we could not detect any GFP-positive cell, indicative of interference of the KI cassette with its own expression; most likely this was due to decreased mRNA stability due to the insertion of the distal LoxP site within the 3'-UTR region or rather owing to the IRES sequence (decreased translation was not likely, given that we detected the expression changes at the mRNA level, see below). Nevertheless, we observed a notable reduction in the Mendelian proportions at birth of mice from the *Sox4*$^{lox/lox}$ genotype likely due to mother's disregard after smaller pups, as observed in other settings (Ortega-Molina et al., 2012) or decreased fitness of these pups; we could confirm that these mice were indeed hypomorphic and bear reduced Sox4 levels across tissues by qPCR (Figure 12). We took advantage of this peculiarity and obtained the first viable adult mouse model with reduced Sox4 levels in adult tissues. This allowed us demonstrate for the first time that moderately decreased *Sox4* levels allow the progression throughout embryogenesis and produces viable organisms, in contrast to full abrogation of Sox4 (Bhattaram et al., 2010; Schilham et al., 1996); interestingly, Sox4 global downregulation leads to an earlier onset of several age-related pathologies, pointing out towards a prominent role for Sox4 in maintaining proper adult tissue homeostasis, beyond its roles during embryogenesis. This is of great interest, as before the publication of this thesis there was a recognised vast lack of knowledge with regard to the functions of Sox4 in adult tissues (Sarkar and Hochedlinger, 2013); so far the results of Sox4 abrogation had only been addressed either during embryonic development or in haematopoietic and lymphoid cells obtained from Sox4-null foetal-liver cells or thymic cultures (Schilham et al., 1997); only recently conditional deletion in lymphocytes (Kuwahara et al., 2012; Malhotra et al., 2013; Sun et al., 2013), and in developing kidney and retina have been achieved so far (Huang et al., 2013; Jiang et al., 2013).

A marked reduction was observed in the mean and maximum lifespan of *Sox4*$^{lox/lox}$ mice when compared to WT cohorts. Interestingly, we found decreased cancer-associated pathologies (20% of mice) in these mice when compared to WT mice at the humane end point, meaning that they died because of degenerative lesions rather than cancer, as

opposed to 80% of WT mice (Figure 10 and Table 3). Among the most prominent findings associated to ageing, hypomorphic Sox4 mice presented bone frailty due to decreased bone mineral density. This is an interesting result, according to previous reports showing that Sox4 is expressed in bone and positively regulated through parathyroid hormone signalling specifically in cultured osteoblasts (Reppe et al., 2000). In addition, human patients suffering from osteopetrosis secondary to hyperparathyroidism condition show increased Sox4 mRNA expression as assessed through microarray profiling of transiliacal bone biopsies; interestingly, a two-year follow-up analysis in one of the patients who undertook surgical removal of the parathyroid gland showed a reversion to normal levels of bone remodelling parameter, including Sox4, in response to normalised PTH levels (Reppe et al., 2006). Moreover, Sox4 haploinsufficiency in mice resulted in decreased bone mineral density and reduced trabecular mesh, as seen by DEXA and micro-computerised tomography (μCT), due to a specific defect in osteoblast-mediated bone remodelling. Upon culture of calvarian osteoblasts in the context of Sox4 haploinsufficiency or siRNA-mediated downregulation of Sox4, the authors demonstrated reduced proliferation and differentiation defects in osteoblast-specific markers such as *osterix* and *osteocalcin* in a *Run*x2-independent manner. The differences in BMD grew bigger in old mice, in support of a age-related progressive loss of proper bone homeostasis (Nissen-Meyer et al., 2007). The connection of bone loss with age in a Sox4-dependent manner has further been proven in post-menopausal women through association studies (Duncan et al., 2011; Jemtland et al., 2011), providing exciting insights into possible development of treatments for this type of osteoporosis, and Sox4 hypomorphic mice can be of great use in research in this topic, given that it can model this human condition in a closer fashion to what happens in the real situation.

We also observed other age-associated pathologies and biomarkers such as increased incidence of dilated cardiomyopathy, pyometra and hepatic failure, together with shorter PBMC telomere length in *Sox4*$^{lox/lox}$ mice. There is a reminiscence of the vastly-characterised heart-associated defects during embryonic development in the absence of Sox4 with the incidence of cardiomyopathy in *Sox4*$^{lox/lox}$ mice (Paul et al., 2013; Penzo-Mendez et al., 2007; Schilham et al., 1996; Ya et al., 1998). It is tempting to think of a possible function for Sox4 in the homeostasis of the adult heart, paralleling the prominent role that this protein exerts during heart morphogenesis. The impact of Sox4 in different cell types and in cardiac extracellular matrix remodelling during embryonic development could in our hypomorphic mice either result in congenital, non-lethal defects that only become evident with age or rather a manifestation of a role for Sox4 in adult

heart homeostasis (Paul et al., 2013), an interesting subject of study in the future. The presence of pyometra is also an exciting observation, given its marked association to progressive degeneration of the uterine wall with age (Verstegen J, 2008). Given that Sox4 expression in adult female mice has been found in correlation with oestrus, we cannot discriminate between a side effect of possible hormonal deregulation in the presence of reduced Sox4 levels, or a decline in the integrity of the uterine wall (Hunt and Clarke, 1999). There are no studies showing correlation of liver function with Sox4 thus far, with the exception of the increased Sox4 expression found in tumours (Hur et al., 2010; Liao et al., 2008), therefore we speculate that increased hepatic failure could be, in principle, secondary to the onset of a general degenerative process and progressive loss of cellular fitness overall. An extremely exciting result to us was the correlation of the decreased survival with the reduced mean telomere length in peripheral blood (Figure 11). Telomere length is one of the most acknowledged molecular biomarkers of ageing, given the correlation of replicative age with telomere erosion (Canela et al., 2007; Lopez-Otin et al., 2013; Vera et al., 2012) and the causality of shortened telomeres in the accelerated onset of age-related pathologies, as ascertained from studies in telomerase-deficient mice and telomerase reintroduction or reactivation and its impact on age and lifespan (Bernardes de Jesus and Blasco, 2011; Bernardes de Jesus et al., 2011; Bernardes de Jesus B, 2012). Interestingly, global downregulation of *Sox4* mRNA in *Sox4*$^{lox/lox}$ mice also resulted in a reduced incidence of spontaneous cancer, indicating that Sox4 is necessary for tumour development and providing genetic evidence for previous reports demonstrating oncogenic activity of Sox4 and its requirement for cellular transformation (Penzo-Mendez, 2010; Vervoort et al., 2013b). Further connections of Sox4 with ageing and its impact in cancer were obtained recently, when an inverse correlation of Sox4 expression with age and p16 mRNA levels was observed in mouse lungs and this was proposed to function as an anti-tumour mechanism in small cell lung carcinoma onset (Castillo et al., 2012).

III. Role of Sox4 in skin homeostasis and regeneration

Sox4 is the only SoxC class member whose expression has been detected by in developing hair follicles (Dy et al., 2008). Moreover, during normal hair cycling, expression of Sox4 was observed in the hair progeny during anagen (proliferative), but not during telogen (resting) phase (Lowry et al., 2005). To gain deeper knowledge into the

consequences of *Sox4* abrogation in adult tissues, we generated mice conditionally deleted for *Sox4* in the skin (*Sox4*^{cKO} mice). We expected a dramatic skin condition, in a similar fashion to deletion of other Sox factors expressed in skin such as Sox9, which is also induced during morphogenesis (Nowak et al., 2008). We found a moderate increase in skin atrophy and hyperpigmentation in our hypomorphic Sox4 mouse model (Table 3). However, we did not see any overt defects in skin stratification and mice displayed a largely normal hair coat upon gross examination. Nonetheless, the tail skin hyperpigmentation phenotype that we previously observed in *Sox4*$^{lox/lox}$ mice was incremented upon full Sox4 abrogation. After close examination of *Sox4*^{cKO} mouse skin, we detected decreased proliferation, concomitant with accumulation of short telomeres and DNA damage and senescence/ageing markers such as p16 and p19 at the tail skin epidermis. These results reinforced the pro-ageing phenotype that we detected upon global downregulation of Sox4 in the whole organism in hypomorphic mice.

Decreased mean telomere length and accumulation of short telomeres have been previously observed to happen in a progressive manner in ageing mouse tail skin (Flores et al., 2008). Moreover, reduced telomere length limits the regenerative potential of skin stem cells (Flores et al., 2006; Flores et al., 2005), and this has obvious implications in the accelerated onset of ageing (Donate and Blasco, 2011). The striking longer telomere length observed in *Sox4*^{cKO} mice hair bulge (the main skin stem cell niche in tail skin) is suggestive of decreased replicative history in HFSCs, likely reflecting stem cell resistance to activation cues and thus accounting for the accelerated ageing seen in the most differentiated parts of the skin (Flores et al., 2008). If this hypothesis was true, we should expect a deteriorated response of HFSCs upon forced proliferation cues in the absence of Sox4. Indeed, when we performed hair plucking to compel entry into hair cycle, we saw specific upregulation of Sox4, indicating likely a role for this protein during hair regeneration; moreover, Sox4 depletion resulted in delayed, but not abrogated, wound healing and hair coat regeneration. We also detected accumulation of DNA damage at stem cell compartments and decreased proliferation in Sox4-depleted skin undergoing plucking-induced regeneration.

It has been largely demonstrated that accumulation of DNA damage is one of the driving forces of ageing, and one of its *bona fide* molecular biomarkers (Hoeijmakers, 2009; Lopez-Otin et al., 2013). DNA damage accumulates naturally with age, thus limiting stem cell function (Sharpless and DePinho, 2007); the proof that accumulation of DNA damage leads to accelerated ageing arises from engineered mouse models with deficiencies in distinct DNA repair pathways, that show accelerated ageing due to a faster

stem cell decline (Schumacher et al., 2008). Age-dependent stem cell dysfunction seems to be one of the major determinants in mammalian lifespan regulation due to the accelerated loss of the regenerative capacity of somatic tissues (Lombard et al., 2005; Signer and Morrison, 2013). We have observed an exacerbated DNA damage accumulation at stem cell compartments upon induction of forced proliferation with plucking (Figure 22), likely indicating replication stress sensitivity, in line with previous reports showing an XRCC1-dependent sensitivity to DNA damage and subsequent γH2AX accumulation in Sox4 depleted cells (Chetty et al., 2012). We can hypothesize on the other hand that the accumulation of DNA damage could be indicative of ageing due to defective stem cell activation and tissue maintenance. As we have detected increased γH2AX staining in both resting tail skin (thus indicating a persistent accumulation of DNA damage likely due to stem cell dysfunction and subsequent accelerated ageing) but also in the short-term, right after induction of proliferation of HFSCs upon plucking (thus probably indicating increased sensitivity to RS), we cannot rule out either of the hypothesis, but assume that they act in a concerted manner to contribute to accelerated ageing in skin depleted of Sox4.

In order to further dissect the molecular mechanisms causing accelerated ageing, DNA damage accumulation and hampering stem cell activation, we performed microarray-based transcriptional profiling of WT and cKO mice undergoing hair regeneration. We validated our microarray by confirming downregulation in a Sox4 signature and downregulation of known Sox4 target genes.

We then analysed the gene set enrichment by using the NCI, Reactome and KEGG repositories; we observed a notable downregulation in a number of cell cycle and DNA repair pathways in Sox4-deficient skin undergoing regeneration. This confirms the previously observed resistance to induction of proliferation and accumulation of DNA damage by IHC (Figure 22). On one hand, the cell cycle-inducing abilities of Sox4 have been broadly demonstrated, in the context of cancer cell biology (Bilir et al., 2013; Cai et al., 2011; Yu et al., 2013). On the other hand, the marked downregulation in DNA damage repair pathways in the face of γH2AX accumulation could underline an inefficient DDR in the absence of Sox4, therefore leading to accumulation of unrepaired DNA. There are reports demonstrating that Sox4 is induced upon DNA damage in an ATM/ATR-dependent pathway (Pan et al., 2009); however in this context the authors found a striking tumour-suppressive function for Sox4 in mediating p53 stabilization, inducing apoptosis and preventing cell cycle entry. Other groups have found similar accumulation of Sox4

upon genotoxic agents, associated however in this case to radiation-resistance and linked to p53 downregulation; in fact, Sox4-depleted cells spontaneously accumulate DNA damage and are extremely sensitive to IR (Chetty et al., 2012). In light of these and our results, we propose a model in which Sox4 can be activated to alleviate this stress, and therefore its absence leads to accumulation of stress and blockade of cell cycle progression under certain situations, such as oncogenic or hair follicle stem cell activation (Figure 29).

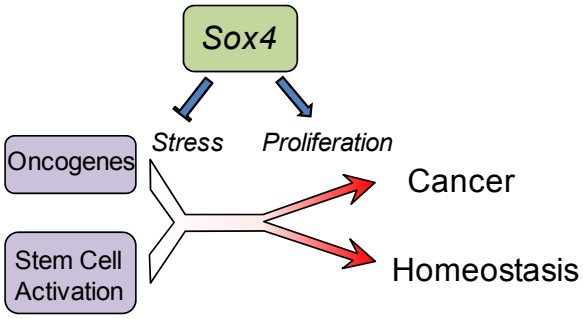

Figure 29. Model for Sox4-mediated alleviation of stress to promote cell cycle progression under oncogenic or replicative stresses, and its impact in cancer and homeostasis.

Interestingly, we also observed a significant downregulation of pathways related to HFSC activity, such as Myc and Hedgehog (Kobielak et al., 2007; Watt et al., 2008). We further confirmed a defective HFSC activation specific to hair plucking-induced hair regeneration by testing a list of genes which have been recently linked to Wnt-activated β-catenin-sensitive plucking-induced transcriptional program. According to this work, Tcf3/4 levels prevent HFSC activation and promote quiescence. When the Wnt pathway becomes activated β-catenin-mediated alleviation of the repression exerted by the Tcf3/4 complex results in transcriptional activation of a subset of genes relevant for the initiation of hair follicle differentiation programs (Lien et al., 2014). The downregulation of these β-catenin-sensitive Wnt targets reveals specific deficiencies in the overcome of the threshold that leads to HFSC activation in the absence of Sox4. Interestingly, Sox4 was itself one of such genes included in the *Cttnb1*-sensitive gene set (Figure 24), in agreement with our results showing Sox4 upregulation upon plucking (Figure 21) and previous results suggesting Sox4 upregulation as a result of hair follicle cycling-mediated Wnt/βcatenin activation (Lowry et al., 2005). In this regard, it has been also demonstrated that Wnt pathway induces Sox4 in several settings to promote tumorigenesis by modulating the Wnt transcriptional output (Bilir et al., 2013; Cai et al., 2011; Lai et al., 2011; Lee et al., 2011). Nevertheless, the molecular mechanism by which Sox4 controls

Wnt/β-catenin signalling still remains poorly understood. There is a clear consensus claiming cooperation among the canonical Wnt pathway and Sox4, in contrast to other Sox members, such as Sox17. In the colon adenocarcinoma cell line SW480, Sox4 was shown to stimulate Wnt/β-catenin activity by preventing proteasomal degradation of β-catenin through direct interaction with β-catenin and TCF/LEF factors (Sinner et al., 2007). A direct interaction with TCF4 has also been reported by independent studies, this time excluding direct interaction of Sox4 with β-catenin during morular differentiation of endometrial carcinomas (Saegusa et al., 2012). Others have attributed the Sox4-dependent modulation of the Wnt pathway to the interaction of Sox4 with Plakoglobin; the formation of a Sox4-plakoglobin transcriptional complex in a Wnt3a-dependent manner induces direct transcriptional regulation of Wnt target genes such as Dicer and Axin2 among others (Lai et al., 2011). In skin, Bmpr1 signalling blocks Wnt-mediated expression of Sox4 and this constitutes a threshold orchestrated by the dermal papilla to govern HFSC activation (Kobielak et al., 2007). All these results indicate a plethora of possibilities for Sox4-mediated regulation of and activation by Wnt signalling pathway. Regardless of the molecular mechanism, that can be highly variable depending on the cell of origin, the metabolic and/or the transformation status of such cells, it is clear that at least in skin Sox4 is induced upon Wnt cues and modulates its transcriptional output, likely by long-range genomic interactions of Wnt-target promoters and Sox4-associated enhancers.

We, in light of our microarray results and current published literature, propose a role for Sox4 in modulating the repression that Tcf3/4 exerts on Wnt targets in resting hair follicles. Upon stimulus that activate the HFSC to initiate proliferation and differentiation programs, Sox4 is induced to counterbalance Tcf3/4 repression and therefore favour β-catenin-mediated activation of genes required for hair regeneration (Figure 30).

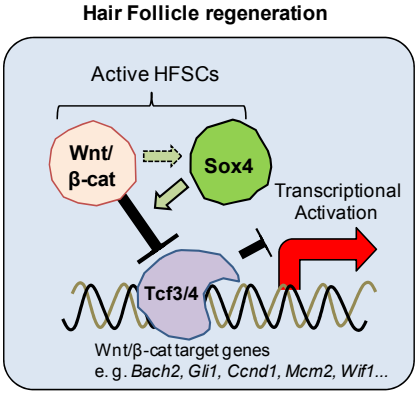

Figure 30. Modulation of Wnt/β-catenin output by Sox4 upon hair regeneration cues.

Interestingly, very recent studies focused on the transcription factor C/EBPα (a major hub in myeloid lineage specific differentiation genes in the haematopoietic compartment) discovered that it is actually a direct repressor of Sox4 (Zhang et al., 2013), and this was shown to function as a preventive mechanism for uncontrolled proliferation, providing a molecular mechanism for the development of a specific subtype of myeloid leukemia (Fung et al., 2013). Besides its implication in tumour development, the authors also discovered that Sox4 is also required for normal haematopoiesis, and when depleted by means of shRNA in total bone marrow cells, there is a progressive loss of colony-forming abilities along passages, an *in vitro* approach to model stem cell ageing. The authors did not go beyond this observation in studying stem cell maintenance, but these results clearly point out towards a requirement of Sox4 for long-term maintenance of competent adult stem cells, given that Sox4 depletion mimics stem cell ageing phenotypes. This goes in line with our own observations in skin, and suggesting a role for Sox4 in regulating somatic stem cells from a broad panel of tissues.

Overall, Sox4 seem to modulate both HFSC activation and alleviation of DNA damage, and both pathways seem to be cross-wired as an adaptive solution to improve survival and tolerate moderate stress levels, at the cost of accelerating the oraganism decline (Rossi et al., 2007).

IV. Sox4 is required for chemically-induced skin carcinogenesis

We observed that hypomorphic Sox4 mice are resistant to spontaneous cancer onset. This appreciation goes in line with a general reduction of Sox4 levels in this mouse model, and provides genetic evidence that highlights the requirement of Sox4 for cellular transformation. Most studies showing the implication of Sox4 in cancer have vastly demonstrated that Sox4 is indeed sufficient for achieving transformation, either alone or in combination with additional pro-oncogenic insults (Vervoort et al., 2013b). However, our results suggest that Sox4 expression can constitute a key event during the acquisition of a malignant phenotype. We further proved that by means of conditional ablation of Sox4 in skin. We demonstrated that not only upon intrinsic cues, but also during multistep chemically-induced carcinogenesis, absence of Sox4 correlates with resistance to cell transformation. This can be explained by a decrease in proliferation, as observed both at early time points after TPA treatment and at benign skin lesions (papilloma). The interest of proving the oncogenic effects of Sox4 in skin stems also from the fact that Sox4 has been detected overexpressed in most types of tumours; however non-melanoma skin cancer is largely disregarded in these studies (Vervoort et al., 2013b). Of note, elevated Sox4 levels associated to stratified epithelial-type cancer, such as squamous cell carcinoma (SCC) from different tissues, displays good correlation with disease progression as ascertained from cancer databases such as Oncomine (Figure 31).

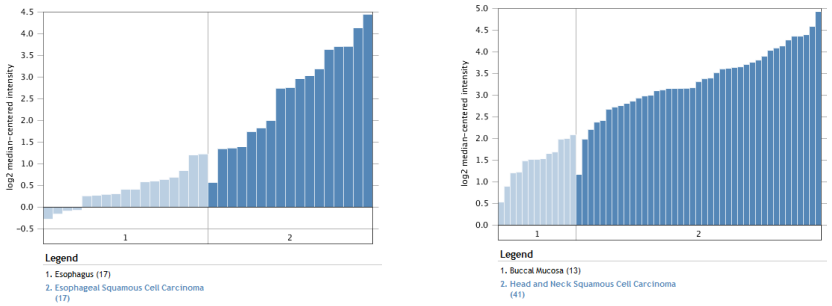

Figure 31. Relative Sox4 expression levels in esophageal SCC (left, dark blue) and head and neck SCC (right, dark blue) compared to normal tissue (light blue). Source: Oncomine.

We have demonstrated that abrogation of Sox4 prevents skin carcinogenesis. The diminished cell transformation is probably due to the resistance to respond to proliferation-

inducing agents, as assessed by reduced Ki67 staining after short or long-term treatment with TPA. This phenotype parallels the delay in hair regeneration and induction of hair cycling upon hair plucking, as shown by of hair coat regeneration dynamics, IHC and transcriptional profiling. Therefore, Sox4 provides a connection between the processes involved in stem cell activation and cancer development. In support of that hypothesis, most of the DEGs that we found in our microarray of skin undergoing regeneration are linked to cancer, further reinforcing the interconnection of stem cell activation with cancer. In this regard, a recent report showing contribution of mobilized *Sox4*-positive, activated HFSC owing to E6/E7 oncoprotein activity suggests an intimate connection between HFSC activation, *Sox4*-positive progeny and skin tumorigenesis (da Silva-Diz et al., 2013). In this context, a resistance to HFSC activation could act as a preventive barrier to the onset of cellular transformation. However, there are a number of reports showing a connection of Sox4 with the acquisition of pro-invasive features typical of EMT, and therefore usually linked to metastatic colonization of distant tissues rather than a prevention in the initial steps of epithelial carcinogenesis (Parvani and Schiemann, 2013; Vervoort et al., 2013a; Wang et al., 2013). Nonetheless, there are other reports showing how Bmpr1 abrogation can lead to deregulated expression of a panel of genes associated to the Wnt signalling pathway, among which they found Sox4. This resulted in loss of the quiescence signalling in the niche, but not in the HFSC, leading to the appearance of tumour-like cysts reminiscent of pylomatrichoma lesions in humans (Kobielak et al., 2007). Therefore we cannot but assume that Sox4 influences carcinogenesis both at early and late stages of cellular transformaction and metastatic colonization.

Finally, an interesting side-observation linked Sox4 to melanomagenesis in the course of the TPA/DMBA assays. While all the treated mice developed melanocytic lesions during the 15-week TPA treatment, Sox4-reduced contexts such as $Sox4^{cKO}$, $Sox4^{lox/lox}$, and $Sox4^{HET}$ mice bore increased number of them from the beginning (not shown). When we stopped the TPA treatment to assess tumour dependence on proliferative cues, we observed progressive disappearance of such lesions in Sox^{WT} mice, but not in the rest of genotypes. In fact, they even increased in size and number, and we even detected a metastatic melanoma in the lymph nodes of a $Sox4^{HET}$ mouse. As mentioned before, melanoma is the only type of tumour in which reduced Sox4 levels seem to be detrimental for tumour prognosis and disease progression, in conflict with the observations in all other types of tumours, in which the roles of Sox4 pinpoint it definitely as an oncogene. Nevertheless, these paradoxical appreciations cannot be consistently reproduced even in studies arising from the same research groups and to our eyes is a

reflection of the paradigmatic intrinsic heterogeneity of this type of tumours, that hampers tumour stratification according to common genetic somatic events (Curtin et al., 2005). It is tempting to speculate that absence of Sox4 can wire a transcriptional program relevant for melanoma malignization without promoting transformation in this cell context, and that in certain situation such as p16 loss, this pre-malignant setting can turn the melanocytic benign nevi into metastatic melanoma (Figure 32).

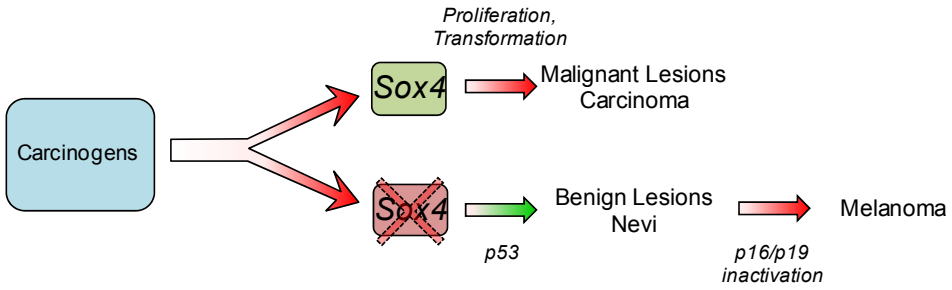

Figure 32. Model for the postulated sequence of events that coonects Sox4 loss with the onset of melanoma.

In this regard, recent studies show that SPARC (secreted peptide acidic and rich in cystein), a protein involved in matrix remodelling and a natural cellular inhibitor of Sox4 (Coskunpinar et al., 2013; Chiodoni et al., 2010), has opposing roles to Sox4 in most tumours and its overexpression usually leads to apoptosis, while its loss is associated with disease progression and radioresistance, as expected (Chetty et al., 2012; Said et al., 2013). Interestingly, melanoma constitutes an exception to this precept, and SPARC is usually increased during melanoma progression in contrast to Sox4, and its depletion prevents cancer cell growth (Maloney et al., 2009), in support for a negative role for Sox4 in this specific type of cancer, whose origins still remain to be investigated

Our results, overall, show that Sox4 is an important factor in modulating the pace of somatic stem cell activation. Its deletion leads to delayed stem cell activation and regeneration of damaged tissues, without excessively compromising their integrity. Its permanent ablation or reduced levels can lead to accelerated ageing and loss of normal tissue homeostasis; however, the most notable effect of Sox4 deletion is the acquired resistance to chemical skin carcinogenesis. So far, Sox4 had been studied in depth in the

context of most tumour types but non-melanoma skin cancer. Our results suggest that the inhibition of Sox4 could prove useful in preventing the expansion of malignant cells, and our new mouse model contributes to a better understanding of the *in vivo* roles of Sox4 in adult tissues in organ homeostasis, cancer and ageing.

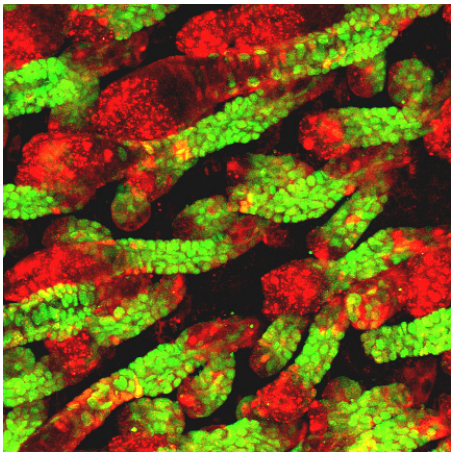

Conclusiones

"(…)
—Más o menos —concedió Oliveira—. Es increíble lo que te cuesta captar las nociones abstractas. Unidad, pluralidad... ¿No sos capaz de sentirlo sin necesidad de ejemplos? No, no sos capaz. En fin, vamos a ver: tu vida, ¿es una unidad para vos?
—No, no creo. Son pedazos, cosas que me fueron pasando. (…)".

Julio Cortázar. Rayuela, Cap 19

1. Sox4 se sobreexpresa durante la diferenciación de células madre embrionarias y se reprime durante la generación de iPS. Sin embargo, Sox4 es dispensable para la generación de iPS y para la diferenciación a todas las capas embrionarias.

2. Los ratones *Sox4*$^{lox/lox}$ con expresión reducida de Sox4 en todos sus tejidos constituyen el primer modelo de ratón con niveles de Sox4 globalmente reducidos en todo el organismo adulto.

3. Los ratones *Sox4*$^{lox/lox}$ nacen en ratios sub-mendelianos; la expresión reducida de Sox4 correlaciona con síntomas de envejecimiento acelerado tales como adiposidad disminuida, fallo hepático crónico, fragilidad ósea y reducción de la supervivencia. Estos ratones presentan telómeros cortos y son resistentes al cáncer espontáneo.

4. La eliminación condicional de Sox4 en epitelio estratificado no altera a la correcta estratificación de la piel pero aumenta la frecuencia de hiperpigmentación y disminuye la proliferación y el grosor epidérmico.

5. La eliminación de Sox4 genera envejecimiento prematura de la piel con reducción de longitud telomérica, acumulación de p53/p16/p19 y daño en el DNA en la IFE de la piel de cola. Los telómeros alargados en el compartimento de células madre de la piel sugieren mayor quiescencia en ausencia de Sox4.

6. Sox4 se induce con la depilación de forma específica y secuencial. La ausencia de Sox4 resulta en la acumulación de daño en el DNA y menor proliferación de keratinocitos, generando un retraso en la regeneración del pelaje. La ausencia de Sox4 también causa retraso en el cierre de heridas.

7. La ausencia de Sox4 genera desregulación específica de genes relacionados con las vías de ciclo celular, respuesta a daño en el DNA y Myc/Hedgehog/Wnt, durante la regeneración del pelo post-depilatoria.

8. La expresión de Sox4 es necesaria para la carcinogénesis química y su ausencia reduce la incidencia de tumores y aumenta la resistencia a transformación celular. Por el contrario, el número de lesiones melanocíticas aumenta, sugiriendo un papel para dicha proteína en melanomagenesis.

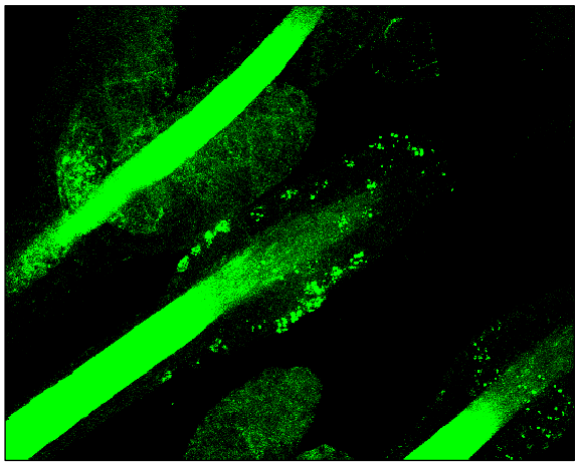

Conclusions

"(…) se entrara por una puerta cualquiera a un jardín cualquiera, a un jardín alegórico para los demás, como los mandalas son alegóricos para los demás (…) a lo mejor todo eso no era más que una nostalgia del paraíso terrenal, un ideal de pureza, solamente que la pureza venía a ser un producto inevitable de la simplificación, (…)".

Julio Cortázar. Rayuela, Cap 18

1. Sox4 is overexpressed during mES differentiation and repressed during iPS reprogramming. Sox4 expression is dispensable for the generation of iPS cells and differentiation into all the embryonic layers.

2. Hypomorphic *Sox4*$^{lox/lox}$ mice, bearing decreased *Sox4* mRNA across tissues constitute the first viable mouse model with globally-reduced Sox4 expression in the adulthood. These mice are viable and fertile.

3. *Sox4*$^{lox/lox}$ mice are born at sub-mendelian ratios; reduced Sox4 levels result in a premature onset of age-associated pathologies such as reduced adiposity, chronic hepatic failure, bone frailty and reduced lifespan. These mice also bear short telomeres and are cancer-resistant.

4. Conditional ablation of *Sox4* in stratified epithelia results in normal skin stratification but increased skin hyperpigmentation, reduced proliferation and epidermal thinning.

5. Sox4 abrogation causes premature skin ageing, as evidenced by shortened telomeres, accumulation of p53, p16/p19 mRNA and DNA damage in tail skin IFE. Longer telomeres at the HFSC compartment are suggestive of increased quiescence in the absence of Sox4.

6. Sox4 mRNA is specifically induced after plucking in a stepwise manner. Hair depilation in a Sox4-depleted context results in DNA damage accumulation and reduced proliferation in skin keratinocytes, resulting in delayed hair coat regeneration. Sox4 depletion also results in a slowed-down wound healing.

7. Sox4 depletion correlates with a specific downregulation of cell cycle, DNA damage response and Myc/Hedgehog/Wnt pathways, as assessed by microarray profiling, during plucking-induced hair regeneration.

8. Expression of Sox4 is required for chemical skin carcinogenesis and its absence results in strongly reduced tumour burden, and resistance to cell transformation *in vitro*. The number and size of melanocytic lesions are increased in Sox4-reduced

contexts upon DMBA/TPA treatment, suggesting a role for this protein in melanomagenesis.

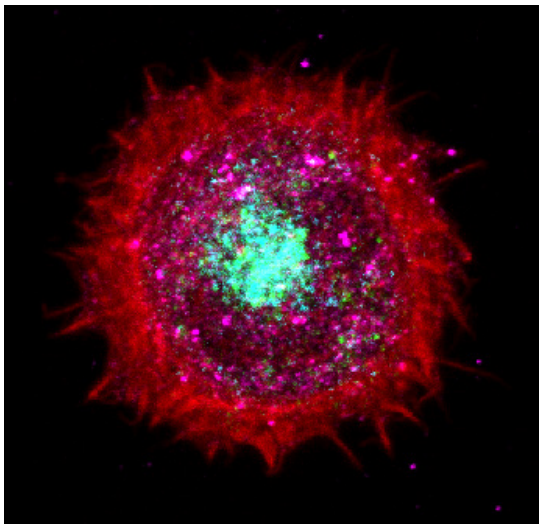

References

"(…) La melancolía de una vida demasiado corta para tantas bibliotecas. Cuando creés que has aprehendido plenamente cualquier cosa, la cosa lo mismo que un iceberg tiene un pedacito por fuera y te lo muestra, y el resto enorme está más allá de tu límite.(…)".

Julio Cortázar. Rayuela, Cap 84

Alonso, L., and Fuchs, E. (2006). The hair cycle. J Cell Sci *119*, 391-393.

Arwert, E.N., Hoste, E., and Watt, F.M. (2012). Epithelial stem cells, wound healing and cancer. Nat Rev Cancer *12*, 170-180.

Aue, G., Du, Y., Cleveland, S.M., Smith, S.B., Dave, U.P., Liu, D., Weniger, M.A., Metais, J.Y., Jenkins, N.A., Copeland, N.G.*, et al.* (2011). Sox4 cooperates with PU.1 haploinsufficiency in murine myeloid leukemia. Blood *118*, 4674-4681.

Bernardes de Jesus, B., and Blasco, M.A. (2011). Aging by telomere loss can be reversed. Cell Stem Cell *8*, 3-4.

Bernardes de Jesus, B., Schneeberger, K., Vera, E., Tejera, A., Harley, C.B., and Blasco, M.A. (2011). The telomerase activator TA-65 elongates short telomeres and increases health span of adult/old mice without increasing cancer incidence. Aging Cell *10*, 604-621.

Bernardes de Jesus B, V.E., Schneeberger K, Tejera AM, Ayuso E, Bosch F, Blasco MA. (2012). Telomerase gene therapy in adult and old mice delays aging and increases longevity without increasing cancer. EMBO Mol Med *4*, 691-704.

Berta, M.A., Baker, C.M., Cottle, D.L., and Watt, F.M. (2010). Dose and context dependent effects of Myc on epidermal stem cell proliferation and differentiation. EMBO Mol Med *2*, 16-25.

Bhattaram, P., Penzo-Mendez, A., Sock, E., Colmenares, C., Kaneko, K.J., Vassilev, A., Depamphilis, M.L., Wegner, M., and Lefebvre, V. (2010). Organogenesis relies on SoxC transcription factors for the survival of neural and mesenchymal progenitors. Nat Commun *1*, 9.

Bies, J., Sramko, M., Fares, J., Rosu-Myles, M., Zhang, S., Koller, R., and Wolff, L. (2010). Myeloid-specific inactivation of p15Ink4b results in monocytosis and predisposition to myeloid leukemia. Blood *116*, 979-987.

Bilir, B., Kucuk, O., and Moreno, C.S. (2013). Wnt signaling blockage inhibits cell proliferation and migration, and induces apoptosis in triple-negative breast cancer cells. J Transl Med *11*, 280.

Blanpain, C., and Fuchs, E. (2006). Epidermal stem cells of the skin. Annu Rev Cell Dev Biol *22*, 339-373.

Blanpain, C., and Fuchs, E. (2009). Epidermal homeostasis: a balancing act of stem cells in the skin. Nat Rev Mol Cell Biol *10*, 207-217.

Blanpain, C., and Simons, B.D. (2013). Unravelling stem cell dynamics by lineage tracing. Nat Rev Mol Cell Biol *14*, 489-502.

Bowles, J., Schepers, G., and Koopman, P. (2000). Phylogeny of the SOX family of developmental transcription factors based on sequence and structural indicators. Dev Biol *227*, 239-255.

Boyd, K.E., Xiao, Y.Y., Fan, K., Poholek, A., Copeland, N.G., Jenkins, N.A., and Perkins, A.S. (2006). Sox4 cooperates with Evi1 in AKXD-23 myeloid tumors via transactivation of proviral LTR. Blood *107*, 733-741.

Braun, K.M., Niemann, C., Jensen, U.B., Sundberg, J.P., Silva-Vargas, V., and Watt, F.M. (2003). Manipulation of stem cell proliferation and lineage commitment: visualisation of label-retaining cells in wholemounts of mouse epidermis. Development *130*, 5241-5255.

Cai, H., Ni, A., Li, W., and Li, J. (2011). Inhibition of melanoma cell proliferation by targeting Wnt/beta-catenin pathway through Sox4 RNA interference. J Huazhong Univ Sci Technolog Med Sci *31*, 565-569.

Canela, A., Vera, E., Klatt, P., and Blasco, M.A. (2007). High-throughput telomere length quantification by FISH and its application to human population studies. Proc Natl Acad Sci U S A *104*, 5300-5305.

Castillo, S.D., Matheu, A., Mariani, N., Carretero, J., Lopez-Rios, F., Lovell-Badge, R., and Sanchez-Cespedes, M. (2012). Novel transcriptional targets of the SRY-HMG box transcription factor SOX4 link its expression to the development of small cell lung cancer. Cancer Res *72*, 176-186.

Collado, M., Blasco, M.A., and Serrano, M. (2007). Cellular senescence in cancer and aging. Cell *130*, 223-233.

Coskunpinar, E., Oltulu, Y.M., Orhan, K.S., Tiryakioglu, N.O., Kanliada, D., and Akbas, F. (2013). Identification of a differential expression signature associated with tumorigenesis and metastasis of laryngeal carcinoma. Gene.

Cui, R., Widlund, H.R., Feige, E., Lin, J.Y., Wilensky, D.L., Igras, V.E., D'Orazio, J., Fung, C.Y., Schanbacher, C.F., Granter, S.R.*, et al.* (2007). Central role of p53 in the suntan response and pathologic hyperpigmentation. Cell *128*, 853-864.

Curtin, J.A., Fridlyand, J., Kageshita, T., Patel, H.N., Busam, K.J., Kutzner H, Cho, K.H., Aiba, S., Bröcker, E.B., LeBoit, P.E.*, et al.* (2005). Distinct sets of genetic alterations in melanoma. N Engl J Med *353*, 2135-2147.

Chen, L., Xiao, Z., Meng, Y., Zhao, Y., Han, J., Su, G., Chen, B., and Dai, J. (2012). The enhancement of cancer stem cell properties of MCF-7 cells in 3D collagen scaffolds for modeling of cancer and anti-cancer drugs. Biomaterials *33*, 1437-1444.

Chetty, C., Dontula, R., Gujrati, M., Dinh, D.H., and Lakka, S.S. (2012). Blockade of SOX4 mediated DNA repair by SPARC enhances radioresponse in medulloblastoma. Cancer Lett *323*, 188-198.

Chiodoni, C., Colombo, M., and Sangaletti, S. (2010). Matricellular proteins: from homeostasis to inflammation, cancer, and metastasis. Cancer Metastasis Rev *29*, 295-307.

da Silva-Diz, V., Sole-Sanchez, S., Valdes-Gutierrez, A., Urpi, M., Riba-Artes, D., Penin, R.M., Pascual, G., Gonzalez-Suarez, E., Casanovas, O., Vinals, F.*, et al.* (2013). Progeny of Lgr5-expressing hair follicle stem cell contributes to papillomavirus-induced tumor development in epidermis. Oncogene *32*, 3732-3743.

de Jesus, B.B., and Blasco, M.A. (2012). Assessing cell and organ senescence biomarkers. Circ Res *111*, 97-109.

de Lange, T. (2009). How telomeres solve the end-protection problem. Science *326*, 948-952.

Deneault, E., Cellot, S., Faubert, A., Laverdure, J.P., Frechette, M., Chagraoui, J., Mayotte, N., Sauvageau, M., Ting, S.B., and Sauvageau, G. (2009). A functional screen to identify novel effectors of hematopoietic stem cell activity. Cell *137*, 369-379.

Donate, L.E., and Blasco, M.A. (2011). Telomeres in cancer and ageing. Philos Trans R Soc Lond B Biol Sci *366*, 76-84.

Du, Y., Spence, S.E., Jenkins, N.A., and Copeland, N.G. (2005). Cooperating cancer-gene identification through oncogenic-retrovirus-induced insertional mutagenesis. Blood *106*, 2498-2505.

Duncan, E.L., Danoy, P., Kemp, J.P., Leo, P.J., McCloskey, E., Nicholson, G.C., Eastell, R., Prince, R.L., Eisman, J.A., Jones, G.*, et al.* (2011). Genome-wide association study using extreme truncate selection identifies novel genes affecting bone mineral density and fracture risk. PLoS Genet *7*, e1001372.

Dy, P., Penzo-Mendez, A., Wang, H., Pedraza, C.E., Macklin, W.B., and Lefebvre, V. (2008). The three SoxC proteins--Sox4, Sox11 and Sox12--exhibit overlapping expression patterns and molecular properties. Nucleic Acids Res *36*, 3101-3117.

Flores, I., Benetti, R., and Blasco, M.A. (2006). Telomerase regulation and stem cell behaviour. Curr Opin Cell Biol *18*, 254-260.

Flores, I., and Blasco, M.A. (2009). A p53-dependent response limits epidermal stem cell functionality and organismal size in mice with short telomeres. PLoS One *4*, e4934.

Flores, I., Canela, A., Vera, E., Tejera, A., Cotsarelis, G., and Blasco, M.A. (2008). The longest telomeres: a general signature of adult stem cell compartments. Genes Dev *22*, 654-667.

Flores, I., Cayuela, M.L., and Blasco, M.A. (2005). Effects of telomerase and telomere length on epidermal stem cell behavior. Science *309*, 1253-1256.

Frierson, H.F., Jr., El-Naggar, A.K., Welsh, J.B., Sapinoso, L.M., Su, A.I., Cheng, J., Saku, T., Moskaluk, C.A., and Hampton, G.M. (2002). Large scale molecular analysis identifies genes with altered expression in salivary adenoid cystic carcinoma. Am J Pathol *161*, 1315-1323.

Fuchs, E. (1994). Epidermal differentiation and keratin gene expression. Princess Takamatsu Symp *24*, 290-302.

Fuchs, E. (2007). Scratching the surface of skin development. Nature *445*, 834-842.

Fuchs, E. (2009). The tortoise and the hair: slow-cycling cells in the stem cell race. Cell *137*, 811-819.

Fung, T.K., Leung, A.Y., and So, C.W. (2013). Sox4you: A New Player in C/EBPalpha Leukemia. Cancer Cell *24*, 557-559.

Geijsen, N., Uings, I.J., Pals, C., Armstrong, J., McKinnon, M., Raaijmakers, J.A., Lammers, J.W., Koenderman, L., and Coffer, P.J. (2001). Cytokine-specific transcriptional regulation through an IL-5Ralpha interacting protein. Science *293*, 1136-1138.

Goodwin, G.H., Sanders, C., and Johns, E.W. (1973). A new group of chromatin-associated proteins with a high content of acidic and basic amino acids. Eur J Biochem *38*, 14-19.

Goto, H., Tomono, Y., Ajiro, K., Kosako, H., Fujita, M., Sakurai, M., Okawa, K., Iwamatsu, A., Okigaki, T., Takahashi, T.*, et al.* (1999). Identification of a novel phosphorylation site on histone H3 coupled with mitotic chromosome condensation. J Biol Chem *274*, 25543-25549.

Greco, V., Chen, T., Rendl, M., Schober, M., Pasolli, H.A., Stokes, N., Dela Cruz-Racelis, J., and Fuchs, E. (2009). A two-step mechanism for stem cell activation during hair regeneration. Cell Stem Cell *4*, 155-169.

Gurdon, J.B., Elsdale, T.R., and Fischberg, M. (1958). Sexually mature individuals of Xenopus laevis from the transplantation of single somatic nuclei. Nature *182*, 64-65.

Hanahan, D., and Weinberg, R.A. (2011). Hallmarks of cancer: the next generation. Cell *144*, 646-674.

Harley, V., and Lefebvre, V. (2010). Twenty Sox, twenty years. Int J Biochem Cell Biol *42*, 376-377.

Higuchi, T., Nakayama, T., Arao, T., Nishio, K., and Yoshie, O. (2013). SOX4 is a direct target gene of FRA-2 and induces expression of HDAC8 in adult T-cell leukemia/lymphoma. Blood *121*, 3640-3649.

Hoeijmakers, J.H. (2009). DNA damage, aging, and cancer. N Engl J Med *361*, 1475-1485.

Hoser, M., Potzner, M.R., Koch, J.M., Bosl, M.R., Wegner, M., and Sock, E. (2008). Sox12 deletion in the mouse reveals nonreciprocal redundancy with the related Sox4 and Sox11 transcription factors. Mol Cell Biol *28*, 4675-4687.

Huang, J., Arsenault, M., Kann, M., Lopez-Mendez, C., Saleh, M., Wadowska, D., Taglienti, M., Ho, J., Miao, Y., Sims, D.*, et al.* (2013). The transcription factor Sry-related HMG box-4 (SOX4) is required for normal renal development in vivo. Dev Dyn *242*, 790-799.

Hunt, S.M., and Clarke, C.L. (1999). Expression and hormonal regulation of the Sox4 gene in mouse female reproductive tissues. Biol Reprod *61*, 476-481.

Hur, W., Rhim, H., Jung, C.K., Kim, J.D., Bae, S.H., Jang, J.W., Yang, J.M., Oh, S.T., Kim, D.G., Wang, H.J.*, et al.* (2010). SOX4 overexpression regulates the p53-mediated apoptosis in hepatocellular carcinoma: clinical implication and functional analysis in vitro. Carcinogenesis *31*, 1298-1307.

Jackson, S.P., and Bartek, J. (2009). The DNA-damage response in human biology and disease. Nature *421*, 1071-1078.

Jafarnejad, S.M., Ardekani, G.S., Ghaffari, M., and Li, G. (2013a). Pleiotropic function of SRY-related HMG box transcription factor 4 in regulation of tumorigenesis. Cell Mol Life Sci *70*, 2677-2696.

Jafarnejad, S.M., Ardekani, G.S., Ghaffari, M., Martinka, M., and Li, G. (2013b). Sox4-mediated Dicer expression is critical for suppression of melanoma cell invasion. Oncogene *32*, 2131-2139.

Jafarnejad, S.M., Wani, A.A., Martinka, M., and Li, G. (2010). Prognostic significance of Sox4 expression in human cutaneous melanoma and its role in cell migration and invasion. Am J Pathol *177*, 2741-2752.

Jaks, V., Barker, N., Kasper, M., van Es, J.H., Snippert, H.J., Clevers, H., and Toftgard, R. (2008). Lgr5 marks cycling, yet long-lived, hair follicle stem cells. Nat Genet *40*, 1291-1299.

Jauch, R., Ng, C.K., Narasimhan, K., and Kolatkar, P.R. (2012). The crystal structure of the Sox4 HMG domain-DNA complex suggests a mechanism for positional interdependence in DNA recognition. Biochem J *443*, 39-47.

Jemtland, R., Holden, M., Reppe, S., Olstad, O.K., Reinholt, F.P., Gautvik, V.T., Refvem, H., Frigessi, A., Houston, B., and Gautvik, K.M. (2011). Molecular disease map of bone characterizing the postmenopausal osteoporosis phenotype. J Bone Miner Res *26*, 1793-1801.

Jensen, K.B., Collins, C.A., Nascimento, E., Tan, D.W., Frye, M., Itami, S., and Watt, F.M. (2009). Lrig1 expression defines a distinct multipotent stem cell population in mammalian epidermis. Cell Stem Cell *4*, 427-439.

Jensen, K.B., Driskell, R.R., and Watt, F.M. (2010). Assaying proliferation and differentiation capacity of stem cells using disaggregated adult mouse epidermis. Nat Protoc *5*, 898-911.

Jiang, Y., Ding, Q., Xie, X., Libby, R.T., Lefebvre, V., and Gan, L. (2013). Transcription factors SOX4 and SOX11 function redundantly to regulate the development of mouse retinal ganglion cells. J Biol Chem *288*, 18429-18438.

Keyes, B.E., Segal, J.P., Heller, E., Lien, W.H., Chang, C.Y., Guo, X., Oristian, D.S., Zheng, D., and Fuchs, E. (2013). Nfatc1 orchestrates aging in hair follicle stem cells. Proc Natl Acad Sci U S A.

Kobielak, K., Stokes, N., de la Cruz, J., Polak, L., and Fuchs, E. (2007). Loss of a quiescent niche but not follicle stem cells in the absence of bone morphogenetic protein signaling. Proc Natl Acad Sci U S A *104*, 10063-10068.

Kuwahara, M., Yamashita, M., Shinoda, K., Tofukuji, S., Onodera, A., Shinnakasu, R., Motohashi, S., Hosokawa, H., Tumes, D., Iwamura, C*., et al.* (2012). The transcription factor Sox4 is a downstream target of signaling by the cytokine TGF-beta and suppresses T(H)2 differentiation. Nat Immunol *13*, 778-786.

Kvinlaug, B.T., Chan, W.I., Bullinger, L., Ramaswami, M., Sears, C., Foster, D., Lazic, E.C., Okabe, R., Benner, A., Lee, B.H*., et al.* (2011). Common and Overlapping Oncogenic Pathways Contribute to the Evolution of Acute Myeloid Leukemias. Cancer Res *71*, 4117-4129.

Lai, Y.H., Cheng, J., Cheng, D., Feasel, M.E., Beste, K.D., Peng, J., Nusrat, A., and Moreno, C.S. (2011). SOX4 interacts with plakoglobin in a Wnt3a-dependent manner in prostate cancer cells. BMC Cell Biol *12*, 50.

Laurenti, E., Doulatov, S., Zandi, S., Plumb, I., Chen, J., April, C., Fan, J.B., and Dick, J.E. (2013). The transcriptional architecture of early human hematopoiesis identifies multilevel control of lymphoid commitment. Nat Immunol *14*, 756-763.

Lee, A.K., Ahn, S.G., Yoon, J.H., and Kim, S.A. (2011). Sox4 stimulates ss-catenin activity through induction of CK2. Oncol Rep *25*, 559-565.

Lefebvre, V., Dumitriu, B., Penzo-Mendez, A., Han, Y., and Pallavi, B. (2007). Control of cell fate and differentiation by Sry-related high-mobility-group box (Sox) transcription factors. Int J Biochem Cell Biol *39*, 2195-2214.

Li, J., Zhang, Z., and Li, G. (2011). Patient outcome prediction using multiple biomarkers in human melanoma: A clinicopathological study of 118 cases. Exp Ther Med *2*, 131-135.

Li, Z., Kustikova, O.S., Kamino, K., Neumann, T., Rhein, M., Grassman, E., Fehse, B., and Baum, C. (2007). Insertional mutagenesis by replication-deficient retroviral vectors encoding the large T oncogene. Ann N Y Acad Sci *1106*, 95-113.

Liao, Y.L., Sun, Y.M., Chau, G.Y., Chau, Y.P., Lai, T.C., Wang, J.L., Horng, J.T., Hsiao, M., and Tsou, A.P. (2008). Identification of SOX4 target genes using phylogenetic footprinting-based prediction from expression microarrays suggests that overexpression of SOX4 potentiates metastasis in hepatocellular carcinoma. Oncogene *27*, 5578-5589.

Lien, W.H., Polak, L., Lin, M., Lay, K., Zheng, D., and Fuchs, E. (2014). In vivo transcriptional governance of hair follicle stem cells by canonical Wnt regulators. Nat Cell Biol.

Lioubinski, O., Muller, M., Wegner, M., and Sander, M. (2003). Expression of Sox transcription factors in the developing mouse pancreas. Dev Dyn *227*, 402-408.

Liu, P., Ramachandran, S., Ali Seyed, M., Scharer, C.D., Laycock, N., Dalton, W.B., Williams, H., Karanam, S., Datta, M.W., Jaye, D.L.*, et al.* (2006). Sex-determining region Y box 4 is a transforming oncogene in human prostate cancer cells. Cancer Res *66*, 4011-4019.

Lombard, D.B., Chua, K.F., Mostoslavsky, R., Franco, S., Gostissa, M., and Alt, F.W. (2005). DNA Repair, Genome Stability, and Aging. Cell *120*, 497-512.

Lopez-Otin, C., Blasco, M.A., Partridge, L., Serrano, M., and Kroemer, G. (2013). The hallmarks of aging. Cell *153*, 1194-1217.

Lowry, W.E., Blanpain, C., Nowak, J.A., Guasch, G., Lewis, L., and Fuchs, E. (2005). Defining the impact of beta-catenin/Tcf transactivation on epithelial stem cells. Genes Dev *19*, 1596-1611.

Malhotra, N., Narayan, K., Cho, O.H., Sylvia, K.E., Yin, C., Melichar, H., Rashighi, M., Lefebvre, V., Harris, J.E., Berg, L.J.*, et al.* (2013). A network of high-mobility group box transcription factors programs innate interleukin-17 production. Immunity *38*, 681-693.

Maloney, S.C., Marshall, J.C., Antecka, E., Orellana, M.E., Fernandes, B.F., Martins, C., Castiglione, E., Logan, P., and Burnier, M.N., Jr. (2009). SPARC is expressed in human uveal melanoma and its abrogation reduces tumor cell proliferation. Anticancer Res *29*, 3059-3064.

Marion, R.M., Strati, K., Li, H., Tejera, A., Schoeftner, S., Ortega, S., Serrano, M., and Blasco, M.A. (2009). Telomeres acquire embryonic stem cell characteristics in induced pluripotent stem cells. Cell Stem Cell *4*, 141-154.

Marks, H., Kalkan, T., Menafra, R., Denissov, S., Jones, K., Hofemeister, H., Nichols, J., Kranz, A., Stewart, A.F., Smith, A.*, et al.* (2012). The transcriptional and epigenomic foundations of ground state pluripotency. Cell *149*, 590-604.

Martinez, P., Thanasoula, M., Munoz, P., Liao, C., Tejera, A., McNees, C., Flores, J.M., Fernandez-Capetillo, O., Tarsounas, M., and Blasco, M.A. (2009). Increased telomere fragility and fusions resulting from TRF1 deficiency lead to degenerative pathologies and increased cancer in mice. Genes Dev *23*, 2060-2075.

Muller-Rover, S., Handjiski, B., van der Veen, C., Eichmuller, S., Foitzik, K., McKay, I.A., Stenn, K.S., and Paus, R. (2001). A comprehensive guide for the accurate classification of murine hair follicles in distinct hair cycle stages. J Invest Dermatol *117*, 3-15.

Munoz, P., Blanco, R., Flores, J.M., and Blasco, M.A. (2005). XPF nuclease-dependent telomere loss and increased DNA damage in mice overexpressing TRF2 result in premature aging and cancer. Nat Genet *37*, 1063-1071.

Nissen-Meyer, L.S., Jemtland, R., Gautvik, V.T., Pedersen, M.E., Paro, R., Fortunati, D., Pierroz, D.D., Stadelmann, V.A., Reppe, S., Reinholt, F.P.*, et al.* (2007). Osteopenia, decreased bone formation and impaired osteoblast development in Sox4 heterozygous mice. J Cell Sci *120*, 2785-2795.

Nowak, J.A., Polak, L., Pasolli, H.A., and Fuchs, E. (2008). Hair follicle stem cells are specified and function in early skin morphogenesis. Cell Stem Cell *3*, 33-43.

Omidvar, N., Maunakea, M.L., Jones, L., Sevcikova, S., Yin, B., Himmel, K.L., Tennant, T.R., Le Beau, M.M., Largaespada, D.A., and Kogan, S.C. (2013). PML-RARalpha co-

operates with Sox4 in acute myeloid leukemia development in mice. Haematologica *98*, 424-427.

Oro, A.E., and Higgins, K. (2003). Hair cycle regulation of Hedgehog signal reception. Dev Biol *255*, 238-248.

Ortega-Molina, A., Efeyan, A., Lopez-Guadamillas, E., Muñoz-Martin, M., Gómez-López, G., Cañamero, M., Mulero, F., Pastor, J., Martinez, S., Romanos, E.*, et al.* (2012). Pten positively regulates brown adipose function, energy expenditure, and longevity. Cell Metab *15*, 382-394.

Oshimori, N., and Fuchs, E. (2012). The harmonies played by TGF-beta in stem cell biology. Cell Stem Cell *11*, 751-764.

Pan, X., Zhao, J., Zhang, W.N., Li, H.Y., Mu, R., Zhou, T., Zhang, H.Y., Gong, W.L., Yu, M., Man, J.H.*, et al.* (2009). Induction of SOX4 by DNA damage is critical for p53 stabilization and function. Proc Natl Acad Sci U S A *106*, 3788-3793.

Parvani, J.G., and Schiemann, W.P. (2013). Sox4, EMT programs, and the metastatic progression of breast cancers: mastering the masters of EMT. Breast Cancer Res *15*, R72.

Paul, M.H., Harvey, R.P., Wegner, M., and Sock, E. (2013). Cardiac outflow tract development relies on the complex function of Sox4 and Sox11 in multiple cell types. Cell Mol Life Sci.

Penzo-Mendez, A., Dy, P., Pallavi, B., and Lefebvre, V. (2007). Generation of mice harboring a Sox4 conditional null allele. Genesis *45*, 776-780.

Penzo-Mendez, A.I. (2010). Critical roles for SoxC transcription factors in development and cancer. Int J Biochem Cell Biol *42*, 425-428.

Pramoonjago, P., Baras, A.S., and Moskaluk, C.A. (2006). Knockdown of Sox4 expression by RNAi induces apoptosis in ACC3 cells. Oncogene *25*, 5626-5639.

Ramezani-Rad, P., Geng, H., Hurtz, C., Chan, L.N., Chen, Z., Jumaa, H., Melnick, A., Paietta, E., Carroll, W.L., Willman, C.L.*, et al.* (2013). SOX4 enables oncogenic survival signals in acute lymphoblastic leukemia. Blood *121*, 148-155.

Ramirez, A., Page, A., Gandarillas, A., Zanet, J., Pibre, S., Vidal, M., Tusell, L., Genesca, A., Whitaker, D.A., Melton, D.W.*, et al.* (2004). A keratin K5Cre transgenic line appropriate for tissue-specific or generalized Cre-mediated recombination. Genesis *39*, 52-57.

Rendl, M., Polak, L., and Fuchs, E. (2008). BMP signaling in dermal papilla cells is required for their hair follicle-inductive properties. Genes Dev *22*, 543-557.

Reppe, S., Rian, E., Jemtland, R., Olstad, O.K., Gautvik, V.T., and Gautvik, K.M. (2000). Sox-4 messenger RNA is expressed in the embryonic growth plate and regulated via the parathyroid hormone/parathyroid hormone-related protein receptor in osteoblast-like cells. J Bone Miner Res *15*, 2402-2412.

Reppe, S., Stilgren, L., Olstad, O.K., Brixen, K., Nissen-Meyer, L.S., Gautvik, K.M., and Abrahamsen, B. (2006). Gene expression profiles give insight into the molecular pathology of bone in primary hyperparathyroidism. Bone *39*, 189-198.

Rhee, H., Polak, L., and Fuchs, E. (2006). Lhx2 maintains stem cell character in hair follicles. Science *312*, 1946-1949.

Rossi, D.J., J., S., Czechowicz, A., D., B., Bryder, D., and Weissman, I.L. (2007). Hematopoietic stem cell quiescence attenuates DNA damage response and permits DNA damage accumulation during aging. Cell Cycle *6*, 2371-2376.

Saegusa, M., Hashimura, M., and Kuwata, T. (2012). Sox4 functions as a positive regulator of beta-catenin signaling through upregulation of TCF4 during morular differentiation of endometrial carcinomas. Lab Invest *92*, 511-521.

Said, N., Frierson, H.F., Sanchez-Carbayo, M., Brekken, R.A., and Theodorescu, D. (2013). Loss of SPARC in bladder cancer enhances carcinogenesis and progression. J Clin Invest *123*, 751-766.

Sandoval, S., Kraus, C., Cho, E.C., Cho, M., Bies, J., Manara, E., Accordi, B., Landaw, E.M., Wolff, L., Pigazzi, M., *et al.* (2012). Sox4 cooperates with CREB in myeloid transformation. Blood *120*, 155-165.

Sarkar, A., and Hochedlinger, K. (2013). The sox family of transcription factors: versatile regulators of stem and progenitor cell fate. Cell Stem Cell *12*, 15-30.

Schilham, M.W., Moerer, P., Cumano, A., and Clevers, H.C. (1997). Sox-4 facilitates thymocyte differentiation. Eur J Immunol *27*, 1292-1295.

Schilham, M.W., Oosterwegel, M.A., Moerer, P., Ya, J., de Boer, P.A., van de Wetering, M., Verbeek, S., Lamers, W.H., Kruisbeek, A.M., Cumano, A., *et al.* (1996). Defects in cardiac outflow tract formation and pro-B-lymphocyte expansion in mice lacking Sox-4. Nature *380*, 711-714.

Schumacher, B., Garinis, G.A., and Hoeijmakers, J.H. (2008). Age to survive: DNA damage and aging. Trends Genet *24*, 77-85.

Sharpless, N.E., and DePinho, R.A. (2007). How stem cells age and why this makes us grow old. Nat Rev Mol Cell Biol *8*, 703-713.

Shin, M.S., Fredrickson, T.N., Hartley, J.W., Suzuki, T., Akagi, K., and Morse, H.C., 3rd (2004). High-throughput retroviral tagging for identification of genes involved in initiation and progression of mouse splenic marginal zone lymphomas. Cancer Res *64*, 4419-4427.

Signer, R.A., and Morrison, S.J. (2013). Mechanisms that regulate stem cell aging and life span. Cell Stem Cell *12*, 152-165.

Simons, B.D., and Clevers, H. (2011). Strategies for homeostatic stem cell self-renewal in adult tissues. Cell *145*, 851-862.

Sinclair, A.H., Berta, P., Palmer, M.S., Hawkins, J.R., Griffiths, B.L., Smith, M.J., Foster, J.W., Frischauf, A.M., Lovell-Badge, R., and Goodfellow, P.N. (1990). A gene from the human sex-determining region encodes a protein with homology to a conserved DNA-binding motif. Nature *346*, 240-244.

Sinner, D., Kordich, J.J., Spence, J.R., Opoka, R., Rankin, S., Lin, S.C., Jonatan, D., Zorn, A.M., and Wells, J.M. (2007). Sox17 and Sox4 differentially regulate beta-catenin/T-cell factor activity and proliferation of colon carcinoma cells. Mol Cell Biol *27*, 7802-7815.

Smith, A.G. (2001). Embryo-derived stem cells: of mice and men. Annu Rev Cell Dev Biol *17*, 435-462.

Snippert, H.J., Haegebarth, A., Kasper, M., Jaks, V., van Es, J.H., Barker, N., van de Wetering, M., van den Born, M., Begthel, H., Vries, R.G.*, et al.* (2010). Lgr6 marks stem cells in the hair follicle that generate all cell lineages of the skin. Science *327*, 1385-1389.

Sun, B., Mallampati, S., Gong, Y., Wang, D., Lefebvre, V., and Sun, X. (2013). Sox4 is required for the survival of pro-B cells. J Immunol *190*, 2080-2089.

Suzuki, T., Shen, H., Akagi, K., Morse, H.C., Malley, J.D., Naiman, D.Q., Jenkins, N.A., and Copeland, N.G. (2002). New genes involved in cancer identified by retroviral tagging. Nat Genet *32*, 166-174.

Takahashi, K., Tanabe, K., Ohnuki, M., Narita, M., Ichisaka, T., Tomoda, K., and Yamanaka, S. (2007). Induction of pluripotent stem cells from adult human fibroblasts by defined factors. Cell *131*, 861-872.

Takahashi, K., and Yamanaka, S. (2006). Induction of pluripotent stem cells from mouse embryonic and adult fibroblast cultures by defined factors. Cell *126*, 663-676.
Tam, P.P., and Loebel, D.A. (2007). Gene function in mouse embryogenesis: get set for gastrulation. Nat Rev Genet *8*, 368-381.

Tavazoie, S.F., Alarcon, C., Oskarsson, T., Padua, D., Wang, Q., Bos, P.D., Gerald, W.L., and Massague, J. (2008). Endogenous human microRNAs that suppress breast cancer metastasis. Nature *451*, 147-152.

Tejera, A.M., Stagno d'Alcontres, M., Thanasoula, M., Marion, R.M., Martinez, P., Liao, C., Flores, J.M., Tarsounas, M., and Blasco, M.A. (2010). TPP1 is required for TERT recruitment, telomere elongation during nuclear reprogramming, and normal skin development in mice. Dev Cell *18*, 775-789.

Tiwari, N., Tiwari, V.K., Waldmeier, L., Balwierz, P.J., Arnold, P., Pachkov, M., Meyer-Schaller, N., Schubeler, D., van Nimwegen, E., and Christofori, G. (2013). Sox4 is a master regulator of epithelial-mesenchymal transition by controlling Ezh2 expression and epigenetic reprogramming. Cancer Cell *23*, 768-783.

Tumbar, T., Guasch, G., Greco, V., Blanpain, C., Lowry, W.E., Rendl, M., and Fuchs, E. (2004). Defining the epithelial stem cell niche in skin. Science *303*, 359-363.

van de Wetering, M., Oosterwegel, M., van Norren, K., and Clevers, H. (1993). Sox-4, an Sry-like HMG box protein, is a transcriptional activator in lymphocytes. EMBO J *12*, 3847-3854.

Van der Flier, L.G., Sabates-Bellver, J., Oving, I., Haegebarth, A., De Palo, M., Anti, M., Van Gijn, M.E., Suijkerbuijk, S., Van de Wetering, M., Marra, G.*, et al.* (2007). The Intestinal Wnt/TCF Signature. Gastroenterology *132*, 628-632.

Vera, E., Bernardes de Jesus, B., Foronda, M., Flores, J.M., and Blasco, M.A. (2012). The rate of increase of short telomeres predicts longevity in mammals. Cell Rep *2*, 732-737.

Verstegen J, D.G., Verstegen-Onclin K. (2008). Mucometra, cystic endometrial hyperplasia, and pyometra in the bitch: advances in treatment and assessment of future reproductive success. Theriogenology *70*, 364-374.

Vervoort, S.J., Lourenco, A.R., van Boxtel, R., and Coffer, P.J. (2013a). SOX4 mediates TGF-beta-induced expression of mesenchymal markers during mammary cell epithelial to mesenchymal transition. PLoS One *8*, e53238.

Vervoort, S.J., van Boxtel, R., and Coffer, P.J. (2013b). The role of SRY-related HMG box transcription factor 4 (SOX4) in tumorigenesis and metastasis: friend or foe? Oncogene *32*, 3397-3409.

Wagers, A.J., and Weissman, I.L. (2004). Plasticity of adult stem cells. Cell *116*, 639-648.

Wang, L., Zhang, J., Yang, X., Chang, Y.W., Qi, M., Zhou, Z., and Han, B. (2013). SOX4 is associated with poor prognosis in prostate cancer and promotes epithelial-mesenchymal transition in vitro. Prostate Cancer Prostatic Dis *16*, 301-307.

Watt, F.M., Frye, M., and Benitah, S.A. (2008). MYC in mammalian epidermis: how can an oncogene stimulate differentiation? Nat Rev Cancer *8*, 234-242.

Watt, F.M., and Huck, W.T. (2013). Role of the extracellular matrix in regulating stem cell fate. Nat Rev Mol Cell Biol *14*, 467-473.

Wilson, M.E., Yang, K.Y., Kalousova, A., Lau, J., Kosaka, Y., Lynn, F.C., Wang, J., Mrejen, C., Episkopou, V., Clevers, H.C.*, et al.* (2005). The HMG box transcription factor Sox4 contributes to the development of the endocrine pancreas. Diabetes *54*, 3402-3409.

Wong, K.Y., Yim, R.L., Kwong, Y.L., Leung, C.Y., Hui, P.K., Cheung, F., Liang, R., Jin, D.Y., and Chim, C.S. (2013). Epigenetic inactivation of the MIR129-2 in hematological malignancies. J Hematol Oncol *6*, 16.

Ya, J., Schilham, M.W., de Boer, P.A., Moorman, A.F., Clevers, H., and Lamers, W.H. (1998). Sox4-deficiency syndrome in mice is an animal model for common trunk. Circ Res *83*, 986-994.

Yu, X., Song, H., Xia, T., Han, S., Xiao, B., Luo, L., Xi, Y., and Guo, J. (2013). Growth inhibitory effects of three miR-129 family members on gastric cancer. Gene *532*, 87-93.
Zhang, G., and Li, G. (2012). Novel multiple markers to distinguish melanoma from dysplastic nevi. PLoS One *7*, e45037.

Zhang, H., Alberich-Jorda, M., Amabile, G., Yang, H., Staber, P.B., Diruscio, A., Welner, R.S., Ebralidze, A., Zhang, J., Levantini, E.*, et al.* (2013). Sox4 Is a Key Oncogenic Target in C/EBPalpha Mutant Acute Myeloid Leukemia. Cancer Cell *24*, 575-588.

Zhang, J., Liang, Q., Lei, Y., Yao, M., Li, L., Gao, X., Feng, J., Zhang, Y., Gao, H., Liu, D.X.*, et al.* (2012). SOX4 induces epithelial-mesenchymal transition and contributes to breast cancer progression. Cancer Res *72*, 4597-4608.

Zhao, T., Satou, Y., Sugata, K., Miyazato, P., Green, P.L., Imamura, T., and Matsuoka, M. (2011). HTLV-1 bZIP factor enhances TGF-beta signaling through p300 coactivator. Blood *118*, 1865-1876.

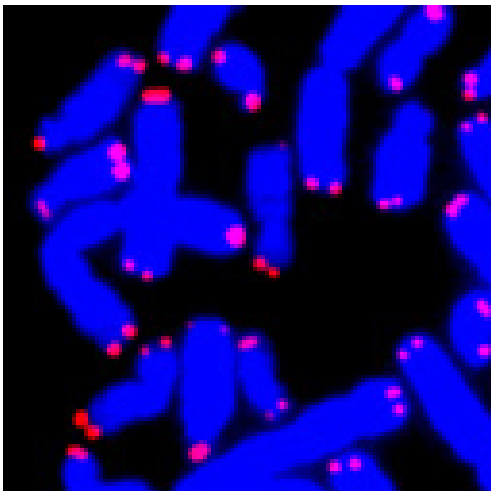

Annex

Música, melancólico alimento para los que vivimos de amor

Julio Cortázar. Rayuela, Cap 2

Publications directly related to the PhD thesis

Miguel Foronda, Stefan Schöftner, Gonzalo Gómez-López, Ralph P. Schneider, Juana M. Flores, Maria A. Blasco. (2014) **Sox4 links tumor suppression to accelerated aging in mice.** Submitted to *Cell Rep*, Feb, 14th 2014.

Other Publications during the execution of the PhD

Ralph P. Schneider, Ianire Garrobo, **Miguel Foronda**, Jose A. Palacios, Rosa M. Marión, Ignacio Flores, Sagrario Ortega, Maria A. Blasco. (2013) **TRF1 is a stem cell marker and is essential for the generation of induced pluripotent stem cells.** *Nat Commun*. **4**:1946.

Andrew J. Ramsay*, Víctor Quesada*, **Miguel Foronda***, Laura Conde, Alejandra Martínez-Trillos, Neus Villamor, David Rodríguez, Agnieszka Kwarciak, Cecilia Garabaya, Mercedes Gallardo, Mónica López-Guerra, López-Guillermo A, Xosé S. Puente, Maria A. Blasco#, Elías Campo#, Carlos López-Otín#. (2013) **POT1 mutations cause telomere dysfunction in chronic lymphocytic leukemia.** *Nat Genet.* **45** (5):526-530.

Elsa Vera, Bruno Bernardes de Jesús, **Miguel Foronda**, Juana M. Flores, Maria A. Blasco. (2013) **Telomerase reverse transcriptase synergizes with calorie restriction to increase health span and extend mouse longevity.** *PLoS One*. **8** (1):e53760.

Elsa Vera*, Bruno Bernardes de Jesús*, **Miguel Foronda**, Juana M. Flores, Maria A. Blasco. (2012) **The rate of increase of short telomeres predicts longevity in mammals.** *Cell Rep.* **2** (4):732-737

Fabian Beier, **Miguel Foronda**, Paula Martínez, Maria A. Blasco. (2012) **Conditional TRF1 knockout in the hematopoietic compartment leads to bone marrow failure and recapitulates clinical features of dyskeratosis congenita.** *Blood* **120** (15):2990-3000

*=Equally contributing first authors

#=Equal senior authorship

Cell Reports
Report

The Rate of Increase of Short Telomeres Predicts Longevity in Mammals

Elsa Vera,[1,3] Bruno Bernardes de Jesus,[1,3] Miguel Foronda,[1] Juana M. Flores,[2] and Maria A. Blasco[1,*]
[1]Telomeres and Telomerase Group, Molecular Oncology Program, Spanish National Cancer Research Center, Melchor Fernández Almagro 3, E-28029 Madrid, Spain
[2]Department of Animal Surgery and Medicine, Facultad de Veterinaria, Universidad Complutense de Madrid, 28029 Madrid, Spain
[3]These authors contributed equally to this work
*Correspondence: mblasco@cnio.es
http://dx.doi.org/10.1016/j.celrep.2012.08.023

SUMMARY

Aberrantly short telomeres result in decreased longevity in both humans and mice with defective telomere maintenance. Normal populations of humans and mice present high interindividual variation in telomere length, but it is unknown whether this is associated with their lifespan potential. To address this issue, we performed a longitudinal telomere length study along the lifespan of wild-type and transgenic telomerase reverse transcriptase mice. We found that mouse telomeres shorten ~100 times faster than human telomeres. Importantly, the rate of increase in the percentage of short telomeres, rather than the rate of telomere shortening per month, was a significant predictor of lifespan in both mouse cohorts, and those individuals who showed a higher rate of increase in the percentage of short telomeres were also the ones with a shorter lifespan. These findings demonstrate that short telomeres have a direct impact on longevity in mammals, and they highlight the importance of performing longitudinal telomere studies to predict longevity.

INTRODUCTION

Telomeres are repeated DNA nucleoprotein structures at the ends of eukaryotic chromosomes (Blackburn, 1991; de Lange, 2005) that protect them from degradation and DNA repair activities, and are essential for chromosomal stability (Chan and Blackburn, 2002). Telomere repeats can be added de novo by telomerase, a reverse transcriptase that elongates telomeres in cells in which it is expressed (Blackburn, 2005; Flores et al., 2006; Greider, 1998; Greider and Blackburn, 1985; Marion et al., 2009). In telomerase-negative cells, telomeres shorten with each round of cell division as a result of end replication and DNA-degrading activities. Short telomeres are passed onto daughter cells, and thus telomere shortening is exacerbated by cell division and increasing age in both humans and mice (Flores et al., 2008; Harley et al., 1990). Critically short telomeres can trigger a persistent DNA damage response that leads to cellular senescence and/or apoptosis (Collado et al., 2007; Deng et al., 2008), eventually compromising the regenerative capacity and function of tissues (Blasco, 2007). Short telomeres are proposed to be sufficient to cause the degenerative pathologies associated with aging even in the presence of telomerase activity (Armanios et al., 2009; Hao et al., 2005).

In further support of this notion, both telomerase-deficient mice and human diseases due to mutations in telomerase components result in accelerated-aging phenotypes and decreased longevity due to premature depletion of stem cells and subsequent organ/tissue failure (Armanios et al., 2007; Blasco et al., 1997; García-Cao et al., 2006; Herrera et al., 1999; Mitchell et al., 1999; Tsakiri et al., 2007; Vulliamy et al., 2001; Yamaguchi et al., 2005). Telomere shortening associated with normal aging can be influenced by known risk factors for disease and premature death, such as psychological stress, smoking, cognitive impairment, and obesity (Canela et al., 2007; Cawthon et al., 2003; Cherkas et al., 2006; Epel et al., 2004; Valdes et al., 2005). However, whether the rate of telomere shortening in individual mammals has an influence on their longevity remains unexplored. In this regard, although serial telomere length measurements were previously obtained in baboons, a correlation with longevity was not sought (Baerlocher et al., 2003). Of interest, it was recently reported that telomere length measured at 25 days of age is a predictor of lifespan in birds (Heidinger et al., 2012).

Evidence from telomerase loss-of-expression and gain-of-expression transgenic mouse models suggests that telomere length may be rate limiting for mouse longevity (García-Cao et al., 2006; Tomás-Loba et al., 2008). Nonetheless, a role for telomere length in normal mouse aging is brought into question by the fact that although mice have very long telomeres compared with humans (~50 kb in young C57BL/6 mice, compared with ~15 kb in young humans) (Gomes et al., 2011; Wright and Shay, 2000), mice have a much shorter maximal lifespan (~5 years in mice of mixed background homozygous [−/−] for the *GHR/BP* gene) (Brown-Borg and Bartke, 2012) than humans (122 years). Although numerous studies have measured the average rate of telomere shortening per year in human population studies, which ranges from 31 base pairs (bp)/year to 72 bp/year in peripheral blood cells (Canela et al., 2007; Hastie et al., 1990; Slagboom et al., 1994; Vaziri et al., 1993), this rate has not been obtained in mice. Moreover, only one study has linked the increase in the percentage of short telomeres with age in humans, which was calculated as a 0.6% increase per year (Canela et al., 2007).

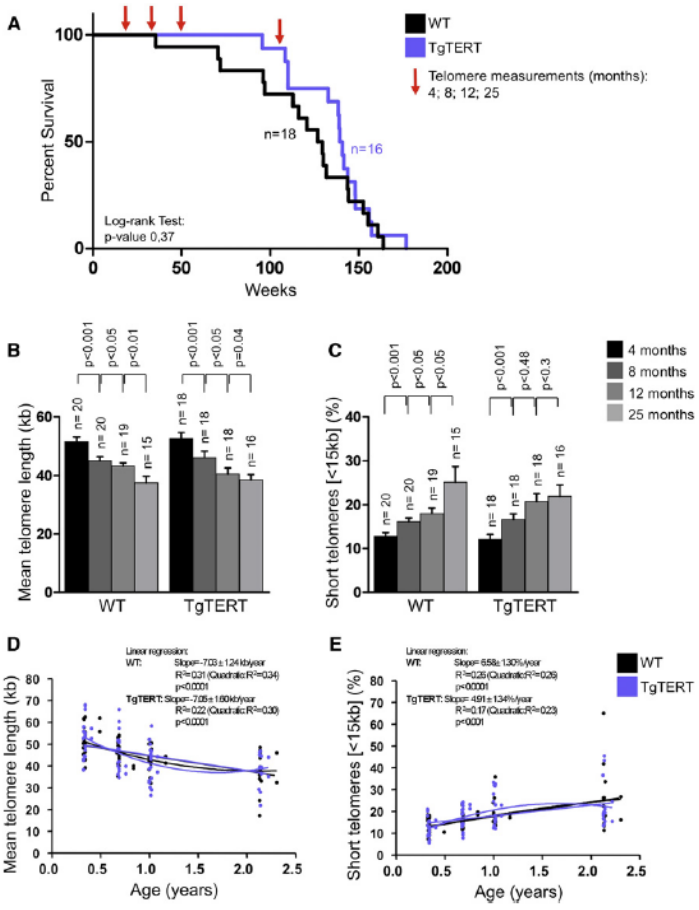

Figure 1. Mouse Telomeres Shorten 100-Fold Faster than Human Telomeres with Aging

(A) Kaplan-Meyer survival curves of the indicated cohorts. Arrows indicate time of blood extraction. (B and C) The mean telomere length (B) and percentage of short telomeres (C) were determined by HT-QFISH on white blood cells (n, number of mice). Values are given as average ± SEM, and statistical significance was determined by one-tailed Student's t test. (B) From left to right (average ± SEM): 51.49 ± 1.633, 45.10 ± 1.322, 43.18 ± 1.118, 37.51 ± 2.241, 52.61 ± 2.049, 46.06 ± 2.142, 40.54 ± 2.053, 38.55 ± 1.801. (C) From left to right (average ± SEM): 12.78 ± 0.8693, 16.19 ± 0.8230, 17.99 ± 1.257, 25.14 ± 3.552, 12.16 ± 1.078, 16.68 ± 1.237, 20.77 ± 1.798, 21.93 ± 2.581.

(D and E) Adjustment of mean telomere length (D) and percentage of short telomeres (E) with aging to a linear or quadratic model. Second-order polynomial adjustment (quadratic) was used for the nonlinear fit model.

Here, we reasoned that the rate of increase in the percentage of short telomeres and the rate of telomere shortening throughout the lifespan of individuals might explain the different longevities of wild-type (WT) mice and humans, as well as the interindividual variations in longevity in mammals.

RESULTS AND DISCUSSION

With the aim of determining the rate of telomere shortening and the rate of increase in the percentage of short telomeres with aging in mice, we performed longitudinal telomere length determinations in the blood of individual mice by using an automated high-throughput quantitative fluorescence in situ hybridization (HT-QFISH) platform (Canela et al., 2007).

To correct for gender and genetic background, as well as to circumvent possible effects of reproduction on telomere length, we used only male mice of a 100% C57BL/6 background. In addition, the mice were individually housed at 3 months of age and fed a defined diet of 92.5 kcal per week (see Experimental Procedures). This caloric intake represents ~10% fewer calories than the average daily intake of C57BL/6 mice, and was used to avoid a possible impact of obesity on longevity. In parallel, we determined the same parameters in a transgenic mouse line overexpressing the mouse catalytic subunit of telomerase reverse transcriptase (TERT) in various epithelial tissues (hereafter termed transgenic TERT [TgTERT]; González-Suárez et al., 2001, 2002). This mouse line has a comparable 100% C57BL/6 background; however, it presents delayed signs of aging compared with WT mice (González-Suárez et al., 2005; this work), as well as a 40% increase in median longevity when combined with overexpression of tumor suppressor genes (Tomás-Loba et al., 2008). As shown in Figure 1A, the TgTERT mice used here show a delayed onset of the first deaths in the colony compared with the WT cohorts (see Figure 1A), in agreement with their increased healthspan. Thus, we set out to study whether any telomere-related parameter could predict longevity in these two independent mouse cohorts (TgTERT and WT) with slightly different longevities.

For cell analyses, we used peripheral blood leukocytes (PBLs), which are widely used for human telomere length studies because hematopoietic stems cells proliferate throughout life and thus reflect on cellular turnover associated with the aging process. Telomere length measurements in the blood have been shown to be representative of the general health status in humans (Canela et al., 2007; Cawthon et al., 2003; Collerton et al., 2007; Mainous et al., 2010; Valdes et al., 2005) and mice (Bernardes de Jesus et al., 2012), and provide an indicator of

Cell PRESS Open ACCESS

the general healthspan. In this regard, although the TERT transgenic mice used here do not target telomerase to blood cells, TERT expression in these mice has systemic beneficial effects that delay aging (Tomás-Loba et al., 2008), as also observed recently when a gene therapy strategy was used to overexpress TERT late in life (Bernardes de Jesus et al., 2012). We extracted 300 μl of blood from the facial vein of each mouse at 4, 8, 12, and 25 months of age (see Experimental Procedures) and the mice were left to age until the end of their lifespan, to obtain their complete longevity curve (Figure 1A). To avoid morbidity associated with this procedure in old mice, blood extractions were not performed after 25 months of age. Of note, we observed a delay in the age at onset of first death in the TgTERT cohort: the first mouse died at >100 weeks of age, compared with <50 weeks of age in the case of the WT cohort (Figure 1A). We determined both the average telomere length and the percentage of short telomeres at the indicated time points per individual mouse by using HT-QFISH (Canela et al., 2007). HT-QFISH is able to measure individual telomere signals at a single-cell level in interphasic nuclei. In this setting, each telomere signal corresponds to a clustering of few individual telomeres. The percentage used to represent short telomeres by HT-QFISH usually corresponds to the 10%–20% percentile in the reference population (in this case, we used 4-month-old WT mice as reference), which is 15 kb. We previously determined that telomere signals <15 kb are a good indicator of the presence of short telomeres in mouse blood cells and reflect differences in telomere length between different cohorts and treatments (Bernardes de Jesus et al., 2012). Therefore, here we set a cutoff of 15 kb to quantify the presence of short telomeres. In addition, we performed correlations with other cutoffs (<2, <5, and <10 kb), but we observed the strongest correlations at the 15 kb cutoff (not shown).

First, it is apparent that even though mouse telomeres are very long at young ages (>50 kb at 4 months of age), they shorten with age, as reflected by both a significant decrease in the mean telomere length and a significant increase in the percentage of short telomeres, detectable at 4 month intervals (Figures 1B and 1C). By adjusting the data to a linear regression model, we determined a rate of telomere shortening (as estimated by the slope of the regression line) of 7,000 bp per year (Figure 1D), which was comparable in both mouse cohorts and is 100 times faster than that obtained for human PBLs using the same technology (Canela et al., 2007). These results indicate that even though mouse telomeres are much longer than human telomeres at younger ages, they exhibit a much faster rate of shortening with age, highlighting the relevance of performing longitudinal telomere length studies rather than measuring telomeres at a single time point. The rate of increase in the percentage of short telomeres per year was 6.6% in WT mice and 4.9% in the TgTERT cohort (as estimated by the slope of the regression line; Figure 1E).

Next, we investigated whether the telomere length or the percentage of short telomeres at any of the studied timepoints is predictive of mouse longevity, as was recently reported for zebra finches (Heidinger et al., 2012). In the case of mice, however, we did not find a significant correlation between either the average telomere length or the percentage of short telomeres with longevity in any of the two mouse cohorts, with the exception of an inverse correlation between average telomere length and longevity at 12 months of age in the TgTERT mice (Figure S1).

Longitudinal studies allow one to examine telomere dynamics in a given individual over time. A given rate of telomere shortening or a rate of increase in the percentage of short telomeres is the result of a longitudinal trend in individual mice that may reflect very complex genetic traits associated with longevity, which cannot be inferred from a single time-point measurement. Therefore, we determined the rate of increase in the percentage of short telomeres per month and the rate of telomere shortening per month for every mouse under study. Strikingly, we found a significant correlation between the rate of increase in the percentage of short telomeres per month and longevity (Figure 2A), which could be observed in both mouse cohorts, and between the rate of telomere shortening per month and longevity (Figure 2B), which was only observed in WT mice. We also observed a significant correlation between the rates of increase in the percentage of short telomeres and mean telomere shortening (Figure 2C). Together, these results indicate that the rate of increase in the percentage of short telomeres is a reliable and robust predictor of mouse longevity in two different mouse strains with different TERT expression levels and different longevities. The mice with the higher rates of increase in the percentage of short telomeres were the ones that had shorter lives, while those with lower rates of increase in the percentage of short telomeres were the ones that enjoyed longer lives.

The fact that the TgTERT cohorts did not show a correlation between the rate of telomere shortening per month and longevity prompted us to address whether this was the consequence of TgTERT mice showing a delayed time of onset of the first death in the colony. In particular, to assess whether lifespan can influence the rate of telomere shortening or the rate of increase in the percentage of short telomeres, we plotted these two parameters at different time intervals of measurement (Figure S2). Indeed, age influenced the rate of mean telomere shortening per month in a discontinuous manner, so that we found higher rates of telomere shortening per month in young mice compared with older mice (Figure S2B). Of interest, this was not the case for the rate of increase in the percentage of short telomeres per month, which was quite constant at different age intervals in both mouse cohorts, with the exception of lower rates of increase in the percentage of short telomeres in old TgTERT mice (Figure S2A). The fact that the rate of telomere shortening per month was not constant with age in both mouse cohorts could account for the significant correlation between the rate of mean telomere shortening per month and longevity in the WT mice but not in the TgTERT mice (Figure 2B), because a significant fraction of WT mice (versus only one TgTERT mouse) died before measurement of the four time points. Indeed, even if we exclude the single TgTERT mouse that died before the fourth measurement, we observe a strong correlation between the rate of increase in the percentage of short telomeres and longevity (Figure S3). These findings indicate that the rate of increase in the percentage of short telomeres is a robust and reliable telomere marker for longevity studies.

It is of interest to note that differences in telomere length and longevity could not be attributed to differences in gender,

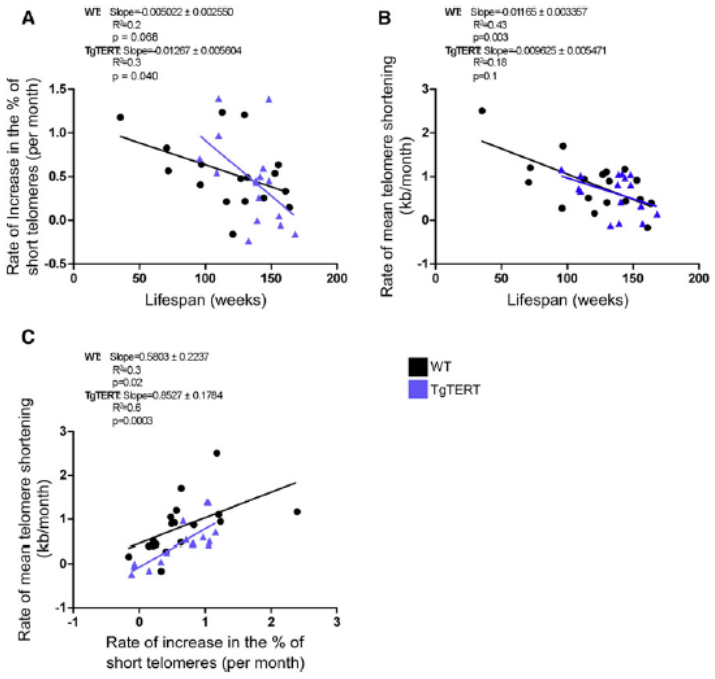

Figure 2. The Rate of Increase in the Percentage of Short Telomeres and the Rate of Telomere Shortening Predicts Mouse Longevity

(A–C) The percentage of short telomeres (<15 kb; A and C) and mean telomere length (B and C) were determined by HT-QFISH on white blood cells (see Figure 1). Linear regression lines were calculated for the values obtained for the rate of increase in the percentage of short telomeres and for the rate of mean telomere length shortening (kb/month) versus lifespan (weeks). (A) Rate of increase in the percentage of short telomeres (<15 kb) per month versus lifespan (weeks). (B) Rate of mean telomere length shortening (kb/month) versus the rate of increase in the percentage of short telomeres (per month). (C) Rate of mean telomere length shortening (kb/month) versus the rate of increase in the percentage of short telomeres (<15 kb) per month. The slope of each regression line is indicated.

See also Figures S1, S2, S3, S4, and S5.

reproduction, genetic background, or environmental factors, as only male mice of the C57BL/6 genetic background housed at our specific pathogen-free (SPF) facility were studied. In this regard, we did not find a correlation between the rate of increase in the percentage of short telomeres or rates of telomere shortening and weight gain with age (Figure S4), which together with the fact that the mice were fed a defined diet rules out a possible dietary contribution. These results suggest that differences in the rate of increase in the percentage of short telomeres or in the rate of telomere shortening, which have been shown to vary among individuals of the same age in different species (Canela et al., 2007; Heidinger et al., 2012; Monaghan, 2010), may be the result of small differences in modifier genes, or environmental factors, and offer an experimental platform to uncover new factors for modulation of aging and longevity.

Finally, we sought to determine whether variations in the rate of increase in the percentage of short telomeres had an impact on pathologies found at the time of death. To that end, we performed a full histopathological analysis of mice under study at their endpoint. The more prevalent pathologies found in C57BL/6 mice at their time of death are cancer (in ~50%–80% of mice) and age-associated pathologies (~50%–20%) (González-Suárez et al., 2002; Herranz et al., 2010; Tomás-Loba et al., 2008). We first determined whether the incidence of malignant cancers (lymphoma, sarcoma, and adenocarcinoma) showed any differential prevalence in mice belonging to either the higher or lower quartile of rate of increase in the percentage of short telomeres. We found a similar incidence of cancer or degenerative diseases in both cases, in spite of the fact that mice belonging to the higher quartile of rate of increase in the percentage of short telomeres showed a median age at death of 105 weeks, compared with 140 weeks in the case of mice belonging to the lower quartile (Figure S5). We observed the same tendency in the TgTERT cohort, and mice belonging to the higher quartile of rate of increase in the percentage of short telomeres showed a median age at death of 116 weeks, compared with 149 weeks in the case of mice belonging to the lower quartile.

Collectively, these findings demonstrate that the rate of increase in the percentage of short telomeres during an individual's lifetime, rather than the rate of telomere shortening over time, determines longevity in mice. These results bring into question the prevailing viewpoint that telomere shortening does not influence replicative aging in WT mice (Gomes et al., 2011; Wright and Shay, 2000), and highlight the importance of performing longitudinal telomere studies to predict traits as complex as longevity.

EXPERIMENTAL PROCEDURES

Mice

Male mice of a 100% C57BL/6 background were produced and stored at the SPF barrier area of the Spanish National Cancer Center, in accordance with the recommendations of the Federation of European Laboratory Animal Science Associations.

In this study we used a total of 38 mice (20 WT and 18 TgTERT; Figure 1B). Two mice from each cohort were sacrificed after the last telomere length measurement point for experimentation, and were excluded from the survival curves and other correlations involving final lifespan.

Experimental Setup

After weaning, five mice were housed per cage and fed a nonpurified diet (No. 2018; Harlan) ad libitum. For the aging study, 3-month-old mice were individually housed and were fed 92.5 kcal per week of chemically defined control

diet (AIN-93M, diet No. F05312; Bio-Serv). This caloric intake was ~10% fewer calories than the average daily intake of C57BL/6 mice, to ensure that all food was consumed. Defined diets were cold-packed into 1 g pellets. The mice were fed two-sevenths of the weekly allotment of food on Monday and Wednesday, and three-sevenths of that amount of Friday (Dhahbi et al., 2004; Pugh et al., 1999).

Mice were inspected on a daily basis and sacrificed when they presented signs of illness or tumors, in accordance with the Guidelines for Humane Endpoints for Animals Used in Biomedical Research (Harrison et al., 2009). The date of euthanasia was considered as an estimation of the natural lifespan. The mice were subjected to necropsy and histopathological analysis.

Histological Analysis

Histopathology was performed as previously described (González-Suárez et al., 2001). Briefly, tissues and organs were fixed for 24 hr in a 10% neutral buffered formalin solution at room temperature, dehydrated through graded alcohols and xylene, and embedded in paraffin. Histological analysis was achieved on 4–5 μm sections according to standard procedures. Cancer-related pathologies and senile lesions were grouped as described previously (Tomás-Loba et al., 2008).

HT-QFISH on PBLs

Blood was extracted from the facial vein at the indicated time points. Upon erythrocyte lysis (buffer EL; Qiagen), PBLs were plated on a clear-bottom, black-walled, 96-well plate, and HT-QFISH was performed as previously described (Canela et al., 2007). The accuracy and sensitivity of HT-QFISH are similar to those of telomere QFISH on metaphasic chromosomes (Canela et al., 2007). We analyzed telomere length values using individual telomere spots (>5,000 per sample) corresponding to the specific binding of a Cy3-labeled telomeric probe. Fluorescence intensities were converted into kilobases as described previously (Canela et al., 2007; McIlrath et al., 2001).

Statistical Analysis

A log-rank test was used to calculate statistical differences in the survival curves. Student's t-test was used to calculate the statistical significance of the mean telomere and short telomere variation over time. To calculate the rate of increase in the percentage of short telomeres and the rate of mean telomere shortening, linear regression lines were calculated for each mouse with GraphPad Prism, representing the best-fit values of the four values calculated at the different time points (either percentage of short telomeres or mean telomere length). For mice that died before the acquisition of all time points, linear regression lines were determined from the available measurements. The p value was calculated by dividing the slope by its standard error, and represents the correlation between the axes (slope significantly different from zero). Pathological analysis was calculated with the χ^2 test.

SUPPLEMENTAL INFORMATION

Supplemental Information includes five figures and can be found with this article online at http://dx.doi.org/10.1016/j.celrep.2012.08.023.

LICENSING INFORMATION

ACKNOWLEDGMENTS

We are indebted to Rosa Serrano for mouse colony management. The Blasco laboratory is funded by the Spanish Ministry of Science and Innovation, European Union (GENICA and TELOMARKER), European Research Council (Advanced Grant), Fundación Botín, and Fundación Lilly. E.V. performed most of the experimental work. B.B.J. and M.F. analyzed data and wrote the paper. J.M.F. did the pathological analysis. M.A.B. directed the project and wrote the paper.

Received: May 3, 2012
Revised: July 11, 2012
Accepted: August 21, 2012
Published online: September 27, 2012

REFERENCES

Armanios, M., Alder, J.K., Parry, E.M., Karim, B., Strong, M.A., and Greider, C.W. (2009). Short telomeres are sufficient to cause the degenerative defects associated with aging. Am. J. Hum. Genet. *85*, 823–832.

Armanios, M.Y., Chen, J.J., Cogan, J.D., Alder, J.K., Ingersoll, R.G., Markin, C., Lawson, W.E., Xie, M., Vulto, I., Phillips, J.A., 3rd., et al. (2007). Telomerase mutations in families with idiopathic pulmonary fibrosis. N. Engl. J. Med. *356*, 1317–1326.

Baerlocher, G.M., Mak, J., Röth, A., Rice, K.S., and Lansdorp, P.M. (2003). Telomere shortening in leukocyte subpopulations from baboons. J. Leukoc. Biol. *73*, 289–296.

Bernardes de Jesus, B., Vera, E., Schneeberger, K., Tejera, A.M., Ayuso, E., Bosch, F., and Blasco, M.A. (2012). Telomerase gene therapy in adult and old mice delays aging and increases longevity without increasing cancer. EMBO Mol. Med. *4*, 691–704.

Blackburn, E.H. (1991). Structure and function of telomeres. Nature *350*, 569–573.

Blackburn, E.H. (2005). Telomeres and telomerase: their mechanisms of action and the effects of altering their functions. FEBS Lett. *579*, 859–862.

Blasco, M.A. (2007). Telomere length, stem cells and aging. Nat. Chem. Biol. *3*, 640–649.

Blasco, M.A., Lee, H.W., Hande, M.P., Samper, E., Lansdorp, P.M., DePinho, R.A., and Greider, C.W. (1997). Telomere shortening and tumor formation by mouse cells lacking telomerase RNA. Cell *91*, 25–34.

Brown-Borg, H.M., and Bartke, A. (2012). GH and IGF1: roles in energy metabolism of long-living GH mutant mice. J. Gerontol. A Biol. Sci. Med. Sci. *67*, 652–660.

Canela, A., Vera, E., Klatt, P., and Blasco, M.A. (2007). High-throughput telomere length quantification by FISH and its application to human population studies. Proc. Natl. Acad. Sci. USA *104*, 5300–5305.

Cawthon, R.M., Smith, K.R., O'Brien, E., Sivatchenko, A., and Kerber, R.A. (2003). Association between telomere length in blood and mortality in people aged 60 years or older. Lancet *361*, 393–395.

Collado, M., Blasco, M.A., and Serrano, M. (2007). Cellular senescence in cancer and aging. Cell *130*, 223–233.

Collerton, J., Martin-Ruiz, C., Kenny, A., Barrass, K., von Zglinicki, T., Kirkwood, T., and Keavney, B.; Newcastle 85+ Core Study Team. (2007). Telomere length is associated with left ventricular function in the oldest old: the Newcastle 85+ study. Eur. Heart J. *28*, 172–176.

Chan, S.W., and Blackburn, E.H. (2002). New ways not to make ends meet: telomerase, DNA damage proteins and heterochromatin. Oncogene *21*, 553–563.

Cherkas, L.F., Aviv, A., Valdes, A.M., Hunkin, J.L., Gardner, J.P., Surdulescu, G.L., Kimura, M., and Spector, T.D. (2006). The effects of social status on biological aging as measured by white-blood-cell telomere length. Aging Cell *5*, 361–365.

de Lange, T. (2005). Shelterin: the protein complex that shapes and safeguards human telomeres. Genes Dev. *19*, 2100–2110.

Deng, Y., Chan, S.S., and Chang, S. (2008). Telomere dysfunction and tumour suppression: the senescence connection. Nat. Rev. Cancer *8*, 450–458.

Dhahbi, J.M., Kim, H.J., Mote, P.L., Beaver, R.J., and Spindler, S.R. (2004). Temporal linkage between the phenotypic and genomic responses to caloric restriction. Proc. Natl. Acad. Sci. USA *101*, 5524–5529.

Epel, E.S., Blackburn, E.H., Lin, J., Dhabhar, F.S., Adler, N.E., Morrow, J.D., and Cawthon, R.M. (2004). Accelerated telomere shortening in response to life stress. Proc. Natl. Acad. Sci. USA *101*, 17312–17315.

Flores, I., Benetti, R., and Blasco, M.A. (2006). Telomerase regulation and stem cell behaviour. Curr. Opin. Cell Biol. *18*, 254–260.

Flores, I., Canela, A., Vera, E., Tejera, A., Cotsarelis, G., and Blasco, M.A. (2008). The longest telomeres: a general signature of adult stem cell compartments. Genes Dev. *22*, 654–667.

García-Cao, I., García-Cao, M., Tomás-Loba, A., Martín-Caballero, J., Flores, J.M., Klatt, P., Blasco, M.A., and Serrano, M. (2006). Increased p53 activity does not accelerate telomere-driven ageing. EMBO Rep. *7*, 546–552.

Gomes, N.M., Ryder, O.A., Houck, M.L., Charter, S.J., Walker, W., Forsyth, N.R., Austad, S.N., Venditti, C., Pagel, M., Shay, J.W., and Wright, W.E. (2011). Comparative biology of mammalian telomeres: hypotheses on ancestral states and the roles of telomeres in longevity determination. Aging Cell *10*, 761–768.

González-Suárez, E., Samper, E., Ramírez, A., Flores, J.M., Martín-Caballero, J., Jorcano, J.L., and Blasco, M.A. (2001). Increased epidermal tumors and increased skin wound healing in transgenic mice overexpressing the catalytic subunit of telomerase, mTERT, in basal keratinocytes. EMBO J. *20*, 2619–2630.

González-Suárez, E., Flores, J.M., and Blasco, M.A. (2002). Cooperation between p53 mutation and high telomerase transgenic expression in spontaneous cancer development. Mol. Cell. Biol. *22*, 7291–7301.

González-Suárez, E., Geserick, C., Flores, J.M., and Blasco, M.A. (2005). Antagonistic effects of telomerase on cancer and aging in K5-mTert transgenic mice. Oncogene *24*, 2256–2270.

Greider, C.W. (1998). Telomerase activity, cell proliferation, and cancer. Proc. Natl. Acad. Sci. USA *95*, 90–92.

Greider, C.W., and Blackburn, E.H. (1985). Identification of a specific telomere terminal transferase activity in Tetrahymena extracts. Cell *43*, 405–413.

Hao, L.Y., Armanios, M., Strong, M.A., Karim, B., Feldser, D.M., Huso, D., and Greider, C.W. (2005). Short telomeres, even in the presence of telomerase, limit tissue renewal capacity. Cell *123*, 1121–1131.

Harley, C.B., Futcher, A.B., and Greider, C.W. (1990). Telomeres shorten during ageing of human fibroblasts. Nature *345*, 458–460.

Harrison, D.E., Strong, R., Sharp, Z.D., Nelson, J.F., Astle, C.M., Flurkey, K., Nadon, N.L., Wilkinson, J.E., Frenkel, K., Carter, C.S., et al. (2009). Rapamycin fed late in life extends lifespan in genetically heterogeneous mice. Nature *460*, 392–395.

Hastie, N.D., Dempster, M., Dunlop, M.G., Thompson, A.M., Green, D.K., and Allshire, R.C. (1990). Telomere reduction in human colorectal carcinoma and with ageing. Nature *346*, 866–868.

Heidinger, B.J., Blount, J.D., Boner, W., Griffiths, K., Metcalfe, N.B., and Monaghan, P. (2012). Telomere length in early life predicts lifespan. Proc. Natl. Acad. Sci. USA *109*, 1743–1748.

Herranz, D., Munoz-Martin, M., Canamero, M., Mulero, F., Martinez-Pastor, B., Fernandez-Capetillo, O., and Serrano, M. (2010). Sirt1 improves healthy ageing and protects from metabolic syndrome-associated cancer. Nat. Commun. *1*, 3.

Herrera, E., Samper, E., Martín-Caballero, J., Flores, J.M., Lee, H.W., and Blasco, M.A. (1999). Disease states associated with telomerase deficiency appear earlier in mice with short telomeres. EMBO J. *18*, 2950–2960.

Mainous, A.G., 3rd, Codd, V., Diaz, V.A., Schoepf, U.J., Everett, C.J., Player, M.S., and Samani, N.J. (2010). Leukocyte telomere length and coronary artery calcification. Atherosclerosis *210*, 262–267.

Marion, R.M., Strati, K., Li, H., Tejera, A., Schoeftner, S., Ortega, S., Serrano, M., and Blasco, M.A. (2009). Telomeres acquire embryonic stem cell characteristics in induced pluripotent stem cells. Cell Stem Cell *4*, 141–154.

McIlrath, J., Bouffler, S.D., Samper, E., Cuthbert, A., Wojcik, A., Szumiel, I., Bryant, P.E., Riches, A.C., Thompson, A., Blasco, M.A., et al. (2001). Telomere length abnormalities in mammalian radiosensitive cells. Cancer Res. *61*, 912–915.

Mitchell, J.R., Wood, E., and Collins, K. (1999). A telomerase component is defective in the human disease dyskeratosis congenita. Nature *402*, 551–555.

Monaghan, P. (2010). Telomeres and life histories: the long and the short of it. Ann. N Y Acad. Sci. *1206*, 130–142.

Pugh, T.D., Klopp, R.G., and Weindruch, R. (1999). Controlling caloric consumption: protocols for rodents and rhesus monkeys. Neurobiol. Aging *20*, 157–165.

Slagboom, P.E., Droog, S., and Boomsma, D.I. (1994). Genetic determination of telomere size in humans: a twin study of three age groups. Am. J. Hum. Genet. *55*, 876–882.

Tomás-Loba, A., Flores, I., Fernández-Marcos, P.J., Cayuela, M.L., Maraver, A., Tejera, A., Borrás, C., Matheu, A., Klatt, P., Flores, J.M., et al. (2008). Telomerase reverse transcriptase delays aging in cancer-resistant mice. Cell *135*, 609–622.

Tsakiri, K.D., Cronkhite, J.T., Kuan, P.J., Xing, C., Raghu, G., Weissler, J.C., Rosenblatt, R.L., Shay, J.W., and Garcia, C.K. (2007). Adult-onset pulmonary fibrosis caused by mutations in telomerase. Proc. Natl. Acad. Sci. USA *104*, 7552–7557.

Valdes, A.M., Andrew, T., Gardner, J.P., Kimura, M., Oelsner, E., Cherkas, L.F., Aviv, A., and Spector, T.D. (2005). Obesity, cigarette smoking, and telomere length in women. Lancet *366*, 662–664.

Vaziri, H., Schächter, F., Uchida, I., Wei, L., Zhu, X., Effros, R., Cohen, D., and Harley, C.B. (1993). Loss of telomeric DNA during aging of normal and trisomy 21 human lymphocytes. Am. J. Hum. Genet. *52*, 661–667.

Vulliamy, T., Marrone, A., Goldman, F., Dearlove, A., Bessler, M., Mason, P.J., and Dokal, I. (2001). The RNA component of telomerase is mutated in autosomal dominant dyskeratosis congenita. Nature *413*, 432–435.

Wright, W.E., and Shay, J.W. (2000). Telomere dynamics in cancer progression and prevention: fundamental differences in human and mouse telomere biology. Nat. Med. *6*, 849–851.

Yamaguchi, H., Calado, R.T., Ly, H., Kajigaya, S., Baerlocher, G.M., Chanock, S.J., Lansdorp, P.M., and Young, N.S. (2005). Mutations in TERT, the gene for telomerase reverse transcriptase, in aplastic anemia. N. Engl. J. Med. *352*, 1413–1424.

OPEN ACCESS Freely available online

PLOS ONE

Telomerase Reverse Transcriptase Synergizes with Calorie Restriction to Increase Health Span and Extend Mouse Longevity

Elsa Vera[1], Bruno Bernardes de Jesus[1], Miguel Foronda[1], Juana M. Flores[2], Maria A. Blasco[1]*

1 Telomeres and Telomerase Group, Molecular Oncology Program, Spanish National Cancer Research Centre, Melchor Fernández Almagro 3, Madrid, Spain, **2** Animal Surgery and Medicine Department, Facultad de Veterinaria, Universidad Complutense de Madrid, Madrid, Spain

Abstract

Caloric restriction (CR), a reduction of food intake while avoiding malnutrition, can delay the onset of cancer and age-related diseases in several species, including mice. In addition, depending of the genetic background, CR can also increase or decrease mouse longevity. This has highlighted the importance of identifying the molecular pathways that interplay with CR in modulating longevity. Significant lifespan extension in mice has been recently achieved through over-expression of the catalytic subunit of mouse telomerase (mTERT) in a cancer protective background. Given the CR cancer-protective effects in rodents, we set to address here whether CR impacts on telomere length and synergizes with mTERT to extend mouse longevity. CR significantly decreased tumor incidence in TERT transgenic (TgTERT) mice and extended their lifespan compared to wild-type (WT) controls under the same diet, indicating a synergy between TgTERT and CR in increasing mouse longevity. In addition, longitudinal telomere length measurements in peripheral blood leukocytes from individual mice showed that CR resulted in maintenance and/or elongation telomeres in a percentage of WT mice, a situation that mimics telomere dynamics in TgTERT cohorts. These results demonstrate that CR attenuates telomere erosion associated to aging and that synergizes with TERT over-expression in increasing "health span" and extending mouse longevity.

Citation: Vera E, Bernardes de Jesus B, Foronda M, Flores JM, Blasco MA (2013) Telomerase Reverse Transcriptase Synergizes with Calorie Restriction to Increase Health Span and Extend Mouse Longevity. PLoS ONE 8(1): e53760. doi:10.1371/journal.pone.0053760

Editor: Jose Vina, University of Valencia, Spain

Received September 28, 2012; **Accepted** December 4, 2012; **Published** January 22, 2013

Funding: Blasco lab is funded by Spanish Ministry of Science and Innovation, European Union (GENICA and TELOMARKER), European Research Council Advanced Grant, Fundación Botín and Fundación Lilly. The funders had no role in study design, data collection and analysis, decision to publish, or preparation of the manuscript.

Competing Interests: The authors have declared that no competing interests exist.

* E-mail: mblasco@cnio.es

Introduction

Caloric restriction (CR) in various organisms, including primates, delays the development of some age-related diseases such as cancer, atherosclerosis, diabetes, and neuro-degenerative and respiratory failures, among others [1,2,3], thus increasing the so-called "health span". At the metabolic level, CR results in improved insulin sensitivity and subsequent decrease in the fasting glucose, protecting from age-dependent metabolic syndrome and diabetes [2,4,5]. CR in humans also reduces the risk factor for diabetes, cardiovascular disease and cancer [4], although it has been reported to negatively impact on bone mineral density and muscular mass [6,7].

In addition to these beneficial effects of CR in increasing "health span", chronic CR is considered among the most robust life-extending interventions, although several recent reports indicate that CR does not always extend and may even shorten lifespan depending on the genotype [2,8], highlighting the importance of finding the genetic pathways which synergize with CR in extending or shortening lifespan. In the particular case of the C57BL/6 mouse strain used in this study, CR has been reported to produce around a 20% life extension when started in 12 months old mice and 40% when started with 19 months old mice [9,10,11,12]. Similar strategies were employed in younger mice and rats and, although the duration was different from the actual study, some beneficial effects could be observed (for a comprehensive review see [13]).

The exact mechanisms by which CR works are currently debated, although the most widespread theory points to a significant protection from DNA damage due to a reduction of metabolism [14,15]. Understanding the mechanisms underlying CR is of great importance as this could pinpoint new therapeutic targets for age-associated diseases, or for anti-aging therapies. In this regard, the well-documented association between telomere shortening and aging [16] suggests a possible role of telomere dynamics in the systemic effects of CR.

Telomeres protect chromosome ends from degradation and DNA repair activities and, therefore, are essential for chromosome-end integrity (telomere capping) and chromosomal stability [17]. Telomere repeats are maintained by telomerase, a reverse transcriptase that can elongate chromosome ends *de novo* in those cells where it is expressed at sufficiently high levels, such as embryonic pluripotent stem cells [18]. In telomerase-negative cells, telomeres become shorter associated to each round of cell division due to the end-replication problem and to the action of DNA degrading activities. Short telomeres are passed onto daughter cells and thus telomere shortening is exacerbated with cell division, as well as with increasing age both in humans and mice [19]. Critically short telomeres can trigger a persistent DNA damage response, which leads to cellular senescence and/or apoptosis [20],

thus eventually compromising tissue function and tissue regenerative capacity, and contributing to organismal aging [21]. This progressive telomere shortening is proposed to represent a "molecular clock" that underlies organism aging.

Both telomerase-deficient mice and human diseases involving mutations in telomerase components result in accelerated-aging phenotypes probably due to the depletion of the pools of stem cells followed by organ failure [16,22,23]. In addition, the speed of telomere shortening with aging can be influenced by factors known to be a risk for disease and premature death, such as psychological stress, smoking, cognitive impairment and obesity [24]. Little is known, however, on the potential effect of treatments that increase lifespan, such as CR, on the rate of telomere shortening with aging.

Besides CR, lifespan extension has been also achieved by over-expressing the catalytic subunit of telomerase, mTERT, in a cancer protective backgrounds owe to increase expression of tumor suppressor genes [25] or through telomerase expression in old mice by using a gene therapy approach [26]. In this context, mTERT over-expression was sufficient to decrease telomere damage with age, delay aging, and increase median longevity. Transgenic overexpression of mTERT, however, was found to increase cancer incidence, therefore masking the potential beneficial effects of constitutive telomerase activation [27]. Since CR is partially mimicking a tumor suppressive condition, we set here to study the impact of transgenic telomerase overexpression in a CR model.

To this end, we performed longitudinal telomere length analyses in single mice by using an automated highthroughput (HT) quantitative telomere FISH platform, HT-QFISH [28], which allows the quantification of individual telomeric spots, and therefore the percentage of short telomeres, in individual cells from large human and mice cohorts. The abundance of critically short telomeres, rather than the mean telomere length, is indicative of telomere dysfunction [29], and thus likely to be useful as biomarker of aging and age-associated diseases.

In summary, we address here the effect of CR on telomere dynamics and telomere function longitudinally during the lifetime of wild-type and telomerase transgenic mice in a C57BL/6 genetic background, as well as study its impact on several health indicators, cancer, and longevity. In this context, we demonstrate that CR slows down telomere shortening and the accumulation of telomere damage with aging in CR WT mice, a situation that mimics mTERT over-expression. These positive effects of CR on telomere length are observed in a wide range of tissues, including peripheral blood mononuclear cells. Importantly, under our experimental settings TgTERT mice under CR show a significant lifespan extension compared to wild-type mice under CR. In contrast, wild-type mice under CR did not present a significant lifespan extension compared to wild-type control mice. These results demonstrate that CR synergizes with telomerase expression resulting in a significant lifespan extension. A similar synergism was previously observed between telomerase expression and higher level of tumor suppressors, which result in a safe cancer protective background for telomerase expression [25]. Hypothetically, the synergism between telomerase expression and caloric restriction could be ruled though the same mechanism.

Results

Calorie Restriction Leads to Significant Weight Loss in both WT and TgTERT Mice

We first set to address whether CR impacts on telomere length dynamics in mice. To this end, we established 4 cohorts of mice, including wild-type and TgTERT mice under either a control or a CR diet. All mice had an identical genetic background, which was a pure C57BL/6 (Materials and Methods). When mice were 3 months of age, those mice to be under CR where shifted to a diet containing 40% of the calories of those of the control diet group. Of note, control mice were not fed *ad libitum*, thus avoiding individual variations in caloric intake in this group (Materials and Methods). One month after the start of diets, the body weight of WT and TgTERT mice under CR was significantly lower than that of the corresponding cohorts under the control diet, and we did not detect differences associated to telomerase over-expression (**Fig. 1A**; $p<0.0001$). After 12 months of diet, both wild-type and TgTERT mice under CR were 35% lighter than the corresponding controls (**Fig. 1A**) and this difference was reduced to 20% at 24 months of diet (**Fig. 1A**; $p<0.0001$). Total fat mass values as determined by DEXA (Materials and Methods), were significantly reduced following 16 months of CR diet in both genotypes compared to the corresponding cohorts under the control diet (**Fig. 1B,C**). Those differences were maintained after 24 months of diet, at which point mice under the control diet also presented reduced fat most likely owe to the normal aging process (**Fig. 1B,C**). Interestingly, old TgTERT mice under the control diet showed significantly higher total fat mass than the age-matched WT cohort under the same diet (**Fig. 1C**; $p=0.02$), in accordance with our previous observations that TERT over-expression leads to improved health status and delayed aging associated pathologies [25].

Stronger Effect of CR in Delaying Age-associated Pathologies in Mice Over-expressing TERT

To test the potential synergistic effects of CR and TgTERT in protecting from age-associated pathologies, we first examined the metabolic capacity of mice under CR compared to mice under the control diet. Glucose intolerance and insulin resistance are common indicators of aging in control conditions. In turn, enhanced glucose tolerance and insulin sensitivity normally accompany lifespan extension in mammals and are also observed after long-term CR [7,30] as well as in some long-lived genetically modified mice, such as mice with enhanced expression of TERT or with enhanced expression of certain tumor suppressor genes [25]. As expected, after 12 months of diet (at 15 months of age), both WT and TgTERT mice under CR showed a significantly improved glucose tolerance compared to the corresponding cohorts under the control diet (**Fig. 1D,E**; $p=0.007$ and $p=0.003$, respectively), as indicated by a faster glucose uptake following glucose injection in fasting (Materials and Methods). Fasting plasma insulin levels (**Fig. 1F**) showed a trend to be lower in CR WT mice, and this trend reached statistical significance in TgTERT mice after 12 months of CR diet compared to the corresponding cohorts under a control diet (**Fig. 1F**; $p=0.006$). Similarly, insulin sensitivity after 12 months of treatment tended to be lower in CR WT, and this trend became significant only in CR TgTERT mice (**Fig 1G**; $p=0.04$), as assessed using the homeostatic model assessment score (HOMA) [31].

Another common feature of aging is the development of osteoporosis, a process were bone mineral density (BMD) is reduced [32]. In line with this, both WT and TgTERT mice showed BMD loss through life, as measured by DEXA, however, bone loss was significantly higher in mice under the control diet compared to calorie restricted mice (**Fig 1H**; $p=0.05$ and $p=0.006$ for WT and TgTERT, respectively; **Fig. 1I** for representative image). Of note, in the first 16 months of diet, CR led to decreased BMD in both genotypes compared to the control diet, in agreement with previous observations (**Fig. S1A–C**) [6,7]. In summary, these findings suggest a long-term

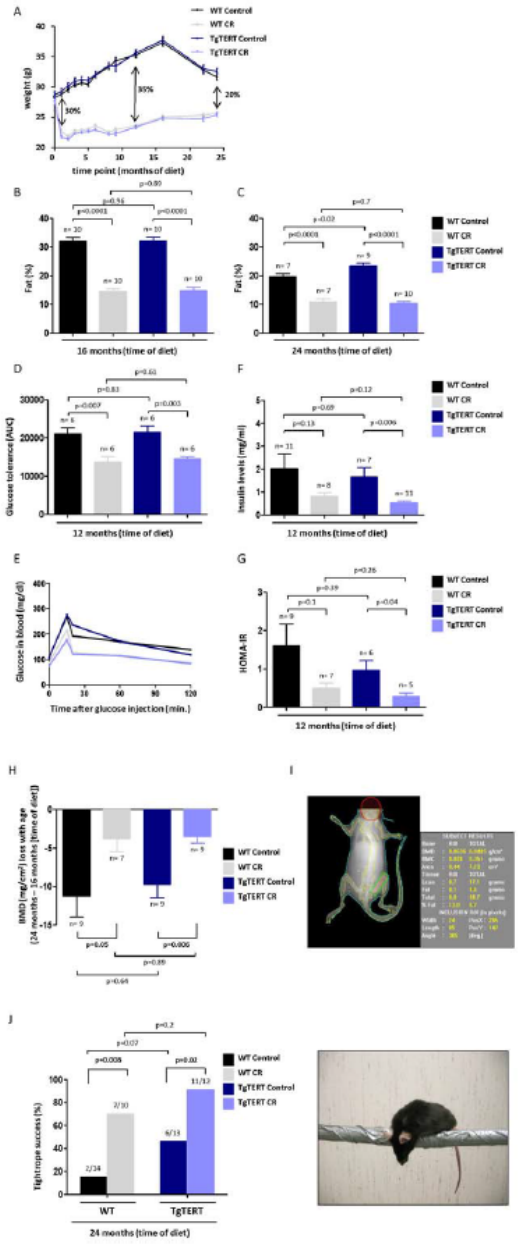

Figure 1. Impact of long-term calorie restriction on metabolic homeostasis and age-associated pathologies. (A) Weight given as average ± SEM of WT and TgTERT mice fed with control or CR diet (see Materials and Methods). One way ANOVA was used to assess statistical significance between the four groups (WT Control vs. Wt CR: $p<0.0001$; TgTERT Control vs. TgTERT CR: $p<0.0001$; WT Control vs. TgTERT Control: $p=0.72$; WT CR vs. TgTERT CR: $p=0.46$). (B and C) Total fat mass of the indicated cohorts was measured at 16 months of diet (B) and 24 months of diet (C). Values are given as average ± SEM, and statistical significance was determined by the two-tailed Student's t-test. (D and E) Glucose tolerance test (GTT) was performed at 12 months of diet. Integrated AUCs (area under the curve; (D)) and curves (E) are shown. Values are given as average ± SEM, and statistical significance was determined by the two-tailed Student's t-test. (F) Fasting plasma insulin levels, given as mean ± SEM, was measured in the different cohorts at 12 months of diet. Statistical significance was determined by the two-tailed Student's t-test. (G) Insulin sensitivity, estimated using the homeostatic model assessment score (HOMA-IR), was performed at 12 months of diet. Values are given as average ± SEM, and statistical significance was determined by the two-tailed Student's t-test. (H) Femur bone mineral density (BMD) variation through lifetime of WT and TgTERT mice under control and CR diets. Values are given as average ± SEM, and statistical significance was determined by the two-tailed Student's *t*-test. (I) Representative DEXA image used for BMD and fat mass calculations. (J) Neuromuscular coordination was quantified as the percentage of mice that pass with success the tightrope test. Numbers above the bars represent the number of mice that successfully pass the test over the total number of mice tested. Student's *t*-test was used to assess significance between control and CR mice. Values are given as average ± SEM, and statistical significance was determined by the two-tailed Student's *t*-test.
doi:10.1371/journal.pone.0053760.g001

protective effect of CR in the onset of osteoporosis in both genotypes in spite of an initial negative impact of CR on bone density.

An additional biomarker of aging is the progressive loss of neuromuscular coordination that can be measured by the tightrope success test [33]. In this assay, CR mice from both genotypes performed significantly better than mice under the control diet (**Fig. 1J**; $p=0.008$ and 0.02 for WT and TgTERT mice, respectively). Of notice, TgTERT mice under the control diet performed better than WT mice under the same diet, although the differences did not reach statistical significance (**Fig. 1J**; $p=0.08$), in line with an improved health status and delayed aging associated to TERT over-expression [25]. In summary, CR has a measurable positive effect on neuromuscular coordination in WT mice and this effect seems to be synergistic with that of TgTERT expression.

Together, these results demonstrate that the long-term calorie restriction protocol performed here delays the onset of age-associated pathologies such as glucose intolerance, osteoporosis, and impaired neuromuscular coordination both in WT and TgTERT mice, although in some assays the effects tended to be of a greater magnitude in the TgTERT cohorts (i.e. insulin levels or tightrope test).

The Impact of CR Decreasing Molecular Markers of Aging is More Apparent in Mice Over-expressing TERT

Calorie restriction, similarly to the effect of some longevity-enhancing mutations in mice, has been shown to reduce IGF1 serum levels, particularly in aged rodents [34,35]. In our study, however, we did not find significant differences in IGF-1 levels between WT mice under either CR or a control diet (**Fig. S1D**; $p=0.2$). Interestingly, IGF-1 levels where higher in TgTERT mice compared WT mice under control diet (**Fig. S1D**; $p=0.01$), in agreement with previous findings [25], and these levels were significantly reduced in TgTERT cohorts under CR (**Fig. S1D**; $p=0.04$). Growth hormone (GH) levels were significantly increased in TgTERT mice under CR (**Fig. S1E**; $p=0.04$) compared to the control diet cohorts.

An additional molecular marker of aging is the accumulation of phosphorylated histone H2AX (γ-H2AX) foci in aged tissues, which has been shown to co-localize with double strand breaks (DSBs) as well as with critically short/dysfunctional telomeres [36,37,38,39,40,41]. We found a tendency to have decreased levels of γ-H2AX in the kidney of WT and TgTERT CR mice

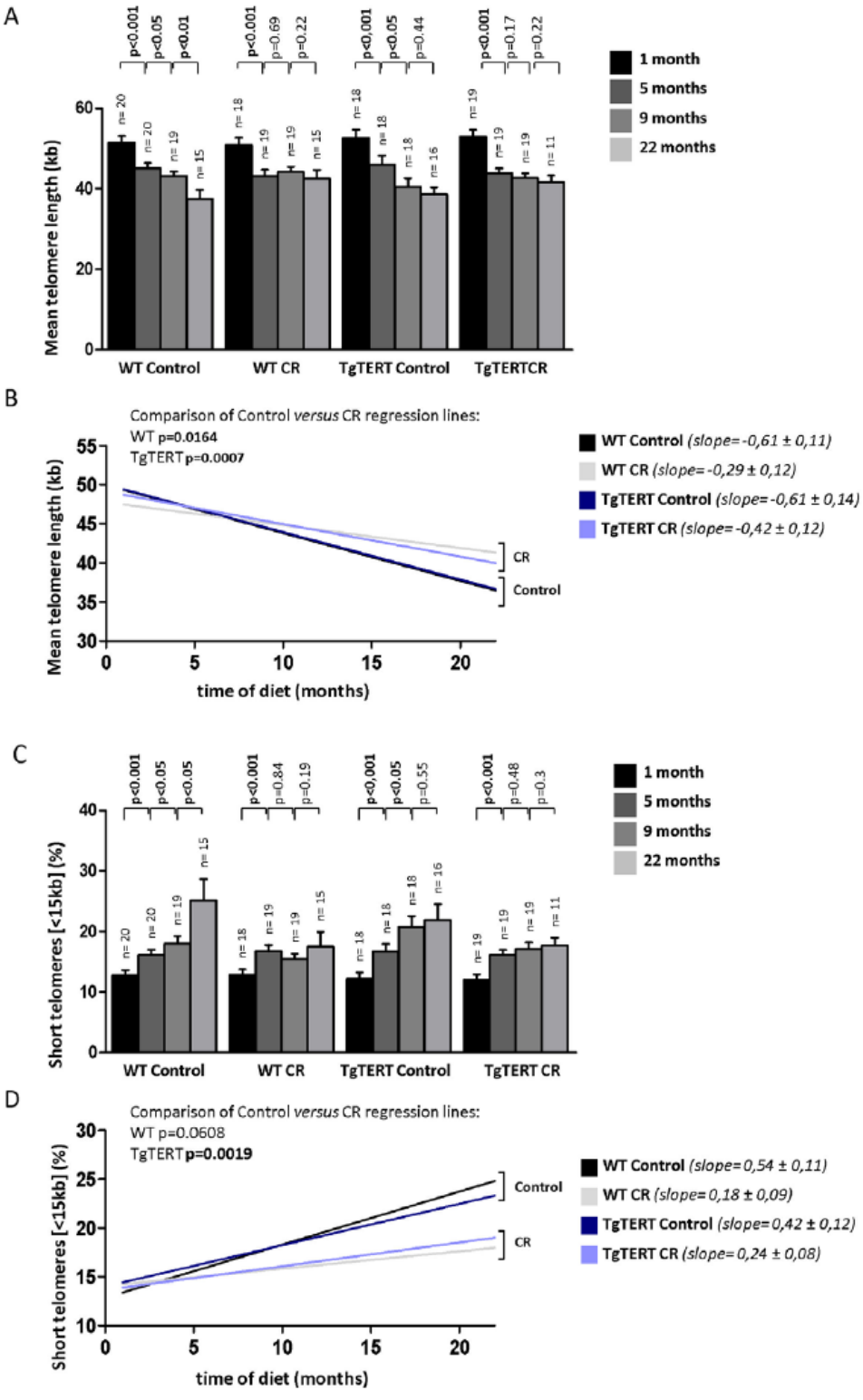
A
p<0.001
p<0.05
p<0.01
p<0.001
p=0.69
p=0.22
p<0,001
p<0.05
p=0.44
p<0.001
p=0.17
p=0.22
n= 20
n= 20
n= 19
n= 15
n= 18
n= 19
n= 19
n= 15
n= 18
n= 18
n= 18
n= 16
n= 19
n= 19
n= 19
n= 11
Mean telomere length (kb)
60
40
20
0
WT Control
WT CR
TgTERT Control
TgTERTCR
1 month
5 months
9 months
22 months
B
Comparison of Control versus CR regression lines:
WT p=0.0164
TgTERT p=0.0007
Mean telomere length (kb)
55
50
45
40
35
30
0
5
10
15
20
time of diet (months)
CR
Control
WT Control (slope=-0,61 ± 0,11)
WT CR (slope=-0,29 ± 0,12)
TgTERT Control (slope=-0,61 ± 0,14)
TgTERT CR (slope=-0,42 ± 0,12)
C
p<0.001
p<0.05
p<0.05
p<0.001
p=0.84
p=0.19
p<0,001
p<0.05
p=0.55
p<0.001
p=0.48
p=0.3
n= 20
n= 20
n= 19
n= 15
n= 18
n= 19
n= 19
n= 15
n= 18
n= 18
n= 18
n= 16
n= 19
n= 19
n= 19
n= 11
Short telomeres [<15kb] (%)
40
30
20
10
0
WT Control
WT CR
TgTERT Control
TgTERT CR
1 month
5 months
9 months
22 months
D
Comparison of Control versus CR regression lines:
WT p=0.0608
TgTERT p=0.0019
Short telomeres [<15kb] (%)
30
25
20
15
10
0
5
10
15
20
time of diet (months)
Control
CR
WT Control (slope=0,54 ± 0,11)
WT CR (slope=0,18 ± 0,09)
TgTERT Control (slope=0,42 ± 0,12)
TgTERT CR (slope=0,24 ± 0,08)

Figure 2. Slower age-dependent telomere shortening in mice under calorie restriction. (A and C) Mean telomere length (A) and percentage of short telomeres (C) was determined by HT QFISH on white blood cells from the indicated mice under CR and control diet. The number of mice is indicated on the top of each bar (n). Values are given as average ± SEM, and statistical significance was determined by one-tailed Student's *t*-test. (B and D) Linear regression lines of the values obtained for mean telomere length (B) and percentage of short telomeres (D) measured in white blood cells. The slope ± SD of each regression line is indicated and represents the rate of telomere loss with time.
doi:10.1371/journal.pone.0053760.g002

compared to those cohorts under control diet, although the differences were not significant (**Fig. S2A,B**). The accumulation of γ-H2AX was significantly attenuated, however, only in CR TgTERT mice compared to CR WT cohorts (**Fig. S2A,B**; $p = 0.03$), suggesting that TERT and CR may contribute in a synergic way to prevent DNA damage with aging something not surprising, since telomerase over-expression prevents telomeres shortening [26,42] (a form of DNA damage [41]) and CR has been extensively linked to DNA damage protection [43].

Calorie Restriction Decreases the Rate of Telomere Shortening with Aging in Longitudinal Studies

To address the effect of CR in telomere length dynamics, we performed a longitudinal telomere length study in individual WT and TgTERT mice under calorie restriction or under a control diet. The most widely used cell type for human and mouse telomere studies are peripheral blood leukocytes (PBL). Telomere length in PBLs has been proposed to reflect on the speed of aging process as hematopoietic stems cells proliferate throughout life. To this end, first, we measured telomere length and the percentage of short telomeres (arbitrarily set to <15 kb as this cutoff has been previously shown by us to be indicative of presence of short telomeres in mice [26]; see also **Fig. S3A–C** for additional cutoffs) in PBLs by using the highthroughput QFISH (HT-QFISH) method previously developed by us for blood samples (Materials and Methods) [28]. Blood was extracted from each individual mouse after 1, 5, 9 and 22 months of diet. We represented changes in mean telomere length and the percentage of short telomeres (<15 Kb) with time. As recently reported by us, WT mice under the control diet showed significant telomere attrition with age, which was detectable when comparing 4 months intervals, as reflected both by a significant decrease in mean telomere length and by a significant increase in the percentage of short telomeres (**Fig. 2A,C and Fig. S3A–C**), demonstrating that mice undergo telomere shortening associated to the aging process [44]. A similar trend was observed for TgTERT under a control diet, however, in this background telomeres shortened only during the first 9 months of diet, after which telomere erosion rate as well as the rate of increase of short telomeres were decreased, most likely as the consequence of increased TERT expression (Fig. 2A,C). Interestingly, in both CR WT and CR TgTERT mice, after an initial telomere shortening during 1 to 5 months of diet, telomeres were stabilized and did not show significant shortening until the end of the experiment (**Fig. 2A**). A similar trend was observed for the percentage of short telomeres, which showed an initial increase at 5 month of diet but was stabilized from 5 to 22 month of diet (**Fig. 2C and Fig. S3C**). These results are also illustrated by the linear regression of telomere length with time of the different groups. In particular, the rate of telomere shortening, as represented by the slope of the regression line, was significantly slower in CR mice of both genotypes compared to the corresponding cohorts under the control diet (**Fig. 2B**; $p = 0.0164$ and $p = 0.0007$ for WT and TgTERT, respectively). Similarly, WT and TgTERT mice under CR showed a lower rate of accumulation of short telomeres compared to the corresponding cohorts under the control diet (**Fig. 2D**; $p = 0.0608$ and $p = 0.0019$ for WT and TgTERT, respectively). These results further reinforce our findings that long-term CR decreases the rate of telomere shortening associated with aging, and protects form the appearance of short telomeres. This links two major cellular pathways involved in the aging process demonstrating for the first time that caloric restriction impacts on telomere dynamics.

Calorie Restriction Leads to Maintenance and/or Elongation of Telomeres in Individual Mice

To understand how CR is impacting on telomere length, we studied telomere dynamics with time in individual mice of both genotypes. First, we plotted both mean telomere values and the percentage of short telomeres at different time points for each mouse and adjusted these values to either a linear model (linear regression) or a non-linear model (quadratic) (**Fig. 3A–L**). In a recent report, we described that the rate of telomere shortening per year in both WT mice and TgTERT mice under a control diet is 100-times faster than in humans [44]. Interestingly, here we first show that both the rate of telomere shortening and the rate of accumulation of short telomeres were affected by CR in WT mice (p-value = 0.06 for mean telomere length and p-value<0.01 for the percentage of short telomeres), but not in the TgTERT group (**Fig. 3I–L**). These findings indicate that the effects of CR on telomere maintenance are smaller in the telomerase over-expressing mice, suggesting that they could be partially mediated by TERT.

To address this, we studied different patterns of telomere length behavior per individual mice with time (**Fig. 4A–F**). Interestingly, we observed three different trends for mean telomere length behavior: shortening of telomeres, maintenance of telomeres, and elongation of telomeres. Similarly, for the percentage of short telomeres, we found increased, decrease or maintenance in the percentage of short telomeres. These different behaviors are consistent with the fact that leukocytes can activate telomerase [45]. The frequency of these patterns in different genotype mice under CR or control diet may be informative on the effects of CR or TERT over-expression on telomere length dynamics with aging. To this end, we studied the changes in telomere length in 3 time intervals: 1–22, 5–22 and 9–22 months of diet (**Fig. 4A–F and Fig. S4A–F**). When considering behavior of telomeres in individual mice during 1–22 months of diet period, all WT mice under the control diet showed telomere shortening with time and none of them showed maintenance or elongation of telomeres during this period. In contrast, both WT mice under CR and TgTERT mice under both diets showed a number of individuals (~20%) that either elongated or maintained telomere length. This was paralleled by the abundance of short telomeres. Representative examples of each pattern are represented (**Fig. 4G,H**). These findings indicate that CR can stop or reverse the trend of continuous telomere shortening with aging, in an analogous manner to that observed for TERT over-expression.

Calorie Restriction Results in Longer Telomeres in Various Adult Mouse Tissues

To further study the impact of CR in telomere maintenance in the context of the organism, we measured telomere length in a variety of tissues (lung, kidney-cortex, muscle-fibers) from WT and TgTERT mice that had been under CR or a control diet during a

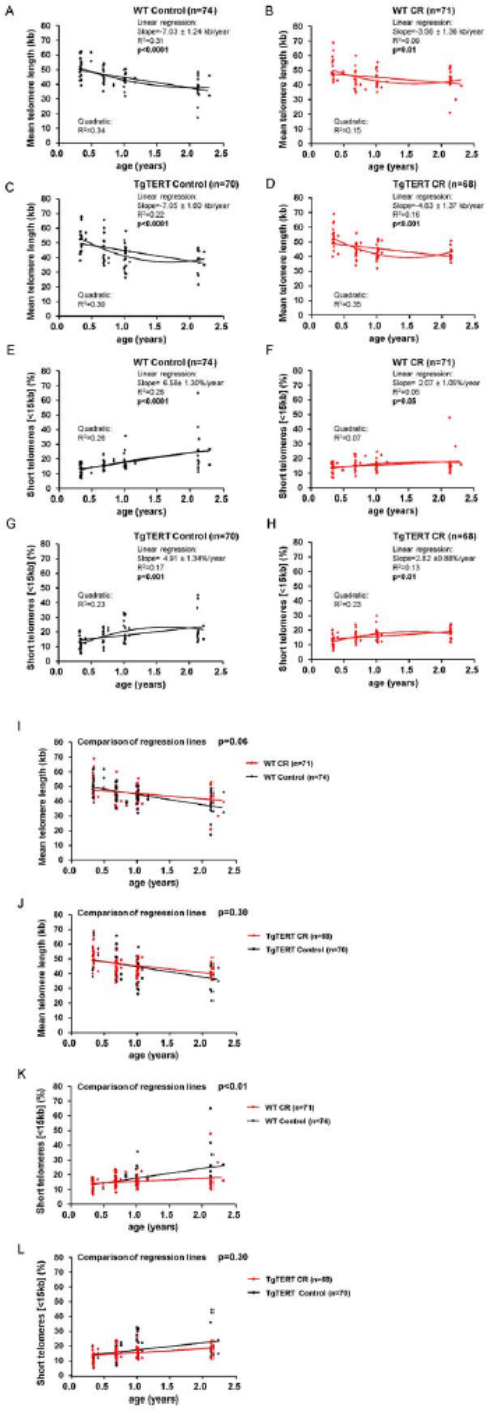

Figure 3. Longitudinal telomere length analyses. (A, B, C and D) Adjustment of mean telomere length values with aging to a linear model or, alternatively, to a quadratic model in the indicated mouse cohorts. Linear regression analysis was used to measure the association between age and mean telomere length. The slope of the regression line is indicated and represents the rate of telomere shortening per year (Kb). Second order polynomial adjustment (quadratic) was used for the non-linear fit model. The R^2 indicates the goodness of the data adjustment to each model. The number of mice per group is shown (n). (E, F, G and H) Adjustment of the percentage of short telomeres (<15kb) to a linear model or alternatively to a quadratic model in the indicated mouse cohorts. Linear regression analysis was used to measure the association between age and the percentage of short telomeres. The slope of the regression line is indicated and represents the percentage of short telomeres enrichment per year. Second order polynomial adjustment (quadratic) was used for the non-linear fit model. The R^2 indicates the goodness of the data adjustment to each model. The number of mice per group is shown (n). (I and J) Linear regression lines of the association between age and mean telomere length are shown for mice under CR (red lines) or a control diet (black lines), in both WT (I) and TgTERT (J) backgrounds. Multiple regression analysis was used to evaluate the statistical differences between the slopes of the different linear regression lines. The number of mice in each group is indicated (n). (K and L) Linear regression lines of the association between age and the percentage of short telomeres (<15 kb) are shown for mice under CR (red lines) or a control diet (black lines), in both WT (K) and TgTERT (L) backgrounds. Multiple regression analysis was used to assess the statistical differences between the different linear regression lines. The number of mice in each group is indicated (n).
doi:10.1371/journal.pone.0053760.g003

total of 23 months. To this end, we used a quantitative telomere FISH method (QFISH) on mouse tissue sections (Materials and Methods). In agreement with the results obtained in leukocytes, tissues from CR mice showed significantly longer telomeres than those of mice under a control diet, as reflected both by higher mean telomere length and by a lower percentage of nuclei with short telomeres (**Fig. 5A–H** and representative images in **Fig. 5K**). These results were confirmed by quantitative QFISH on metaphasic chromosomes from bone marrow (BM) cells, which allows measuring all individual telomeres per nuclei. In particular, mice under CR showed longer telomeres and a lower percentage of chromosome ends with undetectable telomere signals by QFISH (or signal-free ends) compared to the corresponding genotypes under a control diet (**Fig. 5H,I**). Together, these results indicate a systemic effect of CR on telomere length maintenance in multiple organs in mice.

Calorie Restriction Decreases Accumulation of Telomere-originated Chromosomal Aberrations with Aging

Telomeres protect chromosome ends from recombination and DNA repair activities, thus preventing end-to-end fusions and other telomere-related chromosomal aberrations [46,47]. Telomere shortening below a critical length has been shown to lead to loss of telomere protection, chromosomal instability, as well as severe cellular defects (senescence/apoptosis), which eventually can contribute to development of cancer and/or aging.

Here, we used telomere QFISH on BM metaphases to determine the impact of CR on telomere-originated chromosomal aberrations. After 23 months of dietary restriction, CR mice of both genotypes presented a tendency to have less telomere fusions and chromosomes with multitelomeric signals, a telomere aberration recently related to telomere fragility [48], as well as other types of aberrations such as chromosome breaks and fragments (**Fig. 5J–O**; representative images at **Fig. 5M,O**).

Altogether, these results indicate that long-term calorie restriction results in protection from telomere damage and occurrence of telomere-originated chromosomal aberrations.

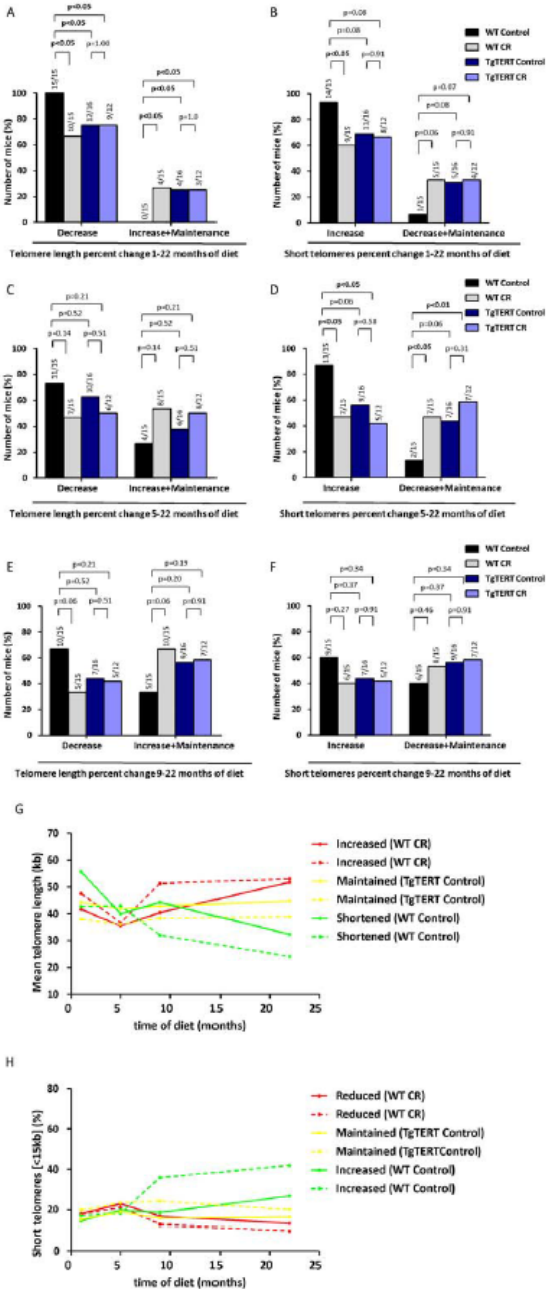

Figure 4. Calorie restriction leads to telomere maintenance and/or elongation with time in a percentage of mice. (A, C and E) The behavior of mean telomere length was classified in two different profiles ("Decrease" and "Increase or Maintenance") at different times of diet (1–22 months of diet, 5–22 months of diet and 9–22 months of diet; A, C and E, respectively) in the indicated groups. Numbers above bars indicate the number of mice showing the profile of interest over the total number of mice. Chi-squared test was used to assess the statistical significance of the differences observed. (B, D and F) The behavior in the percentage of short telomeres (<15 kb) was classified in two different profiles ("Increase" and "Decrease or Maintenance") at different times of diet (1–22 months of diet, 5–22 months of diet and 9–22 months of diet; B, D and F respectively) in the indicated groups. Numbers above bars indicate the number of mice with the profile of interest over the total number of mice. Chi-squared test was used to assess the statistical significance of the differences observed. (G and H) Representative examples of the different assigned profiles for mean telomere length ("Increased", "Maintained", and "Shortened") and percentage of short (<15 kb) telomeres ("Reduced", "Maintained", and "Increased").
doi:10.1371/journal.pone.0053760.g004

CR Synergizes with TERT Over-expression in Extending Mouse Longevity

Finally, we tested the ability of a CR diet to extend the lifespan of both WT and TgTERT cohorts. We observed a tendency to increase the median survival of WT mice under CR compared to those under a control diet (141, 4 weeks compared to 129,6 weeks, respectively; **Fig. 6A–H**), although the differences did not reach significance (**Fig. 6A**). A possible explanation for the lack of lifespan extension associated to CR in the WT cohort could be related to the early age of the mice at the start of the CR protocol, which was of only 3 months. Nevertheless, we observed that WT mice under CR showed a delay in the time of onset of the first deaths in the colony (**Fig. 6A and I–J**) in agreement with an increased "health span" as the result of CR (see also Figs. 1 and 2). Of note, this effect was similar to that seen in TgTERT mice under a control diet, which also showed an increased median survival of 139, 9 weeks compared to 129,6 weeks in the WT controls, as well as a delayed onset of first deaths in the colony (**Fig. 6B–J**), suggesting that the beneficial effects of CR in increasing "health span" in WT mice could be mediated at least in part by TERT over-expression. Interestingly, we observed a significant extension of the median longevity in the TgTERT mice under CR compared to WT mice under a control diet (**Fig. 6C**). These results suggest a synergistic effect between TERT over-expression and CR in increasing mouse longevity (which could be also observed in **Fig 6H**).

In this regard, we have previously demonstrated a synergistic effect between TERT over-expression and increased expression of tumor suppressor genes [25]. As CR has been also previously demonstrated to protect from different cancer types [5,12], we next set to address whether CR was significantly impacting on tumor formation in WT and TgTERT cohorts. To this end, we performed full histopathological analysis of all mice at their time of death. Interestingly, both WT and TgTERT cohorts under CR showed a lower incidence of tumors compared to the corresponding cohorts under the control diet (**Fig. 6I,J**). Of note, the tumor spectrum associated to TERT over-expression was different from that of control mice (**Fig. 6J**), irrespective of this fact, the incidence of cancer in TgTERT mice was reduced to similar levels of those of wild-type mice under a control diet. In summary, CR is able to reduce the increased cancer incidence associated to TERT over-expression, which together with the increased "health span" associated to TERT over-expression could explain the synergistic effects of TERT and CR in increasing longevity (see summary table, **Fig. 6K**).

Discussion

Amelioration of health span, usually alongside with a significant extension of lifespan, has been achieved in the last decades in various species through interventions in major cellular pathways. One of the oldest observations arise from the seminal studies of McCay et al., which reported that rats under a restricted intake of calories showed and extended longevity [49], and that since then

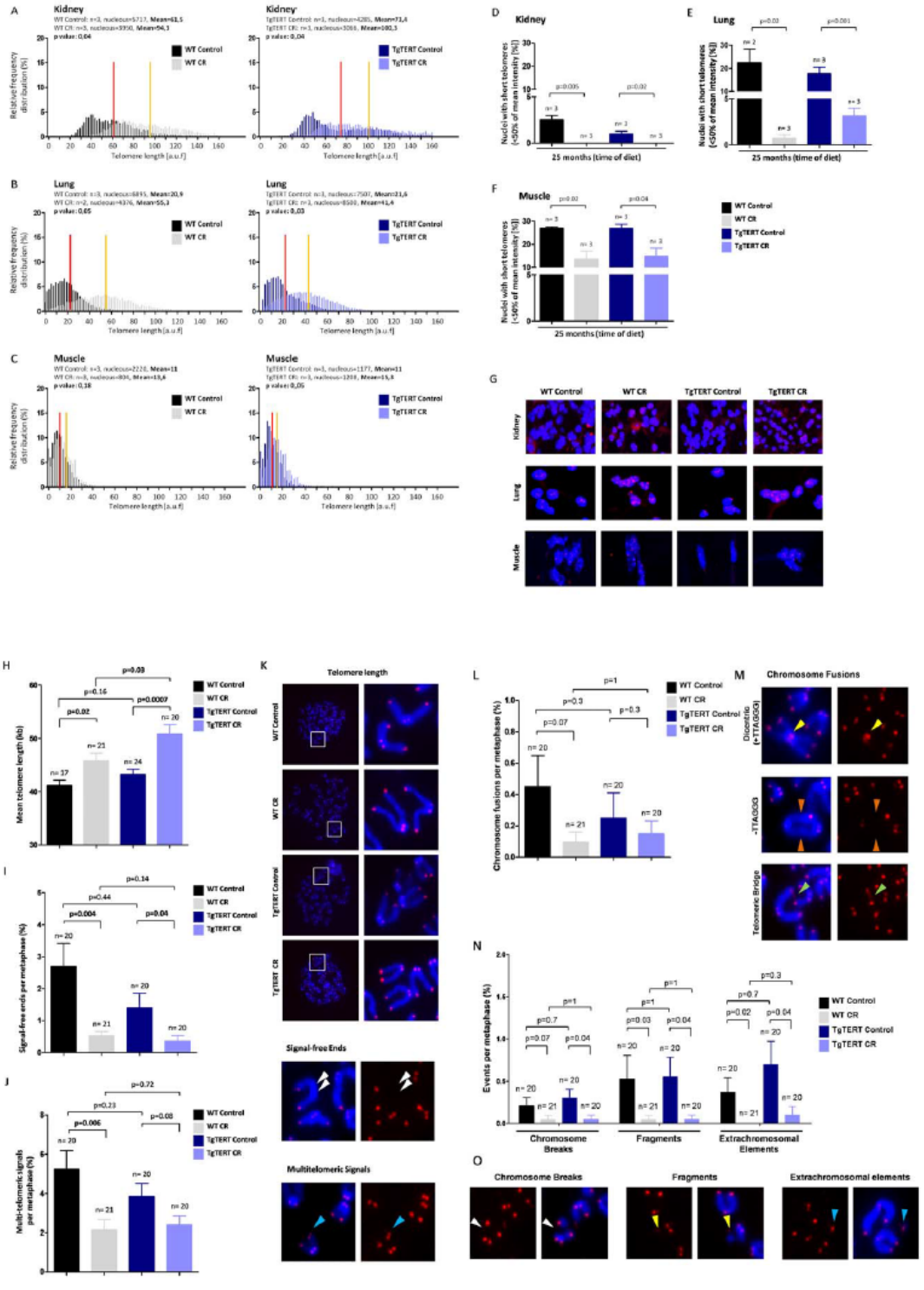
A
Kidney
WT Control
WT CR
TgTERT Control
TgTERT CR
Relative frequency distribution (%)
Telomere length [a.u.f]
B
Lung
C
Muscle
D
Kidney
Nuclei with short telomeres (<50% of mean intensity [%])
25 months (time of diet)
E
Lung
F
Muscle
G
WT Control
WT CR
TgTERT Control
TgTERT CR
Kidney
Lung
Muscle
H
Mean telomere length (kb)
I
Signal-free ends per metaphase (%)
J
Multi-telomeric signals per metaphase (%)
K
Telomere length
Signal-free Ends
Multitelomeric Signals
L
Chromosome fusions per metaphase (%)
M
Chromosome Fusions
Dicentric (>TTAGGG)
-TTAGGG
Telomeric Bridge
N
Events per metaphase (%)
Chromosome Breaks
Fragments
Extrachromosomal Elements
O
Chromosome Breaks
Fragments
Extrachromosomal elements

Figure 5. Calorie restriction prevents telomere shortening in different mouse tissues and protects from telomere-mediated chromosomal aberrations in bone marrow cells. (A,B,C) Telomere fluorescence as determined by QFISH in the indicated tissues from the different mouse cohorts studied here. Histograms represent the frequency (in percentage) of telomere fluorescence per nucleus (in arbitrary units of fluorescence [auf]). Mean telomere length is indicated by a straight line, red for mice under a control diet and yellow for mice under CR. The number of mice (n) and the total number of nuclei analysed is indicated. (D,E,F) Percentage of short telomeres (fraction of telomeres presenting intensity below 50% of the mean intensity) in the indicated tissues from the different mice cohorts studied as determined by QFISH. Students *t*-test was used for statistical analysis. (G) Representative QFISH images for different tissues from the indicated cohorts. Blue colour corresponds to chromosome DNA stained with DAPI; red dots correspond to telomeres (TTAGGG repeats). (H) Telomere length measured in metaphase spreads of BM cells from the different cohorts after hybridization with DAPI and a fluorescent Cy3 labelled PNA-telomeric probe. (I) Frequency of signal-free ends per metaphase in BM cells from the indicated mouse cohorts. (J) Frequency of multitelomeric signals (MTS) per metaphase in BM cells from the indicated mouse cohorts. (K) Representative QFISH images of metaphases from the indicated mouse cohorts. Blue, DNA stained with DAPI; red, telomeres (TTAGGG repeats). (L) Frequency of chromosome fusions per metaphase in BM cells from the indicated mouse cohorts. (M) Representative images of chromosomal fusions. (N) Frequency of other chromosome aberrations (chromosome breaks, fragments and extrachromosomal elements) per metaphase in BM cells from the indicated mouse cohorts. (O) Representative images of the different types of chromosomal aberrations scored. Blue, DAPI staining (DNA); red dots, telomeres (TTAGGG repeats) as detected with a PNA-Cy3 probe.
doi:10.1371/journal.pone.0053760.g005

has been extended to other animal models [3]. However, more recently, it has become apparent that effects of CR in extending longevity are not universal [2]. Indeed, depending on the genetic background CR can either extend or decrease longevity, highlighting the need of identifying the pathways that interplay with CR. In line with this notion, the molecular mechanisms responsible for lifespan extension through CR are still debated. As an example, mammalian *Sirt1* (yeast protein Sir2), which encodes a NAD-dependent deacetylase and was long believed to mediate life extension associated to calorie restriction in different species, such as *C. elegans* and *Drosophila*, [50,51], has been recently challenged [52]. Currently, the most widely accepted model is that CR protects from DNA damage through a decrease of metabolism and mitochondrial activity, and this result in a tissue-protective phenotype [4,53]. Here, we addressed whether CR could impact on telomere dynamics, one of the best-known molecular mechanisms leading to accumulation of DNA damage with aging. In particular, we set to address whether CR may impact on the rate of telomere shortening as well as on the incidence of telomere-originated aberrations associated with aging. Moreover, we set to address whether CR could synergyze with telomerase over-expression in extending life span.

First, we showed that the CR protocol used here was able to protect from the development of pathologies associated with aging in both WT and TgTERT mice, including insulin sensitivity and glucose intolerance, as well as protection from bone loss over time. In addition to protection from age-related pathologies, CR improved other aspects of mouse health such neuromuscular coordination in both genotypes. Together, these results indicate that the CR protocol used in this study was able to increase the "health span" of both WT and TgTERT mice.

In agreement with this, we observed a delayed onset of first deaths in the WT and TgTERT cohorts under CR. Interestingly, WT mice under CR showed a similar median longevity and similar onset of first deaths to that in TgTERT mice under a control diet, suggesting that TERT transgenic expression is partially the beneficial effects of CR.

By using longitudinal telomere length studies, we also describe here that CR delays telomere shortening associated to aging in blood cells from WT mice (PBLs), to an analogous degree to that observed associated to TERT over-expression. Other tissues, such as lung, kidney, bone marrow and muscle, also presented longer telomeres in mice under CR compared to those under the control diet. In agreement with a protection from telomere shortening associated with aging, we also observed that CR protected from telomere-originated DNA damage and chromosomal aberrations. This included "multitelomeric signals", which have been recently associated to increased telomere fragility owing to replication fork stalling at telomeres [48]. The fact that CR reduced the load of telomere fragility, may be suggestive of a reduced replicative stress associated to CR *in vivo*, in agreement with the lower cellular proliferation described for this condition [53,54]. Alternatively, the observed telomere protection associated to CR could also be explained by the reduction of oxidative stress mediated by CR. Oxidative stress accelerates telomere loss, whereas antioxidants decelerate it [55].

Importantly, the slow-down or even increase in telomere length associated to CR in mice, together with the protection from telomere damage, may underlie the delayed onset of age-related diseases upon CR. In support of this notion, there is recent evidence indicating that the rates of accumulation of short telomeres with aging determines mouse longevity [44]. Furthermore, short telomeres are associated with age-related diseases, including heart disease, impaired glucose tolerance, type 2 diabetes and higher plasma oxidative stress [56].

Interestingly, the significantly improved health-span associated to CR in WT mice, also lead to a delay in the onset of first deaths in the cohort, although was not sufficient to significantly increase life-span compared to control mice. Life-span extension in this setting was only achieved in TgTERT over-expressing mice, suggesting a synergy between high TERT expression and CR in extending mouse longevity. The fact that we did not observe a significant increase in the longevity in CR WT mice maybe related to the young age of mice used for this study (3 month of age) compared to other studies (>12 month of age), suggesting the interesting idea that CR may differentially impact on young or adult individuals, in line with the higher proliferative demands of younger organisms.

Finally, our results show a clear impact of CR reducing the tumor incidence associated to the TgTERT genotype. In particular, although TERT overexpressing mice presented a higher incidence of neoplasias than WT mice, the incidence of these neoplasias was reduced to a similar incidence than that of WT mice under CR. This results in a synergistic impact of both mechanisms on survival, mimicking the expression of tumor suppressors under a telomerase overexpression background [25].

In conclusion, we provide evidence of the interaction between two major anti-aging mechanisms in mammals. Further investigation of the interface between telomerase and CR could help unveiling how CR works and could permit to draw new and safer anti-aging treatments.

Materials and Methods

Ethics Statement

Male mice of a 100% C57BL/6 background were produced and stored at a pathogen-free barrier area of the CNIO, in accordance to the recommendations of the Federation of

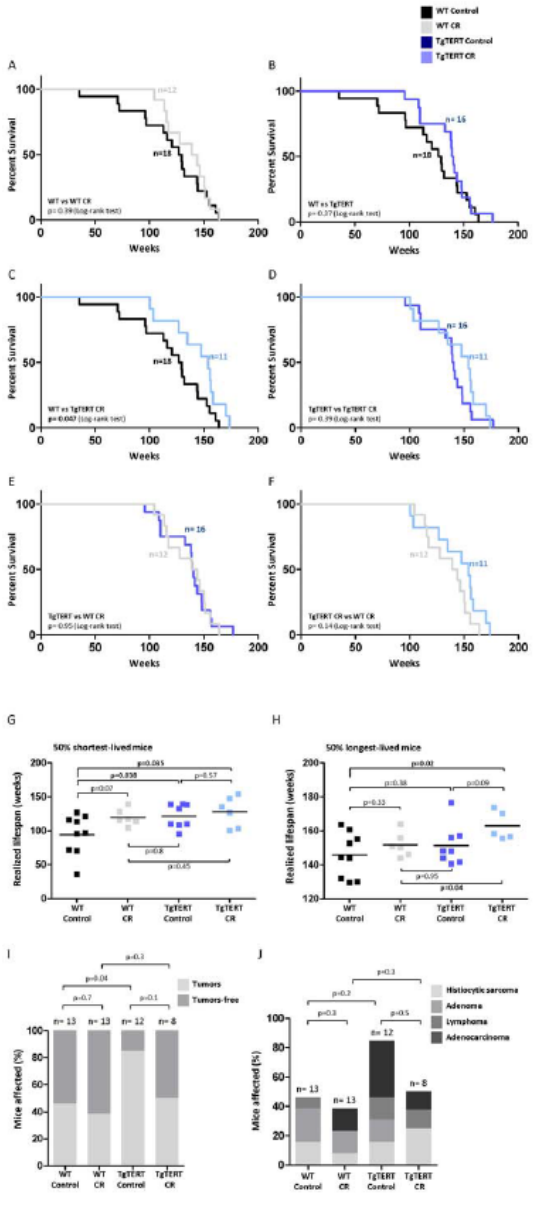

K

	Median Survival (weeks)	Median Survival of the 50% longest lived (weeks)	Mean telomere length – Kidney (a.u.)	Mean telomere length – BM (kb)	Signal-free ends (BM, %)	Mean telomere length after 22 months of diet (kb)	Short telomeres after 22 months of diet (%)
WT	129.6	145.8	61.5	41.2	2.7	37.1	25.1
WT CR	141.4	151.8	94.3	43.2	1.4	42.5	17.5
TgTERT	139.9	151.5	73.4	45.8	0.52	38.6	21.9
TgTERT CR	153.9	162.9	100.3	50.8	0.35	41.6	17.7

Figure 6. Caloric restriction increases median and maximum longevity and protects from cancer. (A–F) Kaplan-Meyer survival curves of the indicated mouse cohorts. The Log rank test was used for statistical analysis. Mice under CR were more susceptible to unexpected stresses such as the blood extraction procedure carried. 5 mice of the WT CR cohort and 6 mice of the TgTERT cohort died during the blood extraction and were excluded from the survival curves (of note, none of the WT or TgTERT mice show sensibility to the blood extraction procedure). (G–H) Realized lifespan of the 50% shortest (G) and longest (H) lived mice of each cohort. Students *t*-test was used for statistical analysis. (I) Percentage of mice with cancer and cancer-free mice in the different cohorts. All death mice were subjected to full histopathological analysis. (J) Percentage of mice in the different cohorts with the indicated tumours at their time of death. (K) Summary table with the findings regarding telomere length and survival of the different cohorts.
doi:10.1371/journal.pone.0053760.g006

European Laboratory Animal Science Associations. Mice were inspected in a daily basis by an authorized animal facility expert and weight monthly the firsts 6 months and each two months thereafter. All the work carried out by the Animal Facility of CNIO (including mice welfare) complies with both national and EU legislation – Spanish Royal Decree RD 1201/2005 and EU Directive 86/609/CEE as modified by 2003/65/CE – for the protection of animals used for research experimentation and other scientific purposes. Mice were sacrificed using carbon dioxide (CO_2) following ISCIII IACUC guidelines, when presenting signs of illness or tumors in accordance to the Guidelines for Humane Endpoints for Animals Used in Biomedical Research [57]. The date of euthanasia was considered as an estimation of the natural life span. The Spanish National Cancer Research Centre (CNIO) is part of the "Carlos III" Health Institute (ISCIII) and all protocols were previously subjected and approved by the Ethical Committee of the ISCIII; approval ID numbers: PA-418/08.

Experimental Set-up

After weaning, five mice were housed per cage and fed *ad libitum* of a non-purified diet (n° 2018, Harlan). For the aging study, three-month old mice were individually housed and randomly assigned to control and CR group of 18–20 mice each group (WT = 20, TgTERT = 18, WT CR = 19, TgTERT CR = 19). Independently of specific cases delineated at the corresponding figure legends, two mice of each cohort were sacrificed after the 25 months' time point for experimentation and were censored from the survival curves. Control mice were fed 92.5 kcal per week of chemically defined control diet (AIN-93M, Diet No. F05312, biodery, Frenchtown, NJ). This caloric intake was found to be ~10% fewer calories than average daily intake of C57BL/6 mice to ensure that all was consumed and allowing the comparison of non-obese controls and CR mice. Caloric restriction was introduced by feeding 74 kcal per week of chemically defined CR diet for two weeks, followed by 59.2 kcal per week of CR diet (AIN-93M 40% Restricted, Diet No. F05314, Bioserv). Defined diets were cold packed into 1 g pellets. Mice were fed two-seventh of the weekly allotment of food on Monday and Wednesdays and three-seventh of that amount of Friday [10,58].

Histological Analysis

Histopathology was performed as described [59]. Briefly, tissues and organs from sacrificed or natural death mice were fixed for 24 h in a 10% neutral-buffered formalin solution at room temperature, dehydrated through graded alcohols and xylene, and embedded in paraffin. Histological analysis was achieved on 4–5 µm sections according to standard procedures.

Bone Density and Fat Content

Bone mineral density and fat content were measured in anesthetized animals (or post-mortem when referred) using a Dual Energy X-ray Absorptiometry (DEXA) scan device.

Intraperitoneal Glucose Tolerance Tests

Mice were fasted for at least 8 hr, and injected intraperitoneally with a 50% dextrose solution (2 g/kg body weight) as previously described. Blood glucose levels were measured at the indicated time points with a glucometer (Glucocard Memory 2, Arkray, Japan), after injection. Analysis of the data was performed as described in [25].

Insulin, HOMA-IR, IGF1 and GH Measurements

Blood insulin levels were measured with an Ultra-Sensitive Mouse Insulin ELISA Kit (Crystal Chem Inc. #90080), following manufacturers protocol. HOMA-IR was calculated as previously described [31]. IGF-1 levels were calculated with a Rat/Mouse IGF-1 ELISA (Novozymes, AC-18F1) and growth hormone with a Rat/Mouse ELISA Kit (Millipore, EZRMGH-45K) following manufactures proceedings. Mice were fasted for at least 6 hr prior to blood insulin, IGF-1 and GH analysis.

Telomere QFISH on Paraffin Sections

Paraffin-embedded tissue sections were hybridized with a PNA-telomeric probe, and fluorescence intensity of telomeres was determined as previously described [59]. Quantitative image analysis was performed using the Definiens Developer Cell software (version XD 1.2; Definiens AG). For statistical analysis a two-tailed Student *t*-test was used to assess significance (GraphPad Prism software).

Quantitative Telomere Fluorescence *in situ* Hybridization (QFISH) on Bone Marrow Cells

Bone marrow cells were isolated and stimulated with IL3 (10 ng/µl) (Sigma) diluted in 25% RPMI (Sigma) 75% Myelocult (Stemcell technologies) culture medias for 72 hr. Cells were incubated with 0.1 mg/mL Colcemid (Gibco) at 37°C overnight to arrest cells in metaphase. Cells were then harvested and fixed in methanol:acetic acid (3:1). Metaphases were spread on glass slides and dried overnight, and QFISH was performed using a PNA-telomeric probe labeled with Cy3 as described previously [29,60,61]. Images were captured at 100× magnification using a COHU CCD camera on a Leica DMRA (Leica, Heidelberg, Germany) microscope. Telomere fluorescence signals were integrated from 17–21 metaphases from 2 animals per diet group and genotyped and quantified by using the TFL-TELO program (gift from Peter Lansdorp, Vancouver, Canada) [60]. Telomere fluorescence values were converted into kb by external calibration with the L5178Y-S and L5178Y-R lymphocyte cell lines with known telomere lengths of 10.2 and 79.7 kb, respectively [61].

High-througput QFISH (HT QFISH) on Peripheral Blood Leukocytes

Blood was extracted from the facial vein while the mice were alive at the indicated time points from the beginning of the diet. Erythrocyte lysis was performed (Buffer EL, Quiagen) and peripheral blood leukocytes were plated on a clear bottom black-walled 96-well plate. HT-QFISH was performed as previously described [28]. Telomere length values were analyzed using individual telomere spots (>5000 per sample) corresponding to the specific binding of a Cy3 labeled telomeric probe. Fluorescence intensities were converted into Kb as previously described [28,61].

Quantification of Phosphorylated H2AX

We performed γ-H2AX (Millipore 05-636, clone JBW301) staining on paraformaldehyde-fixed, paraffin-embedded sections (AxioVision software was used for image analysis; quantitation of immunostainings was determined by counting the number of peroxidase stained nuclei over the total number of hematoxylin-stained nuclei). Samples were processed and acquired under identical conditions.

Neuromuscular Coordination Test

The tightrope test was performed as described elsewhere [25].

Supporting Information

Figure S1 Molecular markers of aging in WT and TgTERT mice under Control and CR diets. (A and B) Femur bone mineral density (BMD) was measured at 16 months of diet (A) and 24 months of diet (B) in mice from the different cohorts. Values are given as average ± SEM, and statistical significance was determined by the two-tailed Student's t-test. (C) Femur bone mineral density (BMD) variation through lifetime of WT and TgTERT mice under control and CR diets. Values are given as average. (D and E) IGF-1 (D) and GH (E) in serum were measured at 16 months of diet in mice of the indicated cohorts. The number of mice is indicated on the top of each bar (n). Values are given as average ± SEM, and statistical significance was determined by the two-tailed Student's *t*-test.
(TIF)

Figure S2 Protection from DNA damage in mice under calorie restriction. (A) Percentage of γ-H2AX positive cells in the kidney of mice from the indicated cohorts. Students t-test was used for statistical assessments. (B) Representative γ-H2AX immunohistochemistry images of kidney from the indicated mice cohorts.
(TIF)

Figure S3 Slower age-dependent telomere shortening in mice under calorie restriction. (A, B and C) Percentage of short telomeres (<2 kb, <5 kb and <10 kb; A, B and C respectively) was determined by HT QFISH on white blood cells from the indicated mice under CR or control diet at different time points. The number of mice is indicated on the top of each bar (n). Values are given as average ± SEM, and statistical significance was determined by one-tailed Student's *t*-test.
(TIF)

Figure S4 Calorie restriction leads to telomere maintenance and/or elongation with time in a percentage of mice. (A, B and C) The behavior of mean telomere length was classified in three different profiles ("Decrease", "Increase", and "Maintenance") at different times of diet (1–22 months of diet, 5–22 months of diet and 9–22 months of diet; A, B and C, respectively) in the indicated groups. Numbers above bars indicate the number of mice showing the profile of interest over the total number of mice. Chi-squared test was used to assess the statistical significance of the differences observed. (D, E and F) The behavior in the percentage of short telomeres (<15 kb) was classified in three different profiles ("Increase", "Decrease", and "Maintenance") at different times of diet (1–22 months of diet, 5–22 months of diet and 9–22 months of diet; D, E and F respectively) in the indicated groups. Numbers above bars indicate the number of mice with the profile of interest over the total number of mice.

Chi-squared test was used to assess the statistical significance of the differences observed.
(TIF)

Author Contributions

Conceived and designed the experiments: MAB EV. Performed the experiments: EV BMB MF JMF. Analyzed the data: EV MAB BMB. Contributed reagents/materials/analysis tools: MF JMF. Wrote the paper: MAB EV BMB.

References

1. Colman RJ, Anderson RM, Johnson SC, Kastman EK, Kosmatka KJ, et al. (2009) Caloric restriction delays disease onset and mortality in rhesus monkeys. Science 325: 201–204.
2. Mattison JA, Roth GS, Beasley TM, Tilmont EM, Handy AM, et al. (2012) Impact of caloric restriction on health and survival in rhesus monkeys from the NIA study. Nature 489: 318–321.
3. Kenyon C (2005) The plasticity of aging: insights from long-lived mutants. Cell 120: 449–460.
4. Fontana L, Klein S (2007) Aging, adiposity, and caloric restriction. JAMA 297: 986–994.
5. Anderson RM, Shanmuganayagam D, Weindruch R (2009) Caloric restriction and aging: studies in mice and monkeys. Toxicol Pathol 37: 47–51.
6. Hamrick MW, Ding KH, Ponnala S, Ferrari SL, Isales CM (2008) Caloric restriction decreases cortical bone mass but spares trabecular bone in the mouse skeleton: implications for the regulation of bone mass by body weight. J Bone Miner Res 23: 870–878.
7. Hempenstall S, Picchio L, Mitchell SE, Speakman JR, Selman C (2010) The impact of acute caloric restriction on the metabolic phenotype in male C57BL/6 and DBA/2 mice. Mech Ageing Dev 131: 111–118.
8. Liao CY, Rikke BA, Johnson TE, Diaz V, Nelson JF (2010) Genetic variation in the murine lifespan response to dietary restriction: from life extension to life shortening. Aging Cell 9: 92–95.
9. Turturro A, Witt WW, Lewis S, Hass BS, Lipman RD, et al. (1999) Growth curves and survival characteristics of the animals used in the Biomarkers of Aging Program. J Gerontol A Biol Sci Med Sci 54: B492–501.
10. Dhahbi JM, Kim HJ, Mote PL, Beaver RJ, Spindler SR (2004) Temporal linkage between the phenotypic and genomic responses to caloric restriction. Proc Natl Acad Sci U S A 101: 5524–5529.
11. Weindruch R, Walford RL (1982) Dietary restriction in mice beginning at 1 year of age: effect on life-span and spontaneous cancer incidence. Science 215: 1415–1418.
12. Weindruch R, Walford RL, Fligiel S, Guthrie D (1986) The retardation of aging in mice by dietary restriction: longevity, cancer, immunity and lifetime energy intake. J Nutr 116: 641–654.
13. Spindler SR (2010) Caloric restriction: from soup to nuts. Ageing Res Rev 9: 324–353.
14. Bordone L, Guarente L (2005) Caloric restriction, SIRT1 and metabolism: understanding longevity. Nat Rev Mol Cell Biol 6: 298–305.
15. Koubova J, Guarente L (2003) How does calorie restriction work? Genes Dev 17: 313–321.
16. Herrera E, Samper E, Martin-Caballero J, Flores JM, Lee HW, et al. (1999) Disease states associated with telomerase deficiency appear earlier in mice with short telomeres. EMBO J 18: 2950–2960.
17. Chan SW, Blackburn EH (2002) New ways not to make ends meet: telomerase, DNA damage proteins and heterochromatin. Oncogene 21: 553–563.
18. Flores I, Benetti R, Blasco MA (2006) Telomerase regulation and stem cell behaviour. Curr Opin Cell Biol 18: 254–260.
19. Harley CB, Futcher AB, Greider CW (1990) Telomeres shorten during ageing of human fibroblasts. Nature 345: 458–460.
20. Collado M, Blasco MA, Serrano M (2007) Cellular senescence in cancer and aging. Cell 130: 223–233.
21. Blasco MA (2007) Telomere length, stem cells and aging. Nat Chem Biol 3: 640–649.
22. Mitchell JR, Wood E, Collins K (1999) A telomerase component is defective in the human disease dyskeratosis congenita. Nature 402: 551–555.
23. Armanios MY, Chen JJ, Cogan JD, Alder JK, Ingersoll RG, et al. (2007) Telomerase mutations in families with idiopathic pulmonary fibrosis. N Engl J Med 356: 1317–1326.
24. Epel ES, Blackburn EH, Lin J, Dhabhar FS, Adler NE, et al. (2004) Accelerated telomere shortening in response to life stress. Proc Natl Acad Sci U S A 101: 17312–17315.
25. Tomas-Loba A, Flores I, Fernandez-Marcos PJ, Cayuela ML, Maraver A, et al. (2008) Telomerase reverse transcriptase delays aging in cancer-resistant mice. Cell 135: 609–622.
26. Bernardes de Jesus B, Vera E, Schneeberger K, Tejera AM, Ayuso E, et al. (2012) Telomerase gene therapy in adult and old mice delays aging and increases longevity without increasing cancer. EMBO Mol Med 4: 1–14.
27. Gonzalez-Suarez E, Geserick C, Flores JM, Blasco MA (2005) Antagonistic effects of telomerase on cancer and aging in K5-mTert transgenic mice. Oncogene 24: 2256–2270.
28. Canela A, Vera E, Klatt P, Blasco MA (2007) High-throughput telomere length quantification by FISH and its application to human population studies. Proc Natl Acad Sci U S A 104: 5300–5305.
29. Hemann MT, Strong MA, Hao LY, Greider CW (2001) The shortest telomere, not average telomere length, is critical for cell viability and chromosome stability. Cell 107: 67–77.
30. Argentino DP, Dominici FP, Munoz MC, Al-Regaiey K, Bartke A, et al. (2005) Effects of long-term caloric restriction on glucose homeostasis and on the first steps of the insulin signaling system in skeletal muscle of normal and Ames dwarf (Prop1df/Prop1df) mice. Exp Gerontol 40: 27–35.
31. Heikkinen S, Argmann CA, Champy MF, Auwerx J (2007) Evaluation of glucose homeostasis. Curr Protoc Mol Biol Chapter 29: Unit 29B 23.
32. Ferguson VL, Ayers RA, Bateman TA, Simske SJ (2003) Bone development and age-related bone loss in male C57BL/6J mice. Bone 33: 387–398.
33. Ingram DK, Reynolds MA (1986) Assessing the predictive validity of psychomotor tests as measures of biological age in mice. Exp Aging Res 12: 155–162.
34. Bartke A (2005) Minireview: role of the growth hormone/insulin-like growth factor system in mammalian aging. Endocrinology 146: 3718–3723.
35. Fontana L, Partridge L, Longo VD (2010) Extending healthy life span–from yeast to humans. Science 328: 321–326.
36. Wang C, Jurk D, Maddick M, Nelson G, Martin-Ruiz C, et al. (2009) DNA damage response and cellular senescence in tissues of aging mice. Aging Cell 8: 311–323.
37. Elyada E, Pribluda A, Goldstein RE, Morgenstern Y, Brachya G, et al. (2011) CKIalpha ablation highlights a critical role for p53 in invasiveness control. Nature 470: 409–413.
38. Herbig U, Ferreira M, Condel L, Carey D, Sedivy JM (2006) Cellular senescence in aging primates. Science 311: 1257.
39. Herbig U, Jobling WA, Chen BP, Chen DJ, Sedivy JM (2004) Telomere shortening triggers senescence of human cells through a pathway involving ATM, p53, and p21(CIP1), but not p16(INK4a). Mol Cell 14: 501–513.
40. Sedelnikova OA, Horikawa I, Redon C, Nakamura A, Zimonjic DB, et al. (2008) Delayed kinetics of DNA double-strand break processing in normal and pathological aging. Aging Cell 7: 89–100.
41. d'Adda di Fagagna F, Reaper PM, Clay-Farrace L, Fiegler H, Carr P, et al. (2003) A DNA damage checkpoint response in telomere-initiated senescence. Nature 426: 194–198.
42. Jaskelioff M, Muller FL, Paik JH, Thomas E, Jiang S, et al. (2011) Telomerase reactivation reverses tissue degeneration in aged telomerase-deficient mice. Nature 469: 102–106.
43. Finkel T, Holbrook NJ (2000) Oxidants, oxidative stress and the biology of ageing. Nature 408: 239–247.
44. Vera E, Bernardes de Jesus B, Foronda M, Flores JM, Blasco MA (2012) The rate of increase of short telomeres predicts longevity in mammals. Cell Reports 2: 732–737.
45. Broccoli D, Young JW, de Lange T (1995) Telomerase activity in normal and malignant hematopoietic cells. Proc Natl Acad Sci U S A 92: 9082–9086.
46. Blasco MA (2005) Telomeres and human disease: ageing, cancer and beyond. Nat Rev Genet 6: 611–622.
47. de Lange T (2005) Shelterin: the protein complex that shapes and safeguards human telomeres. Genes Dev 19: 2100–2110.
48. Martinez P, Thanasoula M, Munoz P, Liao C, Tejera A, et al. (2009) Increased telomere fragility and fusions resulting from TRF1 deficiency lead to degenerative pathologies and increased cancer in mice. Genes Dev 23: 2060–2075.
49. McCay CM, Crowell MF, Maynard LA (1935) The effect of retarded growth upon the length of life span and upon the ultimate body size. J Nutr 10: 63–79.
50. Guarente L, Picard F (2005) Calorie restriction–the SIR2 connection. Cell 120: 473–482.
51. Canto C, Auwerx J (2009) Caloric restriction, SIRT1 and longevity. Trends Endocrinol Metab 20: 325–331.
52. Burnett C, Valentini S, Cabreiro F, Goss M, Somogyvari M, et al. (2011) Absence of effects of Sir2 overexpression on lifespan in C. elegans and Drosophila. Nature 477: 482–485.
53. Longo VD, Fontana L (2010) Calorie restriction and cancer prevention: metabolic and molecular mechanisms. Trends Pharmacol Sci 31: 89–98.
54. Dunn SE, Kari FW, French J, Leininger JR, Travlos G, et al. (1997) Dietary restriction reduces insulin-like growth factor I levels, which modulates apoptosis, cell proliferation, and tumor progression in p53-deficient mice. Cancer Res 57: 4667–4672.
55. von Zglinicki T (2002) Oxidative stress shortens telomeres. Trends Biochem Sci 27: 339–344.
56. Calado RT, Young NS (2009) Telomere diseases. N Engl J Med 361: 2353–2365.

57. Harrison DE, Strong R, Sharp ZD, Nelson JF, Astle CM, et al. (2009) Rapamycin fed late in life extends lifespan in genetically heterogeneous mice. Nature 460: 392–395.
58. Pugh TD, Klopp RG, Weindruch R (1999) Controlling caloric consumption: protocols for rodents and rhesus monkeys. Neurobiol Aging 20: 157–165.
59. Gonzalez-Suarez E, Samper E, Ramirez A, Flores JM, Martin-Caballero J, et al. (2001) Increased epidermal tumors and increased skin wound healing in transgenic mice overexpressing the catalytic subunit of telomerase, mTERT, in basal keratinocytes. EMBO J 20: 2619–2630.
60. Zijlmans JM, Martens UM, Poon SS, Raap AK, Tanke HJ, et al. (1997) Telomeres in the mouse have large inter-chromosomal variations in the number of T2AG3 repeats. Proc Natl Acad Sci U S A 94: 7423–7428.
61. McIlrath J, Bouffler SD, Samper E, Cuthbert A, Wojcik A, et al. (2001) Telomere length abnormalities in mammalian radiosensitive cells. Cancer Res 61: 912–915.

HEMATOPOIESIS AND STEM CELLS

Conditional TRF1 knockout in the hematopoietic compartment leads to bone marrow failure and recapitulates clinical features of dyskeratosis congenita

Fabian Beier,[1] Miguel Foronda,[1] Paula Martinez,[1] and Maria A. Blasco[1]

[1]Telomere and Telomerase Group, Molecular Oncology Program, Spanish National Cancer Research Centre (CNIO), Madrid, Spain

TRF1 is part of the shelterin complex, which binds telomeres and it is essential for their protection. Ablation of TRF1 induces sister telomere fusions and aberrant numbers of telomeric signals associated with telomere fragility. Dyskeratosis congenita is characterized by a mucocutaneous triad, bone marrow failure (BMF), and presence of short telomeres because of mutations in telomerase. A subset of patients, however, show mutations in the shelterin component TIN2, a TRF1-interacting protein, presenting a more severe phenotype and presence of very short telomeres despite normal telomerase activity. Allelic variations in TRF1 have been found associated with BMF. To address a possible role for *TRF1* dysfunction in BMF, here we generated a mouse model with conditional *TRF1* deletion in the hematopoietic system. Chronic TRF1 deletion results in increased DNA damage and cellular senescence, but not increased apoptosis, in BM progenitor cells, leading to severe aplasia. Importantly, increased compensatory proliferation of BM stem cells is associated with rapid telomere shortening and further increase in senescent cells in vivo, providing a mechanism for the very short telomeres of human patients with mutations in the shelterin TIN2. Together, these results represent proof of principle that mutations in *TRF1* lead to the main clinical features of BMF. (*Blood*. 2012;120(15): 2990-3000)

Introduction

Telomeres consist of tandem TTAGGG repeats and associated proteins that form a capping structure at the ends of chromosomes, protecting them from DNA repair activities and from degradation.[1,2] The length of telomeric repeats is mainly regulated by enzyme telomerase, which can add telomeric repeats de novo at chromosome ends because of its reverse transcriptase (TERT) activity that uses an associated RNA component (TERC) as template.[3,4] Telomere repeats are then bound by a 6-protein complex, known as shelterin, encompassing TIN2, TRF1, TRF2, TPP1, POT1, and RAP1, which is needed to form a functional telomere.[2,3,5] TRF1, together with POT1 and TRF2, directly binds telomeric DNA.[2,3,5] TRF1 has been proposed to have roles in the regulation of telomere length and telomere capping, as well as in the prevention of replication fork stalling at telomeres.[1-3,5] TRF1 ablation leads to rapid cellular senescence because of activation of DNA damage response (DDR),[6,7] supporting an essential role of TRF1 in preventing DNA damage at telomeres.

Dyskeratosis congenita (DKC) is considered to be paradigmatic of premature aging syndromes and it is characterized by the classic triad of bone marrow failure (BMF), skin abnormalities, and increased risk of cancer.[8,9] The molecular basis of DKC commonly involves mutations in genes related to telomere maintenance.[8-10] Disturbance of telomere maintenance results in premature telomere shortening and subsequent replicative senescence, leading to premature stem cell exhaustion and tissue failure.[11] The most frequent DKC mutations affect the telomerase complex, including the telomerase RNA component or TERC and the reverse transcriptase subunit or TERT, as well as small nucleolar ribonucleoproteins important for the stability of TERC, such as DKC1, NHP2, or NOP10, and therefore for proper functioning of telomerase.[10,12,13] In addition, mutations of the shelterin protein TIN2 contribute to approximately 10%-20% of all DKC cases.[10,12,13] *TIN2* mutations are autosomal-dominant and generally de novo mutations in contrast to mutations in components of the telomerase complex.[8-10]

Concerning the clinical manifestations of DKC, patients with mutations in *TIN2* appear to have more clinical features and a more severe clinical course than those with mutations in telomerase.[10,14,15] Furthermore, the onset of the disease develops at a younger age in patients with *TIN2* mutations compared with patients with telomerase mutations.[15-17] Strikingly, patients with *TIN2* mutations are characterized by presence of very short telomeres, a feature that correlates with the severity of the disease and that it is used to identify these patients versus other BMF syndromes.[10,14-16,18] In contrast to mutations affecting the telomerase complex, the mechanism underlying the dramatic telomere shortening associated with *TIN2* mutations remains presently unknown. Of note, all known *TIN2* mutations in patients with DKC are found in exon 6, in the proximity of the TRF1 binding site,[18,19] raising the interesting possibility that impaired interaction of TRF1 and TIN2 can contribute to the severe DKC phenotype. In line with this hypothesis, deletion of the TRF1 binding site of TIN2 results in reduced in vitro TRF1 levels in the shelterin complex.[20-23] Further supporting a potential involvement of TRF1 in the pathogenesis of DKC, allelic variations in *TRF1* have been associated with BMF.[24,25] However, solid proof that TRF1 mutations can cause BMF is still pending.

In the present study, we set out to test whether abrogation of TRF1 in the hematopoietic system can recapitulate the clinical features of BMF. To this end, we generated a conditional *TRF1* deletion mouse model for the hematopoietic system. Our results in

Submitted March 28, 2012; accepted August 12, 2012. Prepublished online as *Blood* First Edition paper, August 29, 2012; DOI 10.1182/blood-2012-03-418038.

The online version of this article contains a data supplement.

The publication costs of this article were defrayed in part by page charge payment. Therefore, and solely to indicate this fact, this article is hereby marked "advertisement" in accordance with 18 USC section 1734.

vivo demonstrate that deletion of TRF1 results in BMF. In addition, we were able to reproduce the main clinical features as observed in DKC patients with *TIN2* mutations, such as severe telomere shortening over time, reduced progenitor cells, and progressive development of cytopenia and BMF. In summary, we describe the first mouse model simulating DKC features caused by alteration of the TRF1 shelterin component. Our results also provide the first mechanistic explanation for the severe telomere shortening in the in vivo setting of the bone marrow associated with shelterin mutations in patients with DKC.

Methods

Mice

TRF1$^{flox/flox}$ mice were generated in our laboratory as described.[6] To conditionally delete TRF1 in the bone marrow, homozygous *TRF1*$^{flox/flox}$ mice were crossed with transgenic mice expressing Cre under the control of the endogenous Mx1 promotor (*Mx1-Cre*).[26] Heterozygous *TRF1*$^{flox/wt}$ *Mx1-Cre* mice were crossed with homozygous *TRF1*$^{flox/flox}$ mice to obtain *TRF1*$^{flox/flox}$ *Mx1-Cre* mice. All mice were generated in a pure C57B6 background. Then, 8- to 14-week-old *TRF1*$^{flox/flox}$*Mx1-Cre* and *TRF1*$^{flox/flox}$ *Mx1-wildtype* (*wt*) mice were used as bone marrow donors. Peripheral blood (50-80 μL per mouse) was obtained by jugular puncture and collected into EDTA-coated tubes for further analysis. Peripheral blood counts were measured with the Abacus Junior Vet System (Diatron) or processed for high-throughput (HT), quantitative FISH (QFISH).

Treatment and transplantation protocols were approved by the Ethical Committee of the "Carlos III" Health Institute, and mice were treated in accordance of the Spanish laws and the guidelines for "Humane Endpoints for Animals used in Biomedical Research." All mice were maintained at the Spanish National Cancer Research Center under specific pathogen-free conditions in accordance with the recommendations of the Federation of European Laboratory Animal Science Association.

Bone marrow transplantation and Cre induction

Bone marrow transplantation was performed as described.[27] Groups of 8 wild-type littermates (C57B6 background, 7-10 weeks old) per donor mouse were irradiated with 12 Gy the day before the transplantation. The following day, bone marrow of the donor mice was harvested from the femora and tibiae and 2-3 × 10^6 cells were injected per recipient. All experiments were performed on animals that underwent transplantation after a latency of at least 30 days.

TRF1$^{flox/flox}$*Mx1-Cre* or *TRF1*$^{flox/flox}$*Mx1-wt* mice undergoing long-term polyinosinic-polycytidylic acid (pI-pC; Sigma-Aldrich) injections were used for serial transplantation. A total of 2 × 10^6 cells of donor bone marrow were transplanted into groups of 4 irradiated wild-type littermates as bone marrow recipients.

To induce the Cre expression, 15 μg/g body weight of pI-pC was injected intraperitoneally into animals that had undergone transplantation. Duration and frequency of pI-pC injections is indicated in the respective experiment.

G-CSF ELISA

Peripheral blood of euthanized mice was centrifuged and serum was frozen at −80°C until measurement. ELISA analysis of mouse G-CSF levels was carried out according to the manufacturer (Quantikine; R&D Systems).

FACS analysis and FACS sorting

For detailed bone marrow characterization, 10 × 10^6 bone marrow mononucleated cells (BMMCs) per animal were incubated with 3% BSA (Sigma-Aldrich) for 20 minutes. After washing cells once with PBS, anti–sca-1–PerCP-Cy5.5, lin cocktail-eFluor450, anti–FC-receptor–PE-Cy7, anti–CD34-eFluor660, anti–IL7-Alexa488 (all eBioscience), and anti–c-kit–APC-H7 (BD Pharmingen) antibodies were added and cells were incubated for 30 minutes. After washing cells once with PBS, 2μL of DAPI (200 μg/mL) was added

For BrdU (Sigma-Aldrich) staining and cell-cycle analysis, 150 mg/kg BrdU was injected intraperitoneally 2 hours before the animals were killed. To summarize, 1 × 10^6 BMMCs were fixed for 20 minutes with the use of 70% ethanol and then denatured with 2N HCL solution. After neutralization using 0.1M sodium borate, cells were washed twice with PBS/1% BSA and incubated for 20 minutes with anti-BrdU–FITC antibody (BD Pharmingen). The samples were washed twice with PBS/1% BSA, and cells were resuspended in 10 μg/mL propidiume iodide (Sigma-Aldrich).

For apoptosis measurement, 2 × 10^6 BMMCs per animal were incubated with 3% BSA for 20 minutes. After washing cells once with cell culture media (DMEM; Gibco), samples were resupended in 100 μL of annexin-V binding buffer (Apoptosis detection kit; BD Pharmingen) containing lin cocktail-eFluor450, anti–c-kit–APC-H7, and annexin-V–FITC (BD Pharmingen). Before analysis, 2 μL of Topro-3 (1 μg/mL; Invitrogen) was added to the samples.

For FACS sorting experiments, BMMCs were blocked with 3% BSA for 20 minutes and washed once with PBS. Cells were stained for 30 minutes with lin cocktail-eFluor450, anti–c-kit–APC-H7, and, where required, with anti–sca-1–PerCP-Cy5.5. After washing them once with PBS, we sorted samples by using a FACS Aria II sorter (BD Bioscience).

Colony-forming assay

For short-term colony-forming assay (CFA), 1 × 10^4, 2 × 10^4, or 4 × 10^4 of BMMCs were cultured in 35-mm dishes (StemCell Technologies) containing Methocult (StemCell Technologies) according to the manufacturer's protocol. All experiments were performed as doublets and the number of colonies was counted on day +12 after manufacturer's protocol.

Statistical analysis and experimental groups

Because the pI-pC–induced interferon release has various effects on the hematopoietic system, we used 4 experimental groups to exclude any effect of interferon in our mouse model. *TRF1*$^{flox/flox}$*Mx1-Cre* with and without pI-pC injections and *TRF1*$^{flox/flox}$*Mx1-wt* with and without pI-pC injections were compared with each other. All experiments were carried out with mice from at least 2 different donors, and a comparison of untreated versus pI-pC treated was performed in pairs by the use of mice from the same donor to minimize interindividual differences. In all analysis, a significance level of $\alpha = 0.05$ was considered as statistically significant, and all graphs are displayed as mean value and SE. If not stated otherwise, "n" represents the number of analyzed mice in each experiment. Statistical analysis was performed with GraphPad prism software Version 5.0 (GraphPad).

Results

Acute TRF1 deletion progressively leads to pancytopenia and histopathologically proven BMF but not to telomere shortening

To study the effects of TRF1 deletion in the bone marrow, we crossed *TRF1*$^{flox/flox}$ mice with a conditional knock-out allele for *TRF1*, with *Mx1-Cre* mice, which express the Cre recombinase in the bone marrow as well as in several tissues like liver, heart, spleen, and kidney.[26] To avoid the potentially deleterious and complex effects of TRF1 deletion in other tissues, we used bone marrow transplantation, allowing us to selectively analyze the consequences of TRF1 deletion in the bone marrow. To this end, the bone marrow from *TRF1*$^{flox/flox}$*Mx1-Cre* and *TRF1*$^{flox/flox}$ *Mx1-wt* mice was transplanted into *wild-type* recipient littermates (see "Bone marrow transplantation and Cre induction"). PCR analysis for *TRF1*^{flox} and *TRF1* revealed complete engraftment of the transplanted transgenic bone marrow excluding any relevant participation of the original recipient marrow (Figure 1A). Thirty days after transplantation, we found a complete recovery of the peripheral

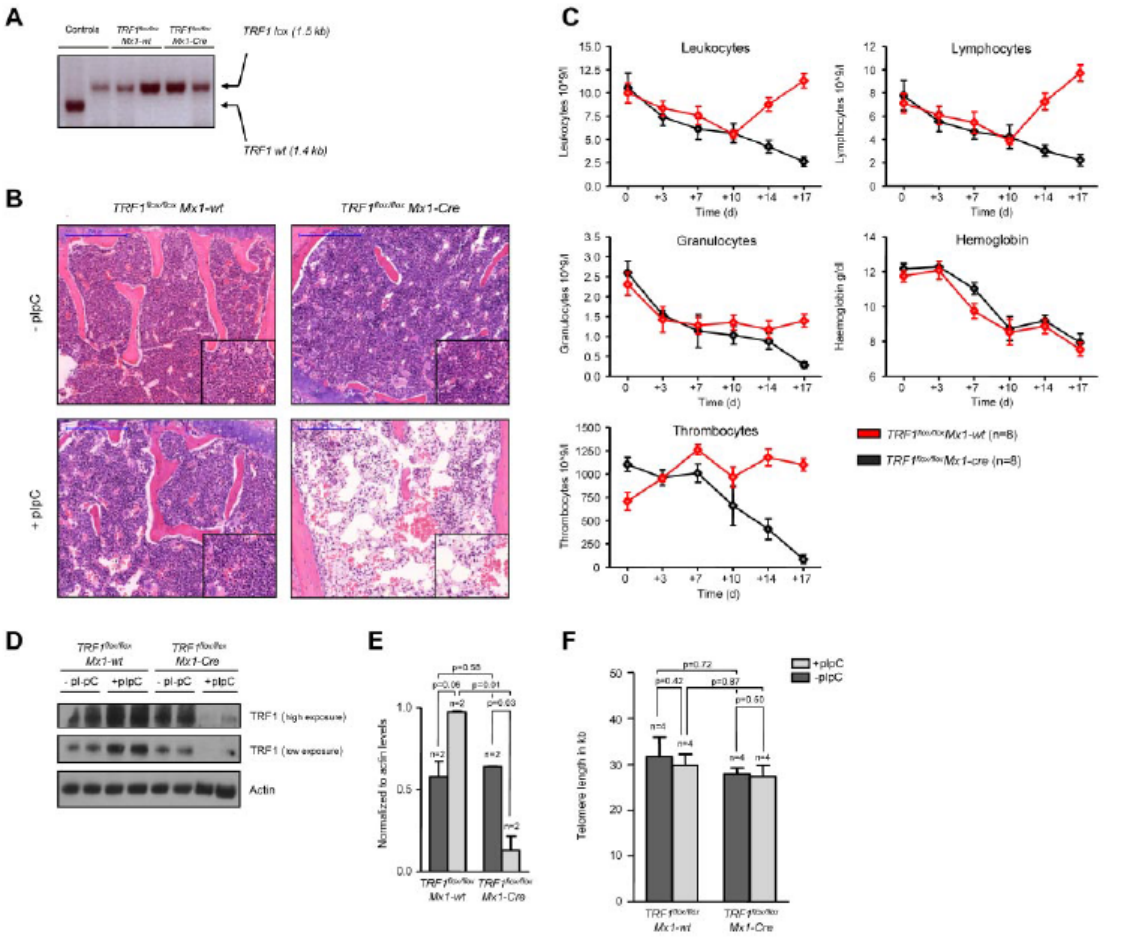

Figure 1. TRF1 deletion progressively leads to pancytopenia and histopathologically proven BMF but not to telomere shortening. (A) PCR for wild-type and floxed *TRF1* confirmed the absence of remaining recipient wild-type bone marrow in *TRF1*$^{flox/flox}$*Mx1-wt* (lane 3 + 4) and *TRF1*$^{flox/flox}$*Mx1-Cre* (lane 5 + 6). Genomic control DNA of *TRF1*^{wt} and *TRF1*$^{flox/flox}$ are shown (lane 1 + 2). (B) Hematoxylin and eosin staining of the sternal bone marrow of *TRF1*$^{flox/flox}$*Mx1-wt* and *TRF1*$^{flox/flox}$*Mx1-Cre* animals without Cre induction and after +18 days. Image was captured with ×10 magnification (blue bar represents 200 μm), small image shows ×40 magnification. (C) Peripheral blood counts measured twice a week of *TRF1*$^{flox/flox}$*Mx1-wt* and *TRF1*$^{flox/flox}$*Mx1-Cre* mice. No statistical difference was found at day 0 in all subpopulations between *TRF1*$^{flox/flox}$*Mx1-wt* and *TRF1*$^{flox/flox}$*Mx1-Cre* mice (all $P > .05$) except for thrombocytes ($P = .005$). At day +18, all *TRF1*$^{flox/flox}$*Mx1-Cre* mice showed statistically significant lower peripheral blood counts (all $P < .005$) except for hemoglobin levels ($P = .55$). Two-sided *t* test was used for statistical comparison. (D) Western blot analysis of TRF1 protein levels of bone marrow protein extracts of *TRF1*$^{flox/flox}$*Mx1-wt* and *TRF1*$^{flox/flox}$*Mx1-Cre* animals without pI-pC injections and after +18 days. Two different exposure times are shown. (E) Quantification of TRF1 protein levels in relation to actin protein levels (without pI-pC, dark gray bars and with pI-pC, light gray bars). Two-sided *t* test was used for statistical comparison. (F) Telomere length analysis using Q-FISH of sternal bone marrow sections of *TRF1*$^{flox/flox}$*Mx1-wt* and *TRF1*$^{flox/flox}$*Mx1-Cre* animals without (dark gray bars) and after 18 days of pI-pC treatment (light gray bars). Two-sided *t* test was used for statistical comparison.

blood counts and normal bone marrow histopathology in both groups (Figure 1B-C), indicating full reconstitution of the recipient bone marrow by the different genotypes.

To delete TRF1 in the bone marrow, we induced Cre expression every second day by treating the mice with pI-pC (see Methods and supplemental Figure 1A, available on the *Blood* Web site; see the Supplemental Materials link at the top of the online article). Eighteen days after induction of Cre (day +18), the mice were sacrificed because they presented with severe pancytopenia and poor health condition. At this end point, we found a significant reduction of TRF1 protein expression in the *TRF1*$^{flox/flox}$*Mx1-Cre* mice, demonstrating a successful abrogation of TRF1 in the treated mice (Figure 1D-E). Reduced TRF1 protein levels also were confirmed by TRF1 immunofluorescence on day +18 at the single-cell level. Of note, although we found dramatically decreased TRF1 protein levels per cell, we did not find any single cell with completely absent TRF1 signals, most likely indicating that these cells are rapidly removed from the bone marrow (supplemental Figure 2A-B).

Histopathologic analysis of the bone marrow at day +18 showed a hypocelluar, aplastic bone marrow (Figure 1B) in the *TRF1*$^{flox/flox}$*Mx1-Cre* group consistent with BMF but no signs of hypocellularity/aplasia in the *TRF1*$^{flox/flox}$*Mx1-wt* mice. In line with the histologic findings, all mice in the *TRF1*$^{flox/flox}$*Mx1-Cre* group developed a progressive decrease of the peripheral blood counts resulting in pancytopenia. In contrast, the *TRF1*$^{flox/flox}$*Mx1-wt* group (Figure 1C) showed stable or even increasing blood counts except for the hemoglobin levels owe to the blood withdrawal.

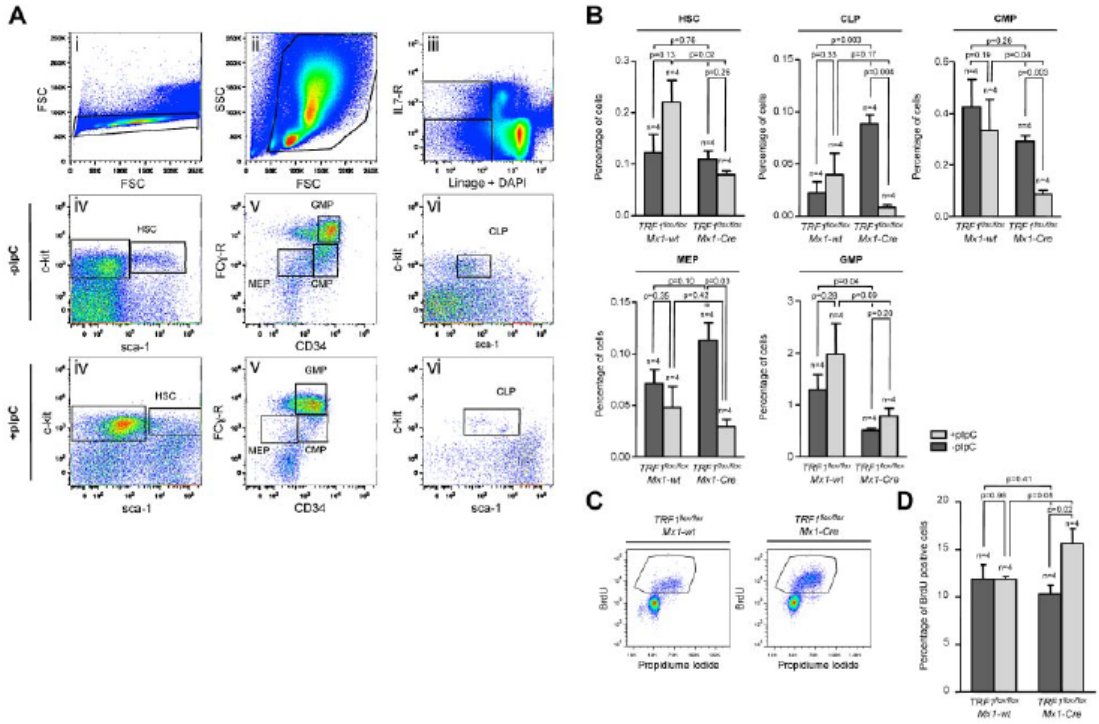

Figure 2. Induction of TRF1 deletion depletes HSC and progenitor cells and leads to increased compensatory proliferation. (A) Representative FACS analysis of the HSC and progenitor cell populations. Single cells in panel Ai were further gated based on forward and side scatter (Aii). Including only viable cells without DAPI incorporation, BMMCs of (Aii) were separated on the basis of being lineage negative and IL-7 receptor positive or negative (Aiii). IL-7 receptor–positive cells were further analyzed based on the sca-1 and c-kit staining (Avi). Common lymphoid progenitors (CLP) were identified as sca-1 and c-kit low(+) cells. Lin and IL-7 receptor–negative cells were further distinguished on the basis of sca-1 and c-kit staining (Aiv). HSCs were identified as c-kit(+), sca-1(+). C-kit(+), sca-1(−) progenitor cells were further differentiated in (Av) on the basis of CD34 and Fc-receptor staining. CD34 and Fc-receptor low(+) cells were identified as megakaryocyte-erythrocyte progenitor cells (MEP), CD34(+), Fc-receptor low–positive cells as common myeloid progenitors (CMP),and CD34(+),Fc-receptor(+) cells were identified as granulocyte-macrophage progenitors (GMP). (B) Quantification of the percentage of the hematopoietic stem and progenitor cell subpopulations. The respective percentage was calculated in relation to the number of cells gated for forward and side scatter in panel Aii. Mice without pI-pC–induced Cre expression are represented by dark gray bars and mice undergoing pI-C injections by light gray bars. Two-sided *t* test was used for statistical comparison between $TRF1^{flox/flox}Mx1\text{-}wt$ and $TRF1^{flox/flox}Mx1\text{-}Cre$ group, student paired *t* test for statistical comparison within the respective group (untreated vs treated). (C) Representative FACS analysis of BrdU incorporation after 2-hour pulse labeling in $TRF1^{flox/flox}Mx1\text{-}wt$ and $TRF1^{flox/flox}Mx1\text{-}Cre$ mice undergoing Cre induction. BMMCs were gated for singlet cells and forward and side scatter (FACS scatter gram not shown) and then further separated on the basis of BrdU and propidium iodide staining. (D) Quantification of BrdU-positive cells. The respective percentage was calculated in relation to the number of cells gated for forward and side scatter. Mice without pI-pC–induced Cre expression are represented by dark gray bars and mice undergoing pI-C injections by light gray bars. Two-sided *t* test and student paired *t* test was used for statistical comparison between respective $TRF1^{flox/flox}Mx1\text{-}wt$ and $TRF1^{flox/flox}Mx1\text{-}Cre$ subgroups.

To investigate the impact of acute TRF1 abrogation on telomere length, telomere length in both groups was measured before and after TRF1 deletion. We observed no significant differences between both groups (Figure 1F). In summary, these findings indicate that TRF1 deletion progressively leads to BMF in the absence of detectable telomere shortening.

Progressive TRF1 deletion significantly reduces the number of HSC and progenitor cells and leads to increased compensatory proliferation

To understand the effect of progressive TRF1 deletion in the bone marrow, we injected pI-pC daily for a total of 7 days (supplemental Figure 1B). Using this approach, we obtained a significant decrease of TRF1 protein levels and a robust decrease of the bone marrow cellularity (supplemental Figure 3A-C), yet at the same time we could obtain sufficient bone marrow cells for further experimentation. First, we performed a detailed analysis of the different bone marrow subpopulations (Figure 2A-B). FACS analysis revealed an increase of HSCs in the pI-pC–treated $TRF1^{flox/flox}Mx1\text{-}wt$ control group but a decrease in the $TRF1^{flox/flox}Mx1\text{-}Cre$ group (Figure 2A-B). In the progenitor cell population, we found a significant decrease in the number of common lymphoid progenitors as well as the common myeloid progenitors in the $TRF1^{flox/flox}Mx1\text{-}Cre$ but not in $TRF1^{flox/flox}Mx1\text{-}wt$ group (Figure 2A-B). We also found a significant decrease in the more differentiated megakaryocyte-erythrocyte progenitors in the $TRF1^{flox/flox}Mx1\text{-}Cre$ mice compared with the $TRF1^{flox/flox}Mx1\text{-}wt$ controls (Figure 2A-B). In contrast, granulocyte-macrophage progenitors did not significantly differ between genotypes (Figure 2A-B).

Because the induction of TRF1 deletion leads to a decrease of the HSC and progenitor cells, we asked whether the observed stem and progenitor cell depletion results in reduced proliferation rates in the bone marrow. To this end, we performed cell-cycle analysis and 2-hour BrdU pulse labeling to analyze for changes in the proliferation rate. Cell-cycle profile revealed significant increased S-phase and G_2-M phase in the $TRF1^{flox/flox}Mx1\text{-}Cre$ mice (supplemental Figure 3E-F). In line with the cell-cycle analysis, the number of BrdU-incorporating cells in the $TRF1^{flox/flox}Mx1\text{-}Cre$ mice was significantly

increased compared with the *TRF1*$^{flox/flox}$*Mx1-wt* controls (Figure 2 C-D). These findings indicate an increased compensatory proliferation of the remaining non-TRF1–deleted cells in the *TRF1*$^{flox/flox}$*Mx1-Cre* mice despite significant reduction of stem and progenitor cells. Supporting the notion of increased compensatory proliferation in response to TRF1 ablation, we found significantly increased G-CSF levels in the blood of the *TRF1*$^{flox/flox}$*Mx1-Cre* mice (supplemental Figure 3D), which is the main growth factor for granulocyte precursors. These results indicate that TRF1 deletion results in increased compensatory proliferation of the remaining non-TRF1–deleted bone marrow cells to compensate for loss of stem and progenitor cells.

Progressive TRF1 deletion leads to increased number of telomere-induced foci, increased p53-mediated induction of p21, and cellular senescence but no apoptosis

γH2AX can form foci that marks the presence of DSBs, and colocalization of γH2AX foci with telomeres indicates the presence of uncapped/dysfunctional telomeres, the so-called telomere damage associated foci or telomere-induced foci (TIFs).[28] To address whether TRF1 ablation results in increased telomeric damage, we combined γH2AX immunofluorescence staining with telomere Q-FISH (immuno-Q-FISH) for colocalization analysis of γH2AX foci and telomeres in bone marrow sections (Figure 3A). We observed a significant increase in the number of TIFs in the pI-pC–treated *TRF1*$^{flox/flox}$*Mx1-Cre* bone marrow but a decrease in similarly treated *TRF1*$^{flox/flox}$*Mx1-wt* control group (Figure 3B). Because dysfunctional telomeres as the result of TRF1 depletion can lead to chromosomal aberrations,[6,7] we next analyzed bone marrow metaphases. We did not observe significant differences in the number of chromosome aberrations between *TRF1*$^{flox/flox}$*Mx1-wt* and *TRF1*$^{flox/flox}$*Mx1-Cre* mice (supplemental Figure 4A-B).

Activation of a persistent DDR as the consequence of dysfunctional telomeres leads to up-regulation of p53 and to cellular senescence mediated by the p53 target gene p21.[29] To address whether conditional TRF1 deletion in the bone marrow induces p53-mediated senescence in vivo, we first analyzed p53 protein levels by Western blotting. We found significantly greater p53 levels in pI-pC–treated *TRF1*$^{flox/flox}$*Mx1-Cre* mice compared with similarly treated *TRF1*$^{flox/flox}$*Mx1-wt* controls (Figure 3C-D). Next, we analyzed p21 mRNA levels by RT-PCR in FACS-sorted bone marrow cells. We found significantly greater p21 mRNA levels in progenitor cells from treated *TRF1*$^{flox/flox}$*Mx1-Cre* mice, as well as in differentiated cells. Interesting, we observed the opposite tendency to have lower p21 mRNA levels in the HSC compartment on TRF1 deletion, which goes in line with compensatory hyperproliferation of this compartment. Immunohistochemistry (IHC) with anti-p21 antibodies directly on bone marrow sections confirmed a significant increase in p21 protein levels in the treated *TRF1*$^{flox/flox}$*Mx1-Cre* group compared with the *TRF1*$^{flox/flox}$*Mx1-wt* controls (Figure 3F-G). Again, we did not detect any relevant changes in p21 mRNA or protein levels in similarly treated *TRF1*$^{flox/flox}$*Mx1-wt* control mice (Figure 3E-G). In summary, elevated p53 and p21 levels are consistent with increased cellular senescence in vivo as the consequence of TRF1 deletion in the bone marrow.

To directly assess induction of senescence in vivo caused by TRF1 deletion, we used β-galactosidase staining directly on freshly isolated bone marrow cells (Figure 3H). The bone marrow from the *TRF1*$^{flox/flox}$*Mx1-Cre*–treated group showed a massive increase in the number of β-galactosidase–positive cells compared with the similarly *TRF1*$^{flox/flox}$*Mx1-wt* control group (Figure 3I). To identify the most affected cellular subpopulation, the bone marrow from treated *TRF1*$^{flox/flox}$*Mx1-Cre* mice was sorted by FACS into differentiated and progenitor cells. Both subpopulations showed significantly increased numbers of β-galactosidase–positive cells, but progenitor cells accounted for the majority β-galactosidase–positive cells (Figure 3I). Interestingly, when we used the same approach for unsorted bone marrow cells with 3 additional days without Cre induction, no increased number of β-galactosidase positive cells was observed, indicating a rapid clearance of the senescent cells (supplemental Figure 4C).

Finally, we wanted to address whether, in addition to cellular senescence, apoptosis also contributed to depletion of HSC and progenitors on TRF1 deletion. Annexin-V analysis of early apoptotic cells (annexin-V positive, TO-PRO-3 negative) of all bone marrow cells and progenitor cells revealed no significant differences between the groups (Figure 3J-K). Our findings demonstrate that conditional TRF1 deletion induces p53-mediated p21 activation and subsequent induction of cellular senescence mainly in the progenitor cells because of persistent telomeric DNA damage in the absence of increased apoptosis.

Long-term induction of TRF1 deletion leads to massive impaired overall survival because of BMF after 8 weeks and massive telomere shortening

Next, we investigated the effects of long-term TRF1 dysfunction by inducing TRF1 deletion at a lower frequency, which could recapitulate a more similar situation to that of human patients with TIN2 mutations. To this end, we induced TRF1 deletion 3 times per week during several weeks (5-13 weeks) in a long-term approach (supplemental Figure 1C). Analysis of the peripheral blood counts revealed a progressive decrease in all 3 lineages over time in the treated *TRF1*$^{flox/flox}$*Mx1-Cre* mice (Figure 4A). In agreement with development of pancytopenia, all treated *TRF1*$^{flox/flox}$*Mx1-Cre* mice showed histopathologic signs of BMF characterized by a hypocellular or aplastic bone marrow (Figure 4B). In contrast, no signs of BMF were found in similarly treated *TRF1*$^{flox/flox}$*Mx1-wt* control animals. In addition, we observed a dramatically reduced median survival of 8.1 weeks for the treated *TRF1*$^{flox/flox}$*Mx1-Cre* mice (Figure 4C).

In this setting of a more chronic TRF1 dysfunction, we next analyzed telomere length in bone marrow sections by using quantitative telomere Q-FISH (Figure 5A). Strikingly, *TRF1*$^{flox/flox}$*Mx1-Cre* mice undergoing long-term Cre-induction/TRF1 deletion showed a dramatic telomere shortening of approximately 15 kb within 7-9 weeks of treatment in comparison with *TRF1*$^{flox/flox}$*Mx1-wt* mice after 13 weeks of treatment (Figure 5B). Telomere length distribution revealed a massive increase in the abundance of shorter telomeres in the treated *TRF1*$^{flox/flox}$*Mx1-Cre* group (Figure 5C). Analysis of the telomere length in relation to the respective untreated counterpart revealed that *TRF1*$^{flox/flox}$*Mx1-wt* animals showed 7.4% shorter telomeres after 13 weeks. Telomeres of *TRF1*$^{flox/flox}$*Mx1-Cre* mice after 7-9 weeks were found to be 44.7% shorter, resulting in an approximately 6-fold increased telomere shortening compared with the *TRF1*$^{flox/flox}$*Mx1-wt* (Figure 5D). These results clearly show that chronic TRF1 dysfunction leads to a severe telomere shortening over time, similar to that observed in human patients with *TIN2* mutations.

Because Q-FISH analysis on bone marrow sections can only determine telomere length at the time of death, we set out to perform longitudinal telomere length studies on induction of TRF1 deletion. To analyze the telomere length dynamics over time, we used the Q-FISH method (HT-Q-FISH), which determines telomere length in a per-cell basis in peripheral blood.[30,31] HT-Q-FISH

BLOOD, 11 OCTOBER 2012 • VOLUME 120, NUMBER 15 TRF1 DEFICIENCY RECAPITULATES FEATURES OF DKC 2995

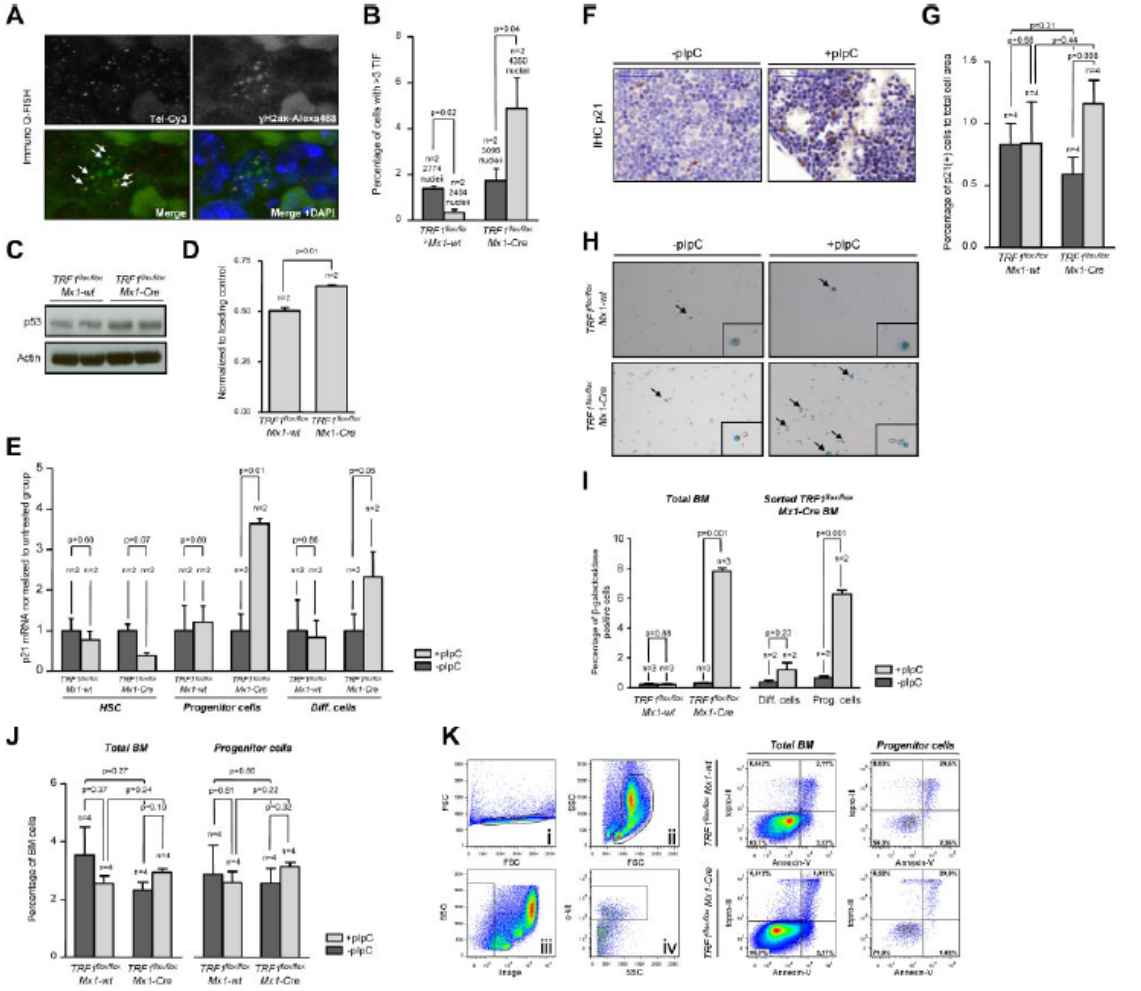

Figure 3. TRF1 deletion leads to increased number of TIFs and cellular senescence via p21 but no induction of apoptosis. (A) Representative image of colocalization (indicated by white arrows) of γH2AX foci and telomeres using immuno Q-FISH. (B) Quantification of the number of TIFs per detected nucleus. Only cells showing 3 or more TIF were included. Mice without pI-pC–induced Cre expression are represented by dark gray bars and mice undergoing pI-C injections by light gray bars. Two-sided *t* test was used for statistical comparison. (C) Western blot analysis of p53 protein levels of pI-pC–treated *TRF1*$^{flox/flox}$*Mx1-wt* and *TRF1*$^{flox/flox}$*Mx1-Cre* mice. (D) Quantification of Western blot analysis of the p53 protein levels in relation to respective actin levels. Two-sided *t* test was used for statistical comparison. (E) Fold change of quantitative PCR of p21 mRNA levels in FACS-sorted bone marrow cells sorted for HSC: lin(−), c-kit (+), sca-1(+); progenitor cells: lin(−), c-kit(+), sca-1 (−); and differentiated cells: lin(+). mRNA of p21 levels were normalized to actin levels, and statistical comparison was conducted with the Student *t* test between untreated and pI-pC–treated *TRF1*$^{flox/flox}$*Mx1-wt* and *TRF1*$^{flox/flox}$*Mx1-Cre* mice. (F) Representative image of p21 IHC staining of *TRF1*$^{flox/flox}$*Mx1-Cre* mice with and without pI-pC injections (×40 magnification, blue bar represents 50 μm). (G) Quantification of the p21 IHC-positive area (brown cells) in relation to the area of all cells. Mice without pI-pC–induced Cre expression are represented by dark gray bars and mice undergoing pI-C injections by light gray bars. Two-sided *t* test and Student paired *t* test was used for statistical comparison between *TRF1*$^{flox/flox}$*Mx1-wt* and *TRF1*$^{flox/flox}$*Mx1-Cre* subgroups. (H) Representative images of β-galactosidase staining in unsorted bone marrow. Images were captured with ×10 magnification, small window represents a magnified (20×) section of the image showing representative β-galactosidase–positive (indicated by black arrows) and –negative cells. (I) Quantification of the percentage of β-galactosidase positive cells per counted dish. Bar graph on the left represents unsorted bone marrow cells. On the right, quantification of FACS-sorted lin(+) differentiated cells and lin(−)c-kit(+) HSC and progenitors cells is shown. Mice without pI-pC–induced Cre expression are represented by dark gray bars and mice undergoing pI-C injections by light gray bars. Two-sided *t* test was used for statistical comparison. (J) Quantification of the percentage of early apoptotic cells in all bone marrow cells and stem and progenitor cells. Quantification on the left represents all bone marrow cells, on the right, quantification of lin(−)c-kit(+) HSC and progenitors cells is shown. Mice without pI-pC–induced Cre expression are represented by dark gray bars, mice undergoing pI-C injections by bright gray bars. Two-sided *t* test and Student *t* test was used for statistical comparison between *TRF1*$^{flox/flox}$*Mx1-wt* and *TRF1*$^{flox/flox}$*Mx1-Cre* subgroups. (K) Representative FACS analysis for apoptosis of pI-pC–treated *TRF1*$^{flox/flox}$*Mx1-wt* and *TRF1*$^{flox/flox}$*Mx1-Cre* mice. Single cells in Ki were further gated on the basis of forward and side scatter (Kii). Selected cells of Kii were analyzed as total bone marrow based on TO-PRO-3 and annexin-V staining or further separated in panel Kiii on the basis of negative linage staining. Lineage(−) cells were further distinguished in c-kit–positive and –negative cells (in Kiv). C-kit(+), lin(−) HSC, and progenitor cells (Kiv) were further analyzed on the basis of TO-PRO-3 and annexin-V staining. Annexin-V–positive and TOP-RO-3–negative cells were identified as early apoptotic cells.

also allows for the determination of the abundance of short telomeres because it can quantify individual telomere signals per cell.[30,31] HT-Q-FISH analysis showed that telomere length progressively shortened over time in the treated *TRF1*$^{flox/flox}$*Mx1-Cre* group (Figure 5E). In addition, HT-Q-FISH revealed a massive accumulation of short telomeres in the treated *TRF1*$^{flox/flox}$*Mx1-Cre* group (Figure 5F). Interestingly, both telomere length and the percentage of short telomeres per individual mice showed a significant

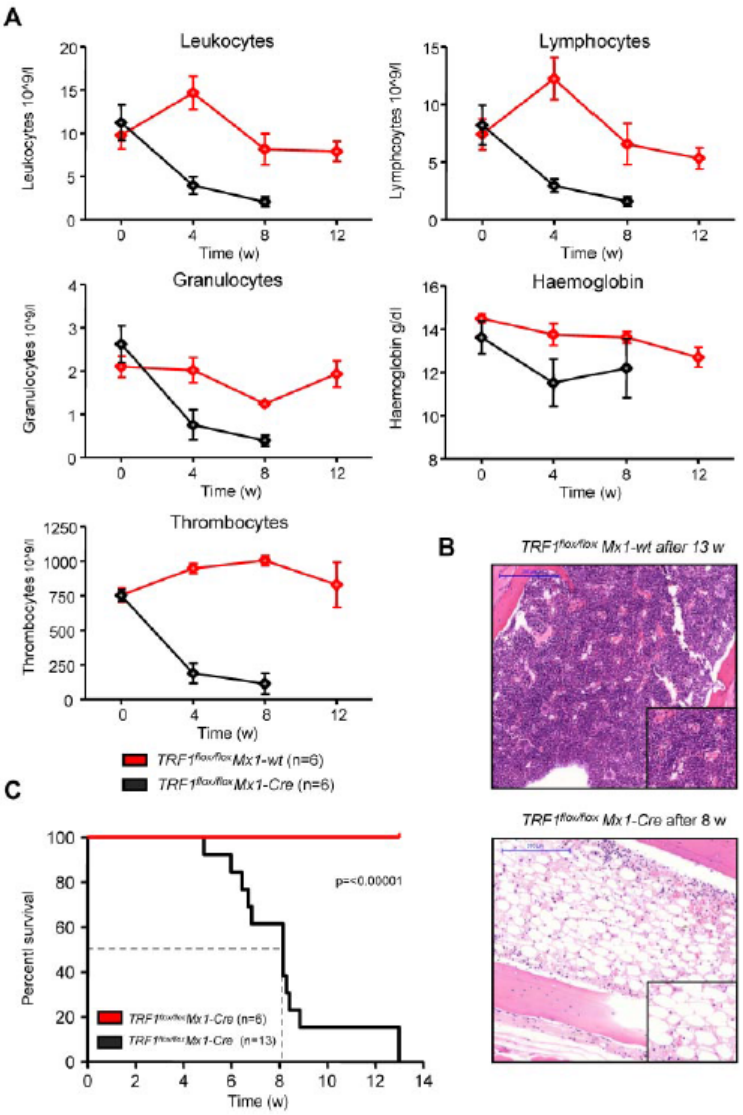

Figure 4. Long-term induction of TRF1 deletion results in BMF and reduced overall survival. (A) Peripheral blood counts measured once a month of *TRF1*$^{flox/flox}$*Mx1-wt* and *TRF1*$^{flox/flox}$*Mx1-Cre* mice during Cre long-term induction via pI-pC. No statistical difference was found at day 0 in all the subpopulations between *TRF1*$^{flox/flox}$*Mx1-wt* and *TRF1*$^{flox/flox}$*Mx1-Cre* mice (all $P > .05$). At 4 and 8 weeks after starting Cre induction, all *TRF1*$^{flox/flox}$*Mx1-Cre* mice showed statistically significant lower peripheral blood counts (all $P < .005$) except for hemoglobin levels ($P = .08$ and $P = .07$ at week +4 and +8, respectively). Two-sided *t* test was used for statistical comparison. (B) Exemplary hematoxylin and eosin staining of the sternal bone marrow of a *TRF1*$^{flox/flox}$*Mx1-wt* and *TRF1*$^{flox/flox}$*Mx1-Cre* animal 13 and 8 weeks, respectively, after the start of Cre induction. Image was captured with ×10 magnification (blue bar represents 200 μm), small image shows ×40 magnification. (C) Overall survival of *TRF1*$^{flox/flox}$*Mx1-wt* and *TRF1*$^{flox/flox}$*Mx1-Cre* mice undergoing long-term Cre induction. Dashed line represents median survival. Log-rank test was used for statistical comparison.

correlation with the remaining overall survival of the individual treated *TRF1*$^{flox/flox}$*Mx1-Cre* mice (Figure 5G-H). These results demonstrate that chronic TRF1 deletion leads to a progressive decrease in telomere length, which eventually determines mouse longevity.

Mice undergoing long-term TRF1 deletion undergo replicative senescence and exhaustion because of telomere shortening

The aforementioned results suggest that the reduction of the HSC and progenitor cells and the consecutive compensatory increased proliferation of the remaining stem and progenitor cells maybe be responsible for the massive telomere shortening and accumulation of short telomeres induced on chronic TRF1 dysfunction, thus providing a molecular mechanism for the observations in human TIN2 patients. To confirm the supposed increased proliferation and replicative stress, we quantified the IHC for phospho-Histone3 and phospho-CHK1, known markers for cell proliferation and replicative stress, respectively.[32] *TRF1*$^{flox/flox}$*Mx1-Cre* mice showed a significant relative increase in proliferation and replicative stress compared with *TRF1*$^{flox/flox}$*Mx1-wt* mice after 4 and 8 weeks of long-term Cre induction (supplemental Figure 5A-D).

BLOOD, 11 OCTOBER 2012 • VOLUME 120, NUMBER 15 TRF1 DEFICIENCY RECAPITULATES FEATURES OF DKC 2997

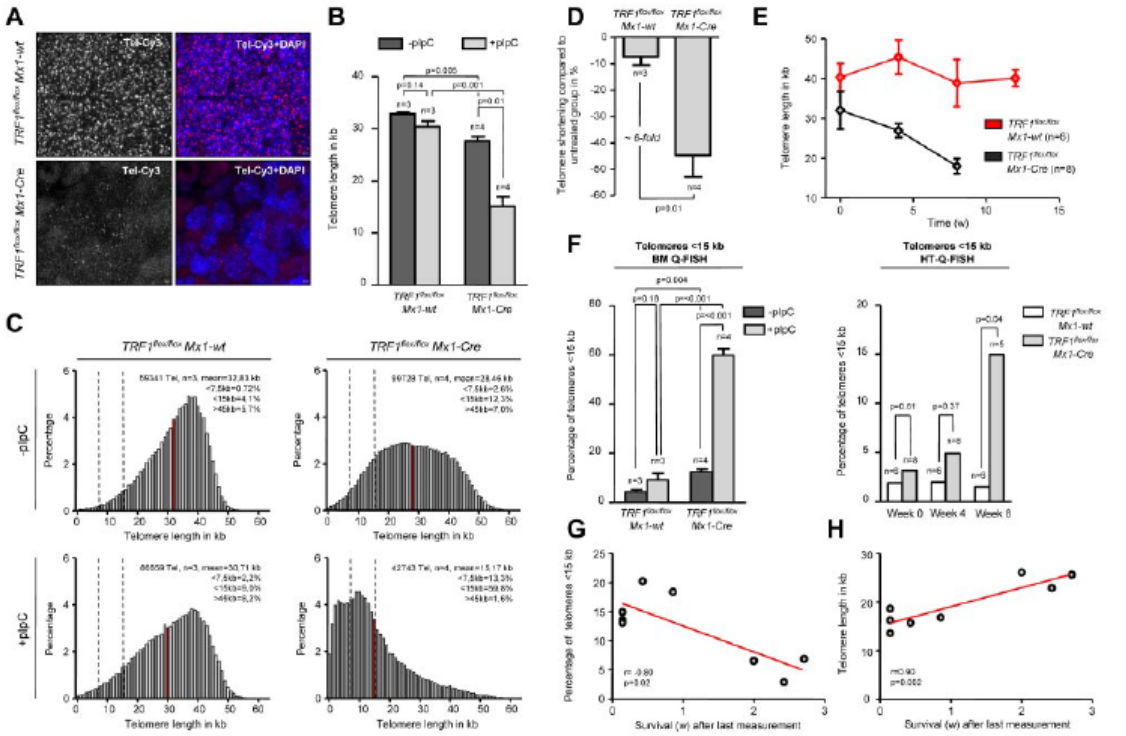

Figure 5. Long-term induction of TRF1 deletion leads to telomere shortening and significant increased number of short telomeres. (A) Representative image of bone marrow Q-FISH of *TRF1*$^{flox/flox}$*Mx1-wt* and *TRF1*$^{flox/flox}$*Mx1-Cre* mice undergoing long-term Cre induction (×63 magnification and ×2 optical zoom). (B) Mean telomere length of *TRF1*$^{flox/flox}$*Mx1-wt* and *TRF1*$^{flox/flox}$*Mx1-Cre* mice with (after 7-9 and 13 weeks, respectively) and without long-term Cre induction. Mice without pI-pC–induced Cre expression are represented by dark gray bars and mice undergoing pI-pC injections by light gray bars. Two-sided *t* test and Student paired *t* test was used for statistical comparison between *TRF1*$^{flox/flox}$*Mx1-wt* and *TRF1*$^{flox/flox}$*Mx1-Cre* subgroups. (C) Telomere length distribution of all measured telomeres in the analyzed *TRF1*$^{flox/flox}$*Mx1-wt* and *TRF1*$^{flox/flox}$*Mx1-Cre* animals with and without Cre induction. Red line indicates the mean value calculated in panel B, and dashed lines represent 7.5 and 15 kb. All percentages given in the graph are calculated represent the mean values of the respective 3 or 4 measured mice. (D) Relative telomere length difference between the respective treated and untreated *TRF1*$^{flox/flox}$*Mx1-wt* and *TRF1*$^{flox/flox}$*Mx1-Cre* mice. Two-sided *t* test was used for statistical comparison. (E) Telomere length over time of peripheral blood leukocytes in *TRF1*$^{flox/flox}$*Mx1-wt* and *TRF1*$^{flox/flox}$*Mx1-Cre* animals undergoing long-term pI-pC injections. *TRF1*$^{flox/flox}$*Mx1-Cre* mice showed significant shorter telomeres after 4 and 8 of Cre induction (both $P < .005$), but no significant difference was observed before Cre induction ($P = .26$). Two-sided *t* test and used for statistical comparison between *TRF1*$^{flox/flox}$*Mx1-wt* and *TRF1*$^{flox/flox}$*Mx1-Cre* subgroups. (F) Quantification of the percentage of telomeres < 15 kb of analyzed mice of (B) using BM-Q-FISH and of (E) using HT-Q-FISH. Two-sided *t* test and used for statistical comparison between *TRF1*$^{flox/flox}$*Mx1-wt* and *TRF1*$^{flox/flox}$*Mx1-Cre* subgroups of BM-Q-FISH, 2-sided Mann-Whitney *U* test was used for comparison between *TRF1*$^{flox/flox}$*Mx1-wt* and *TRF1*$^{flox/flox}$*Mx1-Cre* subgroups of HT-Q-FISH. (G) Correlation between measured short telomeres (< 15 kb) of the last blood sample taken and remaining survival time in weeks of the mice. (H) Correlation between telomere length of the last blood sample taken and remaining survival time in weeks of the mice. Pearson correlation was used for statistical analysis.

In turn, accumulation of short telomeres can induce replicative senescence.[33,34] To analyze the consequences of the massive accumulation of short telomeres in *TRF1*$^{flox/flox}$*Mx1-Cre* mice, we performed β-galactosidase staining in *TRF1*$^{flox/flox}$*Mx1-Cre* and *TRF1*$^{flox/flox}$*Mx1-wt* mice after 4 weeks of long-term Cre induction/TRF1 deletion and 5 days without Cre induction. The *TRF1*$^{flox/flox}$*Mx1-Cre* group showed a significantly increased, approximately 13-fold greater number of β-galactosidase–positive cells (2.19%-0.16%, respectively) compared with the *TRF1*$^{flox/flox}$*Mx1-wt* (Figure 6A-B). The number of β-galactosidase–positive cells in the *TRF1*$^{flox/flox}$*Mx1-wt* group was in the same range as previously found (Figure 3I). To test whether short telomeres affect proliferative capacities of the stem cells, we performed CFA after 4 weeks of long-term Cre induction. CFA showed significantly decreased capacity of forming colonies in the *TRF1*$^{flox/flox}$*Mx1-Cre* group (Figure 6C-D).

To analyze the effects of long-term Cre induction after 8 weeks, we performed IHC of p21 in bone marrow sections. The number of p21-positive bone marrow cells was significantly increased in the *TRF1*$^{flox/flox}$*Mx1-Cre* group, 4.5-fold greater compared with the p21 levels of *TRF1*$^{flox/flox}$*Mx1-wt* mice. p21 levels of *TRF1*$^{flox/flox}$*Mx1-Cwt* mice were in the range as previously observed (Figure 6E-F). To analyze the functional consequences of short telomeres and increased p21 levels, we performed serial bone marrow transplantation after 8 weeks of long-term Cre induction in *TRF1*$^{flox/flox}$*Mx1-wt* and *TRF1*$^{flox/flox}$*Mx1-Cre* mice. The bone marrow of the *TRF1*$^{flox/flox}$*Mx1-wt* mice did not exhibit difficulties to repopulate a second time. In the *TRF1*$^{flox/flox}$*Mx1-Cre* group, we found a tendency for prolonged survival compared with irradiated mice without bone marrow transplantation, but no transplanted bone marrow of the *TRF1*$^{flox/flox}$*Mx1-Cre* group was able to stably repopulate over 4 weeks (Figure 6G). Our data indicate that accumulation of short telomeres because of chronic TRF1 deletion is the underlying mechanism of replicative senescence and impaired proliferative capacity in TRF1 deleted bone marrow.

Discussion

Here, we set out to test whether abrogation of TRF1 in the hematopoietic system recapitulates the clinical features of BMF

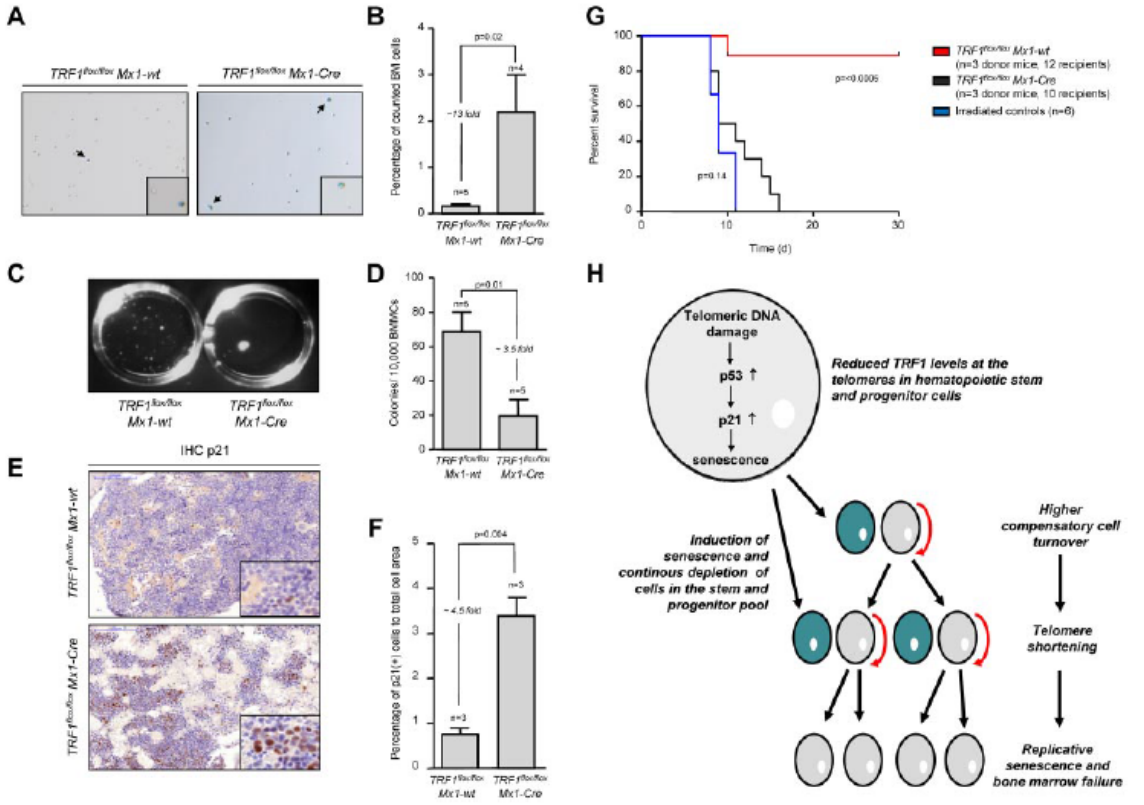

Figure 6. Mice undergoing long-term induction of TRF1 deletion undergo replicative senescence and exhaustion because of telomere shortening. (A) β-galactosidase staining of *TRF1*$^{flox/flox}$*Mx1-wt* and *TRF1*$^{flox/flox}$*Mx1-Cre* mice after 4 weeks of long-term Cre induction and 5 days of pause before measurement to exclude any interferon related effects. Images were captured with ×10 magnification, small window represents a magnified (×20) section of the image showing representative β-galactosidase–positive (indicated by black arrows) and –negative cells. (B) Quantification of β-galactosidase staining of panel A. Two-sided *t* test was used for statistical comparison. (C) Macroscopic view of CFA assays of *TRF1*$^{flox/flox}$*Mx1-wt* and *TRF1*$^{flox/flox}$*Mx1-Cre* mice after 12 days. (D) Quantification of CFU assay of *TRF1*$^{flox/flox}$*Mx1-wt* and *TRF1*$^{flox/flox}$*Mx1-Cre* mice after 4 weeks of long-term Cre induction and 5 days of pause before culturing. Two-sided *t* test was used for statistical comparison. (E) Representative IHC staining for p21 of *TRF1*$^{flox/flox}$*Mx1-wt* and *TRF1*$^{flox/flox}$*Mx1-Cre* mice being bone marrow donor for serial transplantation. Mice underwent 8 weeks of long-term Cre induction and 5 days of pause before being euthanized for serial transplantation. Image was captured with ×20 magnification (blue bar represents 100 μm), small image shows ×80 magnification. (F) Quantification of the percentage of p21-positive area calculated to the area of all cells is shown on the right. Two-sided *t* test was used for statistical comparison. (G) Overall survival of mice undergoing serial transplantation. *TRF1*$^{flox/flox}$*Mx1-wt* and *TRF1*$^{flox/flox}$*Mx1-Cre* bone marrow donor mice underwent 8 weeks of long-term Cre induction and had 5 days of pause before being killed as donors for serial transplantation. Both groups were compared with animals not receiving bone marrow transplantation. Log-rank test was used for comparison between *TRF1*$^{flox/flox}$*Mx1-wt* and *TRF1*$^{flox/flox}$*Mx1-Cre* mice ($P = < .0005$) and *TRF1*$^{flox/flox}$*Mx1-Cre* mice were compared with mice without bone marrow transplantation ($P = .14$). (H) Proposed model of the consequences of reduced TRF1 levels in patients with TIN2 mutations.

associated with mutations in the telomere pathway (ie, patients with telomerase or shelterin mutations). We first show that acute TRF1 deletion results in BMF and progressive cytopenia in the absence of telomere shortening. Because of the severity of the phenotype mice had to be killed only 18 days after the induction of TRF1 ablation, which represents a lifespan of only 8 extra days compared with that of lethally irradiated mice. These findings indicate a severe dysfunction of the HSC/progenitor compartment as observed for chemotherapy and in line with previously studies confirm the essential nature of the *TRF1* gene.[6,35] In the in vivo setting of the BM, TRF1 depletion leads to dysfunctional telomeres and to in vivo induction of cellular senescence via p53 mediated activation of p21.[6]

Cellular senescence was specifically found in progenitor cells and, to a lesser extent, in differentiated cells, in agreement with the fact that these compartments have the highest cell cycle activity.[36] This progenitor cell depletion explains the phenotype observed in the closely clocked acute TRF1 deletion. As a result of the progenitor cell depletion, we found an increased compensatory proliferation of the no-TRF1–depleted stem cell pools (HSCs). This increased proliferation of HSC is mechanistically explained by lower p21 levels in the HSC compartment.[37] Notably, we observed that TRF1-depleted cells did not contribute to cell division and were rapidly cleared of the bone marrow in the absence of increased apoptosis. In this regard, it is likely that phagocytosis of the TRF1 depleted senescent cells by macrophages in the bone marrow as observed for mature granulocytes may explain the clearance of senescent cells.[38]

Next, by deleting TRF1 at a lower frequency and during longer times, we aimed to induce a chronic TRF1 dysfunction, which could resemble more closely the human BMF syndromes associated with telomere dysfunction. In this setting, mice progressively developed cytopenia and BMF over time until reaching their end point. Mice undergoing acute TRF1 deletion did not show telomere shortening because of the acute depletion of the progenitor cell compartment and the short time span. In contrast, telomeres were found

to undergo massive shortening with time in mice receiving less frequent long-term Cre induction. Furthermore, as a consequence of telomere shortening, we observed an accumulation of short telomeres and in vivo induction of replicative senescence in the bone marrow concomitant with impaired replicative capacity.

Importantly, our chronic TRF1 dysfunction mouse model recapitulates various clinical features of DKC patients carrying mutations in the shelterin *TIN2* gene. Similar to the clinical course in DKC patients with *TIN2* mutations, TRF1-deleted mice exhibit progressive pancytopenia over time, resulting in BMF.[10,39] Further, we found a reduced number of colony-forming units, indicating impaired bone marrow function as reported in patients with DKC.[40] In addition, the clinical feature of early onset of symptoms in patients with *TIN2* mutations and the very short telomeres observed in these patients coincidences with the massive and rapid telomere shortening over a period of only few weeks, leading to impaired overall survival as observed in our mice.[14-16] In particular, mice with chronic TRF1 dysfunction showed approximately a 6-fold increase in telomere shortening over time compared with the control group, which is in a similar range to that observed in a prospective study demonstrating a 4-fold increase in telomere shortening in patients with DKC.[14] Furthermore, we found an excellent correlation between telomere length and percentage of short telomeres with the remaining lifespan of mice with TRF1 deletion in the bone marrow, highlighting the role of telomeres as a possible marker for clinical outcome in BMF syndromes. In this regard, in the clinical practice, short telomere length is used to identify DKC patients with *TIN2* mutations[16,18]

Defects in telomere maintenance contribute to various types of BMF syndromes. Previous models for the pathogenesis of DKC proposed that stem cell dysfunction is caused by accelerated telomere shortening because of impaired functionality of the telomerase complex in the HSC because of mutations in the telomerase genes. As a consequence of telomerase deficiency, cycling HSC cannot properly maintain telomere length, resulting in progressive accumulation of short telomeres, a common clinical feature of DKC patients with impaired telomerase activity.[34,41,42] On the basis of our findings, we propose an additional mechanism leading to telomere shortening in the presence of a functional telomerase complex, such as it is the case of DKC patients with *TIN2* mutations. Dysfunctional telomeres lead to activation of DDR and increased number of progenitor cells undergoing cellular senescence. To compensate for the constant progenitor cell lost, a greater cell turnover is needed to maintain blood homeostasis, resulting in telomere shortening and subsequent replicative senescence. We cannot completely rule out the possibility that TRF1-deleted cells can divide and contribute to the phenotype in our mice. However, on the basis of previous studies,[6,7] this possibility is unlikely without additional p53 inactivation.

In line with our findings, recent studies demonstrated that progenitor cells with high levels of DNA damage because of aging or irradiation are cleared from the bone marrow and only progenitor cells without increased DNA damage can contribute to hematopoiesis.[43,44] Further supporting our proposed mechanism, Wang et al demonstrated that mice deficient for the shelterin POT1b develop BMF at the age of 15 months.[45] Absence of POT1b resulted in dysfunctional telomeres, and DDR activation led to an intrinsic growth defect and progressive depletion of the hematopoietic stem cell pool. Interestingly, POT1b-deficient mice with heterozygous telomerase deficiency (mTERC$^{+/-}$) develop even earlier DKC features as BMF and cutaneous phenotypes, highlighting the role of telomere maintenance for the stem cell pool.[46,47]

Interestingly, all known *TIN2* mutations in DKC patients are observed in the exon 6 close-by or in the region encoding for the TRF1 binding site, raising the possibility that impaired TIN2-TRF1 interaction accounts for the pathogenesis of DKC. In vitro studies revealed that deletion of the TRF1 binding site of TIN2 leads to reduced TRF1 levels in the shelterin complex.[20-23] Further supporting this notion, the recent study of Sasa et al reports the case of a 4-year-old patient with a *TIN2* mutation in the TRF1 binding site and very short telomeres.[19] Coimmunoprecipitation assay resulted in a severely impaired ability of the patient's *TIN2* mutation to interact with TRF1. In addition, Kim et al reported that human fibroblasts with a truncated TIN2 protein lacking the TRF1 binding site showed significantly reduced TRF1 levels.[20] In striking similarity to our data, these fibroblasts showed impaired cell growth, an increased number of DNA damage foci on the telomeres indicative for dysfunctional telomeres, and an increased number of β-galactosidase senescent cells. However, despite similarities of our mouse model with the observations in patients with *TIN2* mutations, further data are needed to circumstantiate the hypothesis of impaired *TIN2*-TRF1 interaction responsible for the pathogenesis of DKC. In summary, we provide the first mouse model simulating DKC features caused by alteration of TRF1 and the conditional TRF1 deletion represents a useful model to further investigate the pathogenesis of DKC.

Acknowledgments

The authors thank Rosa Serrano and Ester Collado for the excellent mouse care.

F.B. is funded by the "Mildred-Scheel-Stipendium" of the "Deutsche Krebshilfe." M.F. is funded by the Spanish Ministry of Education through FPU fellowship. P.M. is funded by a "Ramón y Cajal" grant from the Spanish Ministry of Science. Research in the Blasco laboratory is funded by the Spanish Ministry of Economy and Competitiveness Projects SAF2008-05384 and CSD2007-00017, the Madrid Regional Government Project S2010/BMD-2303 (ReCaRe), the European Union FP7 Project FHEALTH-2010-259749 (EuroBATS), The European Research Council (ERC) Project GA#232854 (TEL STEM CELL), the Körber European Science Award from the Körber Foundation, the Preclinical Research Award from Fundación Lilly (Spain), Fundación Botín (Spain), and AXA Research Fund.

Authorship

Contribution: F.B. performed most of the experiments; M.F. performed the experiments in Figure 5E-H and contributed to Figures 4A and 6C and D; P.M. analyzed and interpreted data; and F.B. and M.A.B. conceived the original idea and wrote the manuscript.

Conflict-of-interest disclosure: The authors declare no competing financial interests.

Correspondence: Maria A. Blasco, PhD, Telomere and Telomerase Group, Molecular Oncology Program, Centro Nacional de Investigaciones Oncológicas (CNIO), Calle Melchor Fernández Almagro 3, 28029 Madrid, Spain; e-mail: mblasco@cnio.es.

References

1. Blackburn EH. Switching and signaling at the telomere. *Cell*. 2001;106(6):661-673.
2. de Lange T. Shelterin: the protein complex that shapes and safeguards human telomeres. *Genes Dev*. 2005;19(18):2100-2110.
3. Martinez P, Blasco MA. Telomeric and extra-telomeric roles for telomerase and the telomere-binding proteins. *Nat Rev Cancer*;11(3):161-176.
4. Shore D, Bianchi A. Telomere length regulation: coupling DNA end processing to feedback regulation of telomerase. *EMBO J*. 2009;28(16):2309-2322.
5. Martinez P, Blasco MA. Role of shelterin in cancer and aging. *Aging Cell*;9(5):653-666.
6. Martinez P, Thanasoula M, Munoz P, et al. Increased telomere fragility and fusions resulting from TRF1 deficiency lead to degenerative pathologies and increased cancer in mice. *Genes Dev*. 2009;23(17):2060-2075.
7. Sfeir A, Kosiyatrakul ST, Hockemeyer D, et al. Mammalian telomeres resemble fragile sites and require TRF1 for efficient replication. *Cell*. 2009; 138(1):90-103.
8. Calado RT, Young NS. Telomere maintenance and human bone marrow failure. *Blood*. 2008; 111(9):4446-4455.
9. Calado RT, Young NS. Telomere diseases. *N Engl J Med*. 2009;361(24):2353-2365.
10. Dokal I. Dyskeratosis congenita. *Hematology Am Soc Hematol Educ Program*. 2011:480-486.
11. Blasco MA. Telomere length, stem cells and aging. *Nat Chem Biol*. 2007;3(10):640-649.
12. Dokal I, Vulliamy T. Inherited bone marrow failure syndromes. *Haematologica*. 2010;95(8):1236-1240.
13. Savage SA, Alter BP. The role of telomere biology in bone marrow failure and other disorders. *Mech Ageing Dev*. 2008;129(1-2):35-47.
14. Alter BP, Rosenberg PS, Giri N, Baerlocher GM, Lansdorp PM, Savage SA. Telomere length is associated with disease severity and declines with age in dyskeratosis congenita. *Haematologica*. 2012;97(3):353-359.
15. Vulliamy TJ, Kirwan MJ, Beswick R, et al. Differences in disease severity but similar telomere lengths in genetic subgroups of patients with telomerase and shelterin mutations. *PLoS One*; 6(9):e24383.
16. Alter BP, Baerlocher GM, Savage SA, et al. Very short telomere length by flow fluorescence in situ hybridization identifies patients with dyskeratosis congenita. *Blood*. 2007;110(5):1439-1447.
17. Vulliamy TJ, Marrone A, Knight SW, Walne A, Mason PJ, Dokal I. Mutations in dyskeratosis congenita: their impact on telomere length and the diversity of clinical presentation. *Blood*. 2006; 107(7):2680-2685.
18. Vulliamy T, Beswick R, Kirwan M, Hossain U, Walne A, Dokal I. Telomere length measurement can distinguish pathogenic from non-pathogenic variants in the shelterin component, TIN2. *Clin Genet*. 2012;81(1):76-81.
19. Sasa G, Ribes-Zamora A, Nelson N, Bertuch A. Three novel truncating TINF2 mutations causing severe dyskeratosis congenita in early childhood. *Clin Genet*. 2012;81(5):470-478.
20. Kim SH, Davalos AR, Heo SJ, et al. Telomere dysfunction and cell survival: roles for distinct TIN2-containing complexes. *J Cell Biol*. 2008; 181(3):447-460.
21. Kim SH, Kaminker P, Campisi J. TIN2, a new regulator of telomere length in human cells. *Nat Genet*. 1999;23(4):405-412.
22. Takai KK, Kibe T, Donigian JR, Frescas D, de Lange T. Telomere protection by TPP1/POT1 requires tethering to TIN2. *Mol Cell*. 2011;44(4): 647-659.
23. Ye JZ, de Lange T. TIN2 is a tankyrase 1 PARP modulator in the TRF1 telomere length control complex. *Nat Genet*. 2004;36(6):618-623.
24. Savage SA, Calado RT, Xin ZT, Ly H, Young NS, Chanock SJ. Genetic variation in telomeric repeat binding factors 1 and 2 in aplastic anemia. *Exp Hematol*. 2006;34(5):664-671.
25. Savage SA, Giri N, Jessop L, et al. Sequence analysis of the shelterin telomere protection complex genes in dyskeratosis congenita. *J Med Genet*. 2011;48(4):285-288.
26. Kühn R, Schwenk F, Aguet M, Rajewsky K. Inducible gene targeting in mice. *Science*. 1995; 269(5229):1427-1429.
27. Samper E, Fernandez P, Eguia R, et al. Long-term repopulating ability of telomerase-deficient murine hematopoietic stem cells. *Blood*. 2002; 99(8):2767-2775.
28. Takai H, Smogorzewska A, de Lange T. DNA damage foci at dysfunctional telomeres. *Curr Biol*. 2003;13(17):1549-1556.
29. Deng Y, Chan SS, Chang S. Telomere dysfunction and tumour suppression: the senescence connection. *Nat Rev Cancer*. 2008;8(6):450-458.
30. Canela A, Vera E, Klatt P, Blasco MA. High-throughput telomere length quantification by FISH and its application to human population studies. *Proc Natl Acad Sci U S A*. 2007;104(13): 5300-5305.
31. Bernardes de Jesus B, Schneeberger K, Vera E, Tejera A, Harley CB, Blasco MA. The telomerase activator TA-65 elongates short telomeres and increases health span of adult/old mice without increasing cancer incidence. *Aging Cell*. 2011; 10(4):604-621.
32. Toledo LI, Murga M, Fernandez-Capetillo O. Targeting ATR and Chk1 kinases for cancer treatment: a new model for new (and old) drugs. *Mol Oncol*. 3022;5(4):368-373.
33. Blasco MA. Telomeres and human disease: ageing, cancer and beyond. *Nat Rev Genet*. 2005; 6(8):611-622.
34. Brümmendorf TH, Balabanov S. Telomere length dynamics in normal hematopoiesis and in disease states characterized by increased stem cell turnover. *Leukemia*. 2006;20(10):1706-1716.
35. Karlseder J, Kachatrian L, Takai H, et al. Targeted deletion reveals an essential function for the telomere length regulator Trf1. *Mol Cell Biol*. 2003; 23(18):6533-6541.
36. Engelhardt M, Kumar R, Albanell J, Pettengell R, Han W, Moore MA. Telomerase regulation, cell cycle, and telomere stability in primitive hematopoietic cells. *Blood*. 1997;90(1):182-193.
37. Cheng T, Rodrigues N, Shen H, et al. Hematopoietic stem cell quiescence maintained by p21cip1/waf1. *Science*. 2000;287(5459):1804-1808.
38. Rankin SM. The bone marrow: a site of neutrophil clearance. *J Leukoc Biol*. 2010;88(2):241-251.
39. Steele JM, Sung L, Klaassen R, et al. Disease progression in recently diagnosed patients with inherited marrow failure syndromes: a Canadian Inherited Marrow Failure Registry (CIMFR) report. *Pediatr Blood Cancer*. 2006;47(7):918-925.
40. Dokal I. Dyskeratosis congenita in all its forms. *Br J Haematol*. 2000;110(4):768-779.
41. Kirwan M, Dokal I. Dyskeratosis congenita, stem cells and telomeres. *Biochim Biophys Acta*. 2009; 1792(4):371-379.
42. Mason PJ, Wilson DB, Bessler M. Dyskeratosis congenital—a disease of dysfunctional telomere maintenance. *Curr Mol Med*. 2005;5(2):159-170.
43. Mohrin M, Bourke E, Alexander D, et al. Hematopoietic stem cell quiescence promotes error-prone DNA repair and mutagenesis. *Cell Stem Cell*. 2010;7(2):174-185.
44. Rossi DJ, Bryder D, Seita J, Nussenzweig A, Hoeijmakers J, Weissman IL. Deficiencies in DNA damage repair limit the function of haematopoietic stem cells with age. *Nature*. 2007; 447(7145):725-729.
45. Wang Y, Shen MF, Chang S. Essential roles for Pot1b in HSC self-renewal and survival. *Blood*. 2011;118(23):6068-6077.
46. He H, Wang Y, Guo X, et al. Pot1b deletion and telomerase haploinsufficiency in mice initiate an ATR-dependent DNA damage response and elicit phenotypes resembling dyskeratosis congenita. *Mol Cell Biol*. 2009;29(1):229-240.
47. Hockemeyer D, Palm W, Wang RC, Couto SS, de Lange T. Engineered telomere degradation models dyskeratosis congenita. *Genes Dev*. 2008;22(13):1773-1785.